



SESAME

Research and Innovation Action (RIA)

This project has received funding from the Euratom research and training programme 2014-2018 under grant agreement No 654935.

Start date : 2015-04-01 Duration : 48 Months
<http://sesame-h2020.eu/>



CIRCLE experiment: pre-test, data set and analysis

Authors : Dr. Mariano TARANTINO (ENEA) D. Martelli (ENEA), Vincent Moreau (CRS4), Kevin Zwijssen (NRG)

SESAME - Contract Number: 654935
thermal hydraulics Simulations and Experiments for the Safety Assessment of Metal cooled reactors


Document title	CIRCLE experiment: pre-test, data set and analysis
Author(s)	Dr. Mariano TARANTINO D. Martelli (ENEA), Vincent Moreau (CRS4), Kevin Zwijsen (NRG)
Number of pages	230
Document type	Deliverable
Work Package	WP3
Document number	D3.2
Issued by	ENEA
Date of completion	2017-09-11 14:49:16
Dissemination level	Public

Summary


The present document reports the experimental data obtained in the frame of the EU project SESAME WP3 (deliverable D3.2) on the CIRCE large pool experimental facility. Moreover the pre-test CFD analysis performed at CRS4 and NRG are reported.

Approval


Date	By
2017-09-12 09:22:39	Mrs. Vincent MOREAU (CRS4)
2017-09-12 16:43:24	Dr. Mariano TARANTINO (ENEA)

 DIVISIONE INGEGNERIA SPERIMENTALE	<u>Title</u> D3.2: CIRCE experiments: pre-test, data-set and analysis	<u>Distribution</u> PUBLIC	<u>Emission</u> 09/08/2017	<u>Pag.</u> 3 di 234
		<u>Ref.</u> CI-T-R-292	Rev. 0	

List of Revision	2
Abbreviations and acronyms	5
1 Introduction	6
2 Test Matrix	7
3 Experimental results	9
3.1 Test 1	9
3.2 Test 2	47
3.3 Test 3	85
3.4 Test 4	124
4 CRS4 CFD simulations of CIRCE-ICE	164
4.1 COLD model	164
4.1.1 Geometry	164
4.1.2 Eulerian Multiphase trial	165
4.1.3 VoF and Lagrangian particles	166
4.1.4 Analysis	168
4.2 Hot model	169
4.2.1 Geometry	169
4.2.2 Mesh	170
4.3 Instrumentation	171
4.3.1 Numerical settings	172
4.3.2 Results	174
4.3.3 Analysis	177
5 NRG simulation of CIRCE-ICE	181
5.1 Model description	181
5.1.1 Fuel Pin Simulator	182
5.1.2 Argon Injection	185
5.1.3 Cover gas & free surface	185
5.1.4 Heat exchanger	185
5.1.5 Decay heat removal system	187
5.1.6 Coniugate heat transfer	188
5.2 Mesh generation	188
5.2.1 Simulation Settings	190
5.2.2 Material Properties	190
5.3 Results of the CFD Simulation	191


 DIVISIONE INGEGNERIA SPERIMENTALE	<u>Title</u> D3.2: CIRCE experiments: pre-test, data-set and analysis	<u>Distribution</u> PUBLIC	<u>Emission</u> 09/08/2017	<u>Pag.</u>
		<u>Ref.</u> CI-T-R-292	Rev. 0	4 di 234

5.3.1	Description of SESAME WP3 Test 1	191
5.3.2	Steady-State results.	192
5.3.3	Transient simulation.....	196
6	Conclusions and remarks	201
Annex A:	205
Annex B:	219
Annex C:	227
Distribution List	230

 DIVISIONE INGEGNERIA SPERIMENTALE	<u>Title</u> D3.2: CIRCE experiments: pre-test, data-set and analysis	<u>Distribution</u> PUBLIC	<u>Emission</u> 09/08/2017	<u>Pag.</u>
		<u>Ref.</u> CI-T-R-292	Rev. 0	5 di 234

ABBREVIATIONS AND ACRONYMS

CIRCE	CIRcolazione Eutettico
CRS4	Centro di Ricerca, Sviluppo e studi superiori in Sardegna
DHR	Decay Heat Removal
EC DG RTD	European Commission – Directorate General for Research and Technological Development
ENEA	Agenzia nazionale per le nuove tecnologie, l'energia e lo sviluppo economico sostenibile
FPS	Fuel Pin Simulator
HLM	Heavy Liquid-Metal
HS	Heat Source
HX	Heat Exchanger
HTC	Heat Transfer Coefficient
ICE	Integral Circulation Experiments
LBE	Lead-Bismuth Eutectic
LOF	Loss of Flow
LOFA	Loss Of Flow Accident
NRG	Nuclear Research and consultancy Group
PLOHS	Protected Loss Of Heat Sink
SESAME	Safety Assessment of MEtal cooled reactors
TC	Thermocouple

 DIVISIONE INGEGNERIA SPERIMENTALE	<u>Title</u> D3.2: CIRCE experiments: pre-test, data-set and analysis	<u>Distribution</u> PUBLIC	<u>Emission</u> 09/08/2017	<u>Pag.</u> 6 di 234
		<u>Ref.</u> CI-T-R-292	Rev. 0	

1 INTRODUCTION

In the framework of the Heavy Liquid Metal (HLM) - GEN IV Nuclear reactor development one of the main task deals with the thermal-hydraulics analysis of Heavy Liquid Metal-cooled fast reactor (attention mainly focused on LBE and LEAD cooled reactors), aimed at their safety analysis in response to a hypothetical accidental scenario.


Nowadays numerical simulations and modelling always more play a key role in the design of components and systems and in that scenario new models and new software tools are developed to investigate thermal-hydraulics issues related to HLM technology. All this incoming tools must be validated in order to be used for safety analyses.

The activity proposed within the Safety Assessment of Metal cooled reactor (SESAME [1]) WP3 “Pool Thermal Hydraulics” of the research and innovation program HORIZON2020, is aimed to define, implement and carry out experimental campaigns on the CIRCE experimental facility [2] in order to support the qualification of CFD as a valid tool for the design, control and analysis of complex three dimensional convection patterns in a large pool configuration simulating the primary system of a LBE- LEAD cooled reactor.

In this document the experimental activity on the CIRCE-ICE pool type facility is summarized outcomes of the performed experimental tests are reported.

The proposed experimental test matrix was intended to reproduce steady state forced circulation at full power and steady state natural circulation at decay power (5-7% of the nominal power). Moreover, transition from forced to natural circulation was also investigated simulating a Protected Loss of Flow Accident (PLOFA) scenario.

The second part of the document resume the work performed by CRS4 and NRG in the framework of the SESAME deliverable D3.2: “CIRCE experiment pre-test, data set and analysis”. The general objective is to build a CFD model of CIRCE that can help understand the effective behaviour of the experimental facility, highlight possible improvement, reproduce former experiments and later be validated by predicting the behaviour of CIRCE in new experimental campaign.

 DIVISIONE INGEGNERIA SPERIMENTALE	<u>Title</u> D3.2: CIRCE experiments: pre-test, data-set and analysis	<u>Distribution</u> PUBLIC	<u>Emission</u> 09/08/2017	<u>Pag.</u> 7 di 234
		<u>Ref.</u> CI-T-R-292	Rev. 0	

2 TEST MATRIX

The experimental activity consists in a series of four tests (named Test 1, Test 2, Test 3 and Test 4) simulating the total loss of the secondary circuit and the coolant pump trip (simulated stopping the gas enhanced circulation, with the exception of Test 4) with the consequent reactor scram (reduction of the electric power supplied to the fuel pin simulator) and activation of DHR system to remove the decay heat power (~5% of the nominal value). The boundary conditions of the performed tests are reported from Table 1 to Table 4.

Table 1: Boundary conditions for TEST 1

Nominal Steady State	PLOHS+LOF transient
HS Thermal Power ~800 kW	Isolation of the main HX (isolating the feed water)
HLM flow rate: 60-70 kg/s (by gas lift)	Core "scram" at about 30 kW (decay power)
Argon mass flow rate ~3NI/s	Start-up of the DHR-system (air mass flow rate 0.24 kg/s)
Average velocity into the HS:1m/s	DHR air inlet @ room temperature
Pool LBE initial temperature ~314°C (Vertical gradient in the pool of 3°C 316 T-MS-001, 312 °C T-MS-119)	"Main pump" turn-off (the gas injection is interrupted)
Vessel heating system: not active	Vessel heating system: not-active
HX water flow rate ~ 0.6 kg/s	
HX thermal power removed ~750 kW	
DHR: not active	
HX inlet Water @ room temperature	

Table 2: Boundary conditions for TEST 2

Nominal Steady State	PLOHS+LOF transient
HS Thermal Power ~800 kW	Isolation of the main HX (isolating the feed water)
HLM flow rate: 60-70 kg/s (by gas lift)	Core "scram" at about 30 kW (decay power)
Argon mass flow rate ~2.7 NI/s	Start-up of the DHR-system (air mass flow rate $\dot{m} \sim 0.325 / 0.22 \text{ kg/s}$)
Average velocity into the HS:1m/s	DHR air inlet @ room temperature
Pool LBE initial temperature ~280°C (Vertical gradient in the pool of 4°C 282 T-MS-001, 278 °C T-MS-119)	"Main pump" turn-off (the gas injection is interrupted)
Vessel heating system: not active	Vessel heating system: not-active
HX water flow rate ~ 0.6 kg/s	
HX thermal power removed ~750 kW	
DHR: not active	
HX inlet Water @ room temperature	


 DIVISIONE INGEGNERIA SPERIMENTALE	<u>Title</u> D3.2: CIRCE experiments: pre-test, data-set and analysis	<u>Distribution</u> PUBLIC	<u>Emission</u> 09/08/2017	<u>Pag.</u> 8 di 234
		<u>Ref.</u> CI-T-R-292	Rev. 0	

Table 3: Boundary conditions for TEST 3


Nominal Steady State	PLOHS+LOF transient
HS Thermal Power ~750 kW	Isolation of the main HX (isolating the feed water)
HLM flow rate: 59.6 kg/s (by gas lift)	Core “scram” at about 30 kW (decay power)
Argon mass flow rate ~2.5-2.6 NI/s	Start-up of the DHR-system (air mass flow rate 0.2 kg/s)
Average velocity into the HS: 0.91 m/s	DHR air inlet @ room temperature
Pool LBE initial temperature ~270°C (Vertical gradient in the pool of 1-2°C)	“Main pump” turn-off (the gas injection is interrupted)
Vessel heating system: not active	Vessel heating system: not-active
HX water flow rate ~ 0. 5kg/s	
HX thermal power removed ~411 kW	
DHR: not active	
HX inlet Water @ room tem0070erature	

Table 4: Boundary conditions for TEST 4

Nominal Steady State	PLOHS transient
HS Thermal Power ~750 kW	Isolation of the main HX (isolating the feed water)
HLM flow rate: 59.6 kg/s (by gas lift)	Core “scram” at about 30 kW (decay power)
Argon mass flow rate ~2.5-2.6 NI/s	Start-up of the DHR-system (air mass flow rate 0.2 kg/s)
Average velocity into the HS: 1 m/s	DHR air inlet @ room temperature
Pool LBE initial temperature ~280°C (Vertical gradient in the pool of 4°C)	Gas injection is NOT interrupted
Vessel heating system: not active	Vessel heating system: not-active
HX water flow rate ~ 0. 6 kg/s	
HX thermal power removed ~411 kW	
DHR: not active	
HX inlet Water @ room temperature	

As shown in Table 4, Test 4 differs from the other tests in the fact that the forced circulation is maintained also after the transition to reduced power condition.

Experimental data of each tests are collected in the file Test_i.rar (i=1..4), containing the .txt version of the acquired signals (Test_i.txt) and a file with the name of each signal (Header_test_i.txt). Moreover, the file TEST_i.mat represents the MATLAB version of the experimental data. Finally, the file DATA_Description.xlsx contains for each measurement device a short description, the measurements unit, the name of the technical drawing with the location of the device and the type of the instrumentation.

 DIVISIONE INGEGNERIA SPERIMENTALE	<u>Title</u> D3.2: CIRCE experiments: pre-test, data-set and analysis	<u>Distribution</u> PUBLIC	<u>Emission</u> 09/08/2017	<u>Pag.</u> 9 di 234
		<u>Ref.</u> CI-T-R-292	Rev. 0	

3 EXPERIMENTAL RESULTS

3.1 Test 1

Test 1 is characterized by a nominal power ramp from 0 to 800 kW. The ramp starts at $t = 1083$ s and stops at 1260 s, the mean value of the power during the full power transient is about 804.8 kW with a standard deviation of 7.1 kW. The “full power” transient stops at $t=37128$ s with a descending ramp up to about 30 kW ($t=37332$ s). The end of the low power run is at $t=72339$ s (~20h). The mean value of the power after the simulation of the core scram is 30.7 kW with a standard deviation of 0.5 kW. The electric power (DC-KW) time trend is reported in Figure 1

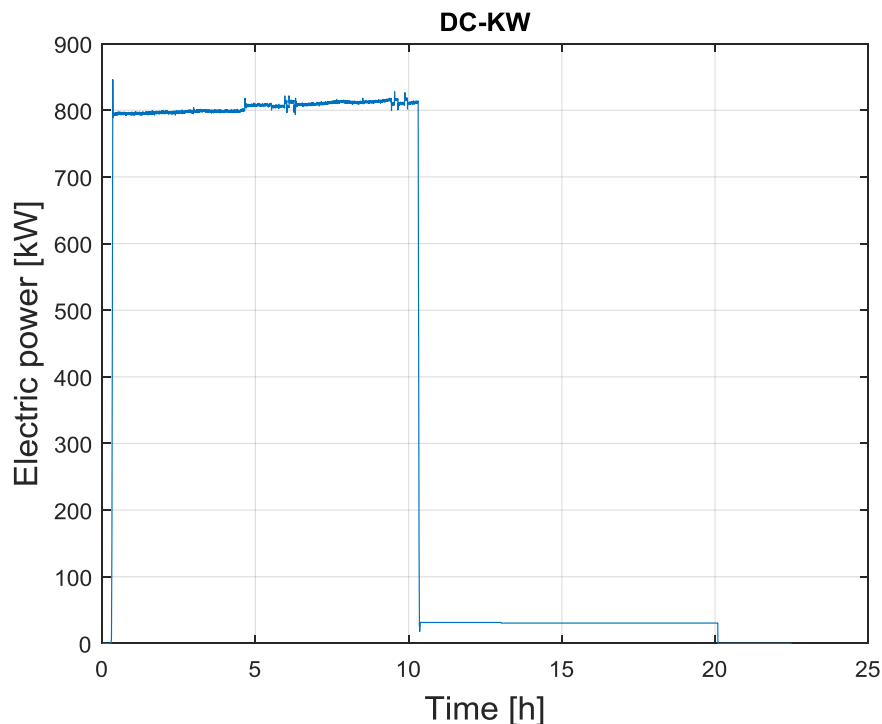



Figure 1: Electric Power [kW]

During the full power transient, the main heat exchanger is fed by a water mass flow rate with a mean value of 0.59 kg/s (FE501 see Figure 2) and a standard deviation 0.02. After the simulation of the accidental scenario the water injection is stopped at about $t=37265$ s. In Figure 2, the value 0.1 kg/s after 10 h is to be considered the full scale of the instrument.

 DIVISIONE INGEGNERIA SPERIMENTALE	<u>Title</u> D3.2: CIRCE experiments: pre-test, data-set and analysis	<u>Distribution</u> PUBLIC	<u>Emission</u> 09/08/2017	<u>Pag.</u> 10 di 234
		<u>Ref.</u> CI-T-R-292	Rev. 0	

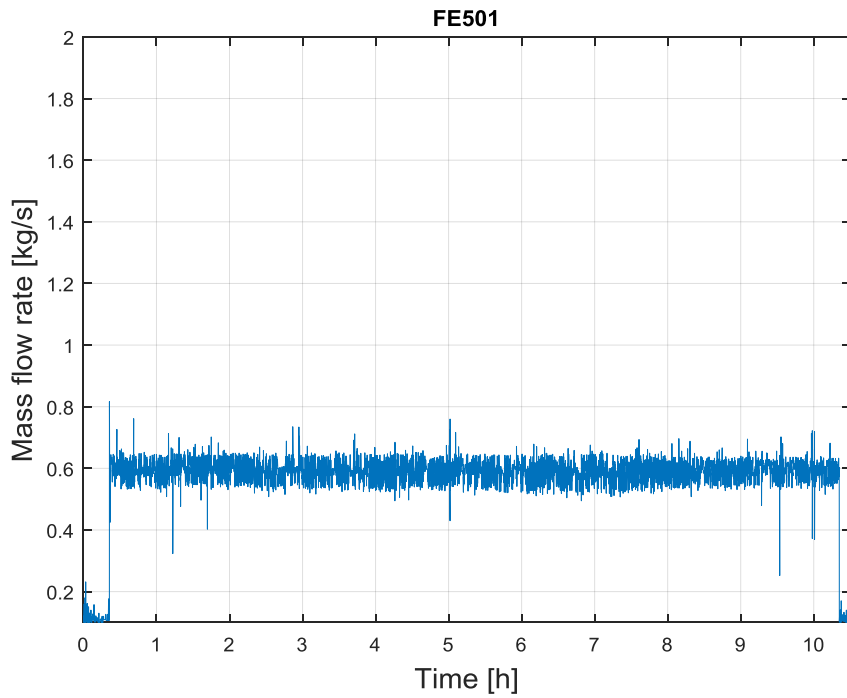


Figure 2: Water mass flow rate

Pressure and temperature of the water at the inlet of the HX are reported in Figure 3 and Figure 4

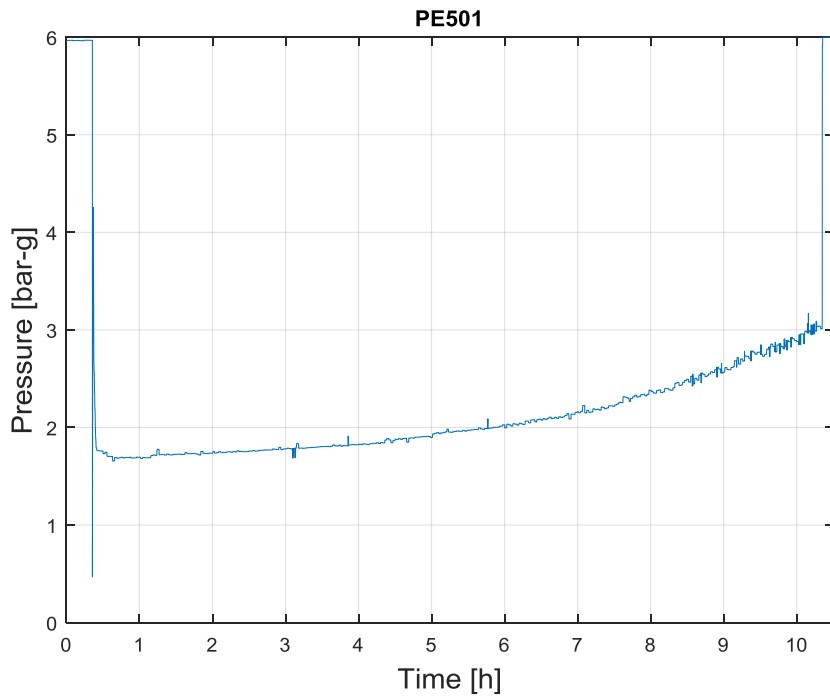



Figure 3: Water inlet pressure

 DIVISIONE INGEGNERIA SPERIMENTALE	<u>Title</u> D3.2: CIRCE experiments: pre-test, data-set and analysis	<u>Distribution</u> PUBLIC	<u>Emission</u> 09/08/2017	<u>Pag.</u> 11 di 234
		<u>Ref.</u> CI-T-R-292	Rev. 0	

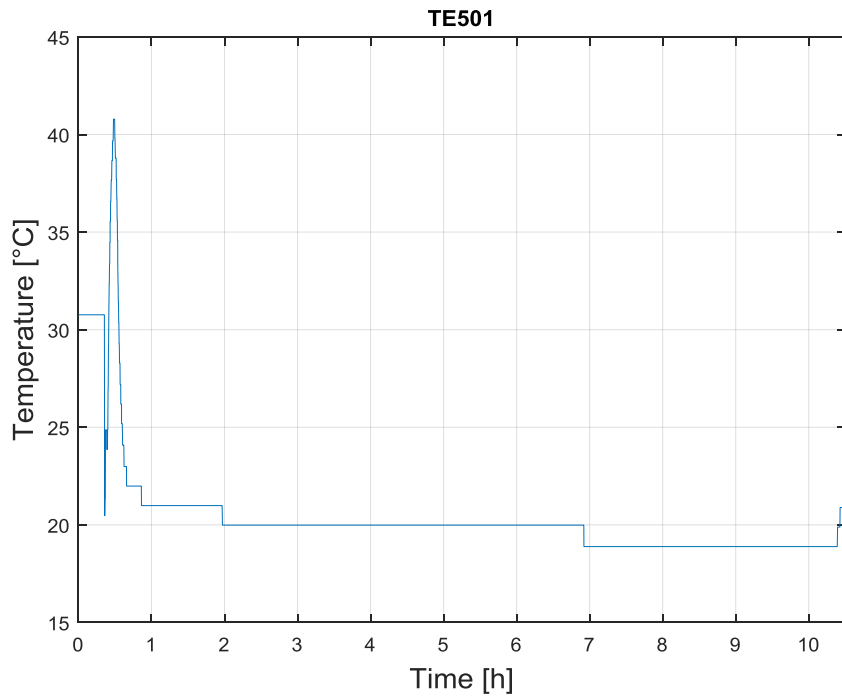


Figure 4: Water inlet temperature

Temperature of the steam at the outlet of the HX is reported in Figure 5

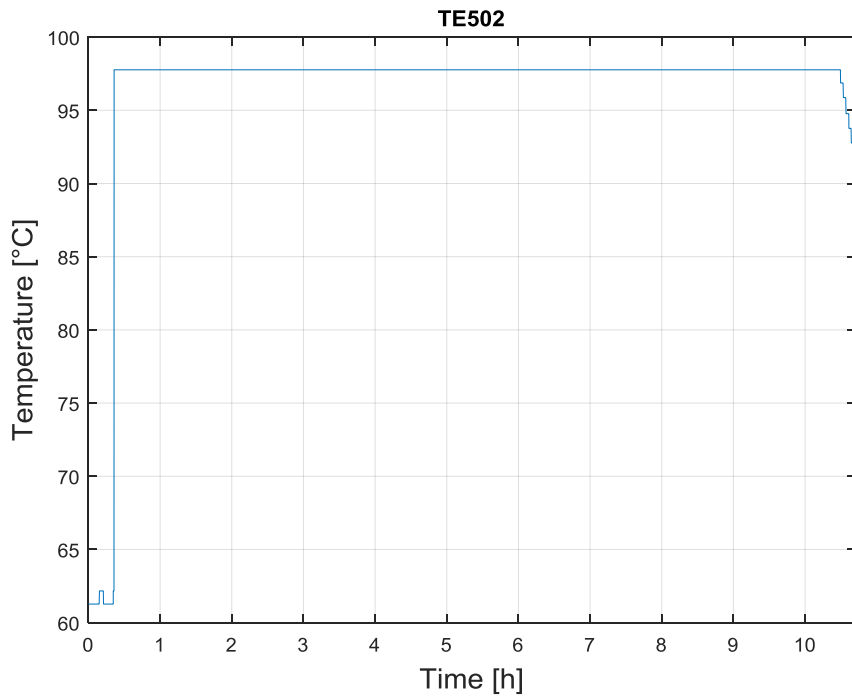



Figure 5: Steam temperature at the outlet of the HX

 DIVISIONE INGEGNERIA SPERIMENTALE	<u>Title</u> D3.2: CIRCE experiments: pre-test, data-set and analysis	<u>Distribution</u> PUBLIC	<u>Emission</u> 09/08/2017	<u>Pag.</u> 12 di 234
		<u>Ref.</u> CI-T-R-292	Rev. 0	

The Temperature of the helium gas entrapped in the gap between the tubes of the HX is reporter in Figure 6

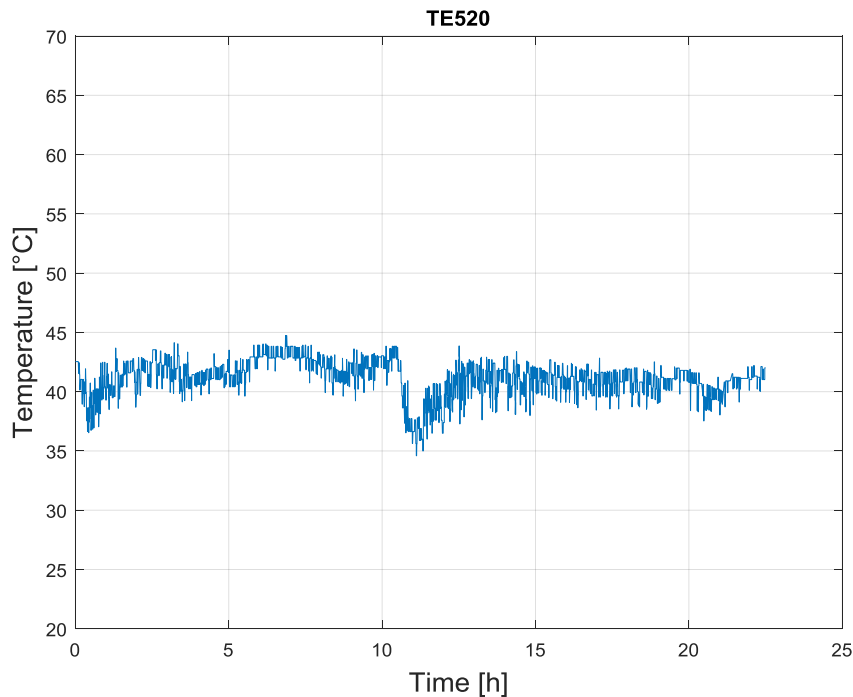


Figure 6: He temperature in the gap between the HX tubes

During the full power run, the LBE is circulated by means of argon gas injection (gas enhanced circulation). The gas injection is usually started before activating the fuel pin simulator in order to avoid the overheating of the pin clads. For this reason the gas injection started at $t=618$ s while it is stopped simultaneously to the stopping of the injection of the water in order to simulate the loss of the heat sink together with the loss of flow ($t=37264$ s, Figure 7). During the gas injection the mean value is 2.53 NI/s and a standard deviation is 0.0347 NI/s. The adopted gas flow meters for TEST 1 was FT-208 B described in Annex B. The zero of the acquired mass flow rate signal was not directly provided by the software, for this reason for Test 1 the signal FE208B was properly shifted.

In the low power transient the decay heat removal system (DHR) is activated injecting air in the bayonet tube of the DHR. The injection of air starts at $t=37267$ s. As shown in Figure 8, the air mass flow rate mean value is 227.3 g/s with a standard deviation of 57 g/s. The DHR air temperature difference is plot in Figure 9. The air temperature must be considered after the activation of the DHR ($t=37267$ s.).

At $t=59550$ the temperature difference suddenly decreases of about 33°C without changes of the boundary conditions (for the physical interpretation of the sudden decrease of the air temperature difference between the DHR inlet and outlet ($t\sim 16.51$ h) refers to Annex C). In Figure 10 the air velocity in the DHR is plotted, the mean value is 26.3 m/s.

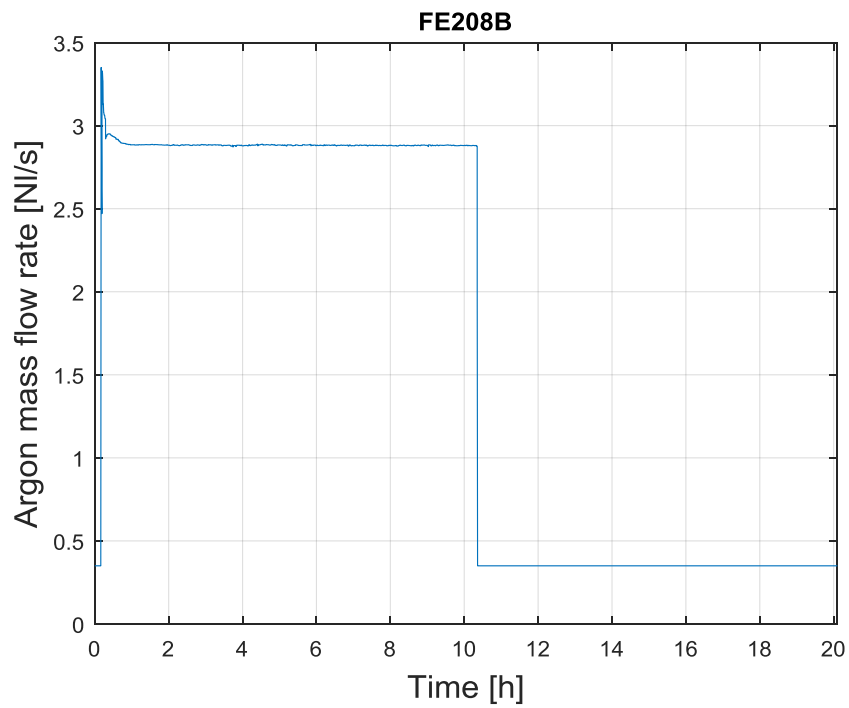


Figure 7: Argon mass flow rate

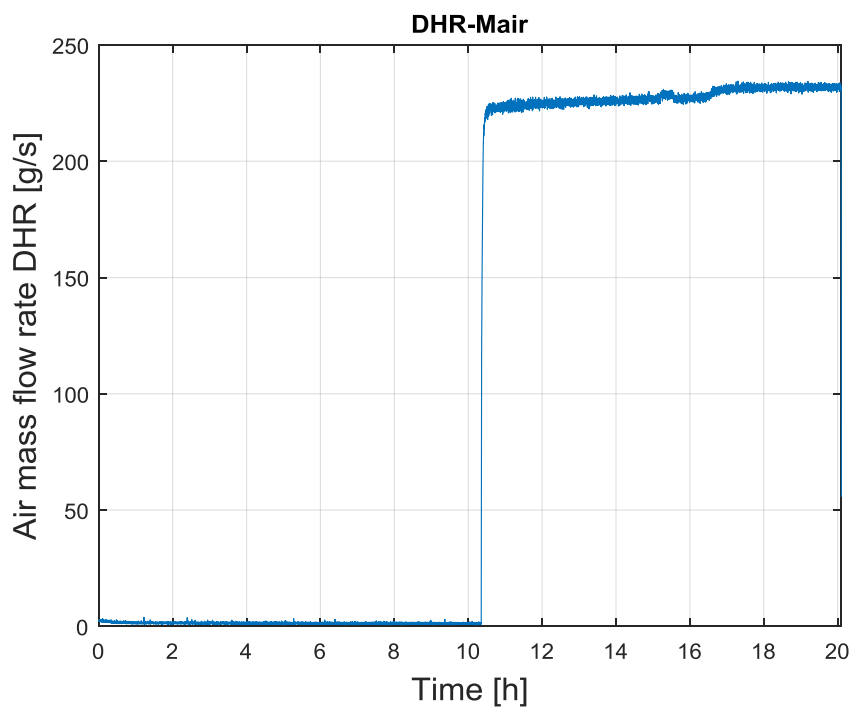


Figure 8: DHR air mass flow rate

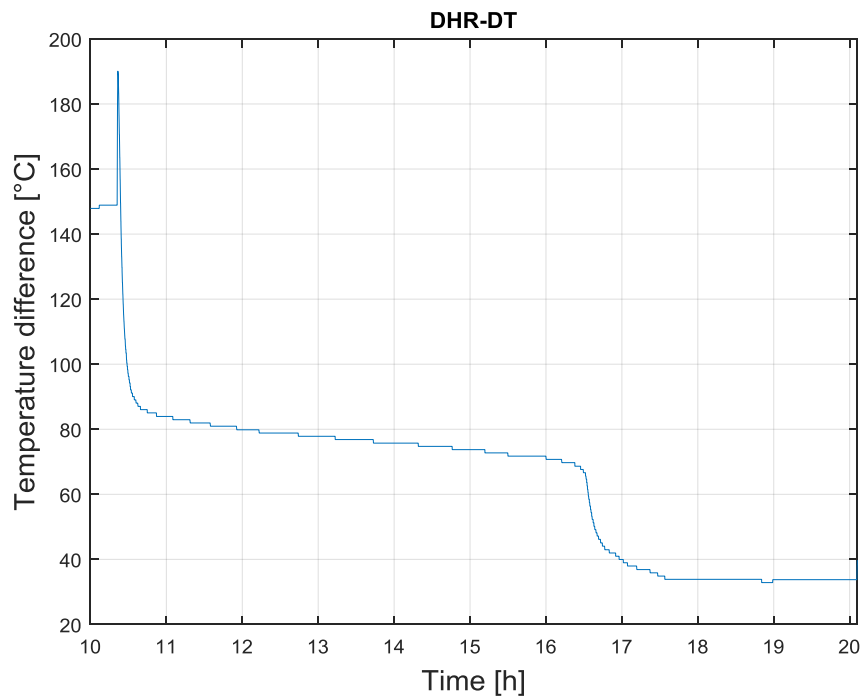


Figure 9: DHR inlet outlet air temperature difference

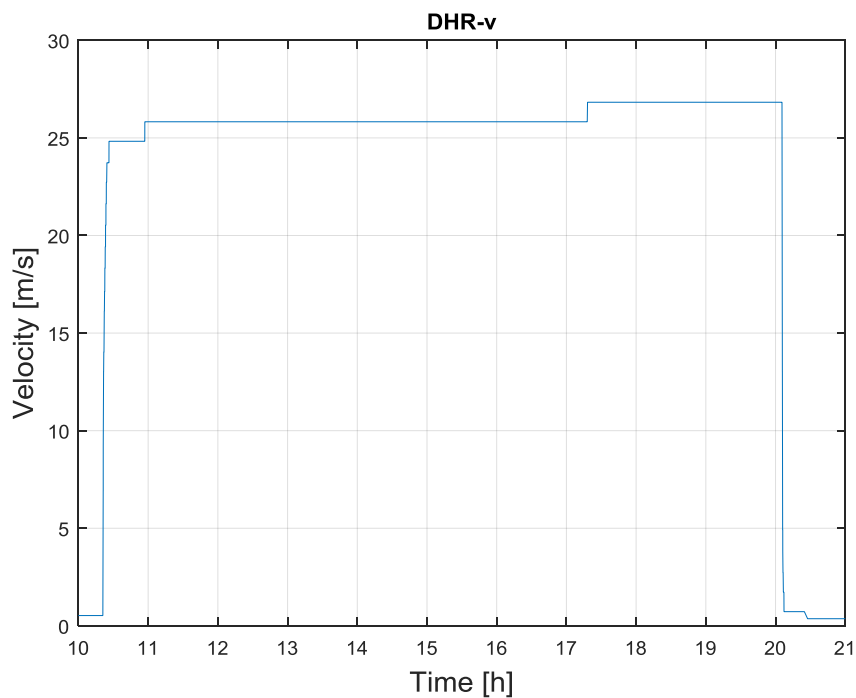



Figure 10: DHR air velocity

 DIVISIONE INGEGNERIA SPERIMENTALE	<u>Title</u> D3.2: CIRCE experiments: pre-test, data-set and analysis	<u>Distribution</u> PUBLIC	<u>Emission</u> 09/08/2017	<u>Pag.</u> 15 di 234
		<u>Ref.</u> CI-T-R-292	Rev. 0	

The pressure difference across the venturi flow meter (see Annex A Fig. 1 Mass flow Meter/08-384-DISEGNO.pdf) used to evaluate the LBE mass flow rate in the ICE test section is plotted in Figure 11. The mean value during the full power run is 343.5 mbar with a standard deviation of 12.6 mbar. During the low power transient the mean pressure difference is 44.2 mbar.

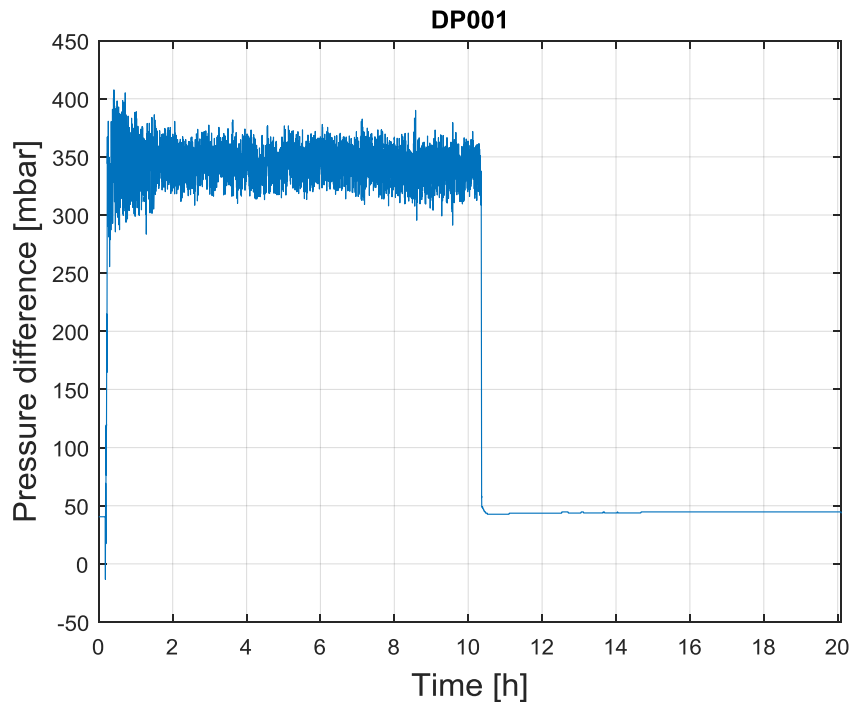


Figure 11: Pressure difference across the venturi flow meter

DP002 (PE009-PE010) represents the pressure difference across the lower spacer grid (for the positioning of the bubble tubes see Annex A Fig. 2 0510 Rev 1-Fuel Pin Simulator.pdf). The mean value of the pressure difference during the full power transient is 251 mbar with a standard deviation of about 3 mbar, while the mean value for the low power run is 212 mbar with a standard deviation of 1 mbar (see Figure 12). PE003 represents the pressure in the fitting volume (Figure 13) while PE004 (Figure 14), PE005 (Figure 15) represent respectively the pressure in the lower and upper section of the riser. For the position of the bubble tubes PE003, PE004, PE005 see Annex A Fig. 3 0016 Instrumentation.pdf.

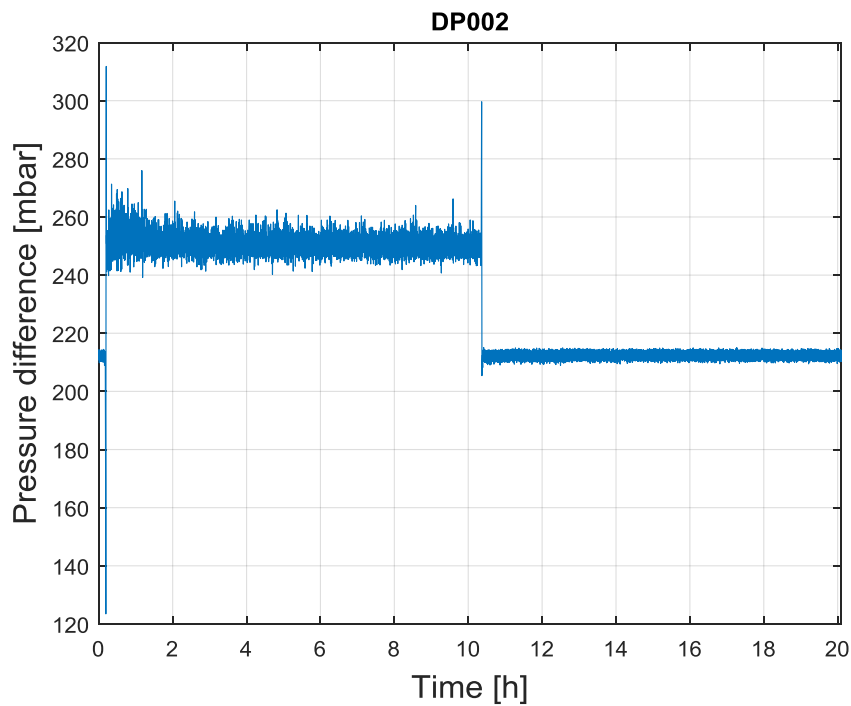


Figure 12: Pressure difference across the FPS lower spacer grid

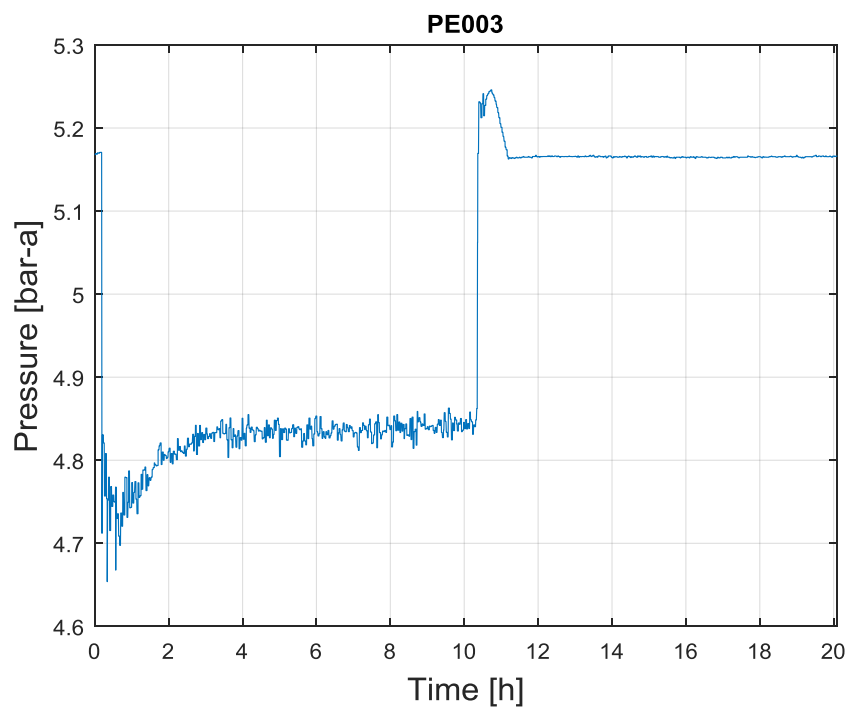


Figure 13: Pressure in the fitting volume

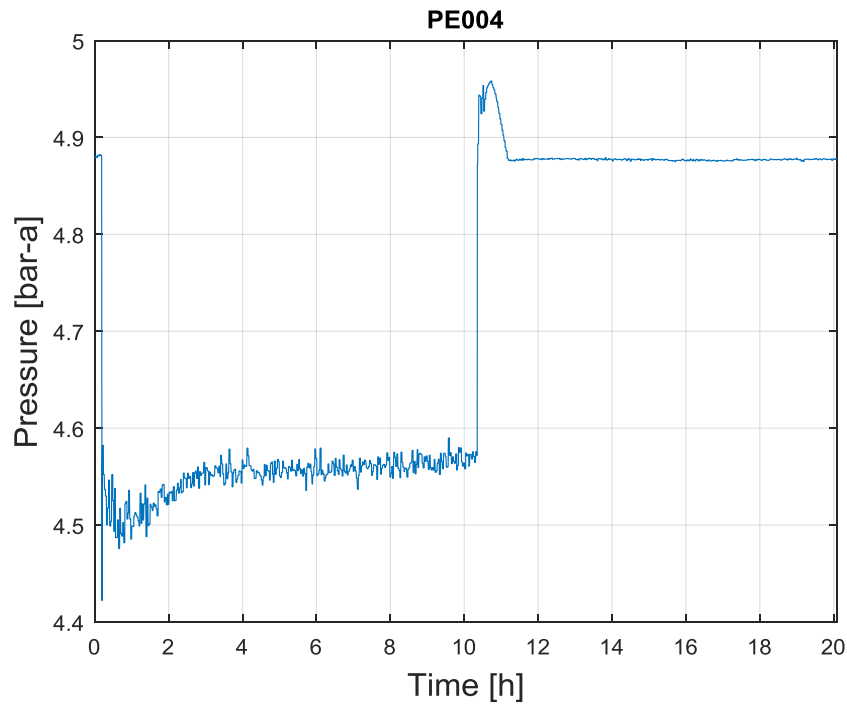


Figure 14: Pressure in the riser (lower section)

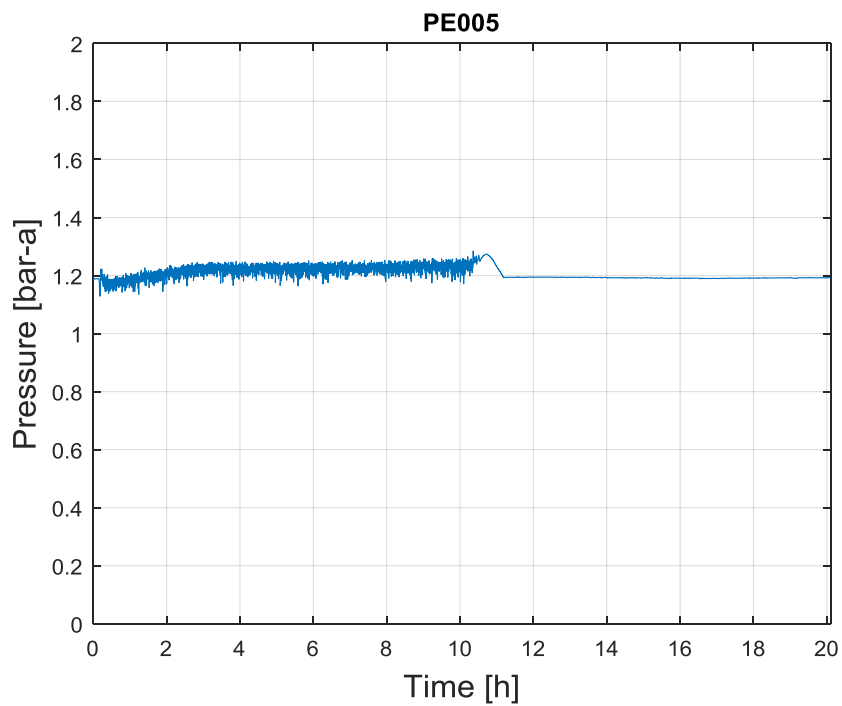



Figure 15: Pressure in the riser (upper section)

 DIVISIONE INGEGNERIA SPERIMENTALE	<u>Title</u> D3.2: CIRCE experiments: pre-test, data-set and analysis	<u>Distribution</u> PUBLIC	<u>Emission</u> 09/08/2017	<u>Pag.</u> 18 di 234
		<u>Ref.</u> CI-T-R-292	Rev. 0	

The LBE inside the pool is operated under a protective atmosphere of argon gas that fill the volume from the LBE free level to the vessel head. A relative small overpressure is maintained in the gas in order to avoid oxygen contamination from the external environment. PE007 is the pressure of the argon measured in the cover gas (see Figure 16), while the temperature of the cover gas is measured through a 3 mm *K*-type thermocouple and it is reported in Figure 17

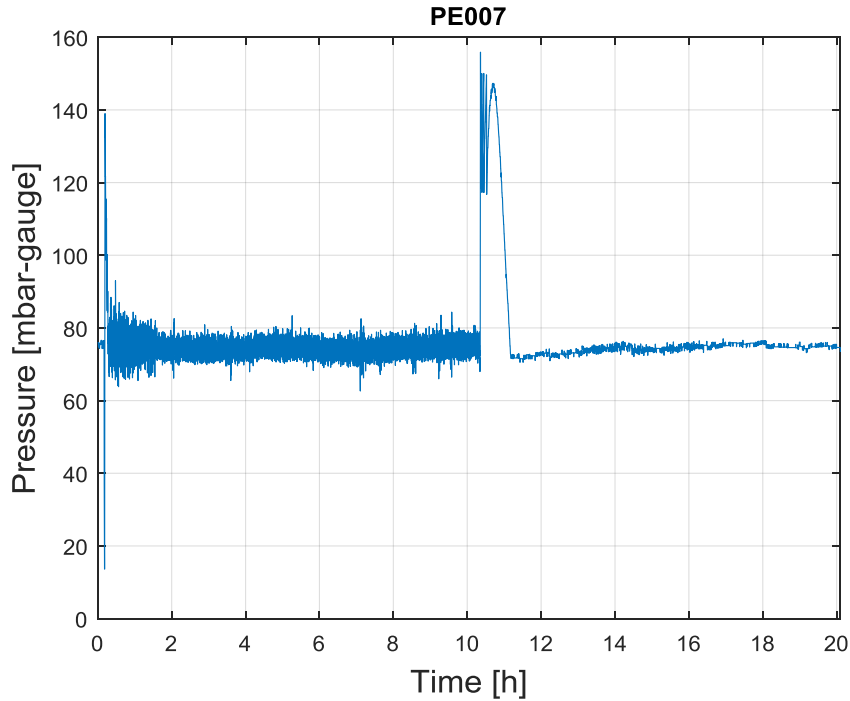



Figure 16: Pressure in the cover gas

 DIVISIONE INGEGNERIA SPERIMENTALE	<u>Title</u> D3.2: CIRCE experiments: pre-test, data-set and analysis	<u>Distribution</u> PUBLIC	<u>Emission</u> 09/08/2017	<u>Pag.</u> 19 di 234
		<u>Ref.</u> CI-T-R-292	Rev. 0	

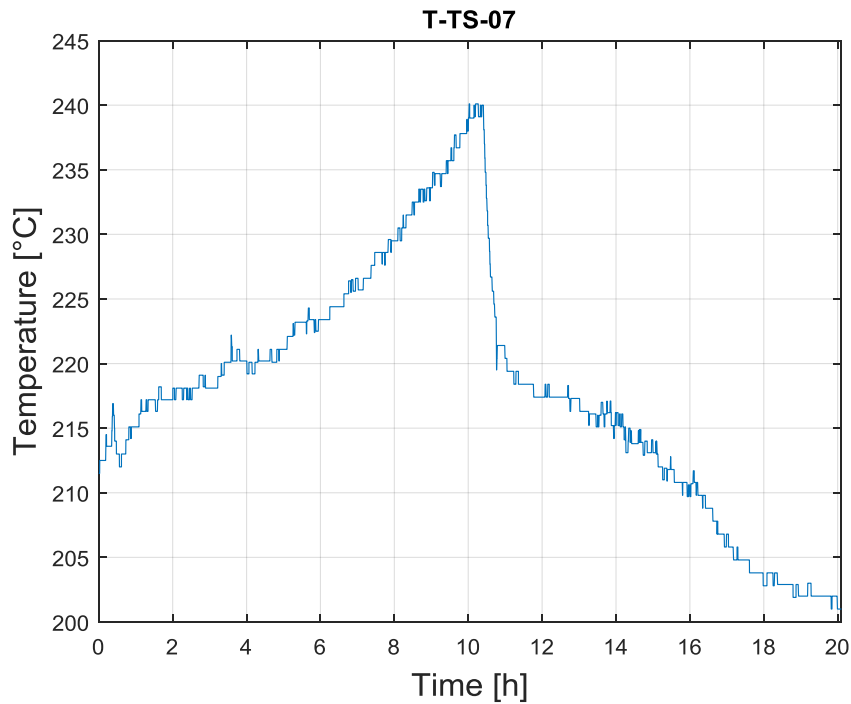



Figure 17: Temperature in the cover gas

For the positioning of the thermocouples in the DHR system refers to Annex A Fig. 4 THINS thermocouples arrangement.pdf and Annex A Fig. 5 T-DHR-0100-Instrumentation DHR.pdf. In Figure 18 the average temperature of the LBE at the inlet and outlet sections of the DHR is reported. After about 16.51 h of transient an inversion of the temperature between the inlet and outlet section occurs (at the same time the air temperature in the DHR suddenly decrease as observed in Figure 9), for the physical interpretation refers to Annex C .

 DIVISIONE INGEGNERIA SPERIMENTALE	<u>Title</u> D3.2: CIRCE experiments: pre-test, data-set and analysis	<u>Distribution</u> PUBLIC	<u>Emission</u> 09/08/2017	<u>Pag.</u> 20 di 234
		<u>Ref.</u> CI-T-R-292	Rev. 0	

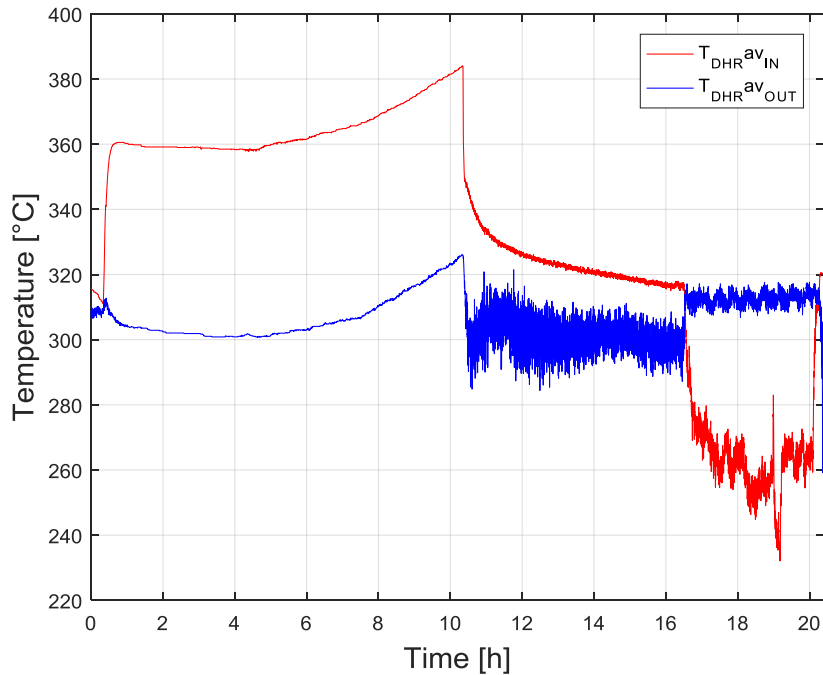



Figure 18: DHR inlet outlet average temperature

The LBE temperature at the FPS entrance was measured by three thermocouples with a diameter of 3 mm (T-FPS-31, 32, 33, Annex A Fig. 6 T-FPS-0100 foglio2-FPS Instrumented). The LBE temperature at the active length exit section of the FPS was measured by three thermocouples (T-FPS-34, 35, 36 Annex A Fig. 6 T-FPS-0100 foglio2-FPS Instrumented) of the same type of those at the entrance. Moreover three thermocouples T-FPS-37, 38, 39 were installed in the slot at the exit of the FPS placed at 120° (see Annex A Fig. 7 T-FPS-0100 foglio1-FPS Instrumented). For the position of the thermocouples inside the bundle refers to Annex A Fig. 8 T-FPS Instrumentation 1 of 2 and Annex A Fig. 9 T-FPS Instrumentation 2 of 2. In Figure 19 the LBE average temperature evaluated at the inlet and outlet sections of the FPS and at the outlet section of the FPS are reported (see Annex A Fig. 7 T-FPS-0100 foglio1-FPS Instrumented).

 DIVISIONE INGEGNERIA SPERIMENTALE	<u>Title</u> D3.2: CIRCE experiments: pre-test, data-set and analysis	<u>Distribution</u> PUBLIC	<u>Emission</u> 09/08/2017	<u>Pag.</u> 21 di 234
		<u>Ref.</u> CI-T-R-292	Rev. 0	

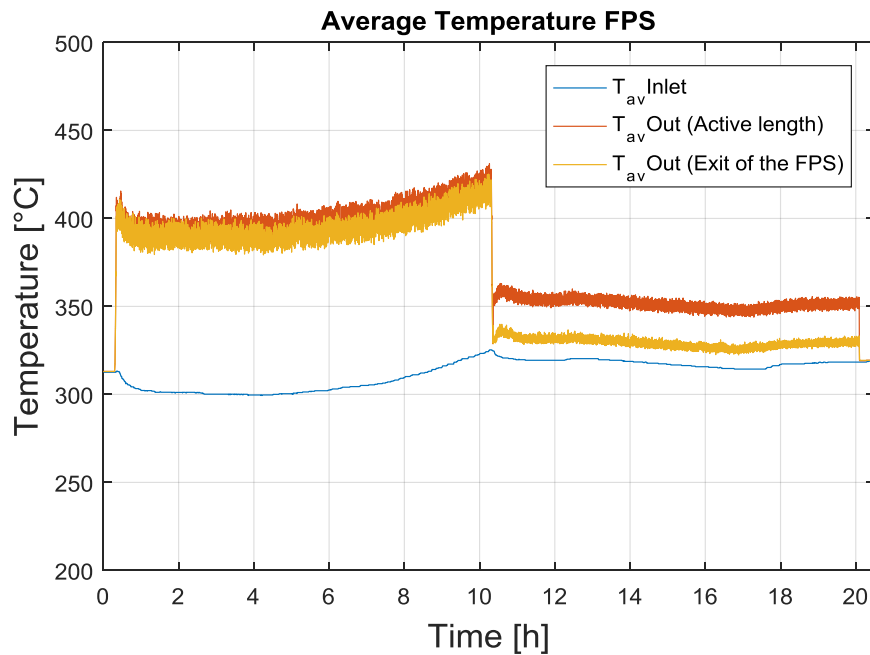


Figure 19: Active length Inlet/Outlet section and FPS Outlet LBE average temperature

From Figure 20 to Figure 48, temperatures in the Fuel Pin Simulator (FPS) are reported. It is worth to be mentioned that T-FPS-013 is damaged and therefore the relative plot is not reported.

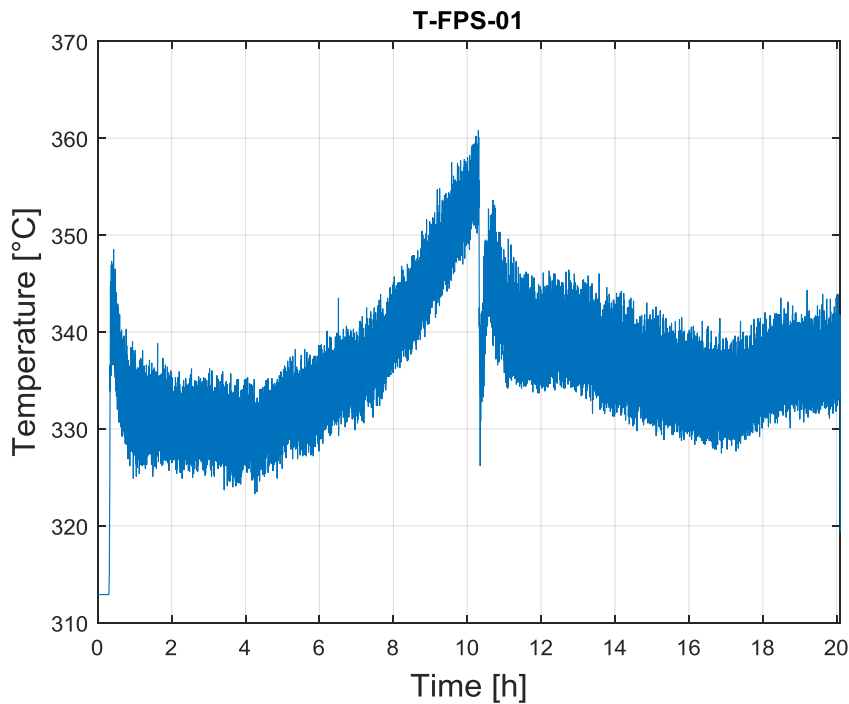


Figure 20: T-FPS-01 LBE temperature

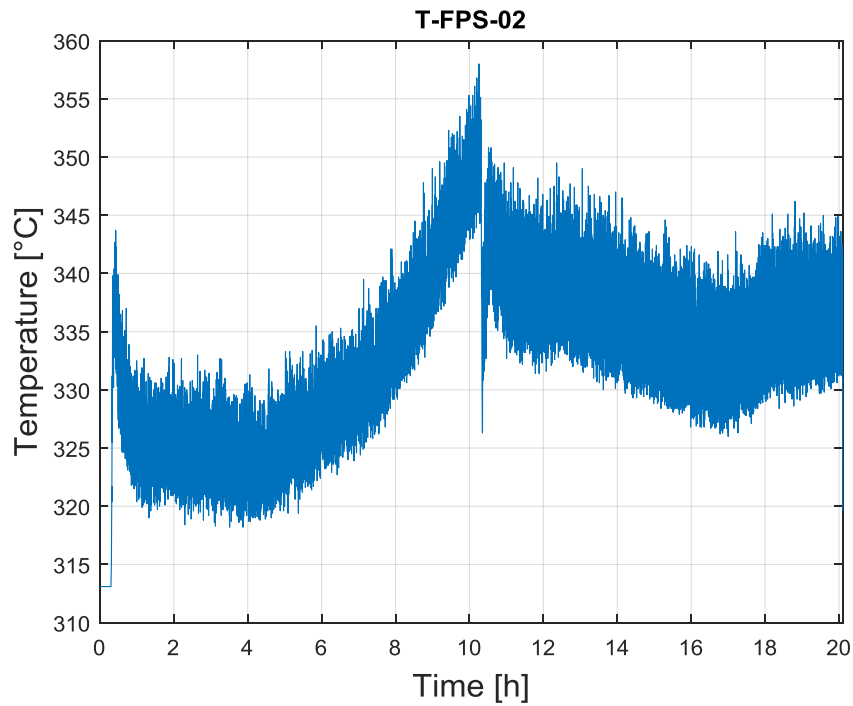


Figure 21: T-FPS-02 LBE temperature

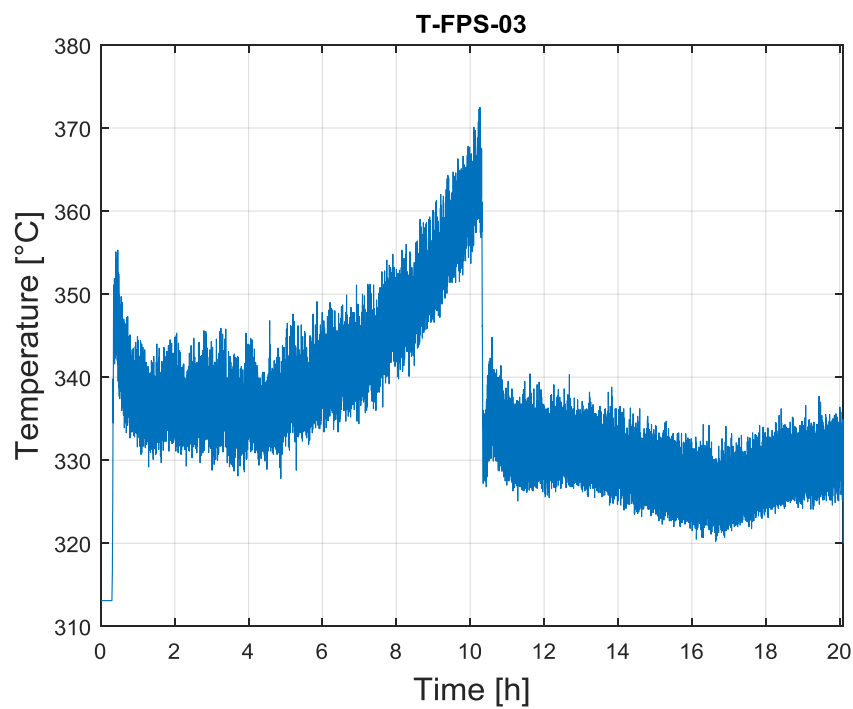


Figure 22: T-FPS-03 LBE temperature

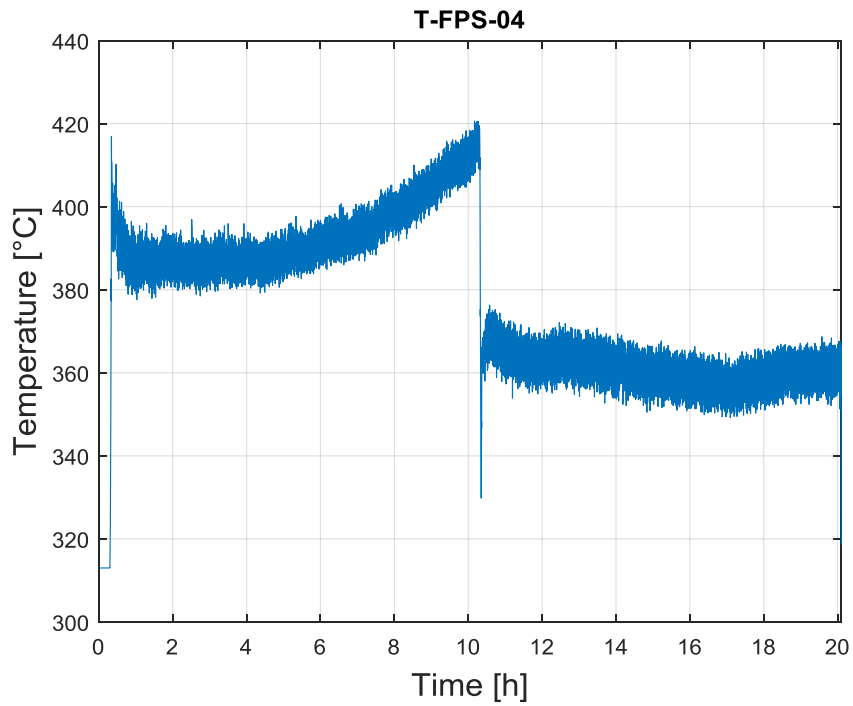


Figure 23: T-FPS-04 LBE temperature

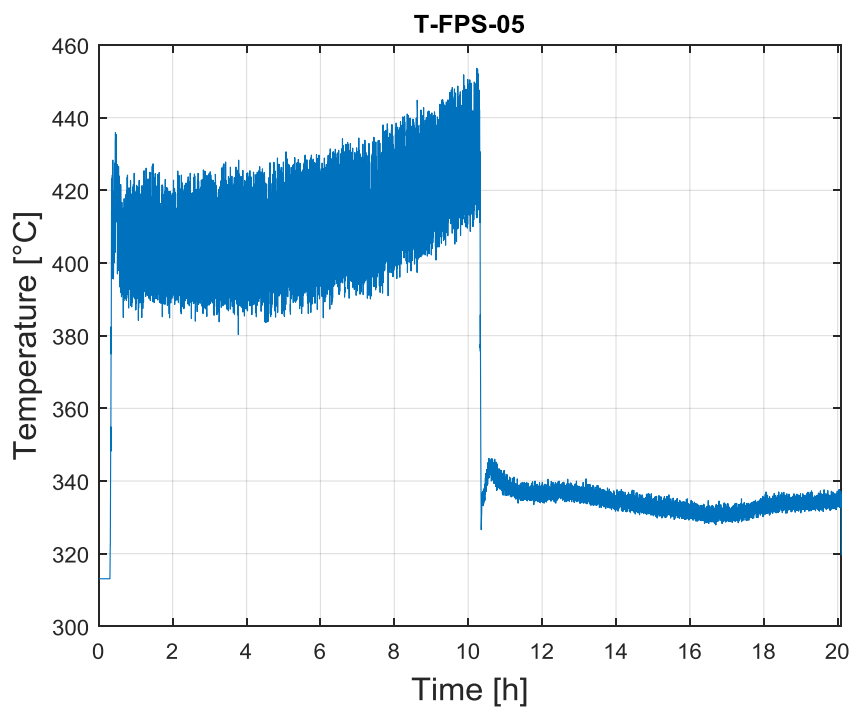


Figure 24: T-FPS-05 LBE temperature

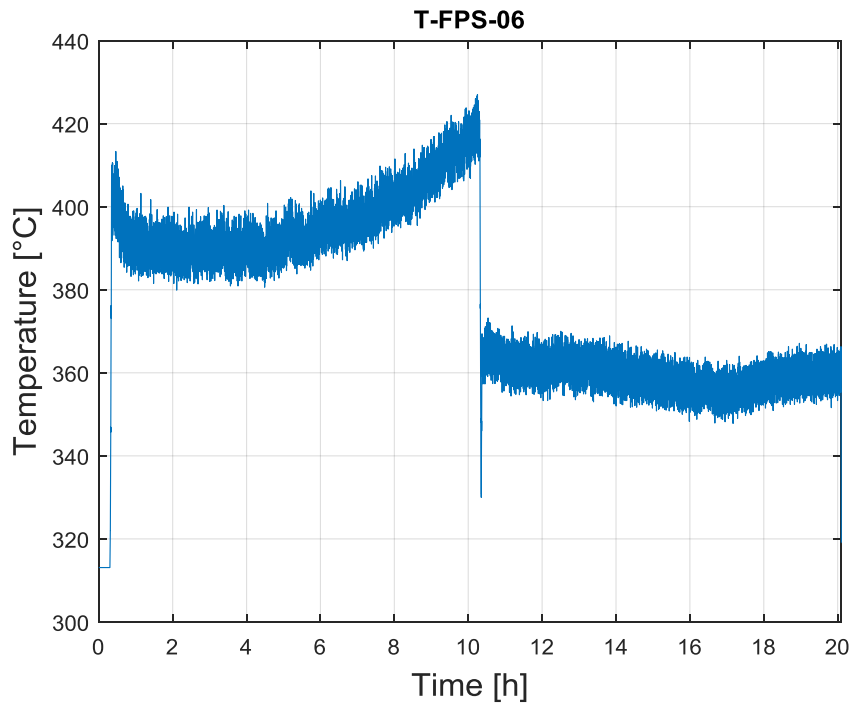


Figure 25: T-FPS-06 LBE temperature

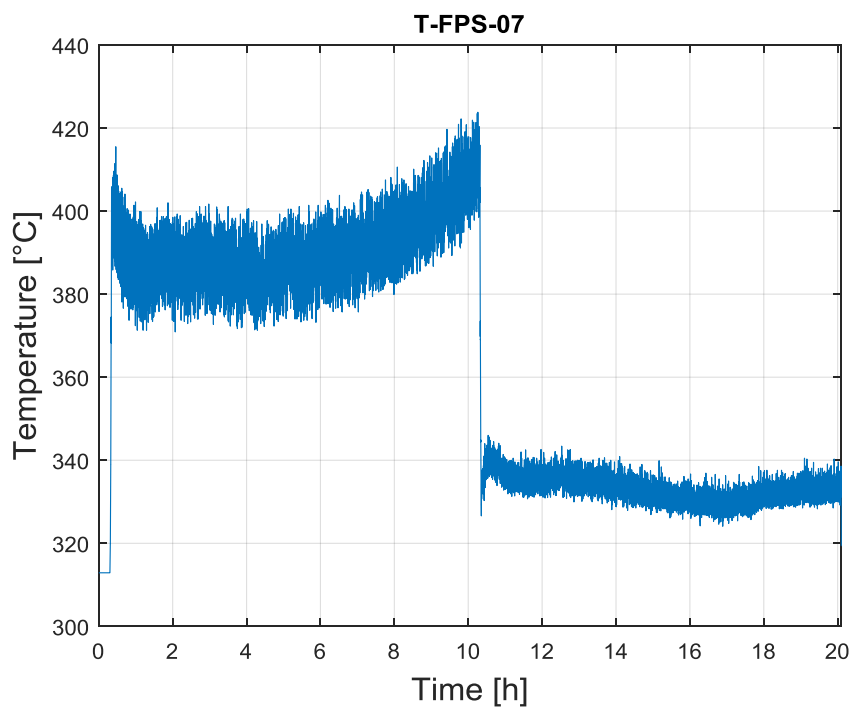


Figure 26: T-FPS-07 LBE temperature

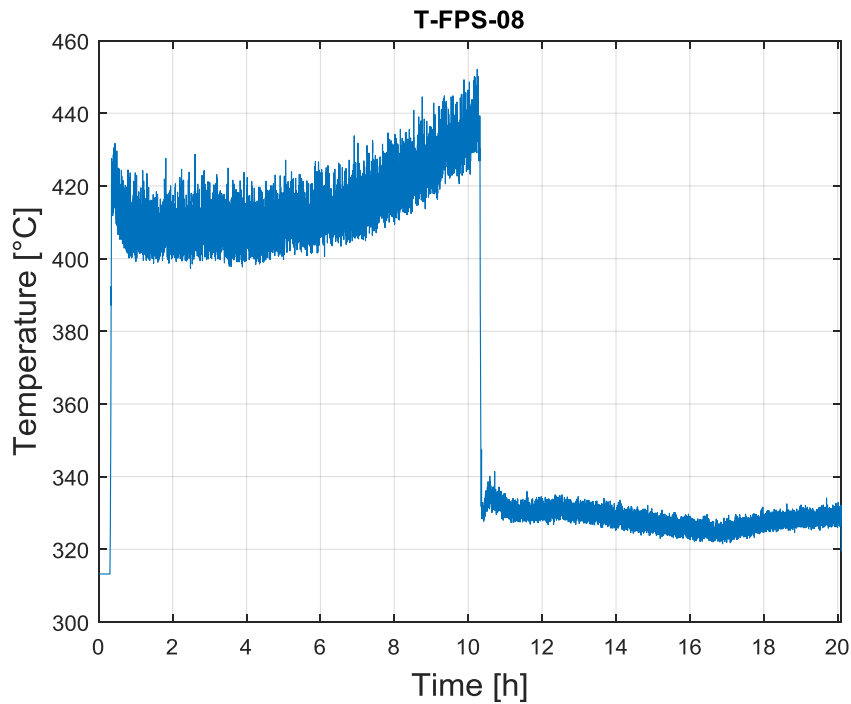


Figure 27: T-FPS-08 LBE temperature

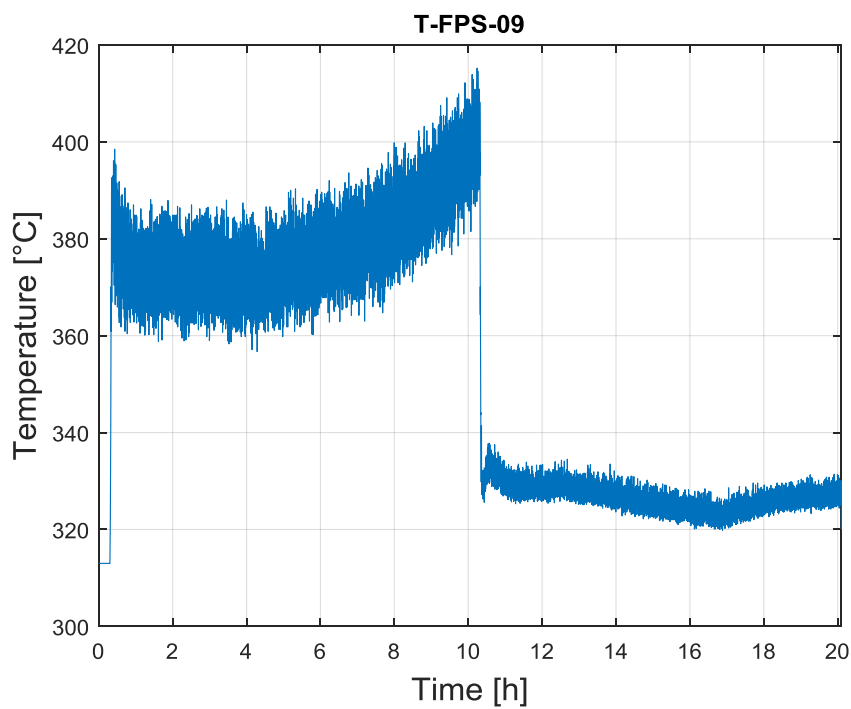


Figure 28: T-FPS-09 LBE temperature

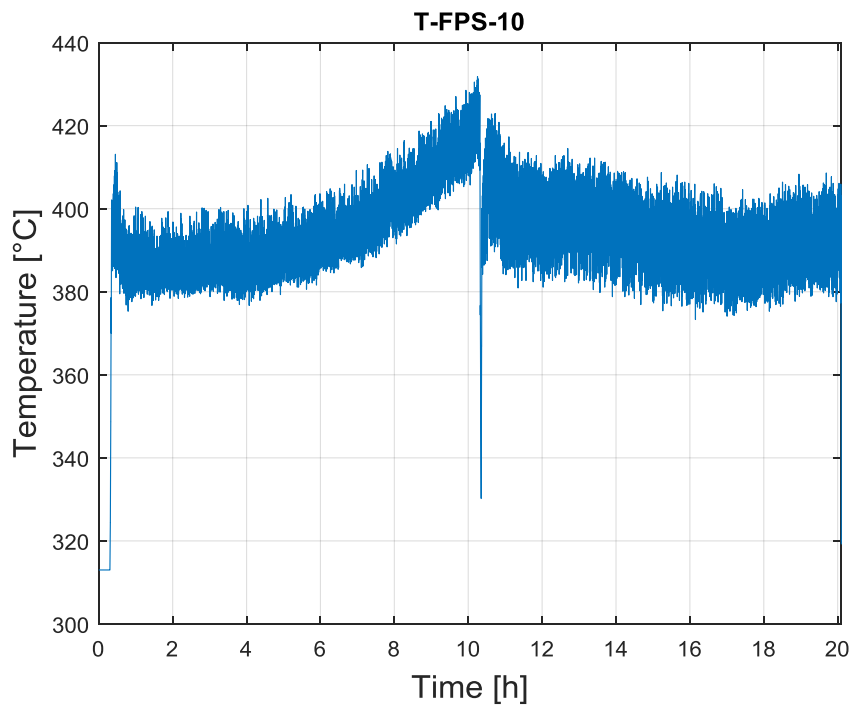


Figure 29: T-FPS-10 LBE temperature

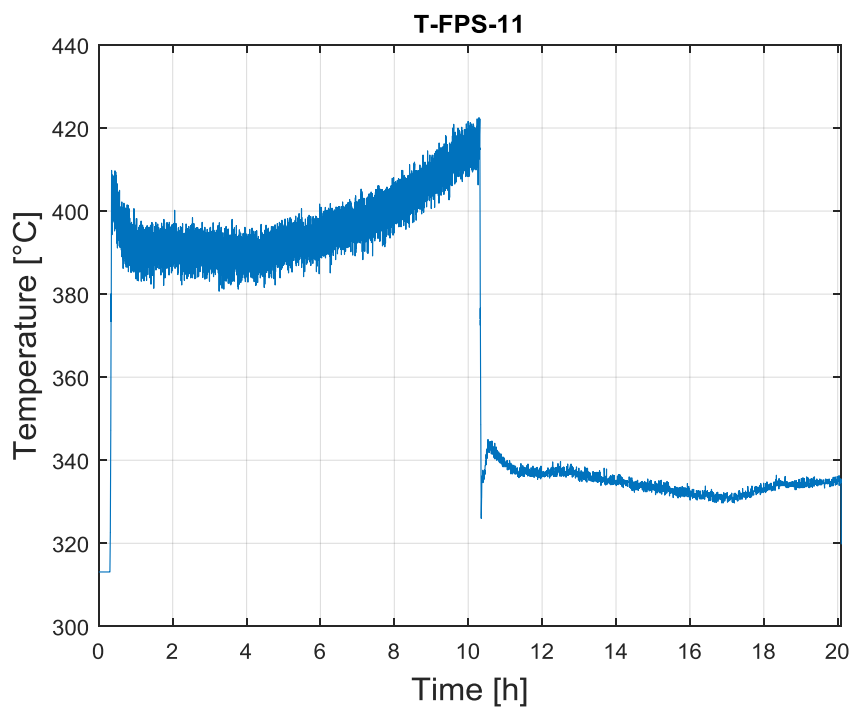


Figure 30: T-FPS-11 LBE temperature

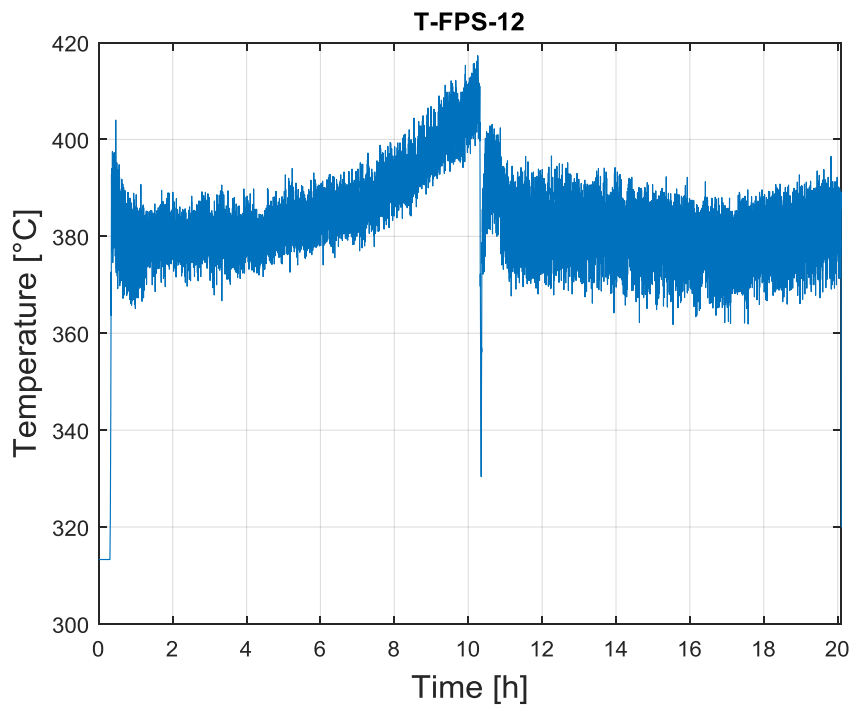


Figure 31: T-FPS-12 LBE temperature

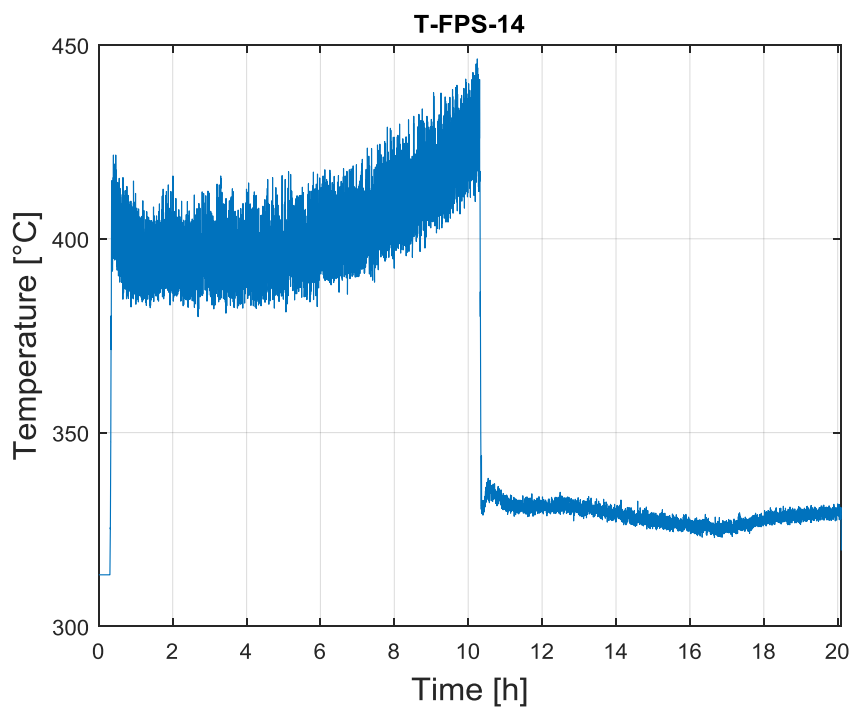


Figure 32: T-FPS-14 LBE temperature

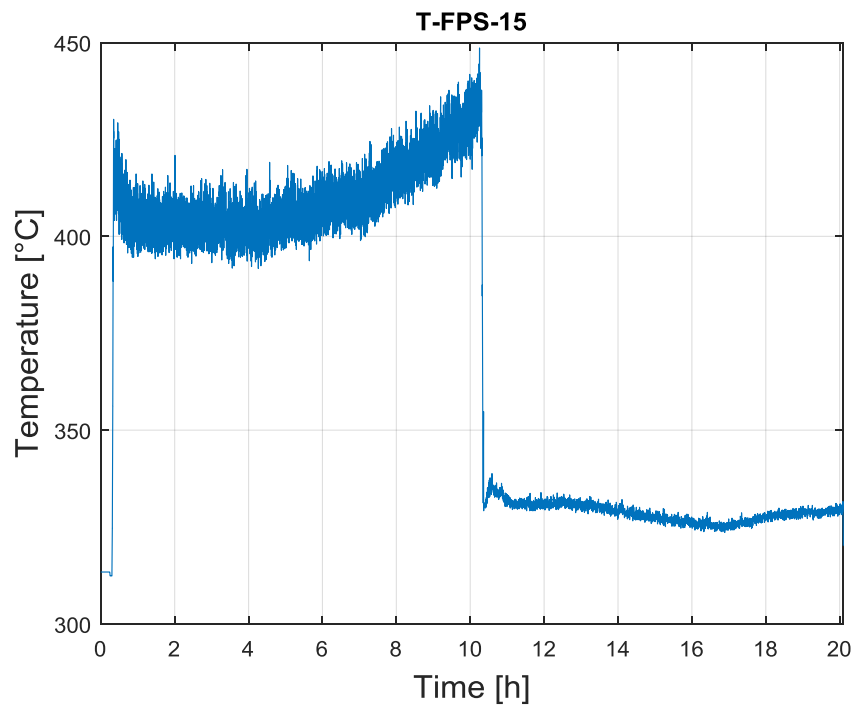


Figure 33: T-FPS-15 LBE temperature

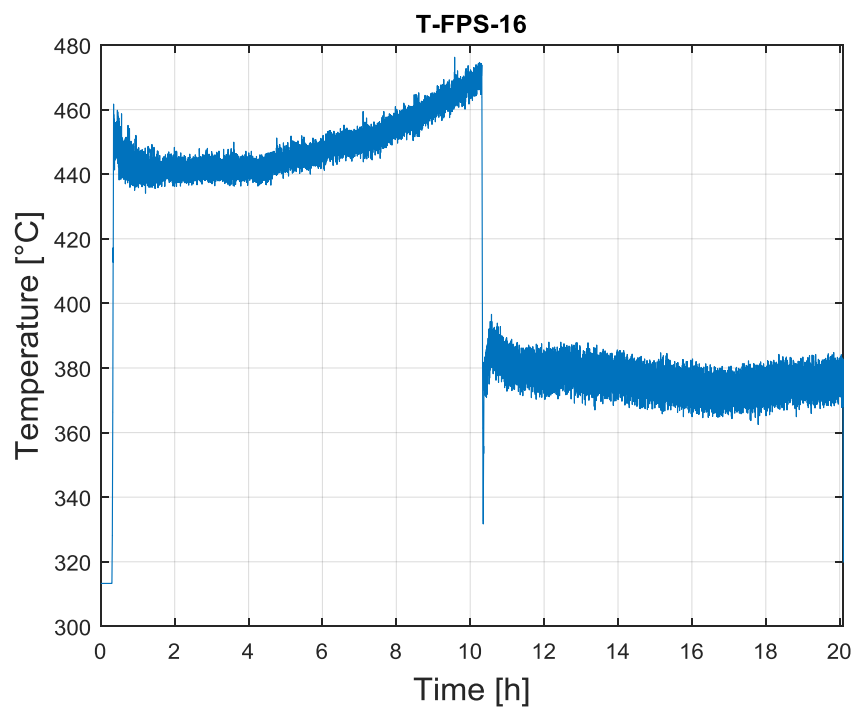


Figure 34: T-FPS-16 LBE temperature

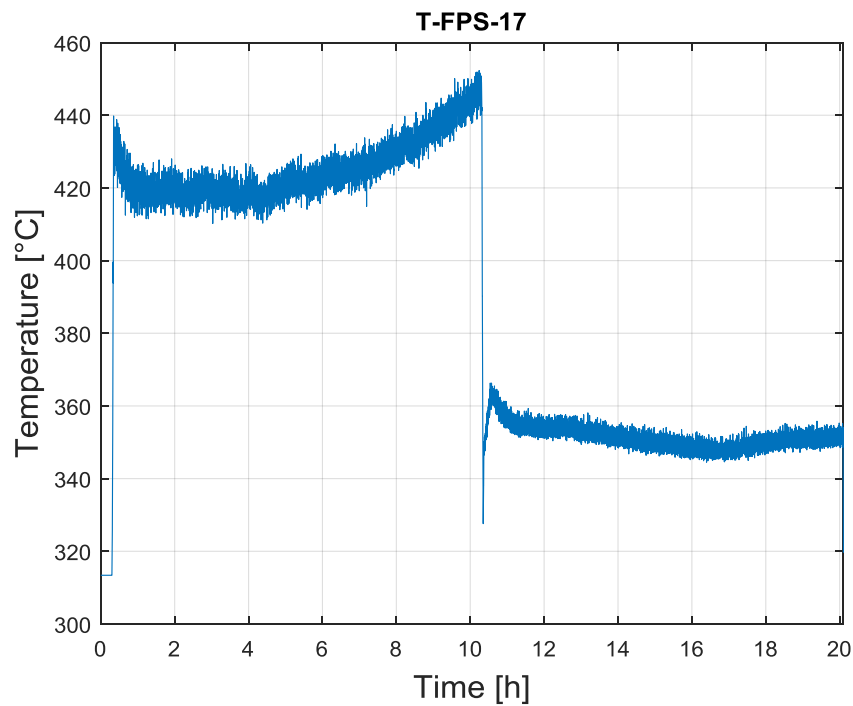


Figure 35: T-FPS-17 LBE temperature

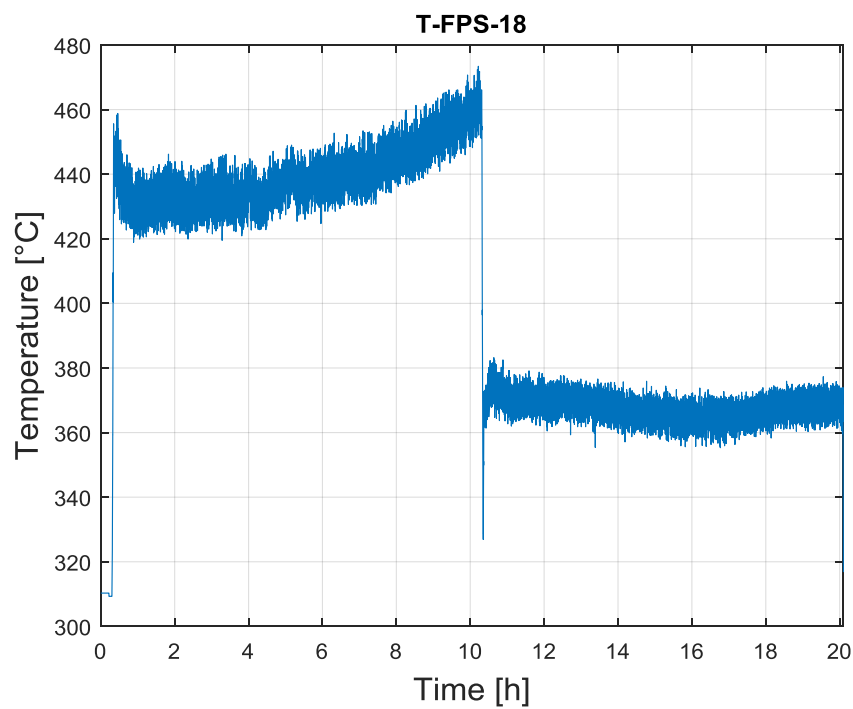


Figure 36: T-FPS-18 LBE temperature

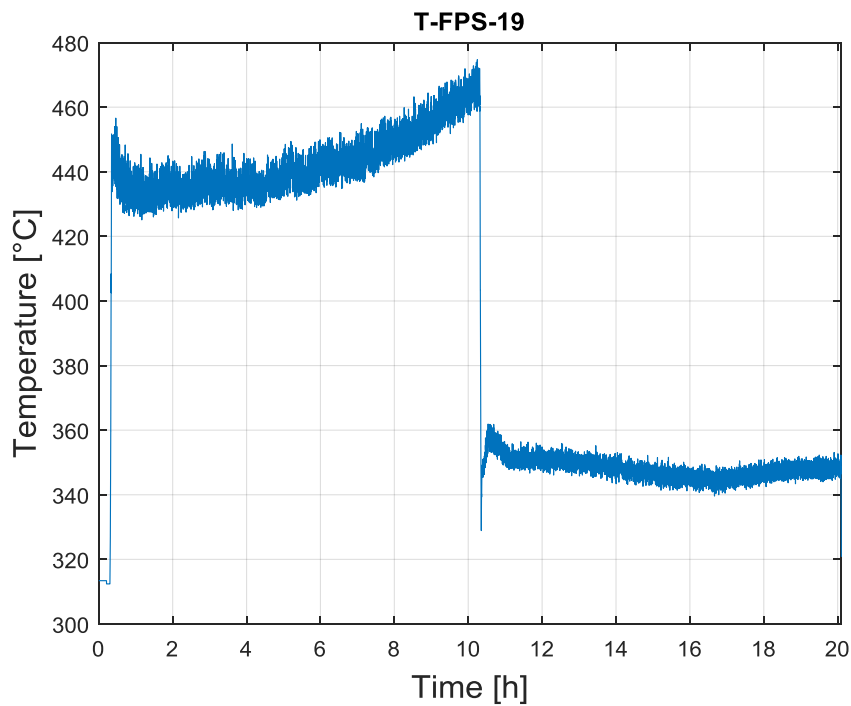


Figure 37: T-FPS-19 LBE temperature

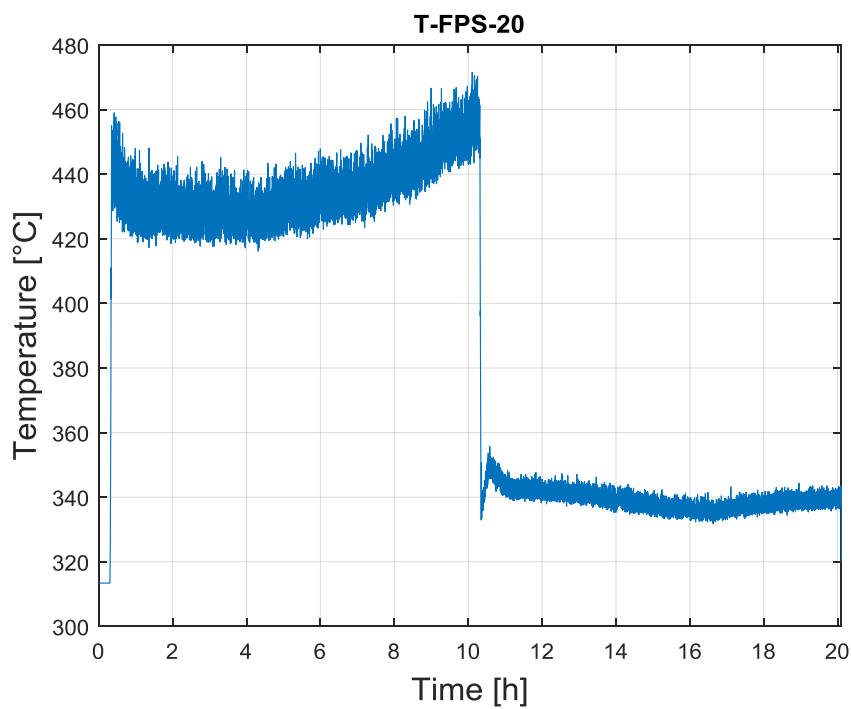


Figure 38: T-FPS-20 LBE temperature

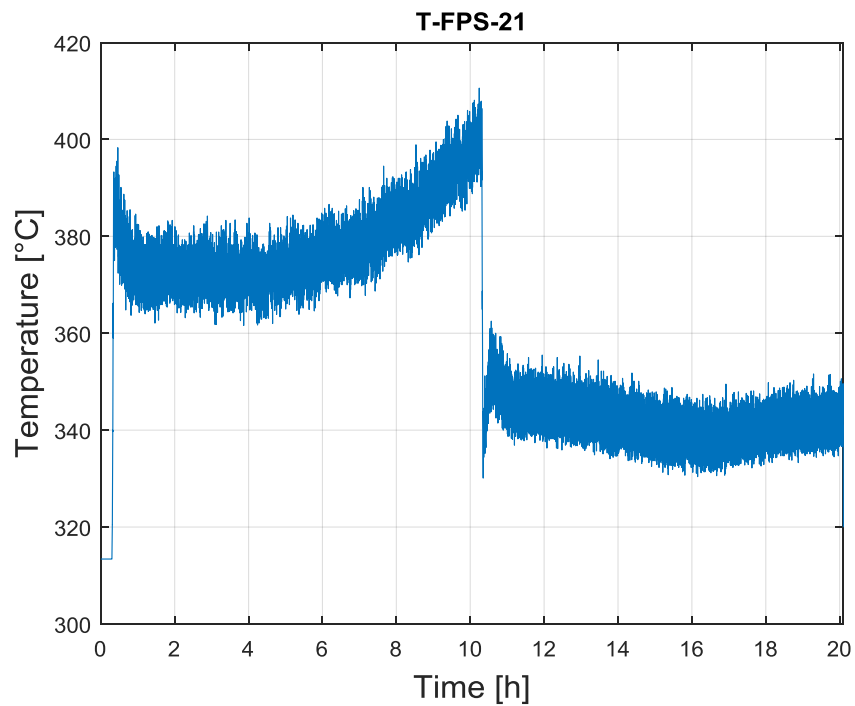


Figure 39: T-FPS-21 LBE temperature

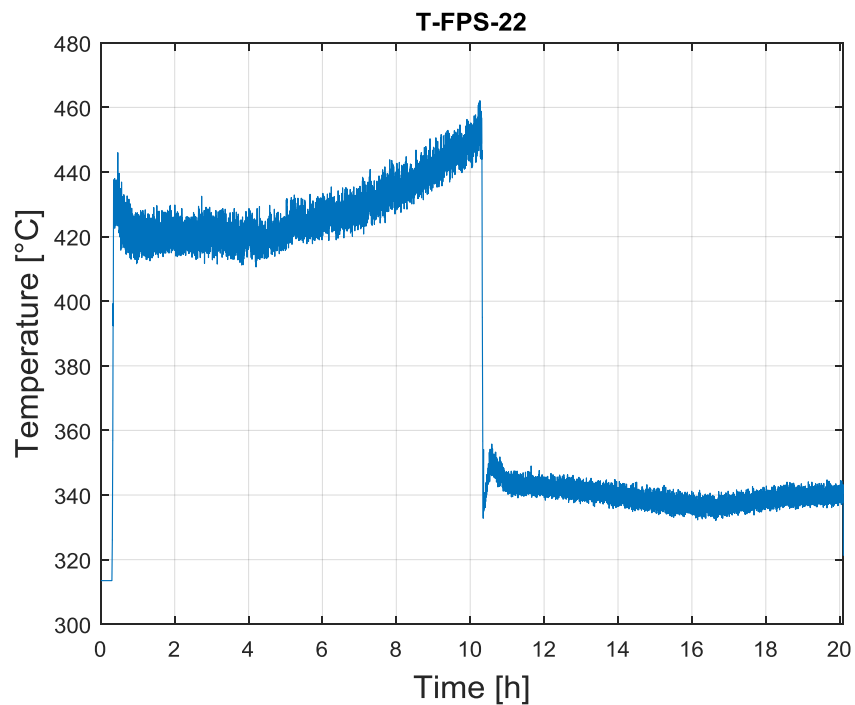


Figure 40: T-FPS-22 LBE temperature

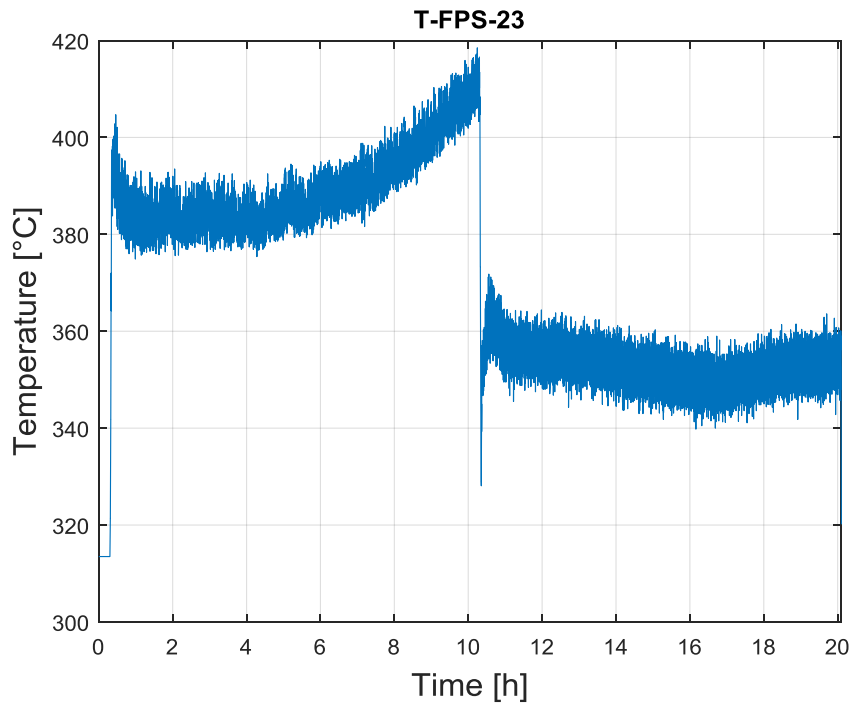


Figure 41: T-FPS-23 LBE temperature

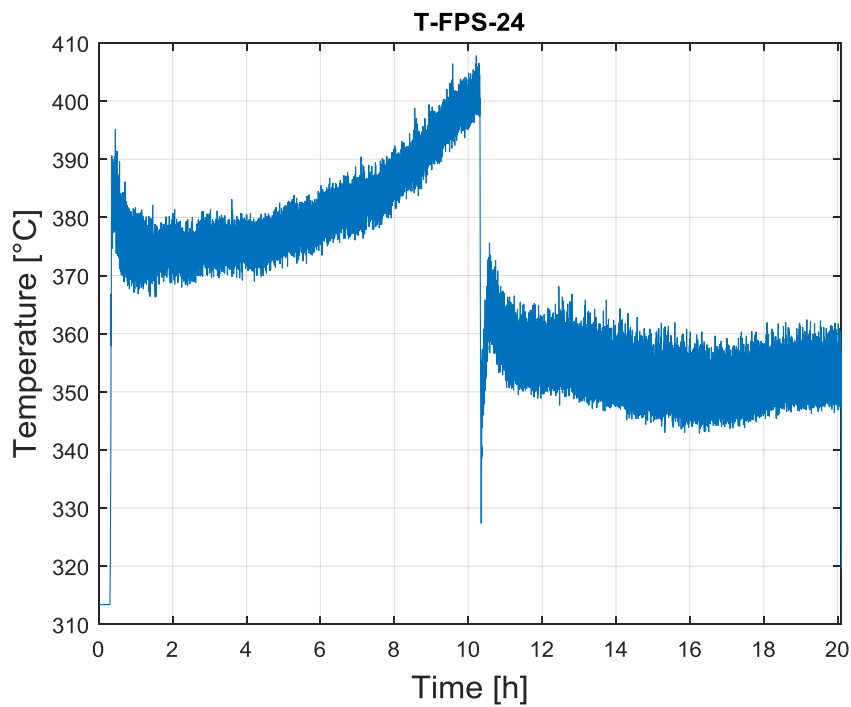


Figure 42: T-FPS-24 LBE temperature

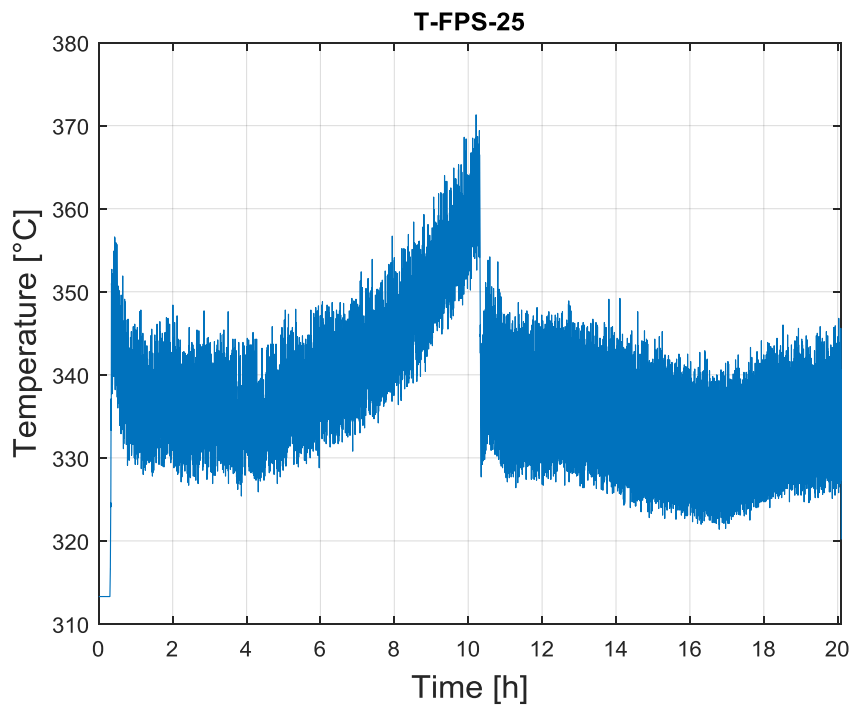


Figure 43: T-FPS-25 LBE temperature

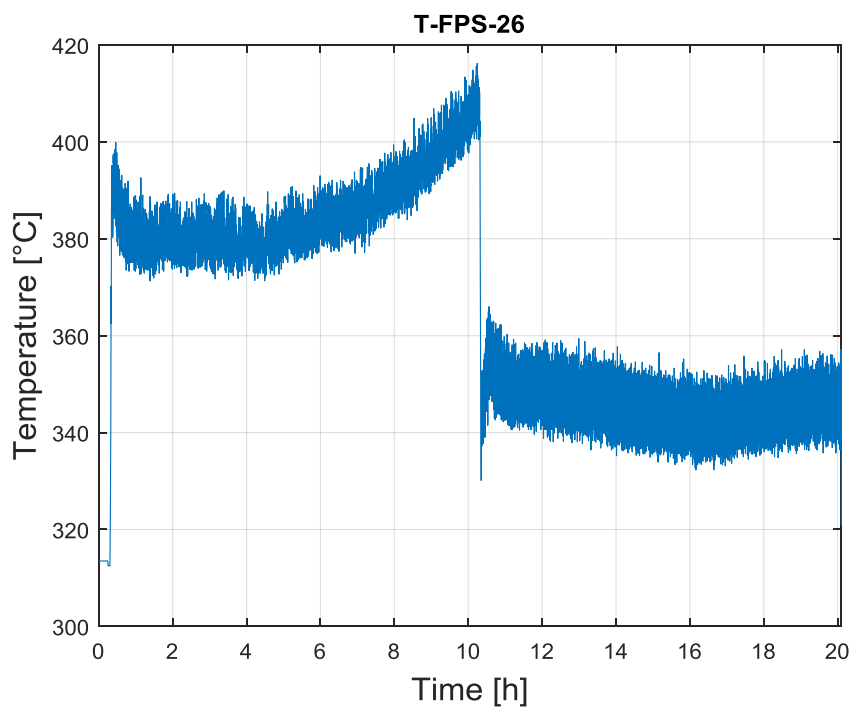


Figure 44: T-FPS-26 LBE temperature

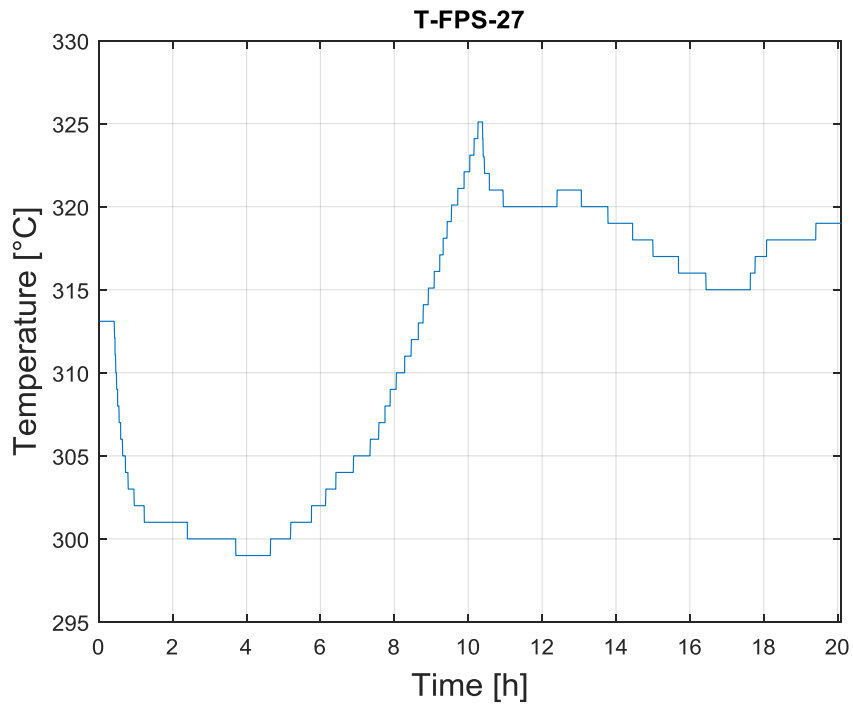


Figure 45: T-FPS-27 LBE temperature

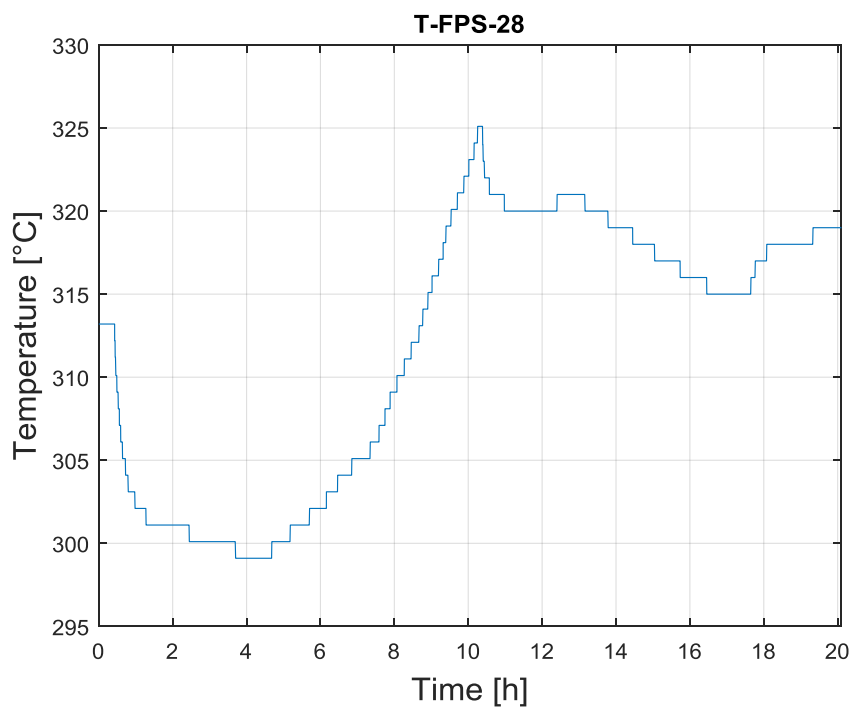


Figure 46: T-FPS-28 LBE temperature

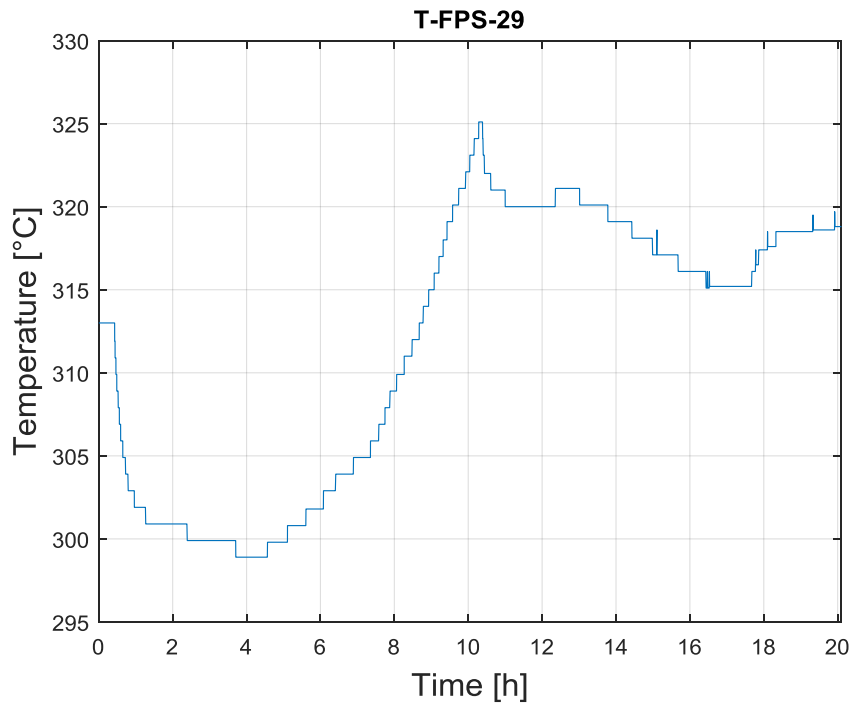


Figure 47: T-FPS-29 LBE temperature

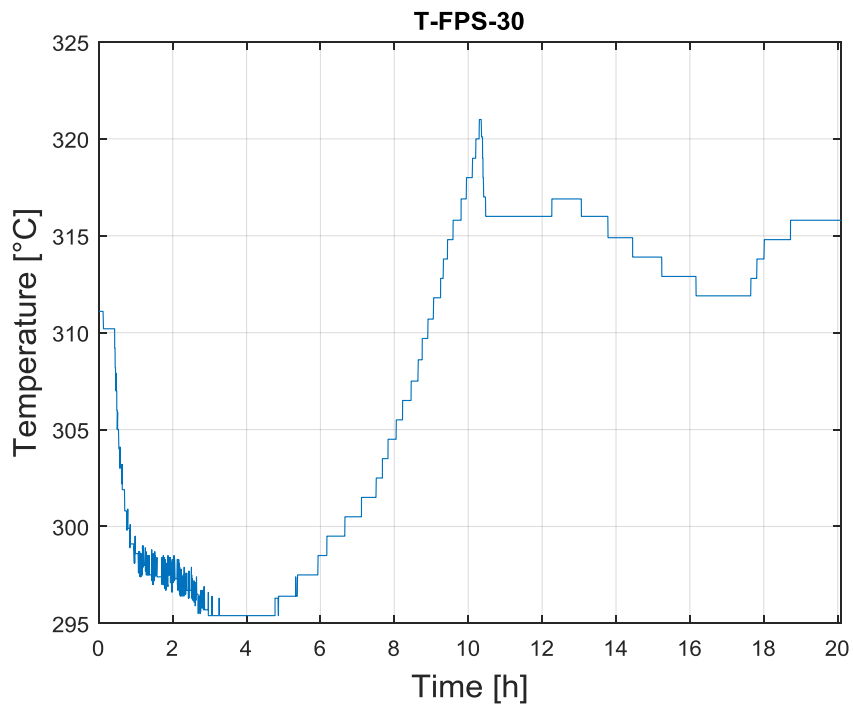



Figure 48: T-FPS-30 LBE temperature

 DIVISIONE INGEGNERIA SPERIMENTALE	<u>Title</u> D3.2: CIRCE experiments: pre-test, data-set and analysis	<u>Distribution</u> PUBLIC	<u>Emission</u> 09/08/2017	<u>Pag.</u> 36 di 234
		<u>Ref.</u> CI-T-R-292	Rev. 0	

The LBE heated by the FPS flows through the fitting volume into the riser (see Annex A Fig. 3 0016 Instrumentation.pdf); here temperatures are measured using TCs with a diameter of 3 mm disposed at the entrance section (T-TS-01 to 03) and at the exit section before the separator (T-TS-04 to 06). Average temperatures at inlet and outlet section of the riser are reported in Figure 49

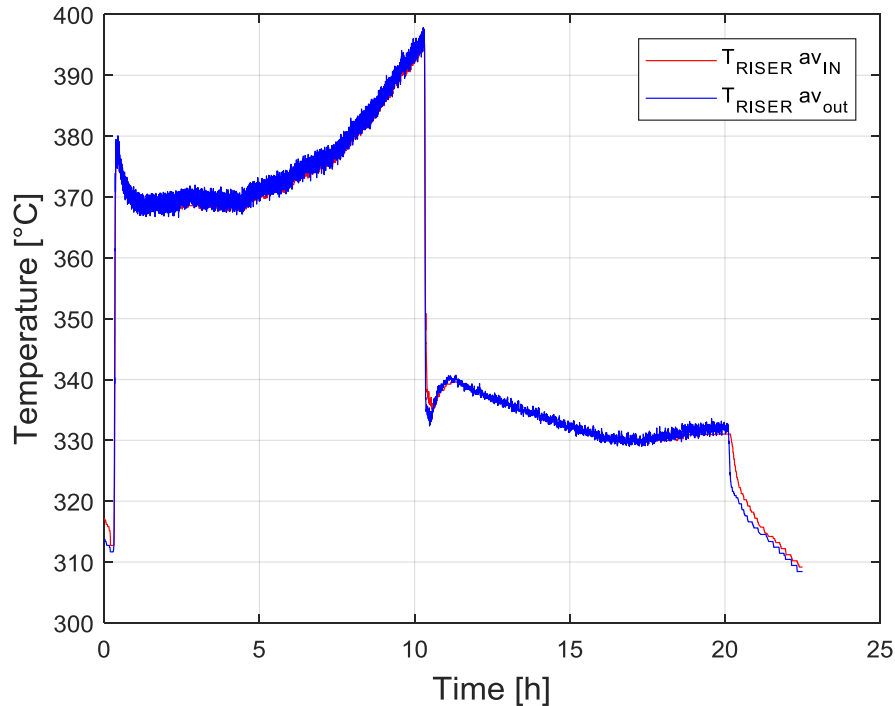



Figure 49: Inlet/Outlet average temperature in the Riser

From the riser exit section, the LBE flows through the Separator into the HX shell, where the temperatures at the entrance section is measured by three TCs placed at 120°, 30 mm from the bottom of the Separator (T-SG-01 ... 03, see Annex A Fig. 4 THINS thermocouples arrangement.pdf).

Sub-channel temperature measurements were taken in a plane placed 30 mm above the lower grid (see Annex A Fig. 10: 0700-Assieme-HX.pdf for the positioning of the grid), according to the scheme shown in Annex A Fig. 11: T-SG-0100-Disposizione TC Sottocanali GV.pdf (T-SG-04 ... 12).

The LBE temperature at the outlet section of the HX is measured by six thermocouples (T-SG-13 ... 18) placed at 60° each and at 100 mm before the HX skirt exit (see Annex A Fig. 12: T-SG-0101-Disposizione TC Uscita GV.pdf). In Figure 50 the LBE temperature averaged at the inlet and outlet sections of the HX is reported.

 DIVISIONE INGEGNERIA SPERIMENTALE	<u>Title</u> D3.2: CIRCE experiments: pre-test, data-set and analysis	<u>Distribution</u> PUBLIC	<u>Emission</u> 09/08/2017	<u>Pag.</u> 37 di 234
		<u>Ref.</u> CI-T-R-292	Rev. 0	

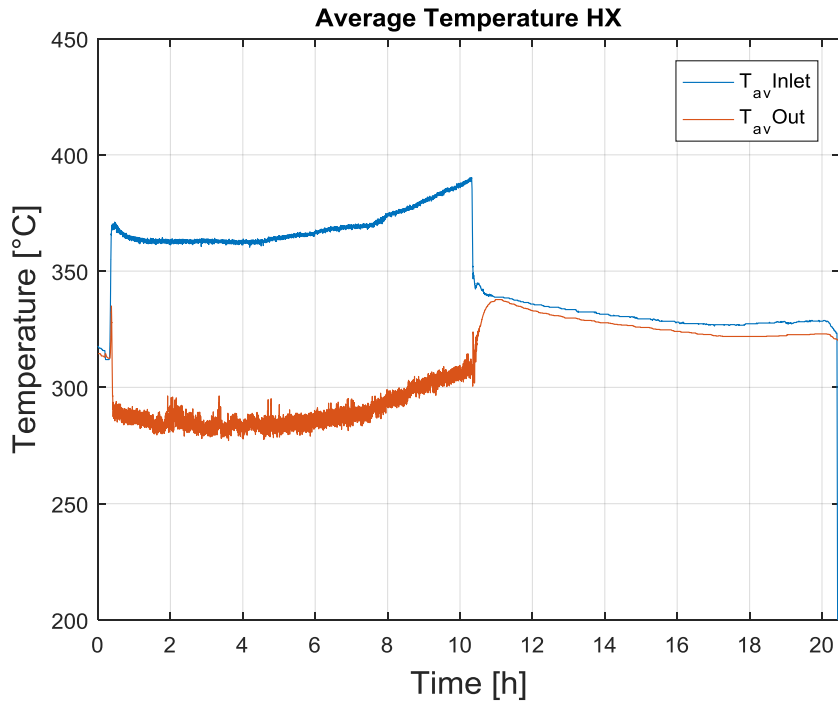


Figure 50: Inlet/Outlet average LBE temperature in the main HX

From Figure 51 to Figure 59, temperatures measured from each single thermocouple in the HX subchannels are reported.

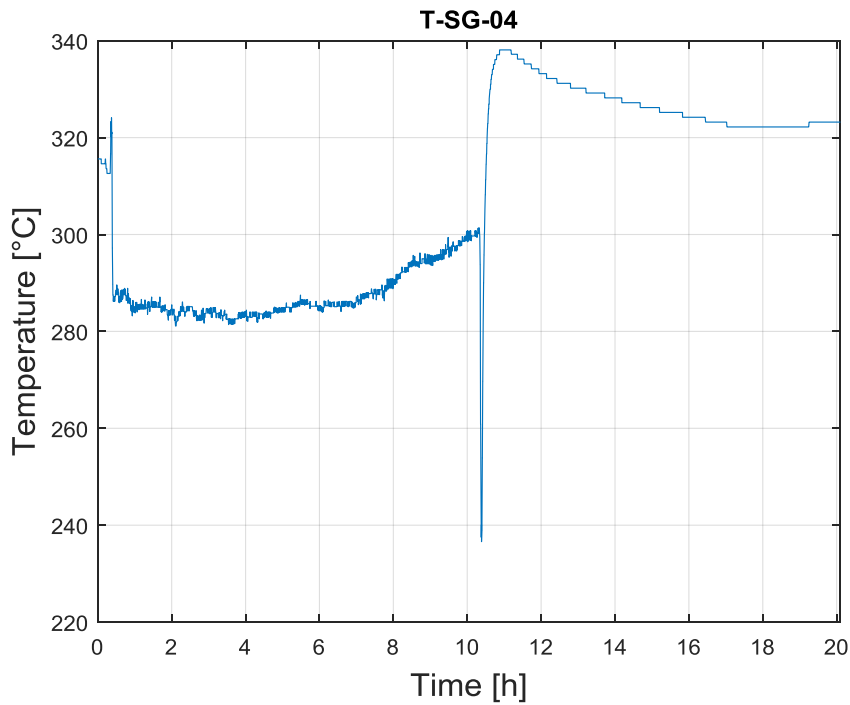


Figure 51: LBE temperature in the sub channel of the HX (T-SG-04)

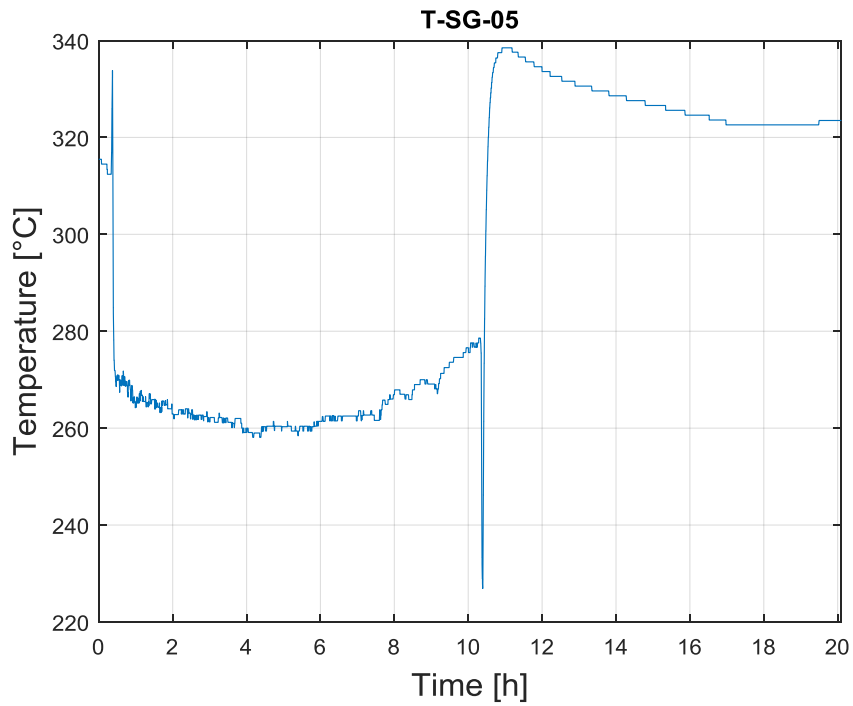


Figure 52: LBE temperature in the sub channel of the HX (T-SG-05)

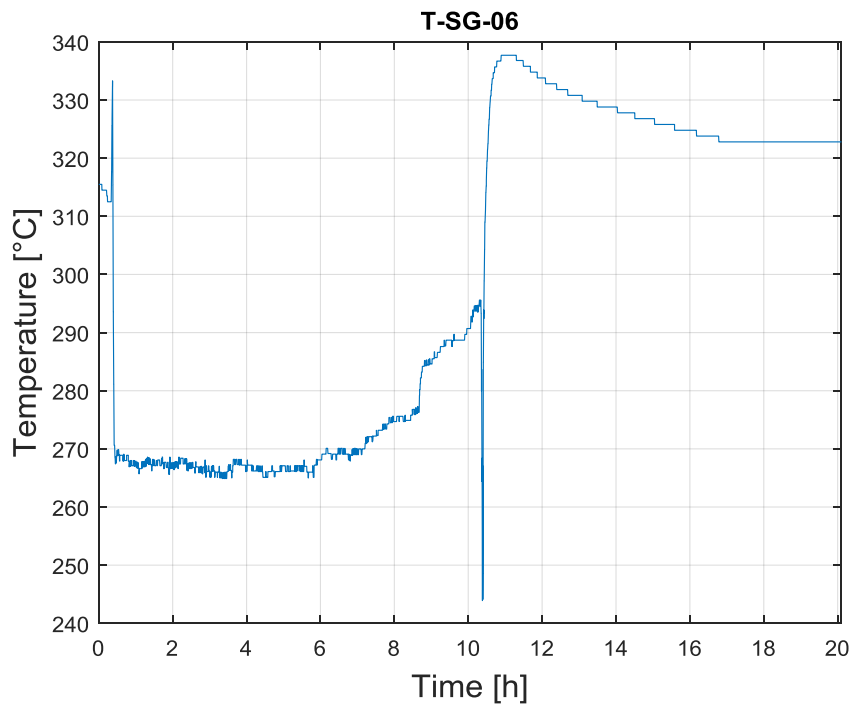


Figure 53: LBE temperature in the sub channel of the HX (T-SG-06)

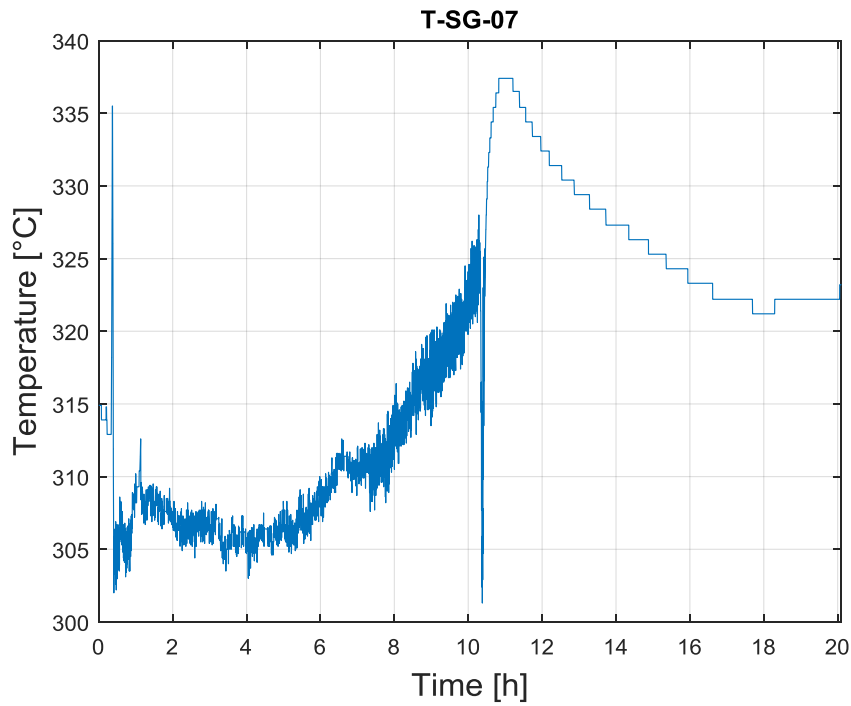


Figure 54: LBE temperature in the sub channel of the HX (T-SG-07)

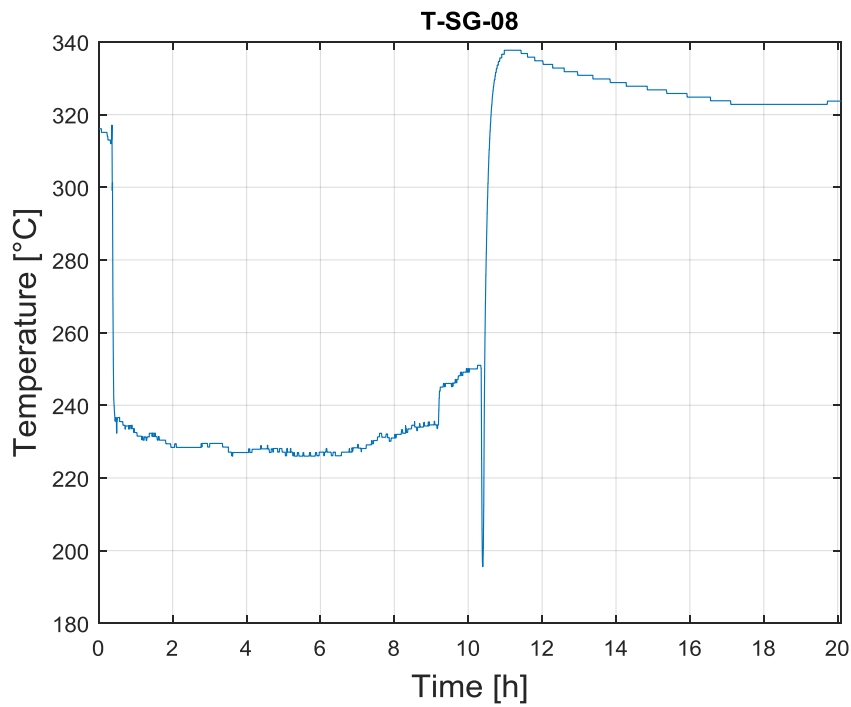


Figure 55: LBE temperature in the sub channel of the HX (T-SG-08)

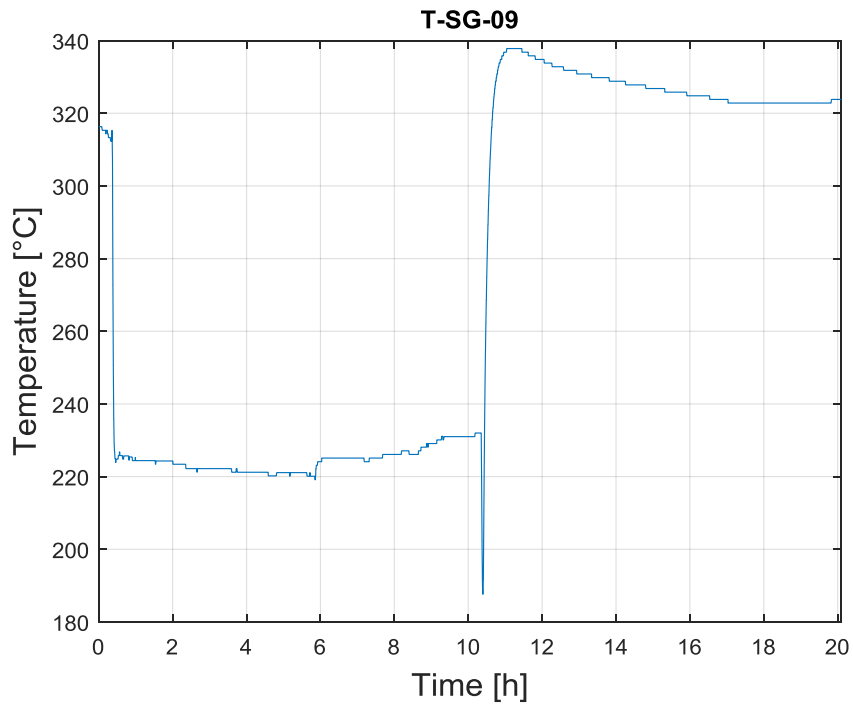


Figure 56: LBE temperature in the sub channel of the HX (T-SG-09)

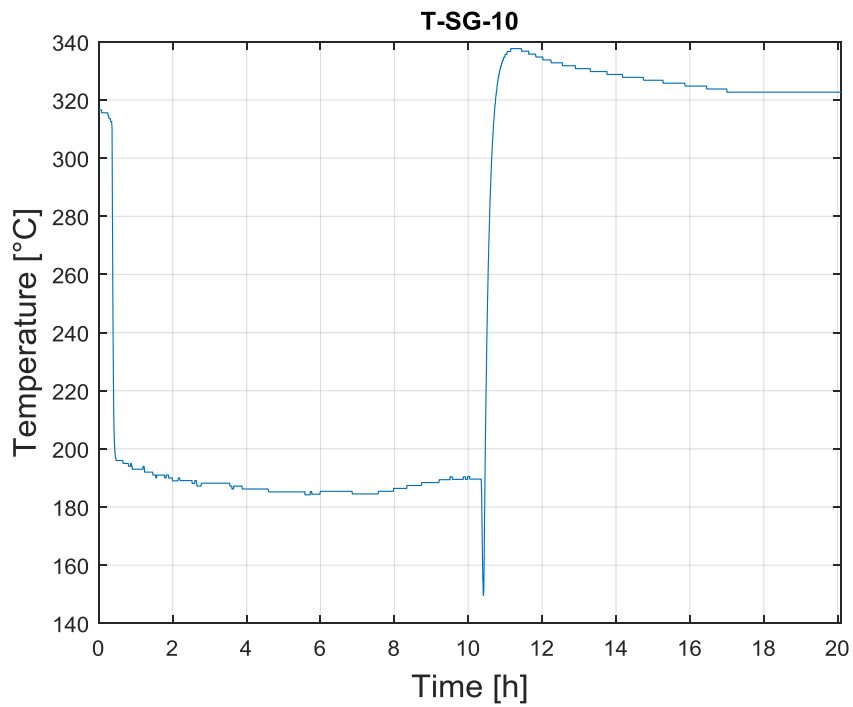


Figure 57: LBE temperature in the sub channel of the HX (T-SG-10)

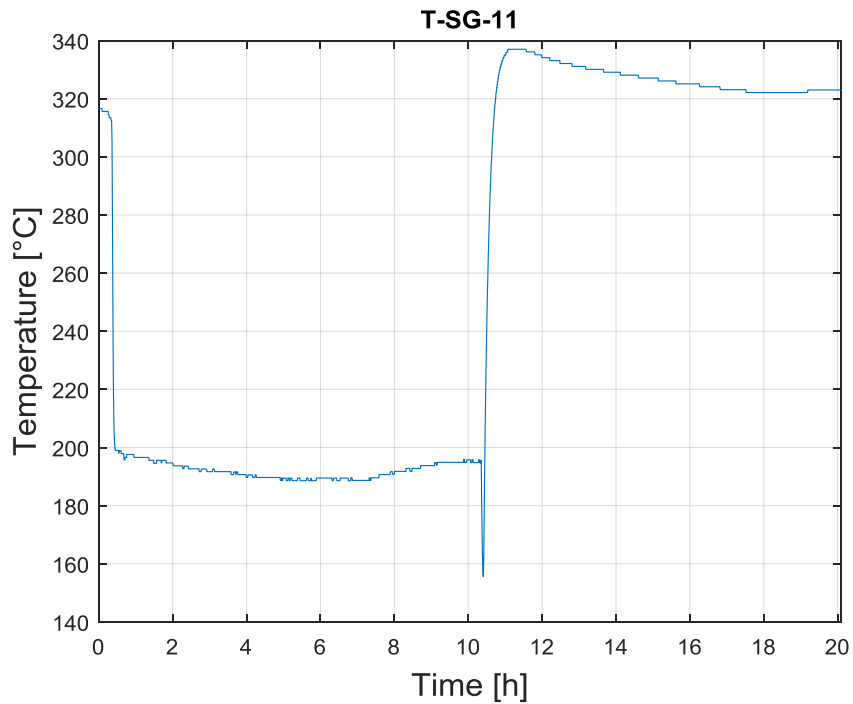


Figure 58: LBE temperature in the sub channel of the HX (T-SG-11)

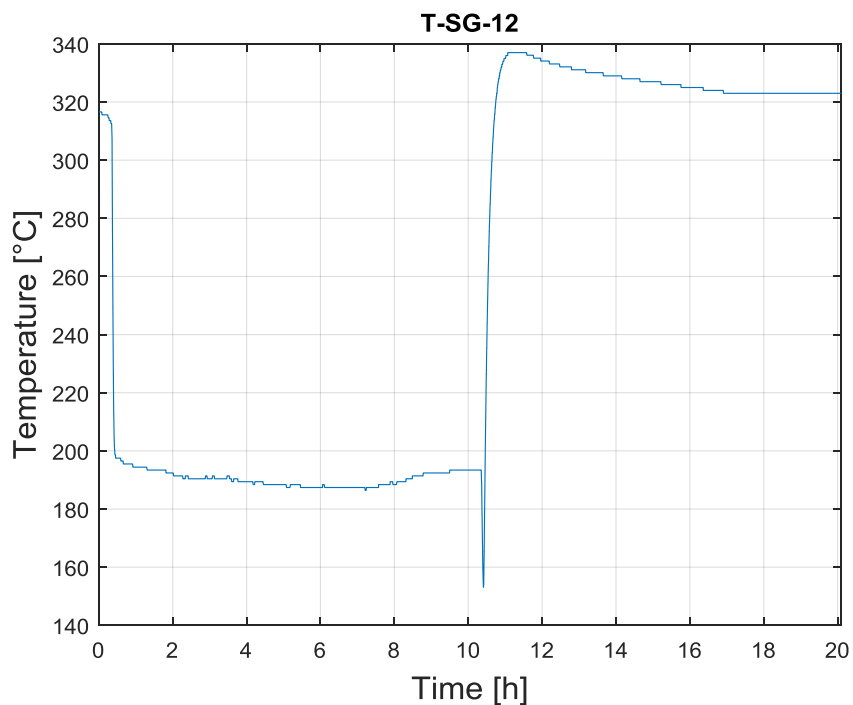



Figure 59: LBE temperature in the sub channel of the HX (T-SG-12)

 DIVISIONE INGEGNERIA SPERIMENTALE	<u>Title</u> D3.2: CIRCE experiments: pre-test, data-set and analysis	<u>Distribution</u> PUBLIC	<u>Emission</u> 09/08/2017	<u>Pag.</u> 42 di 234
		<u>Ref.</u> CI-T-R-292	Rev. 0	

After passing through the HX, the LBE then returned into the pool. Here, thermocouples for the measurements of LBE temperature were maintained in the fixed positions by vertical rods. Thermocouples are fixed at 17 different elevations (see Annex A Fig. 13 T-MS-0101 TC per Mix&Strat.pdf) and 9 different radial positions (see Annex A Fig. 14 T-MS-0100-Posizione TC Mix&Strat su piani di misura.pdf) for a total of 119 TCs with a diameter of 3 mm (T-MS-01 ... 119). In particular, with reference to Annex A Fig. 13 T-MS-0101 TC per Mix&Strat.pdf, TCs on lines *A*, *H*, *I* allow measurement from the bottom side of the test section up to the FPS entrance, while TCs on lines *B*, *C*, *D*, *E*, *F*, *G* allow measurement up to 600 mm below the exit of the DHR.

From Figure 60 to Figure 68 the LBE temperatures in the pool are reported along the vertical lines *A*, *B*, *C*, *D*, *E*, *F*, *G*, *H* and *I* (see Annex A Fig. 14 T-MS-0100-Posizione TC Mix&Strat su piani di misura.pdf)

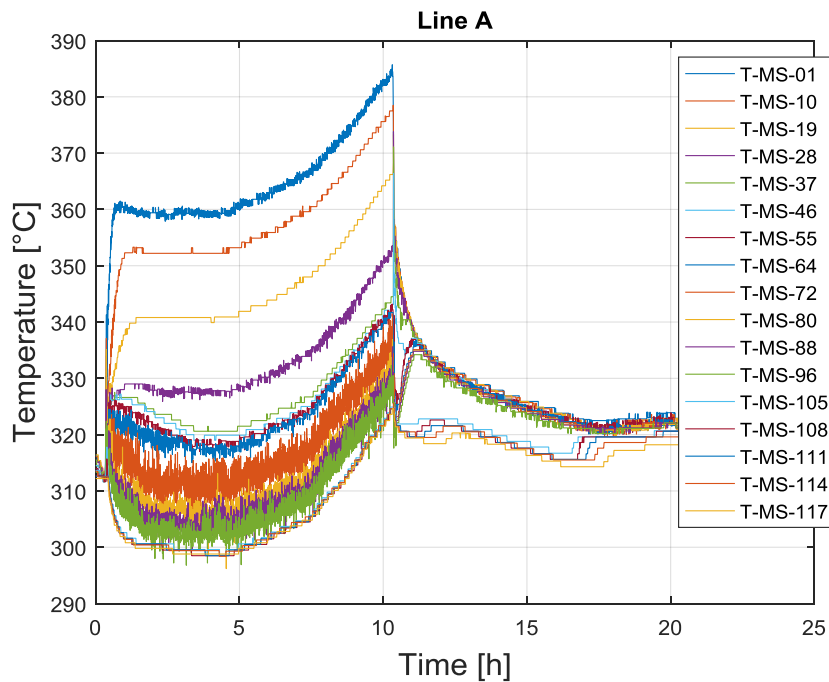


Figure 60: Temperature in the pool along Line A

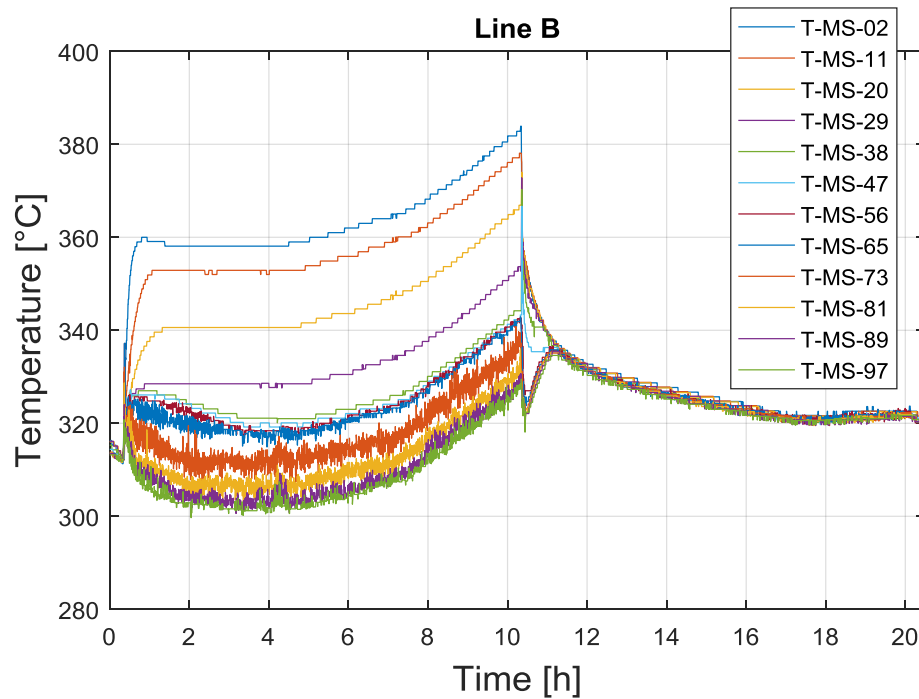


Figure 61: Temperature in the pool along Line B

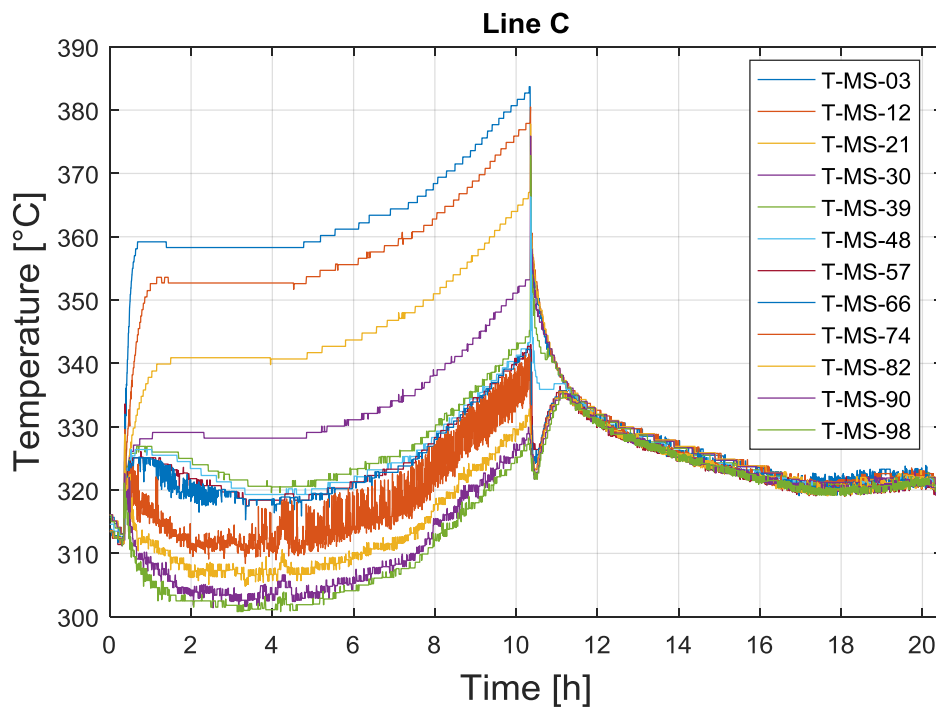


Figure 62: Temperature in the pool along Line C

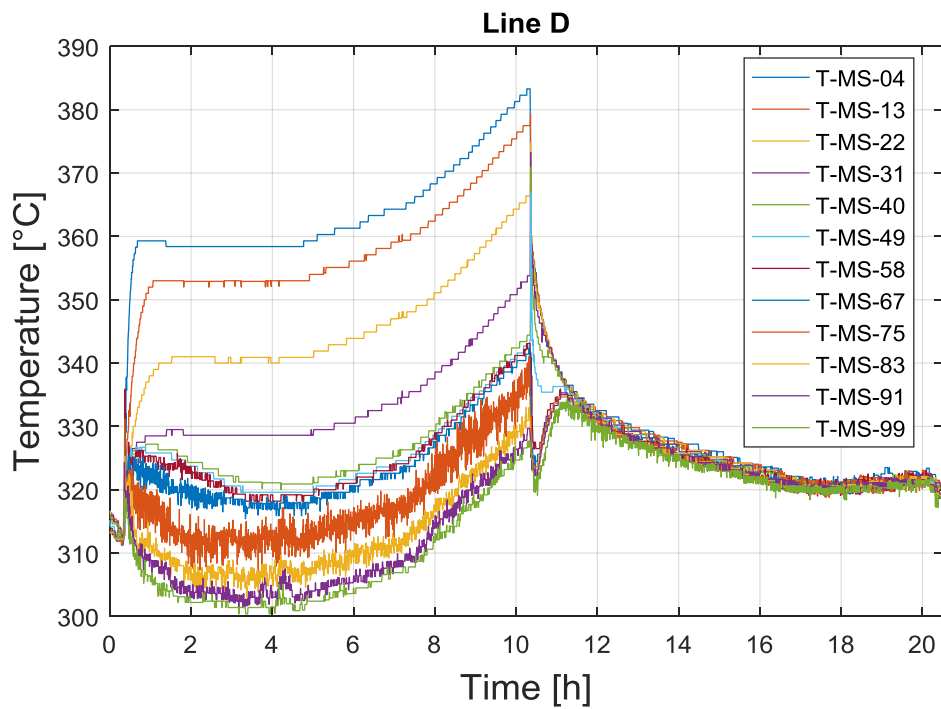


Figure 63: Temperature in the pool along Line D

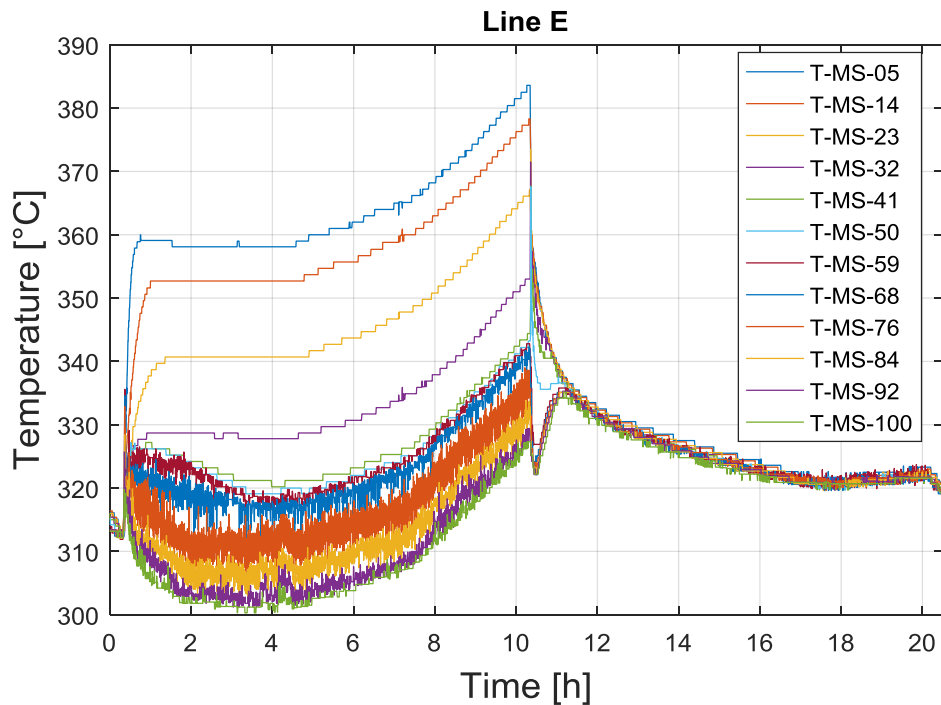


Figure 64: Temperature in the pool along Line E

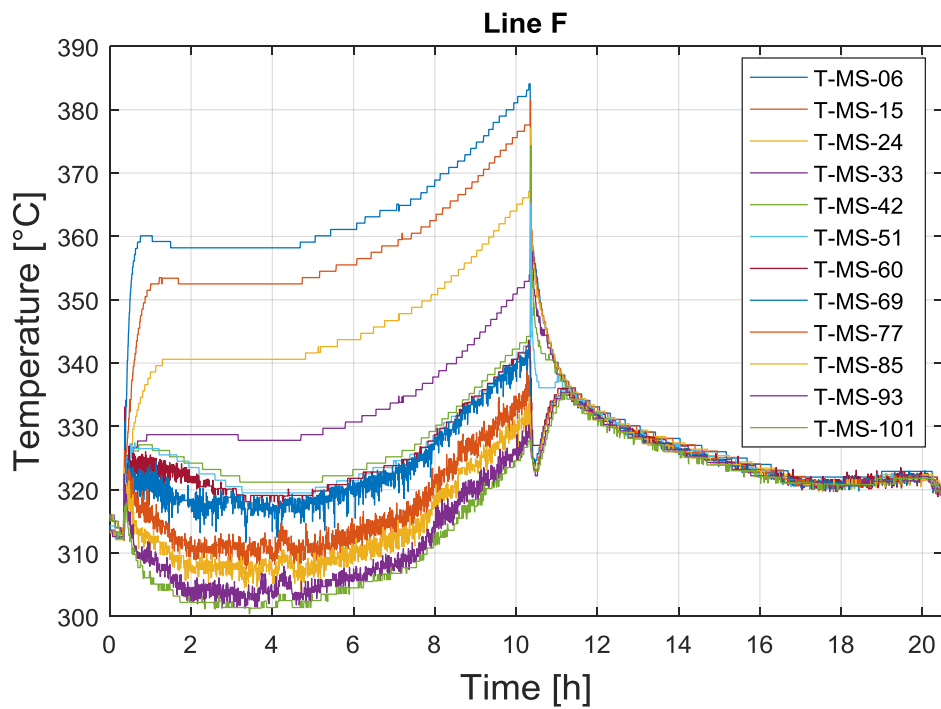


Figure 65: Temperature in the pool along Line F

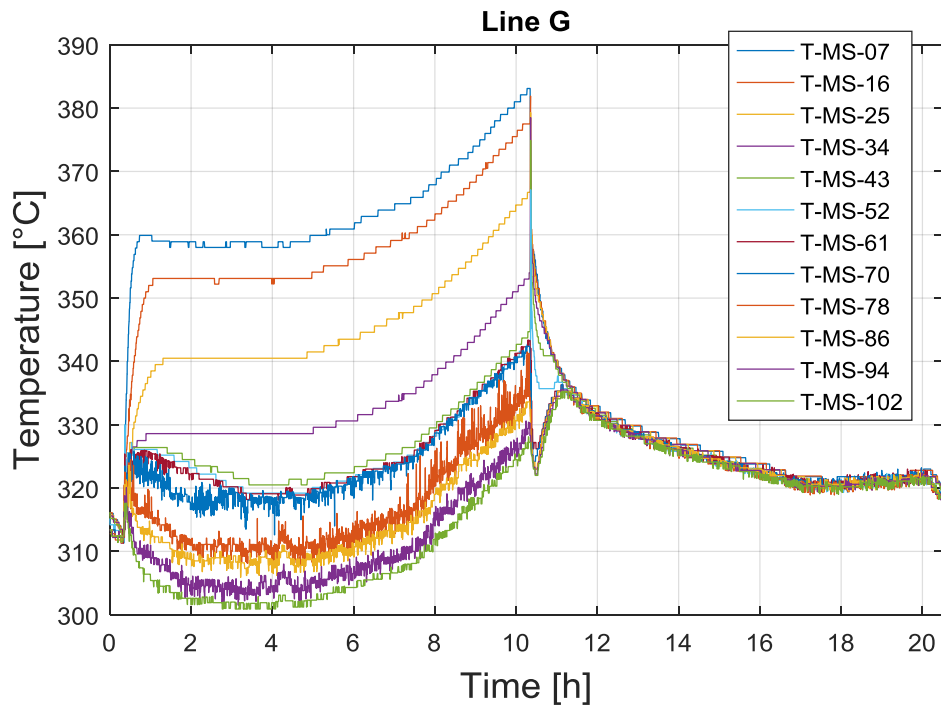


Figure 66: Temperature in the pool along Line G

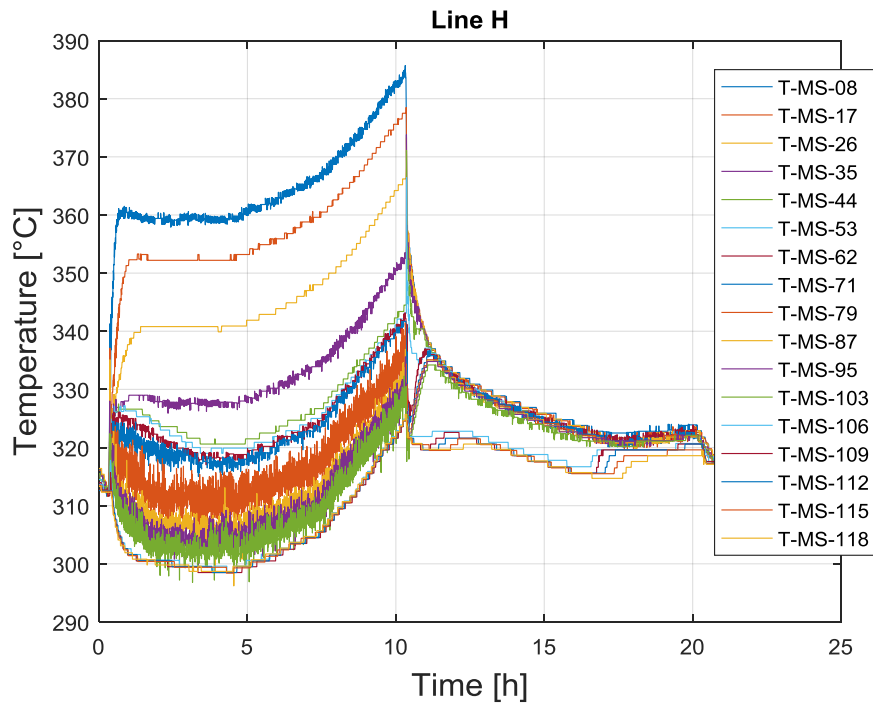


Figure 67: Temperature in the pool along Line H

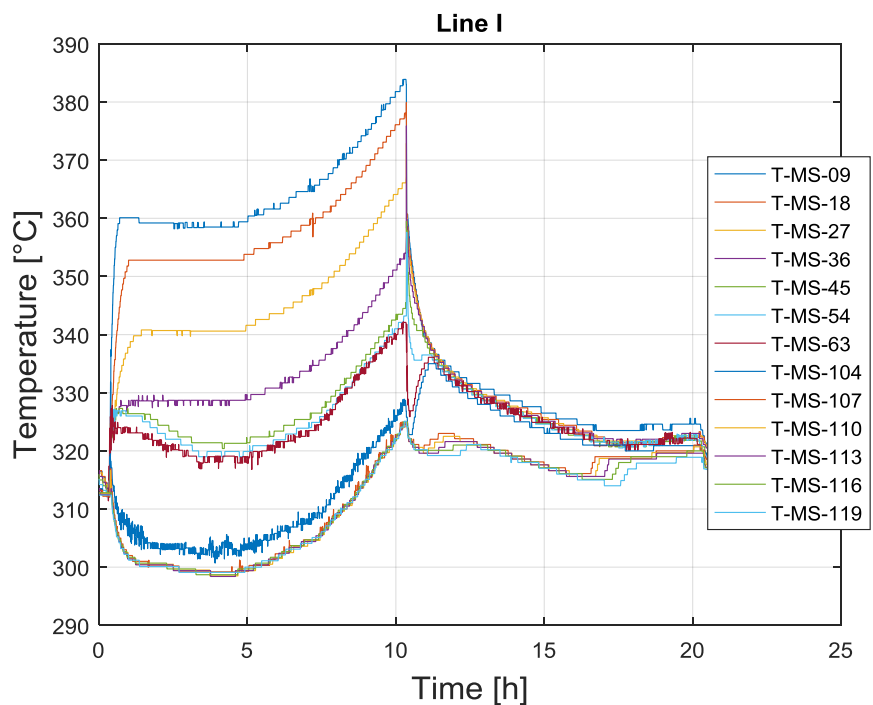



Figure 68: Temperature in the pool along Line I

 DIVISIONE INGEGNERIA SPERIMENTALE	<u>Title</u> D3.2: CIRCE experiments: pre-test, data-set and analysis	<u>Distribution</u> PUBLIC	<u>Emission</u> 09/08/2017	<u>Pag.</u> 47 di 234
		<u>Ref.</u> CI-T-R-292	Rev. 0	

3.2 Test 2

Test 2 is characterized by a nominal power ramp from 0 to 600 kW. The ramp starts at $t= 864$ s and stops at about 1008 s, the mean value of the power during the full power transient is about 600.3 kW with a standard deviation of 1.4 kW. The “full power” transient stops at $t= 8118$ s with a descending ramp up to about 30 kW ($t\sim 8890$ s). The end of the low power run is at $t=22190$ s (~ 6 h). The mean value of the power after the simulation of the core scram is 30.7 kW with a standard deviation of 0.2 kW. The electric power (DC-KW) time trend is reported in Figure 69.

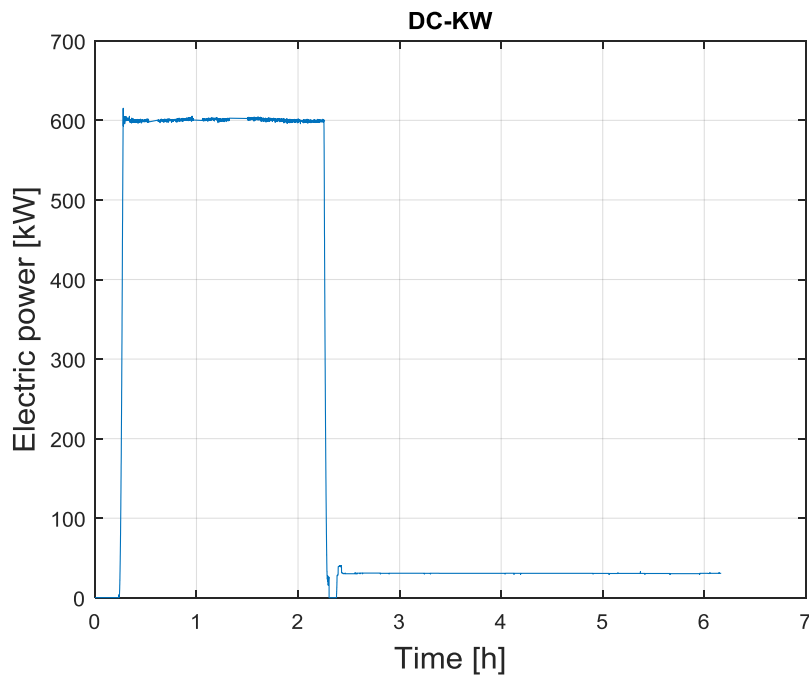



Figure 69: Electric Power [kW] (Test 2)

During the full power transient, the main heat exchanger is fed by a water mass flow rate with a mean value of 0.49 kg/s (FE501 see Figure 70) and a standard deviation 0.02. After the simulation of the accidental scenario the water injection is stopped at about $t=8225$ s.

 DIVISIONE INGEGNERIA SPERIMENTALE	<u>Title</u> D3.2: CIRCE experiments: pre-test, data-set and analysis	<u>Distribution</u> PUBLIC	<u>Emission</u> 09/08/2017	<u>Pag.</u> 48 di 234
		<u>Ref.</u> CI-T-R-292	Rev. 0	

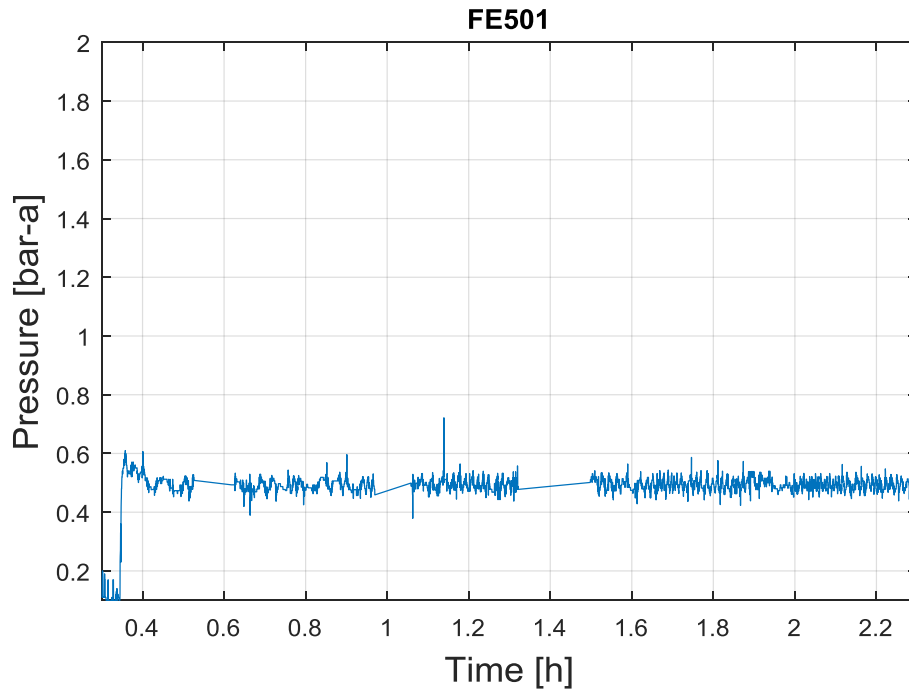


Figure 70: Water mass flow rate (Test 2)

Pressure and temperature of the water at the inlet of the HX are reported in Figure 71 and Figure 72 respectively.

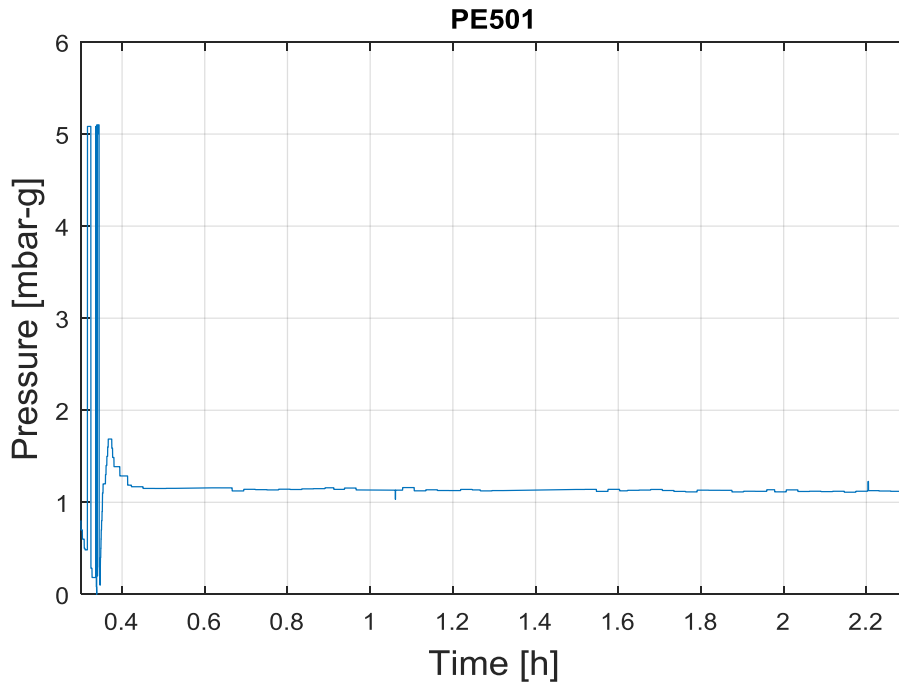



Figure 71: Water inlet pressure (Test 2)

 DIVISIONE INGEGNERIA SPERIMENTALE	<u>Title</u> D3.2: CIRCE experiments: pre-test, data-set and analysis	<u>Distribution</u> PUBLIC	<u>Emission</u> 09/08/2017	<u>Pag.</u> 49 di 234
		<u>Ref.</u> CI-T-R-292	Rev. 0	

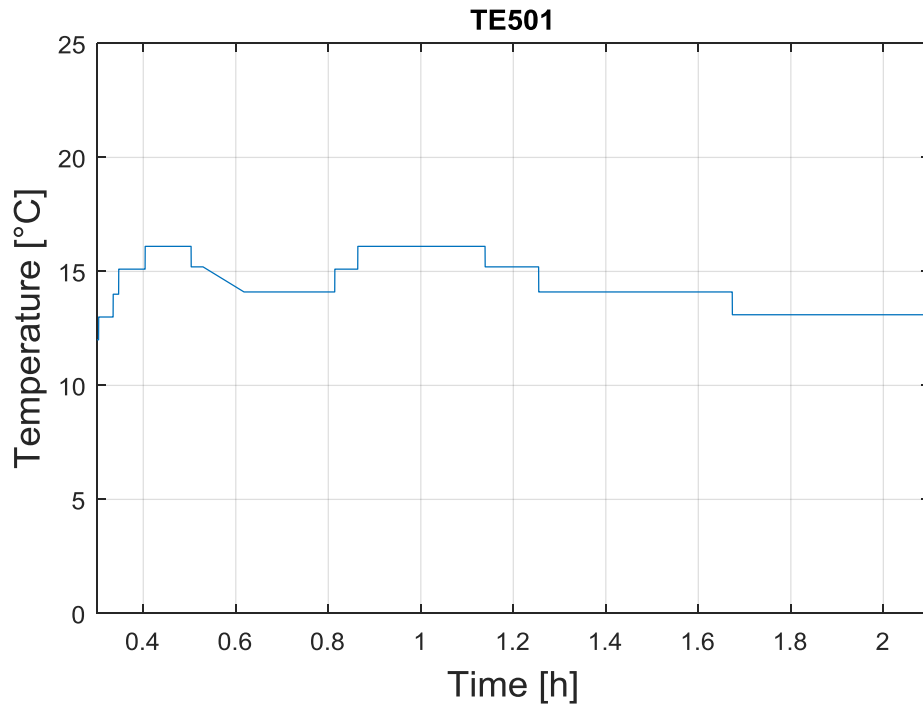


Figure 72: Water inlet temperature (Test 2)

Temperature of the steam at the outlet of the HX is reported in Figure 73.

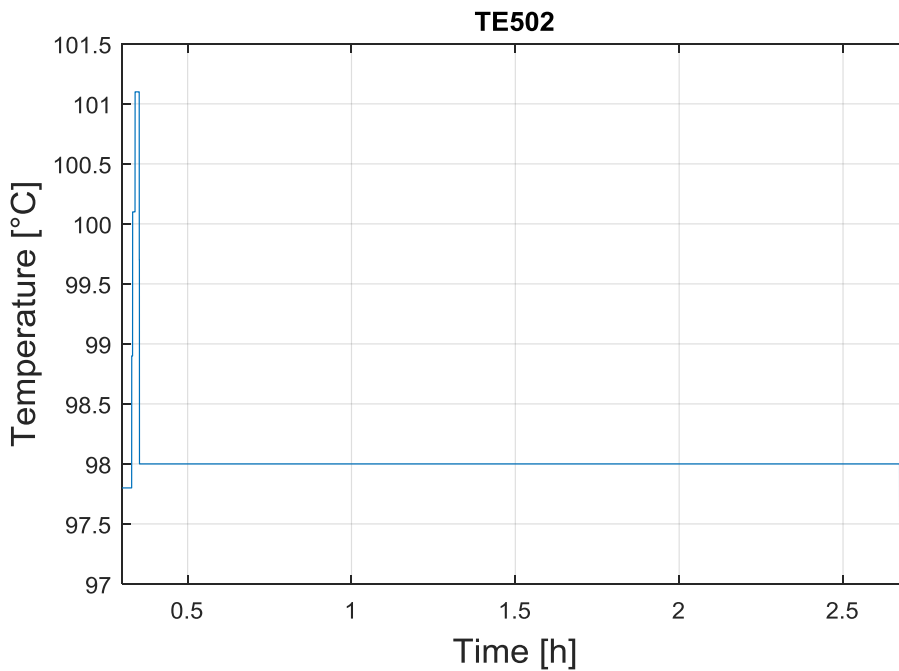



Figure 73: Steam temperature at the outlet of the HX (Test 2)

The Temperature of the helium gas entrapped in the gap between the tubes of the HX is reported in Figure 74.

 DIVISIONE INGEGNERIA SPERIMENTALE	<u>Title</u> D3.2: CIRCE experiments: pre-test, data-set and analysis	<u>Distribution</u> PUBLIC	<u>Emission</u> 09/08/2017	<u>Pag.</u> 50 di 234
		<u>Ref.</u> CI-T-R-292	Rev. 0	

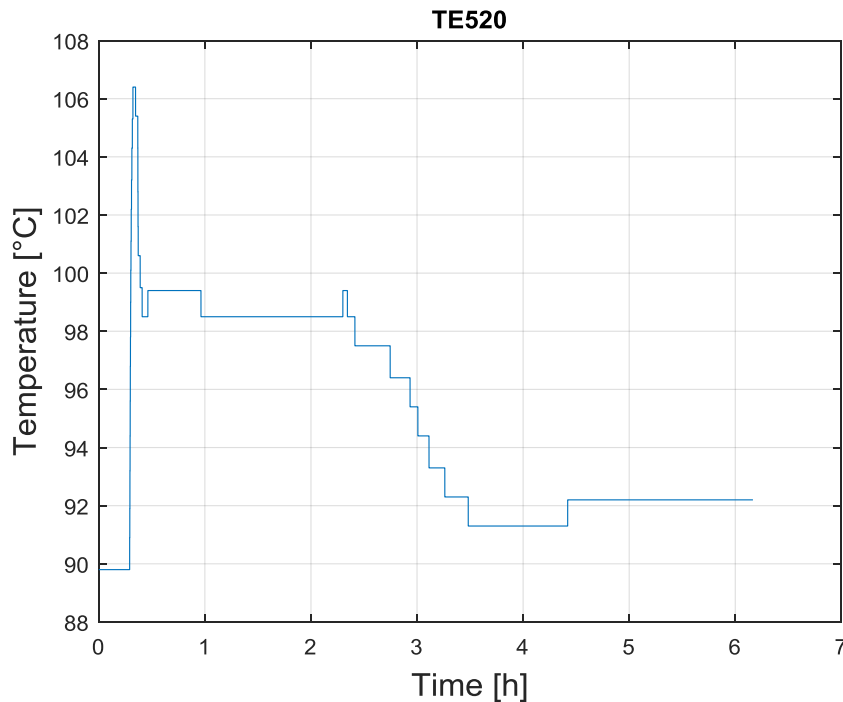


Figure 74: He temperature in the gap between the HX tubes (Test 2)

During the full power run, the LBE is circulated by means of argon gas injection (gas enhanced circulation). The gas injection is usually started before activating the fuel pin simulator in order to avoid the overheating of the pin clads. For this reason the gas injection started at $t=593$ s while it is stopped simultaneously to the stopping of the injection of the water in order to simulate the loss of the heat sink together with the loss of flow ($t=8204$ s, Figure 75). During the injection the mean value is 2.37 NI/s and a standard deviation of 0.021 NI/s. The adopted gas flow meters for TEST 2 was *FT-208 C* described in Annex B. The zero of the acquired mass flow rate signal was not directly provided by the software, for this reason for Test 2 the signal *FT-208 C* was properly shifted.

In the low power transient the decay heat removal system (DHR) is activated injecting air in the bayonet tube of the DHR. The injection of air starts at $t=8230$ s. As shown in Figure 76, the air mass flow rate mean value is 325 g/s up to $t=17770$ s with a standard deviation of 1 g/s. Then the air mass flow rate is reduced to about 218 g/s till the end of the experiment. In TEST 2 a software upgrade allowed the acquisition of both inlet and outlet air temperatures in the DHR as shown in Figure 77 and Figure 78. In Figure 79 the air velocity in the DHR is plotted (mean value ~ 26.3 m/s).

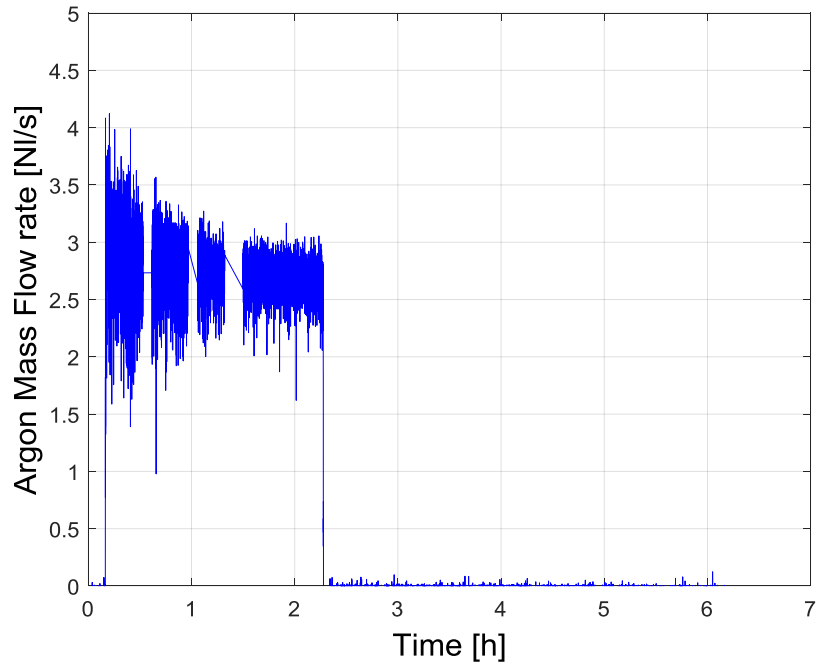


Figure 75: Argon mass flow rate (Test 2)

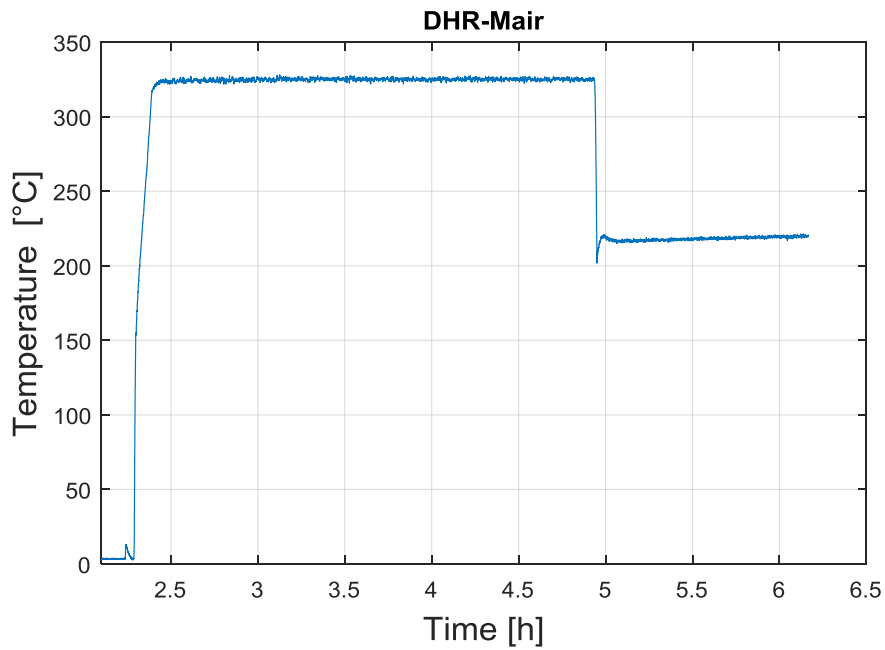


Figure 76: DHR air mass flow rate (Test 2)

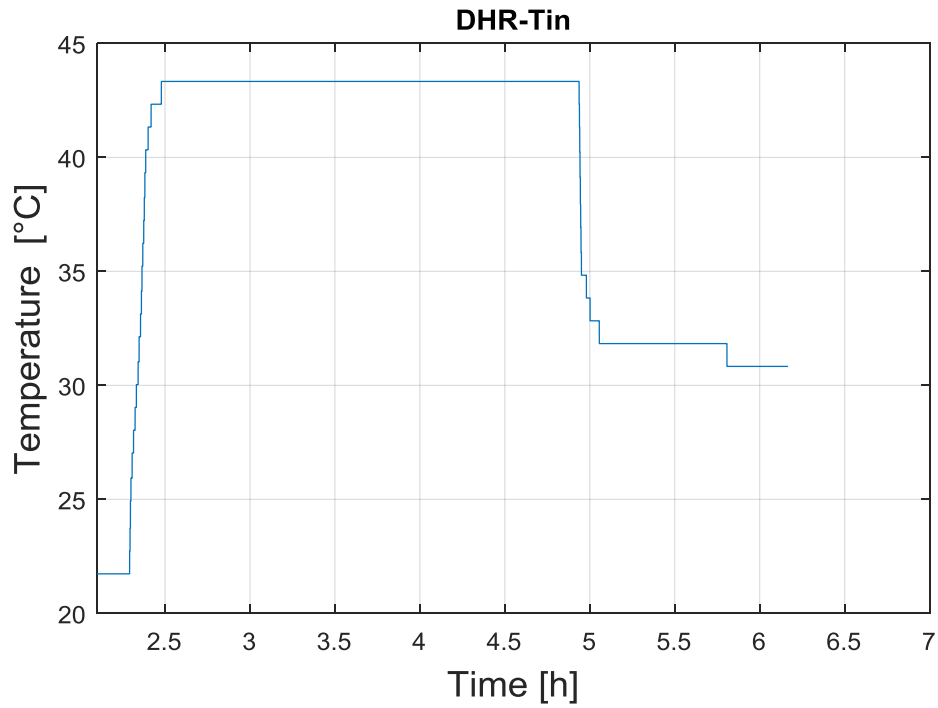


Figure 77: DHR inlet air temperature (Test2)

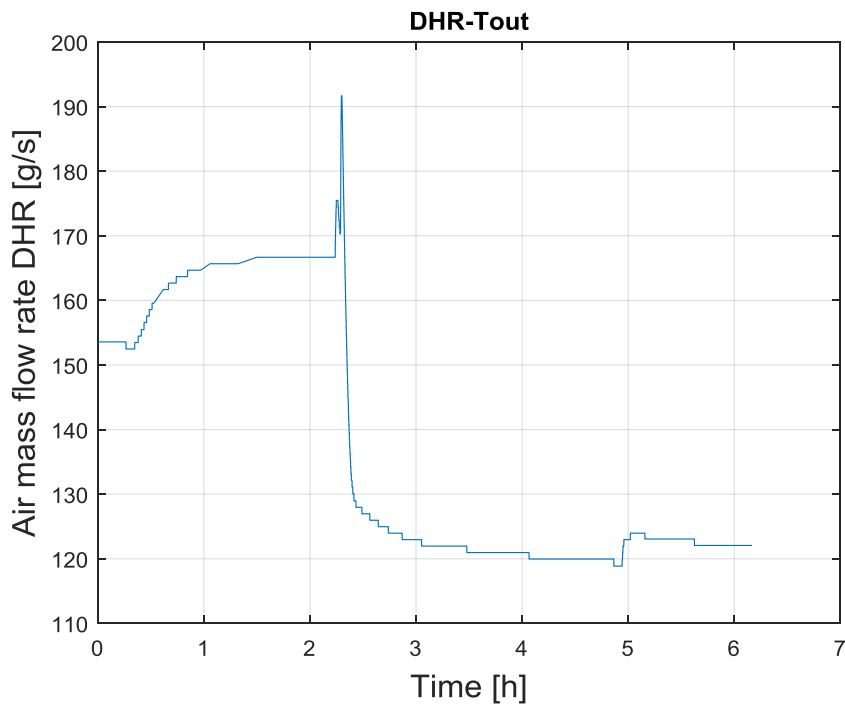



Figure 78: DHR outlet air temperature (Test2)

 DIVISIONE INGEGNERIA SPERIMENTALE	<u>Title</u> D3.2: CIRCE experiments: pre-test, data-set and analysis	<u>Distribution</u> PUBLIC	<u>Emission</u> 09/08/2017	<u>Pag.</u> 53 di 234
		<u>Ref.</u> CI-T-R-292	Rev. 0	

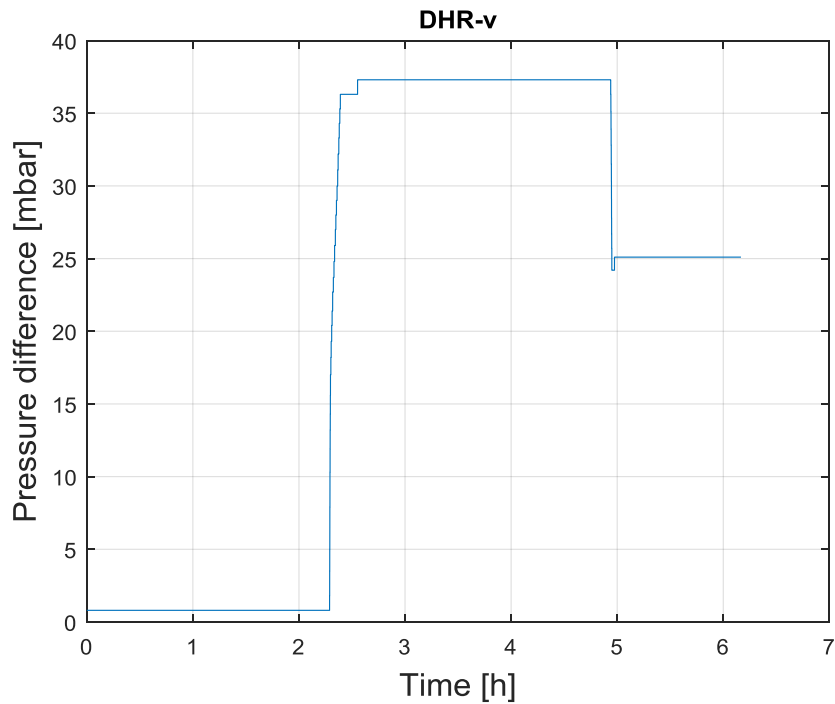



Figure 79: DHR air velocity (Test 2)

The pressure difference across the venturi flow meter (see Annex A Fig. 1 Mass flow Meter/08-384-DISEGNO.pdf) used to evaluate the LBE mass flow rate in the ICE test section is plotted Figure 80. The mean value during the full power run is 330 mbar with a standard deviation of 13.3 mbar. During the low power transient the mean pressure difference is 47.2 mbar.

 DIVISIONE INGEGNERIA SPERIMENTALE	<u>Title</u> D3.2: CIRCE experiments: pre-test, data-set and analysis	<u>Distribution</u> PUBLIC	<u>Emission</u> 09/08/2017	<u>Pag.</u> 54 di 234
		<u>Ref.</u> CI-T-R-292	Rev. 0	

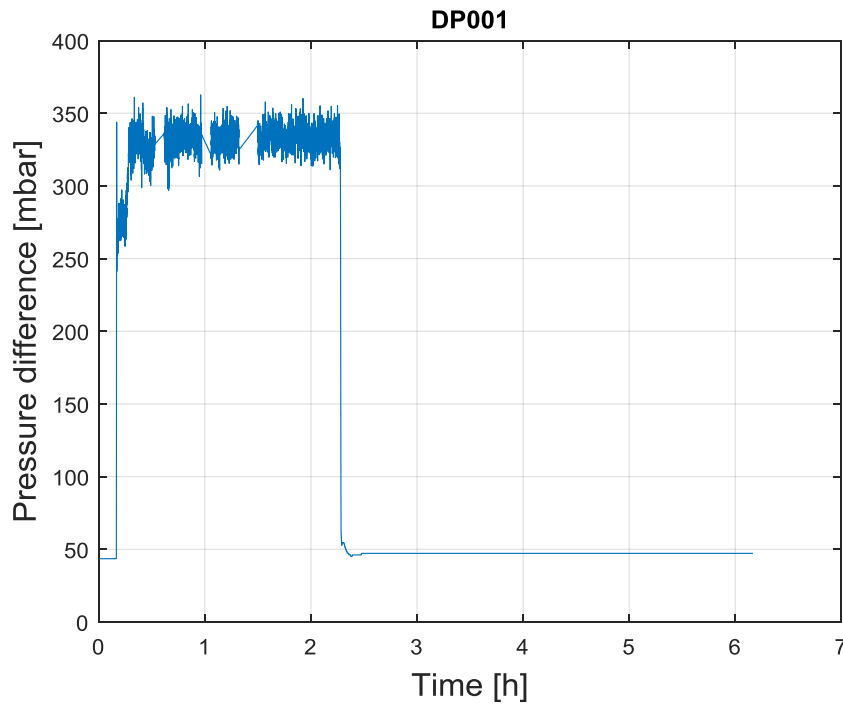



Figure 80: Pressure difference across the venturi flow meter (Test 2)

DP002 (PE009-PE010) represents the pressure difference across the lower spacer grid (for the positioning of the bubble tubes see Annex A Fig. 2 0510 Rev 1-Fuel Pin Simulator.pdf). The mean value of the pressure difference during the full power transient is 247 mbar with a standard deviation of about 2.7 mbar, while the mean value for the low power run is 216 mbar with a standard deviation of 1 mbar (see Figure 81). Pe003 represents the pressure in the fitting volume (Figure 82) while PE004 (Figure 83), PE005 (Figure 84) represent respectively the pressure in the lower and upper section of the riser. For the position of the bubble tubes PE003, PE004, PE005 see Annex A Fig. 3 0016 Instrumentation.pdf.

 DIVISIONE INGEGNERIA SPERIMENTALE	<u>Title</u> D3.2: CIRCE experiments: pre-test, data-set and analysis	<u>Distribution</u> PUBLIC	<u>Emission</u> 09/08/2017	<u>Pag.</u> 55 di 234
		<u>Ref.</u> CI-T-R-292	Rev. 0	

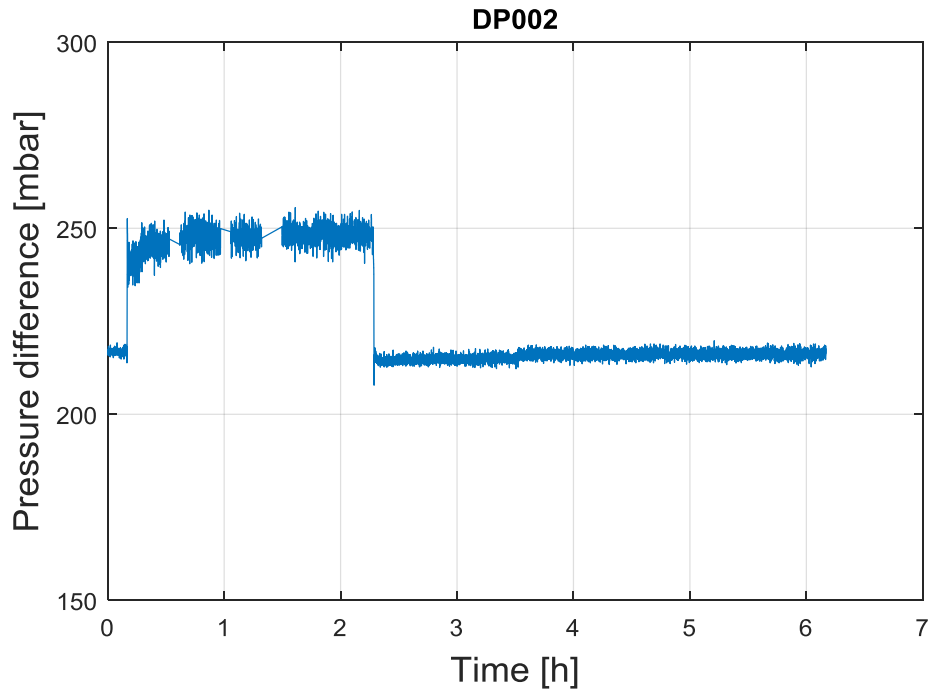


Figure 81: Pressure difference across the FPS lower spacer grid (Test 2)

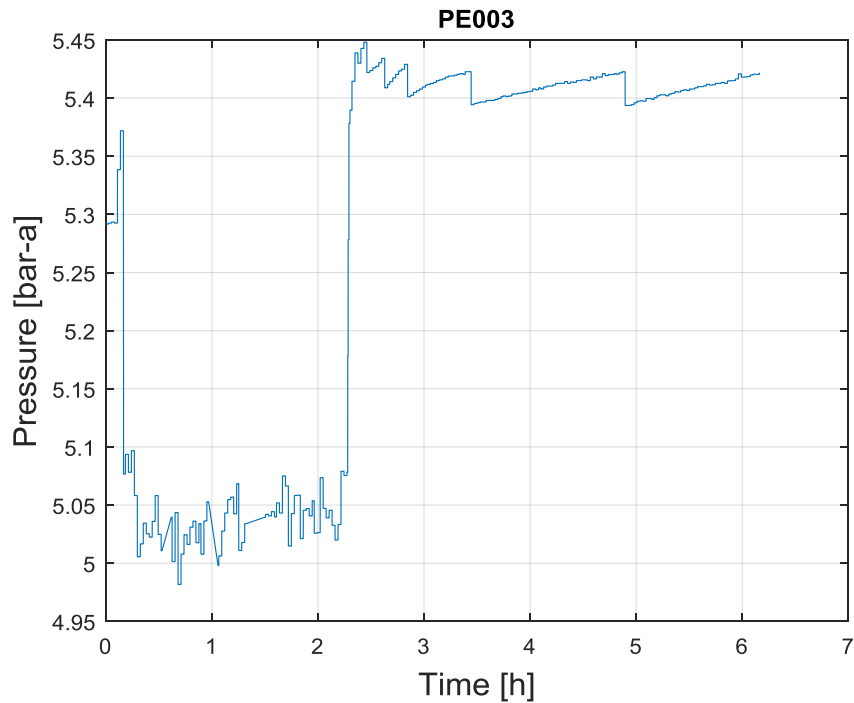


Figure 82: Pressure in the fitting volume (Test 2)

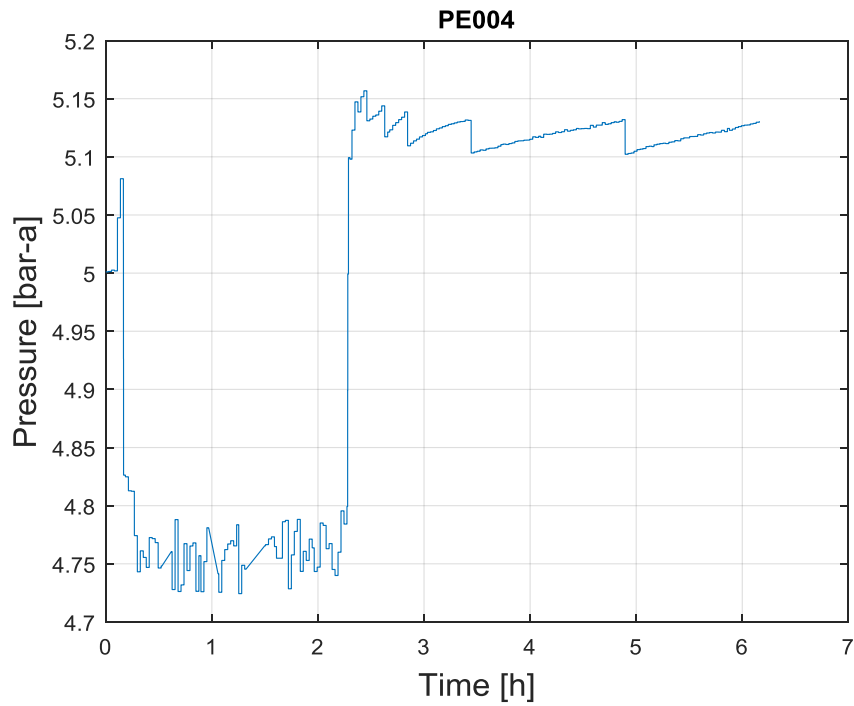


Figure 83: Pressure in the riser (lower section) (Test 2)

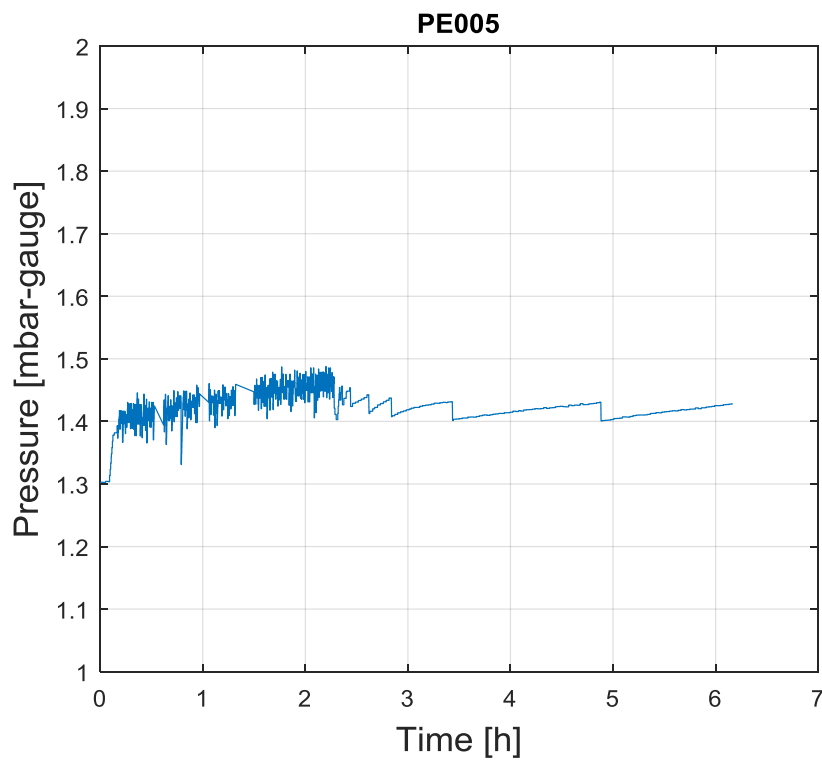



Figure 84: Pressure in the riser (upper section) (Test 2)

 DIVISIONE INGEGNERIA SPERIMENTALE	<u>Title</u> D3.2: CIRCE experiments: pre-test, data-set and analysis	<u>Distribution</u> PUBLIC	<u>Emission</u> 09/08/2017	<u>Pag.</u> 57 di 234
		<u>Ref.</u> CI-T-R-292	Rev. 0	

The LBE inside the pool is operated under a protective atmosphere of argon gas that fill the volume from the LBE free level to the vessel head. A relative small overpressure is maintained in the gas in order to avoid oxygen contamination from the external environment. PE007 is the pressure of the argon measured in the cover gas (pressure gauge, see Figure 85), while the temperature of the cover gas is measured through a 3 mm *K*-type thermocouple and reported in Figure 86.

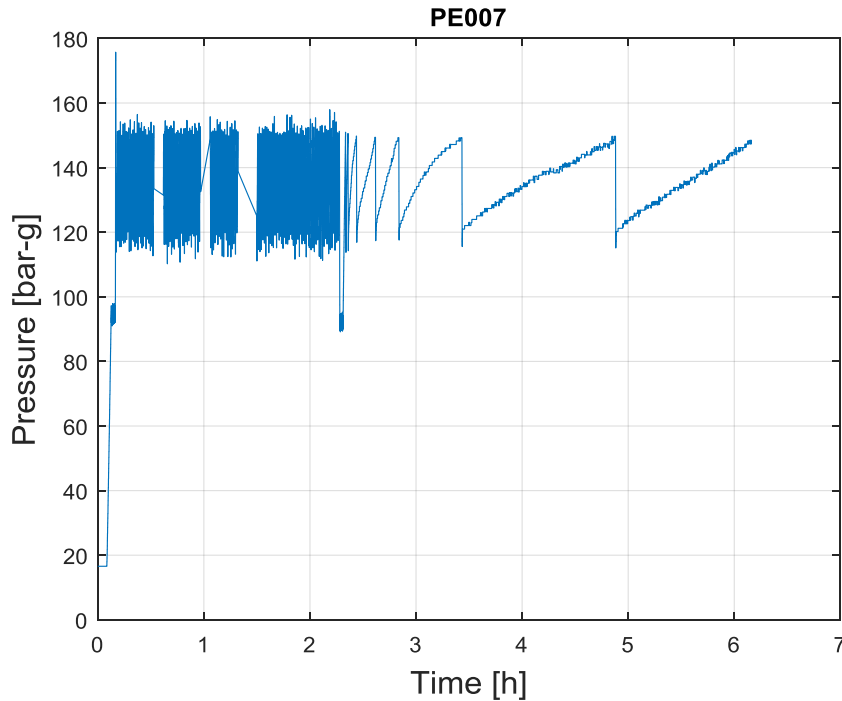



Figure 85: Pressure in the cover gas (Test 2)

 DIVISIONE INGEGNERIA SPERIMENTALE	<u>Title</u> D3.2: CIRCE experiments: pre-test, data-set and analysis	<u>Distribution</u> PUBLIC	<u>Emission</u> 09/08/2017	<u>Pag.</u> 58 di 234
		<u>Ref.</u> CI-T-R-292	Rev. 0	

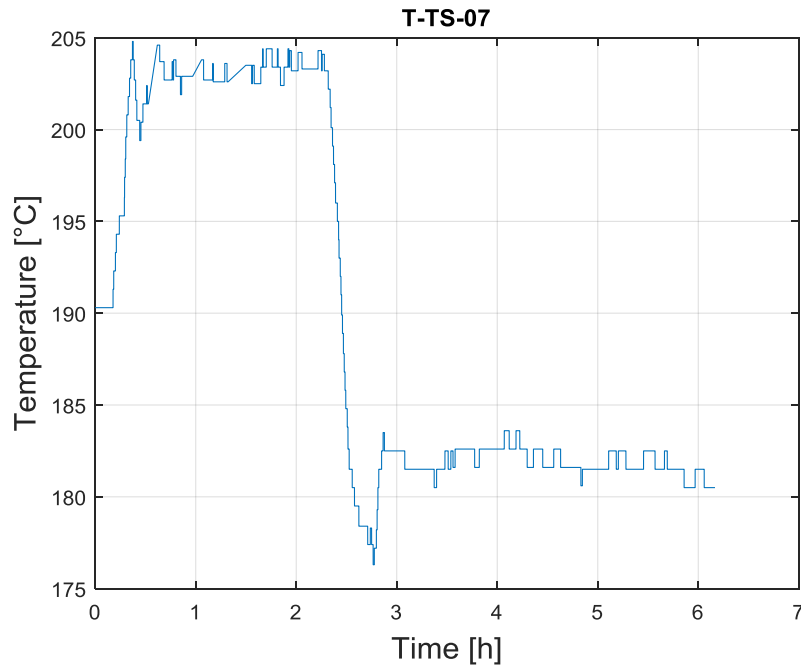


Figure 86: Temperature in the cover gas (Test 2)

For the positioning of the thermocouples in the DHR system refers to Annex A Fig. 4 THINS thermocouples arrangement.pdf and Annex A Fig. 5 T-DHR-0100-Instrumentation DHR.pdf. In Figure 87, the average temperature of the LBE at the inlet and outlet sections of the DHR is reported. Unlike in Test 1, for Test 2 no inversion of the temperature between intel and outlet section of the DHR was detected.

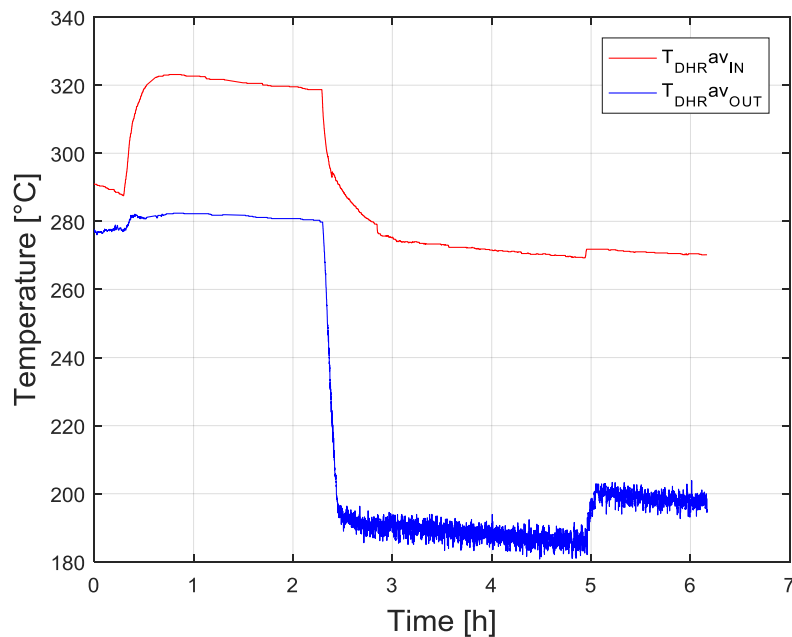



Figure 87: DHR inlet outlet average temperature (Test 2)

 DIVISIONE INGEGNERIA SPERIMENTALE	<u>Title</u> D3.2: CIRCE experiments: pre-test, data-set and analysis	<u>Distribution</u> PUBLIC	<u>Emission</u> 09/08/2017	<u>Pag.</u> 59 di 234
		<u>Ref.</u> CI-T-R-292	Rev. 0	

The LBE temperature at the FPS entrance was measured by three thermocouples with a diameter of 3 mm (T-FPS-31, 32, 33, Annex A Fig. 6 T-FPS-0100 foglio2-FPS Instrumented). The LBE temperature at the active length exit section of the FPS was measured by three thermocouples (T-FPS-34, 35, 36 Annex A Fig. 6 T-FPS-0100 foglio2-FPS Instrumented) of the same type of those at the entrance. Moreover three thermocouples T-FPS-37, 38, 39 were installed in the slot at the exit of the FPS placed at 120° (see Annex A Fig. 7 T-FPS-0100 foglio1-FPS Instrumented). For the position of the thermocouples inside the bundle refers to Annex A Fig. 8 T-FPS Instrumentation 1 of 2 and Annex A Fig. 9 T-FPS Instrumentation 2 of 2. In Figure 88, the LBE average temperature evaluated at the inlet and outlet sections of the FPS and at the outlet section of the FPS are reported (see Annex A Fig. 7 T-FPS-0100 foglio1-FPS Instrumented).

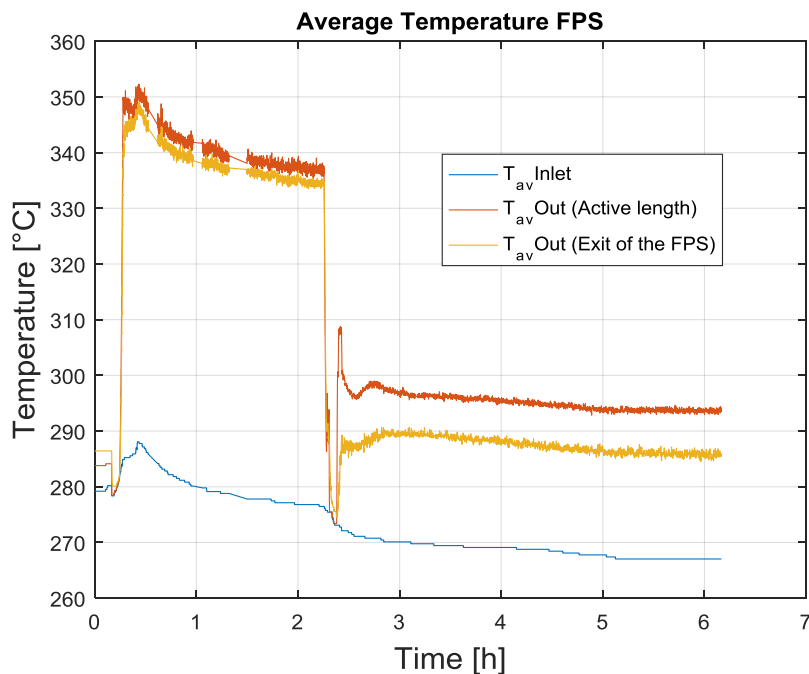


Figure 88: Active length Inlet/Outlet section and FPS Outlet LBE temperature (Test 2)

From Figure 89 to Figure 117 the single temperature in the Fuel Pin Simulator (FPS) are reported. It is worth to be mentioned that T-FPS-013 is broken and therefore the relative plot is not reported, while some problem are encountered with T-FPS-07 as evidenced from Figure 95.

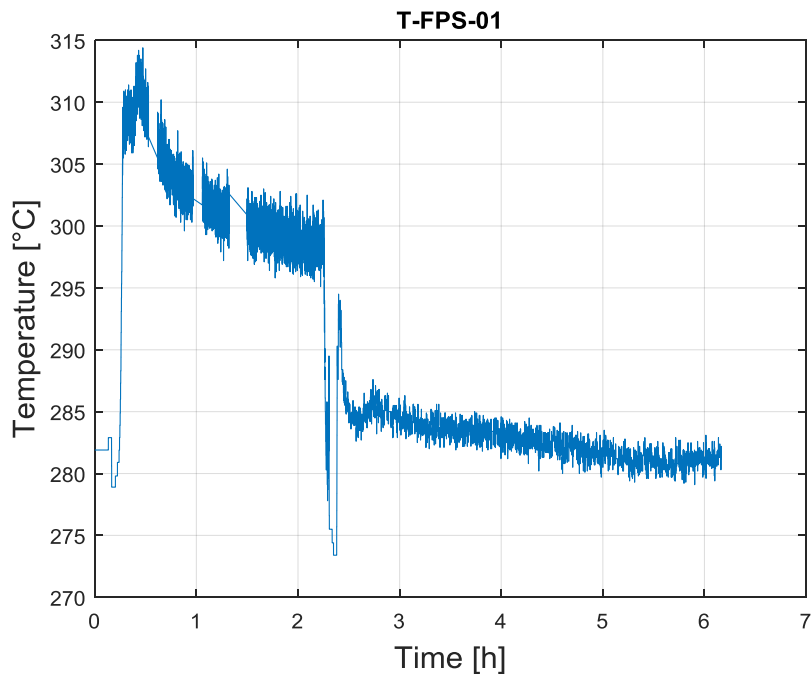


Figure 89: T-FPS-01 LBE temperature (Test 2)

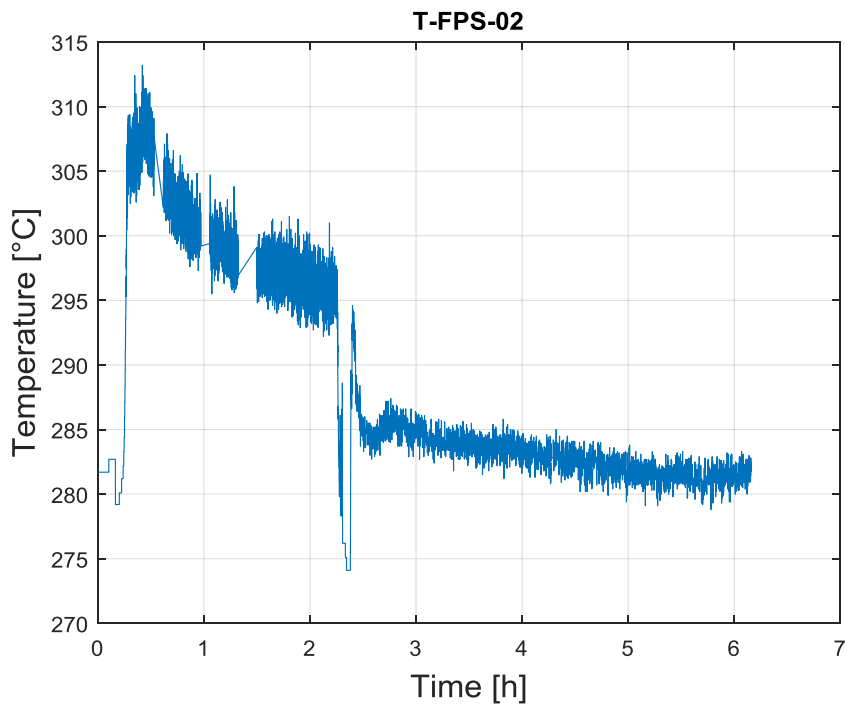


Figure 90: T-FPS-02 LBE temperature (Test 2)

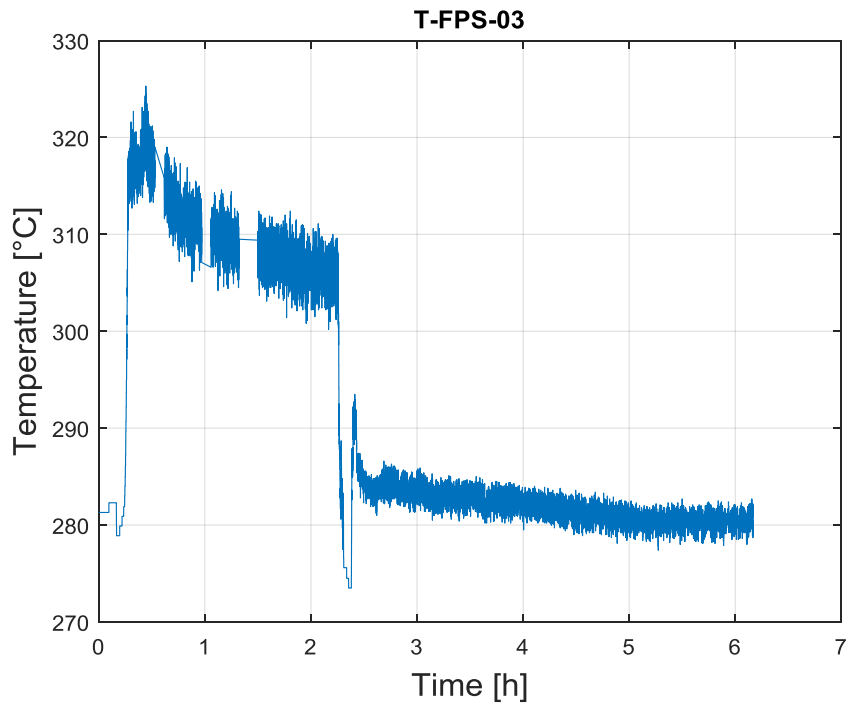


Figure 91: T-FPS-03 LBE temperature (Test 2)

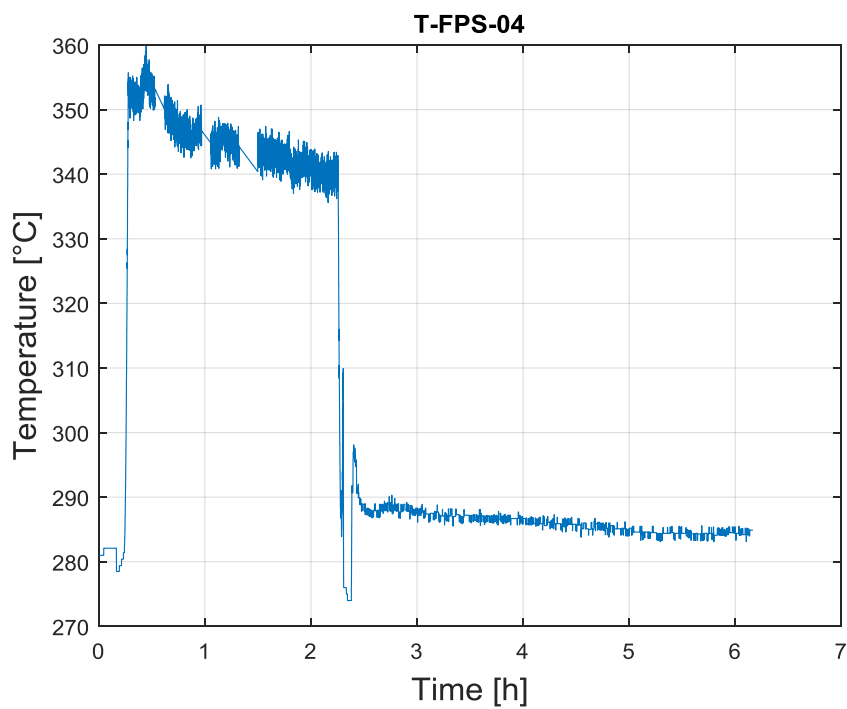


Figure 92: T-FPS-04 LBE temperature (Test 2)

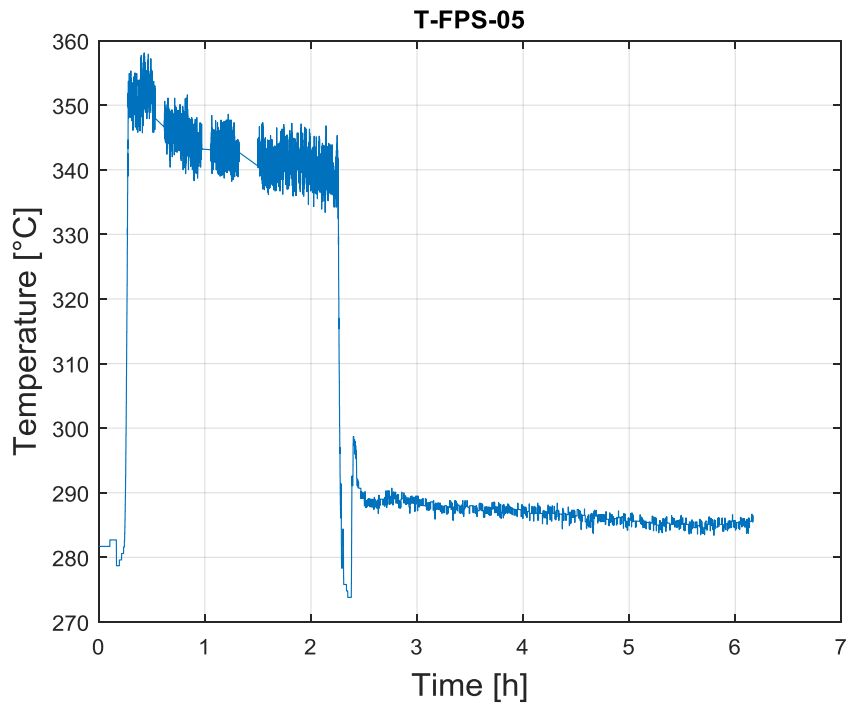


Figure 93: T-FPS-05 LBE temperature (Test 2)

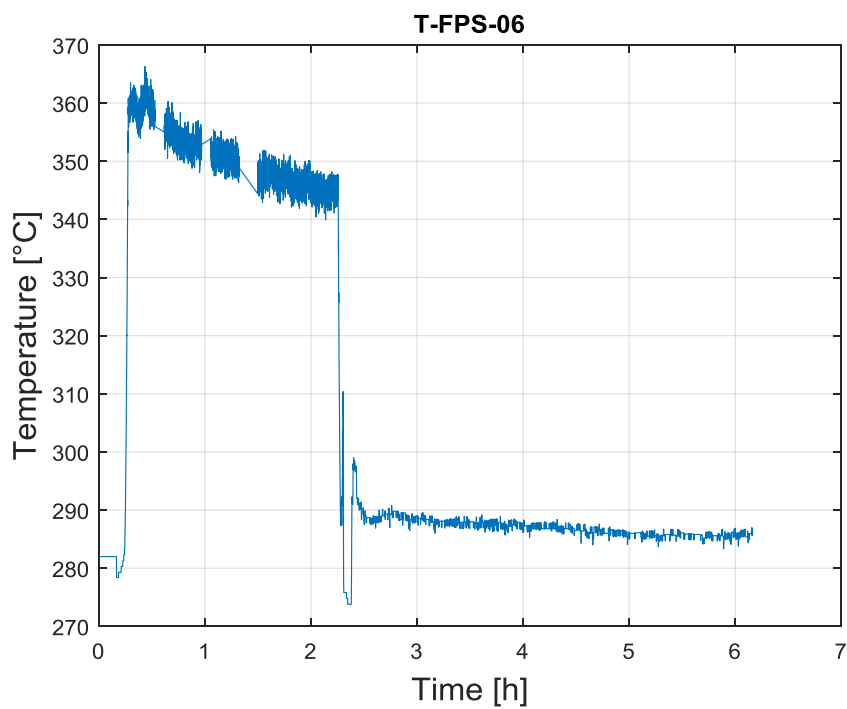


Figure 94: T-FPS-06 LBE temperature (Test 2)

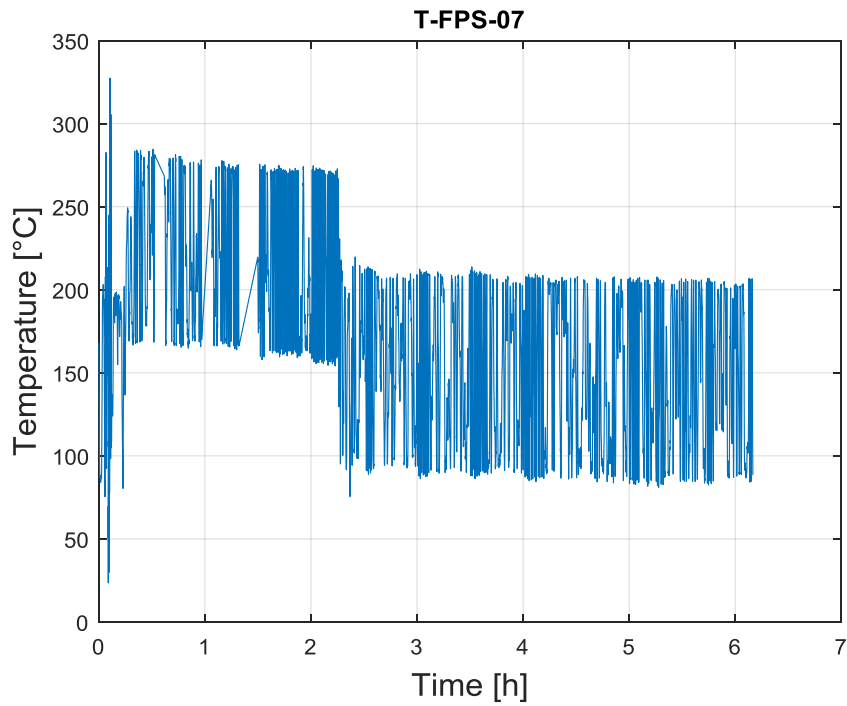


Figure 95: T-FPS-07 LBE temperature (Test 2)

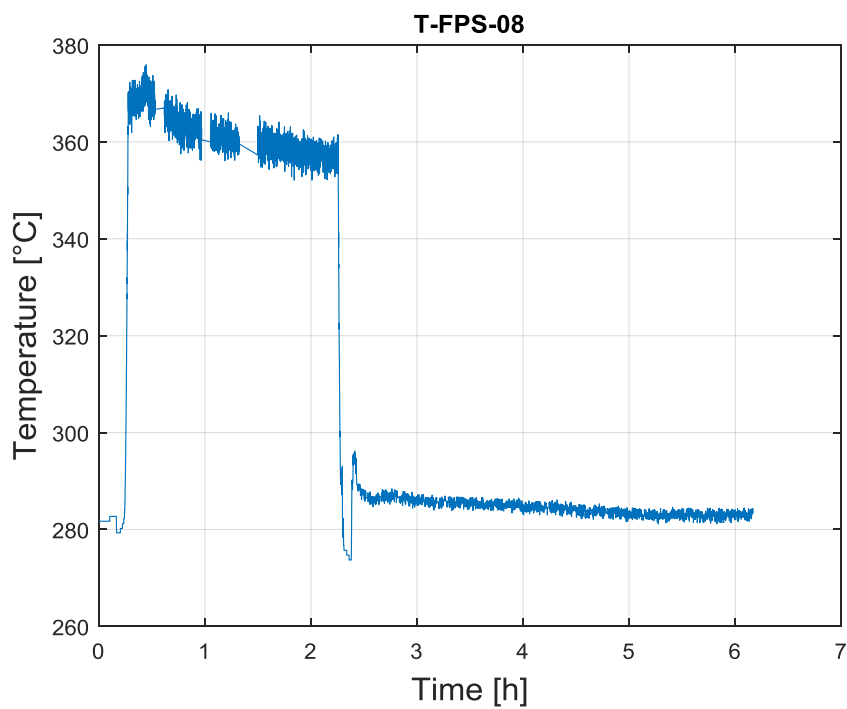


Figure 96: T-FPS-08 LBE temperature (Test 2)

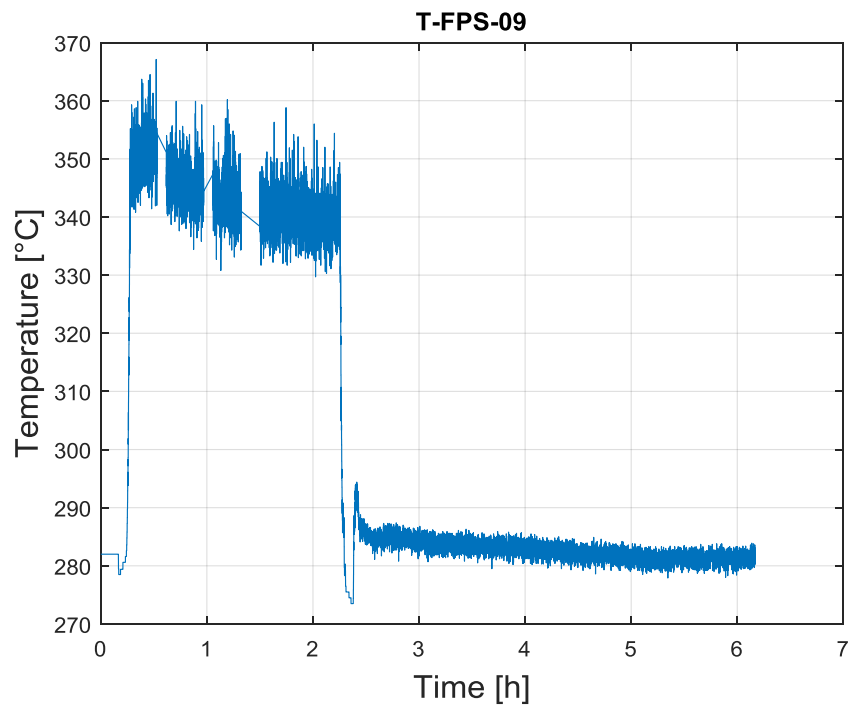


Figure 97: T-FPS-09 LBE temperature (Test 2)

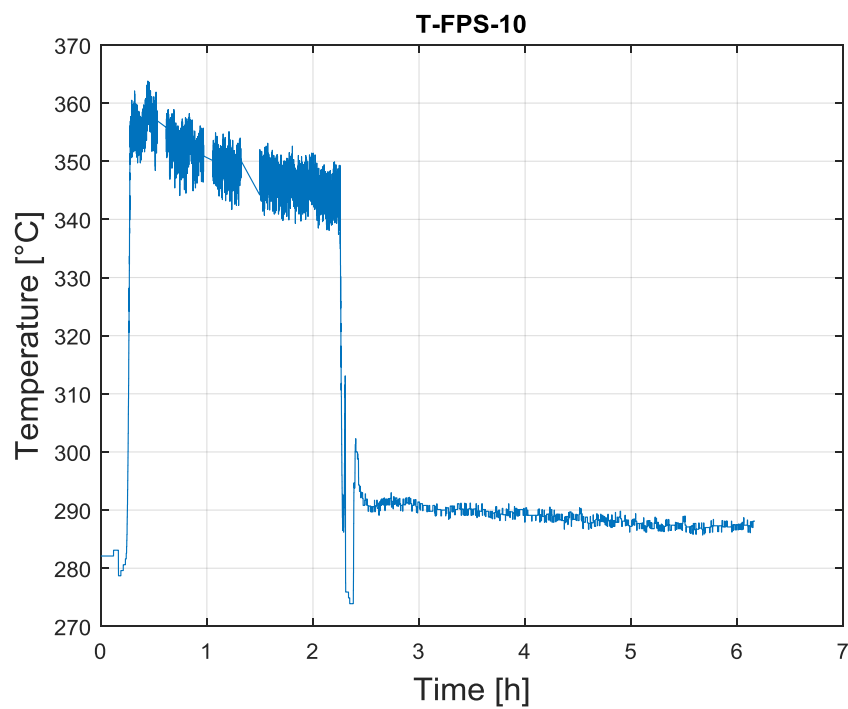


Figure 98: T-FPS-10 LBE temperature (Test 2)

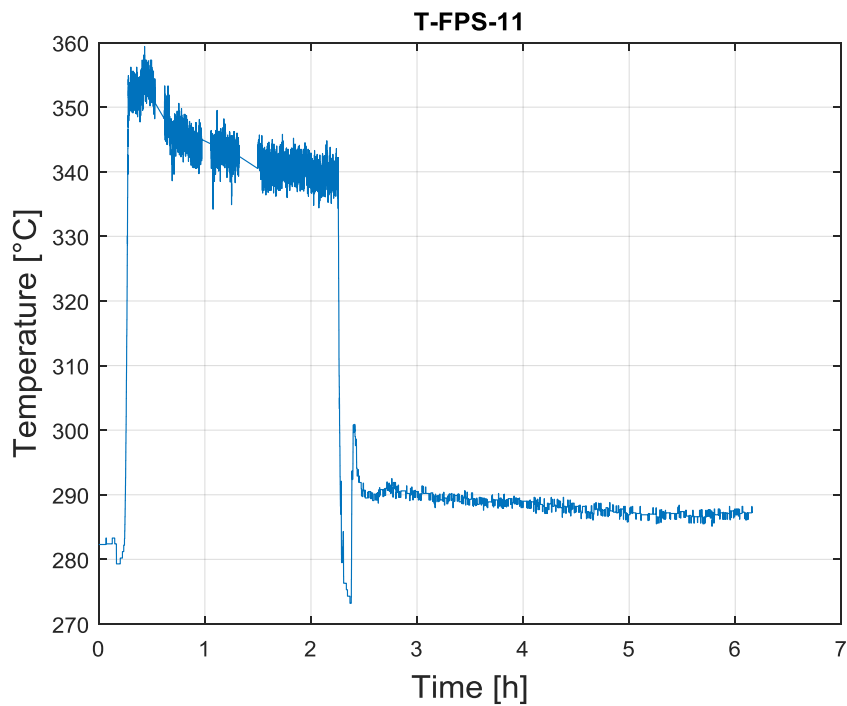


Figure 99: T-FPS-11 LBE temperature (Test 2)

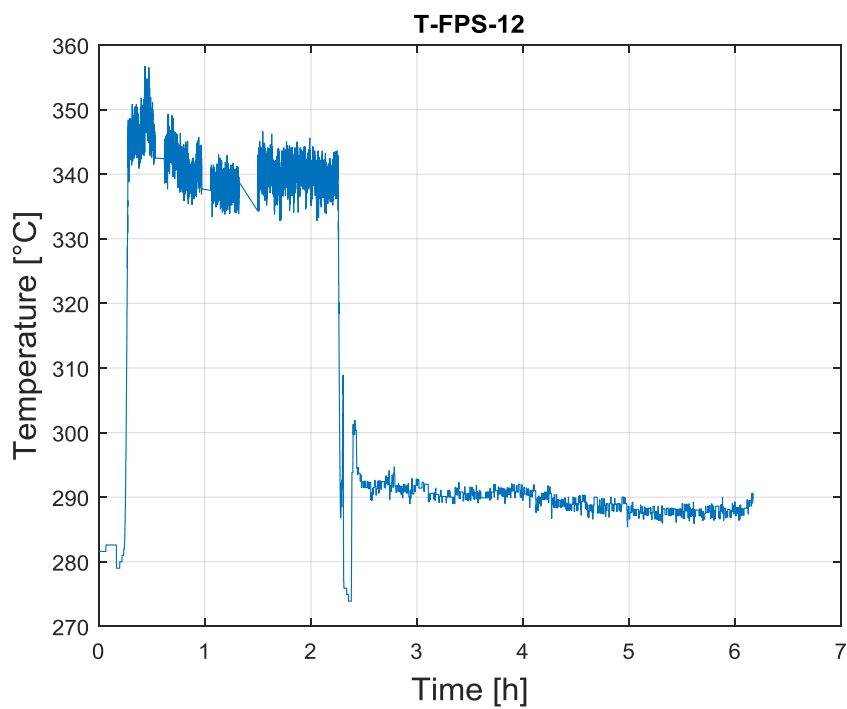


Figure 100: T-FPS-12 LBE temperature (Test 2)

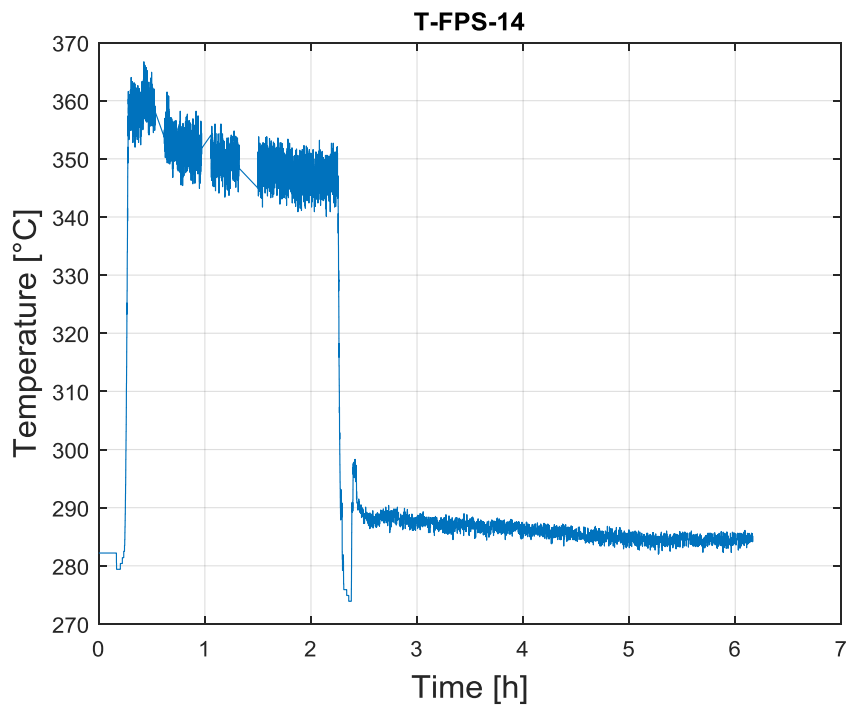


Figure 101: T-FPS-14 LBE temperature (Test 2)

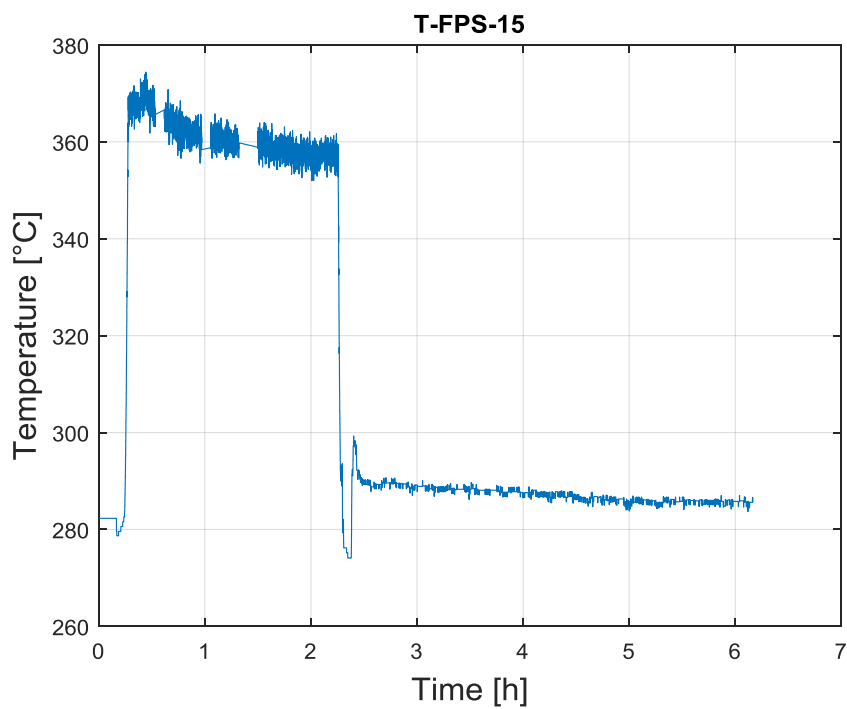


Figure 102: T-FPS-15 LBE temperature (Test 2)

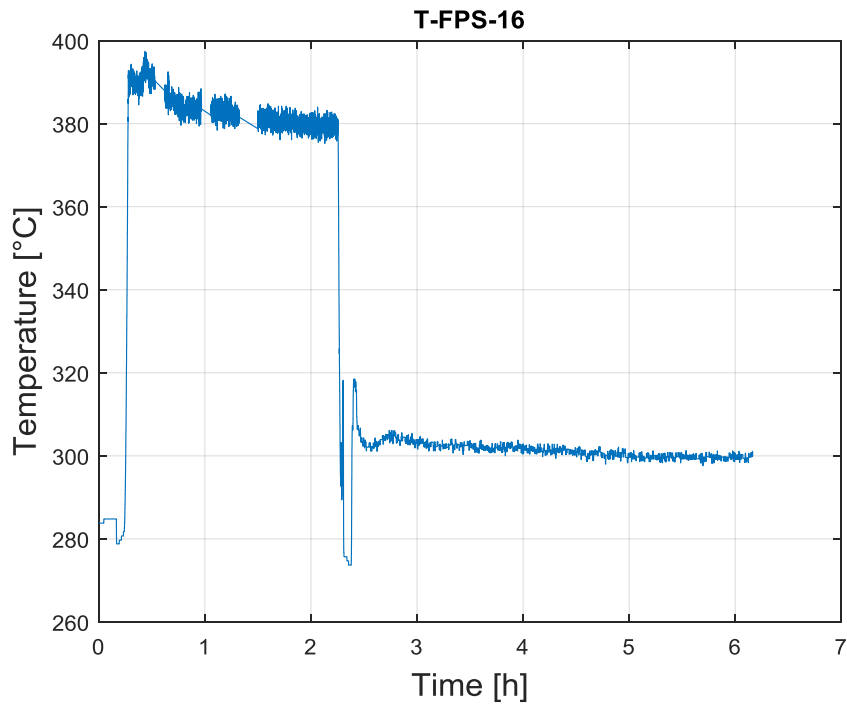


Figure 103: T-FPS-16 LBE temperature (Test 2)

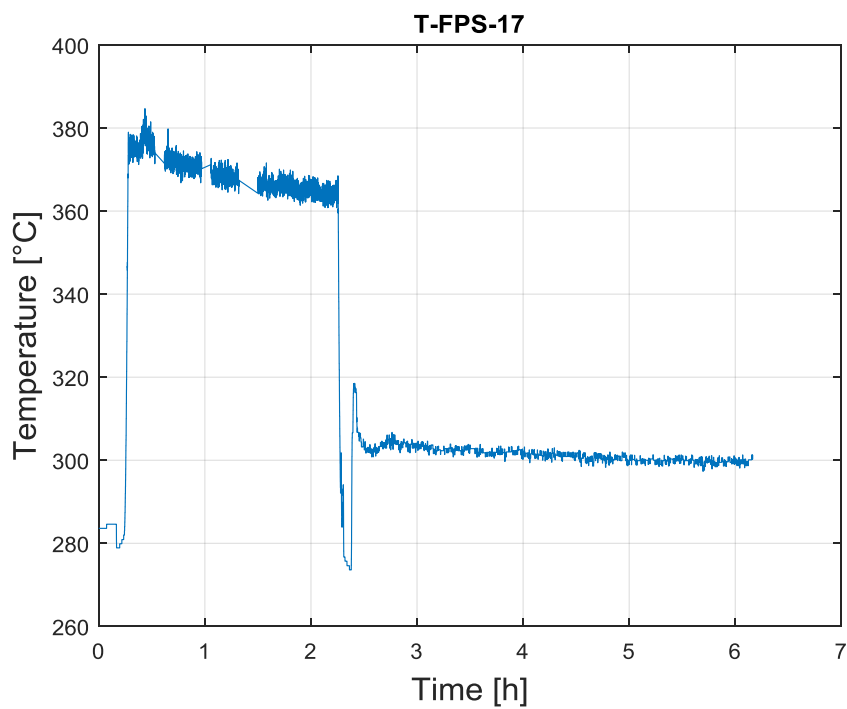


Figure 104: T-FPS-17 LBE temperature (Test 2)

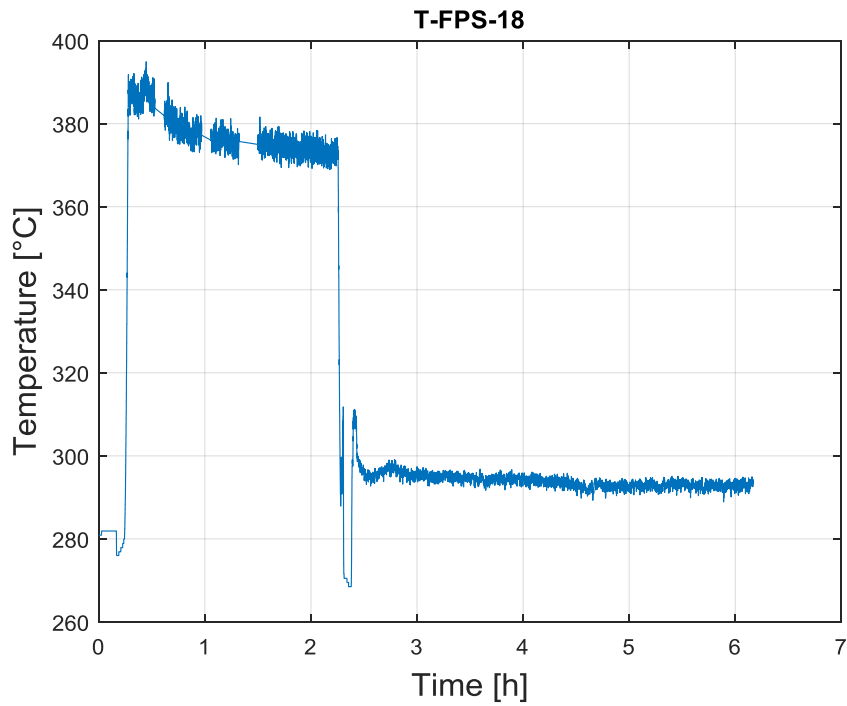


Figure 105: T-FPS-18 LBE temperature (Test 2)

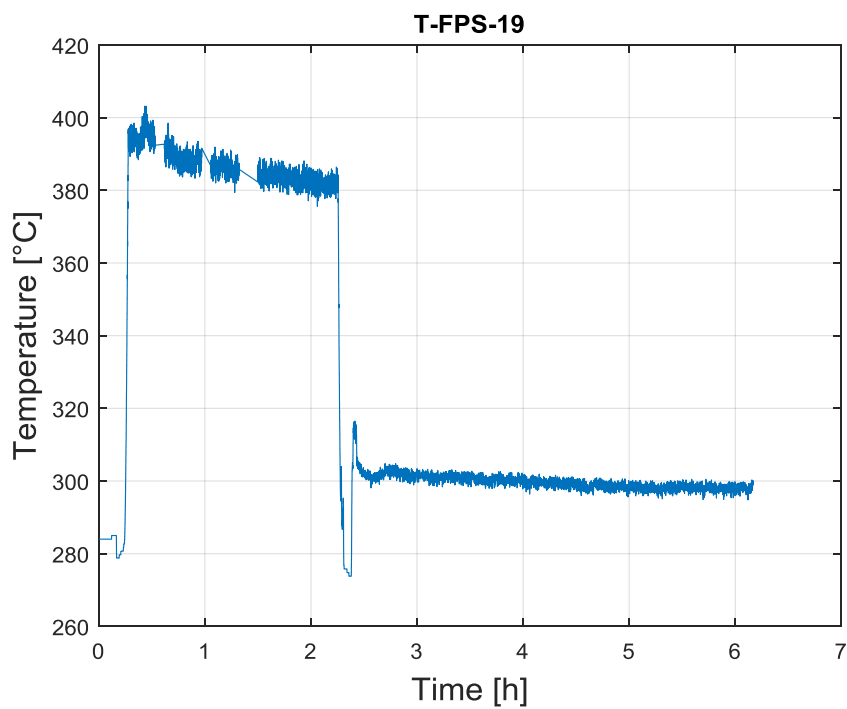


Figure 106: T-FPS-19 LBE temperature (Test 2)

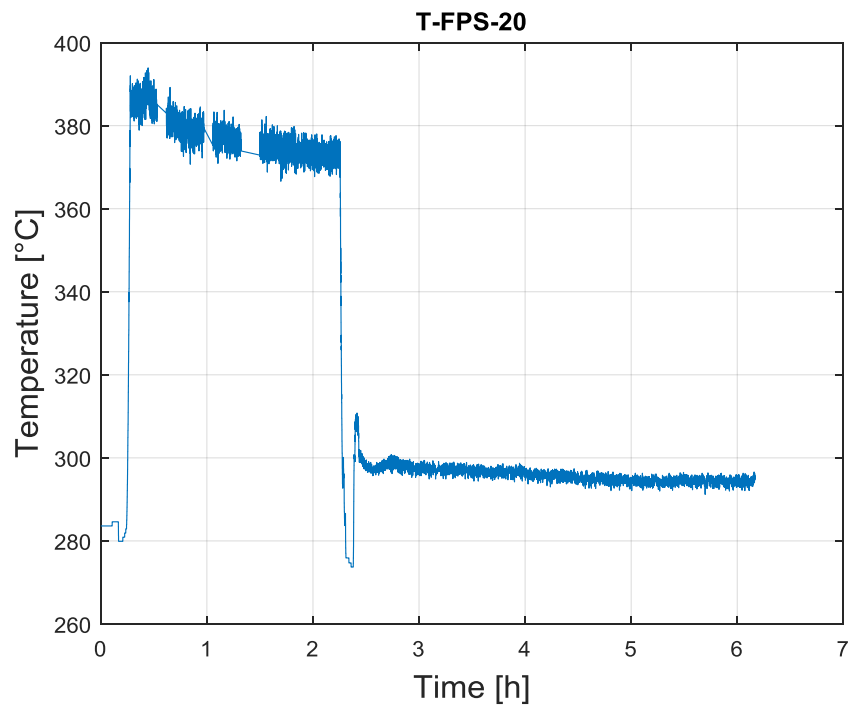


Figure 107: T-FPS-20 LBE temperature (Test 2)

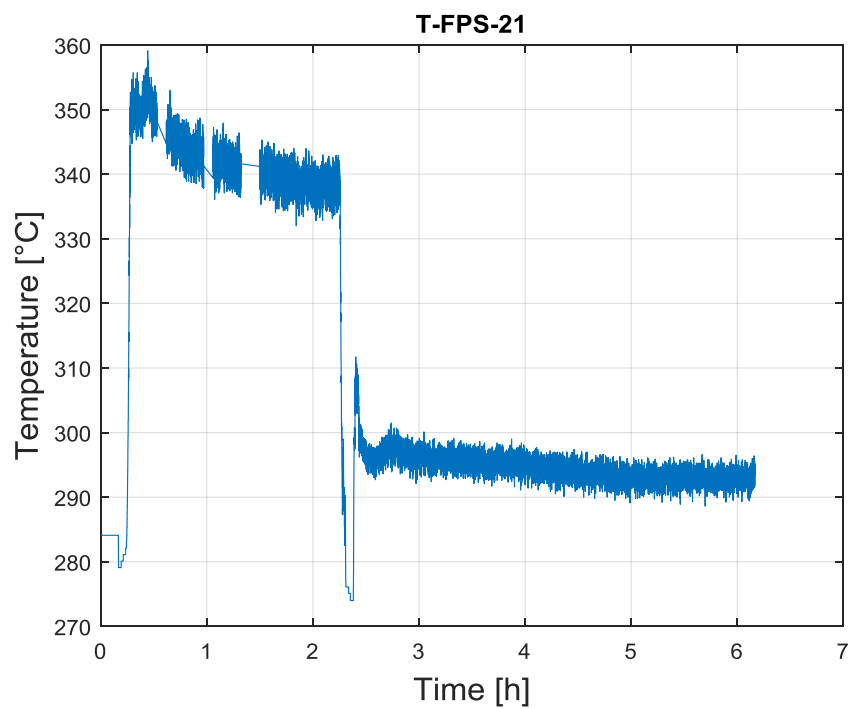


Figure 108: T-FPS-21 LBE temperature (Test 2)

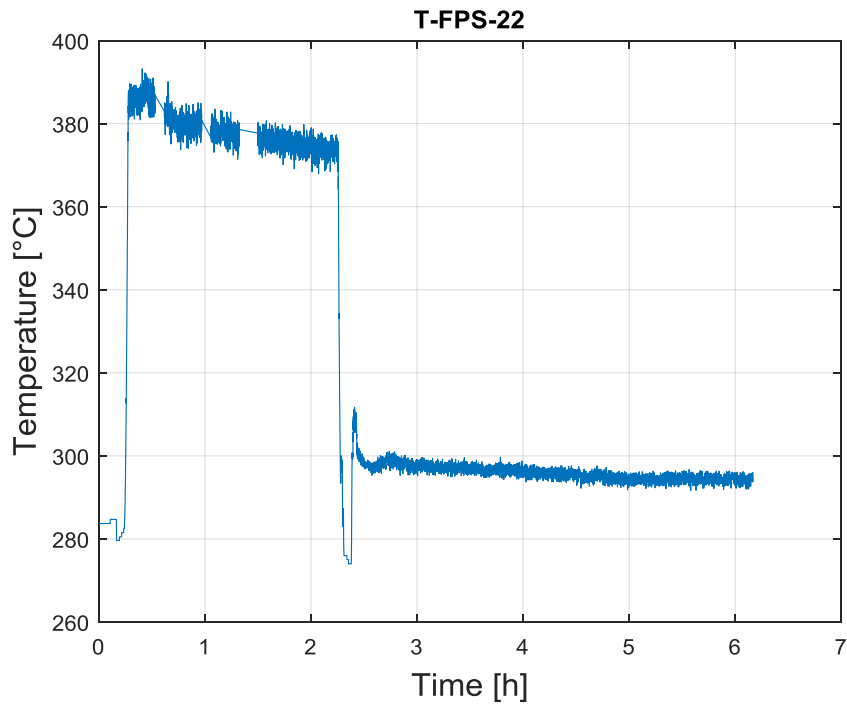


Figure 109: T-FPS-22 LBE temperature (Test 2)

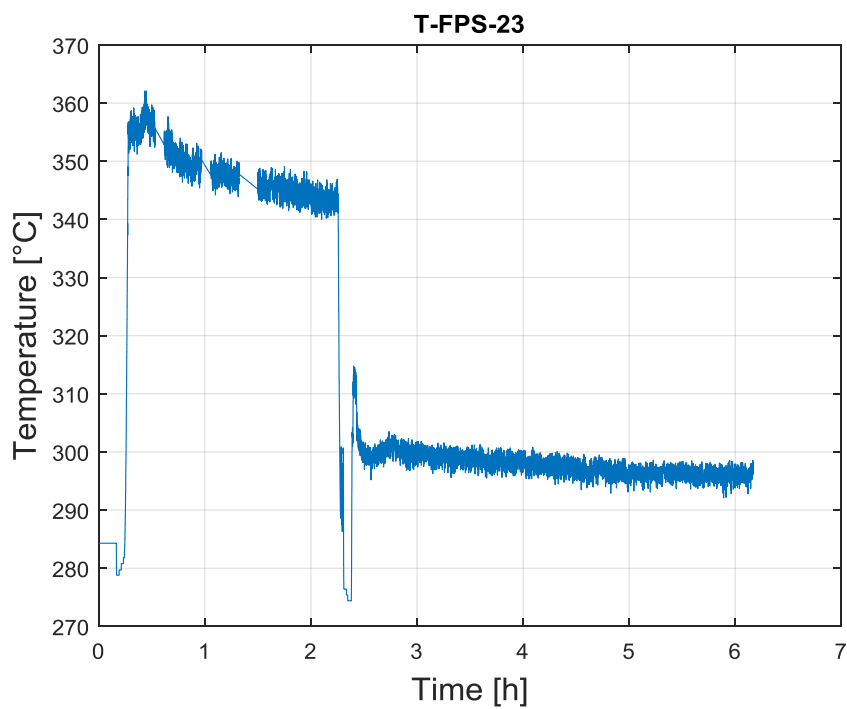


Figure 110: T-FPS-23 LBE temperature (Test 2)

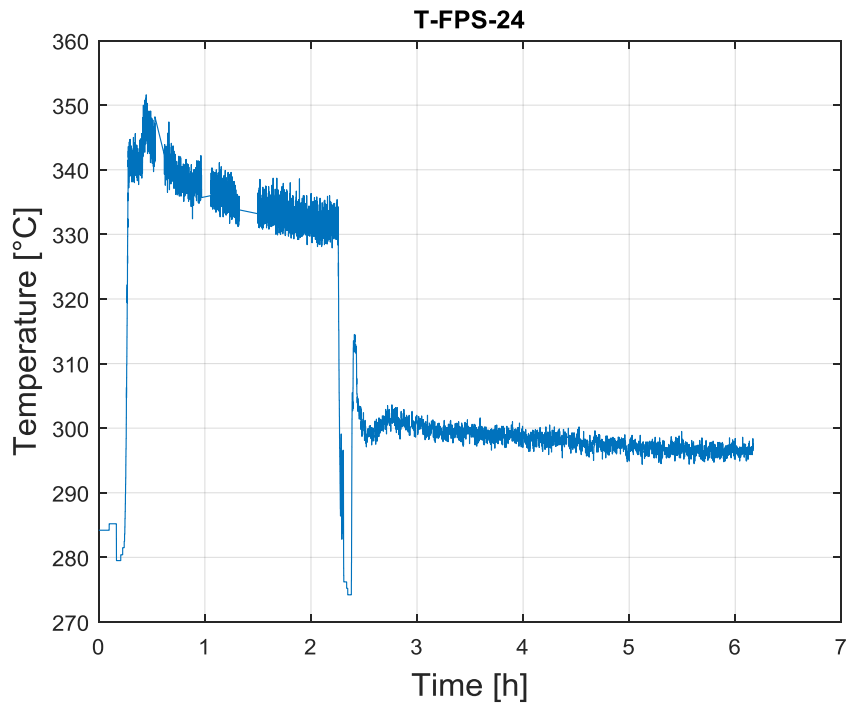


Figure 111: T-FPS-24 LBE temperature (Test 2)

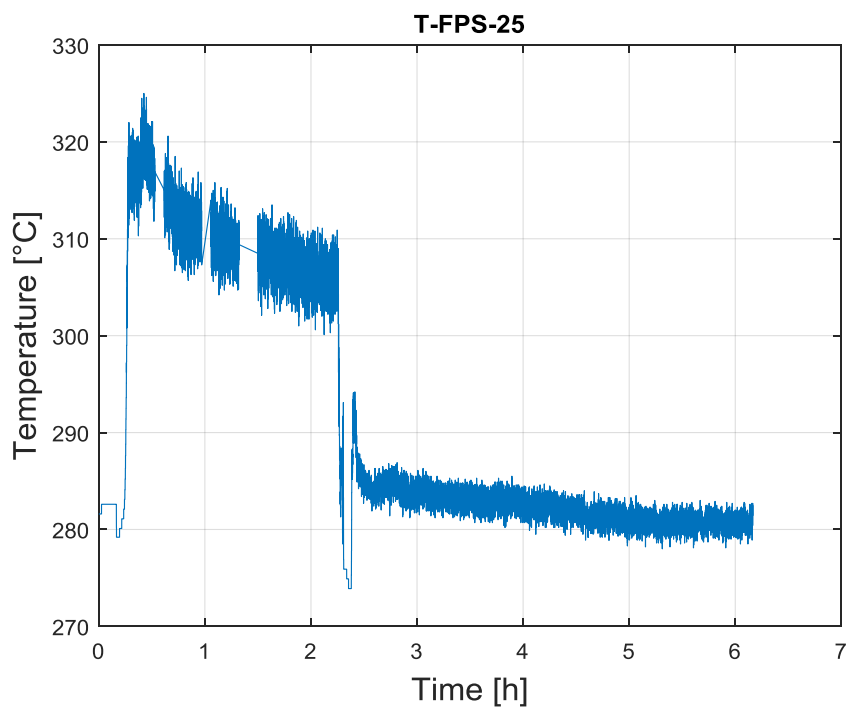


Figure 112: T-FPS-25 LBE temperature (Test 2)

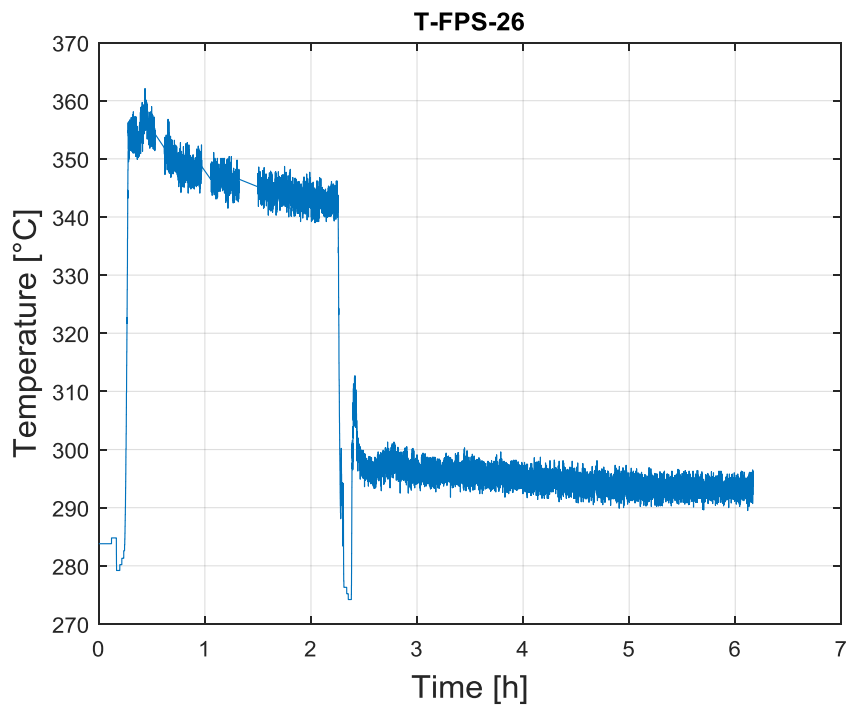


Figure 113: T-FPS-26 LBE temperature (Test 2)

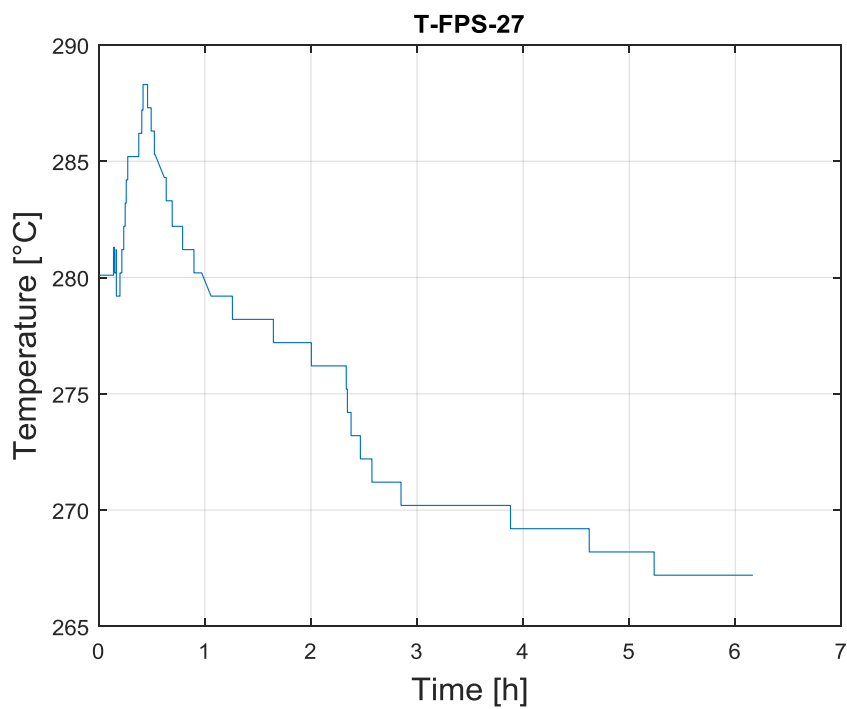


Figure 114: T-FPS-27 LBE temperature (Test 2)

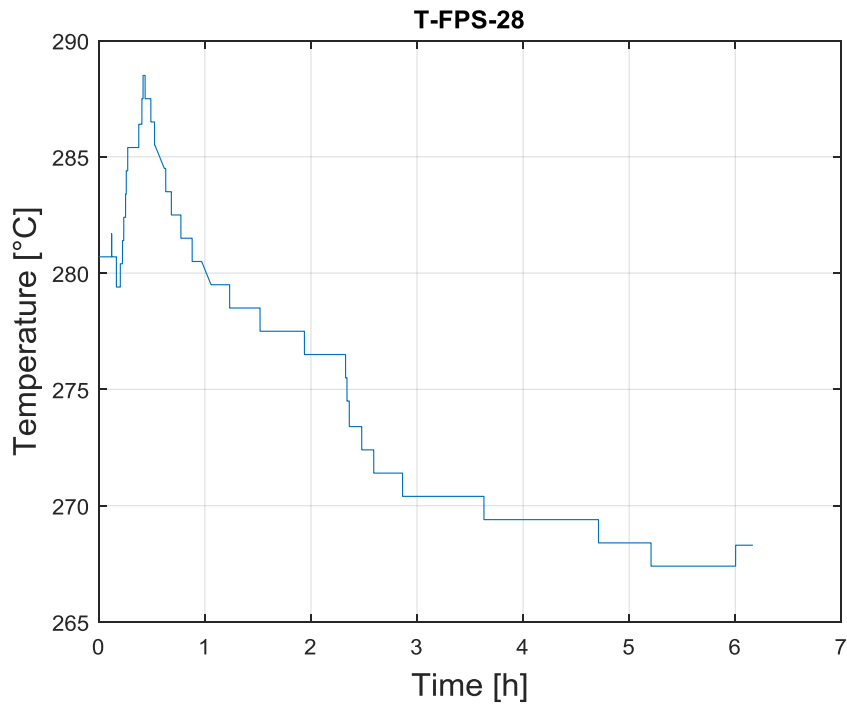


Figure 115: T-FPS-28 LBE temperature (Test 2)

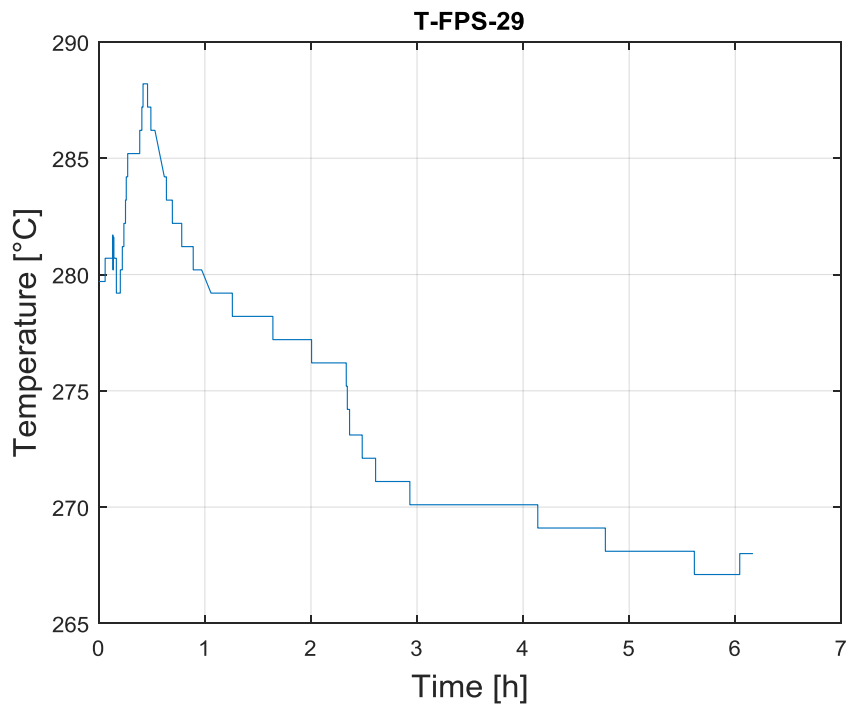



Figure 116: T-FPS-29 LBE temperature (Test 2)

 DIVISIONE INGEGNERIA SPERIMENTALE	<u>Title</u> D3.2: CIRCE experiments: pre-test, data-set and analysis	<u>Distribution</u> PUBLIC	<u>Emission</u> 09/08/2017	<u>Pag.</u> 74 di 234
		<u>Ref.</u> CI-T-R-292	Rev. 0	

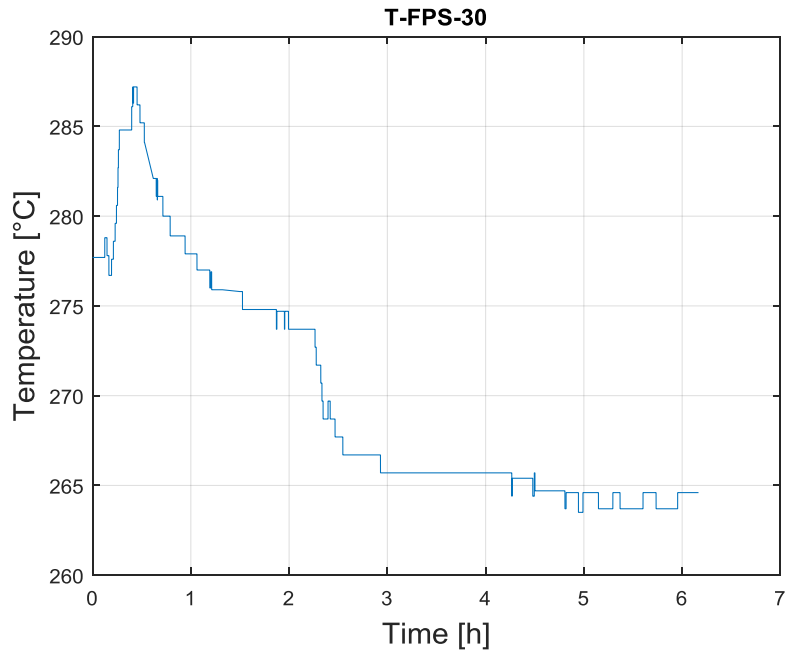


Figure 117: T-FPS-30 LBE temperature (Test 2)

The LBE heated by the FPS flows through the fitting volume into the riser (see Annex A Fig. 3 0016 Instrumentation.pdf); here temperatures are measured using TCs with a diameter of 3 mm disposed at the entrance section (T-TS-01 to 03) and at the exit section before the separator (T-TS-04 to 06). In Figure 118 the riser inlet/outlet averaged temperature is reported.

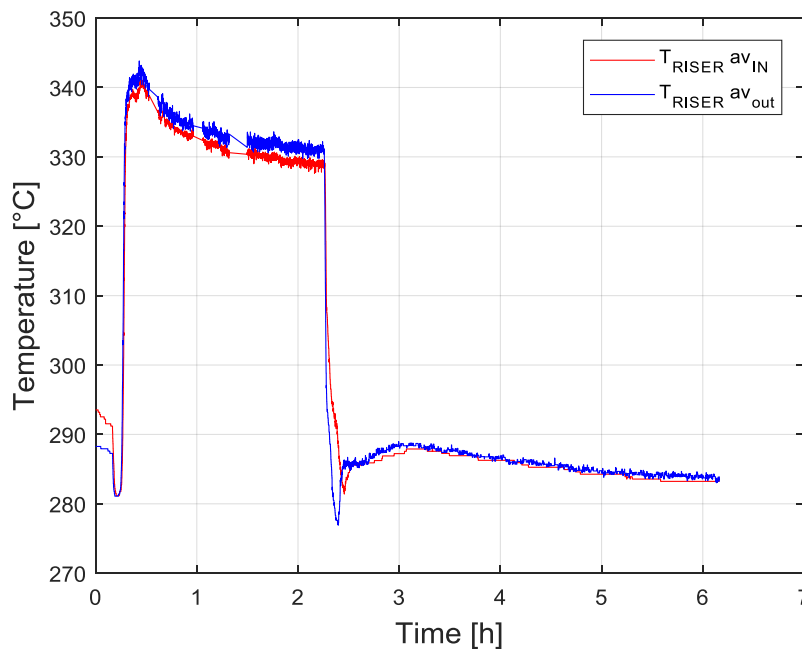



Figure 118: Inlet/Outlet average temperature in the Riser

 DIVISIONE INGEGNERIA SPERIMENTALE	<u>Title</u> D3.2: CIRCE experiments: pre-test, data-set and analysis	<u>Distribution</u> PUBLIC	<u>Emission</u> 09/08/2017	<u>Pag.</u> 75 di 234
		<u>Ref.</u> CI-T-R-292	Rev. 0	

From the riser exit, the LBE flows through the Separator into the HX shell, where the temperature at the entrance section is measured by three TCs placed at 120°, 30 mm from the bottom of the Separator (T-SG-01 ... 03, see Annex A Fig. 4 THINS thermocouples arrangement.pdf).

Sub-channel temperature measurements were taken in a plane placed 30 mm above the lower grid (see Annex A Fig. 10: 0700-Assieme-HX.pdf for the positioning of the grid), according to the scheme shown in Annex A Fig. 11: T-SG-0100-Disposizione TC Sottocanali GV.pdf (T-SG-04 ... 12).

The LBE temperature at the outlet section of the HX is measured by six thermocouples (T-SG-13 ... 18) placed at 60° each and at 100 mm before the HX skirt exit (see Annex A Fig. 12: T-SG-0101-Disposizione TC Uscita GV.pdf). In Figure 119 the average LBE temperature at the inlet and outlet sections of the HX is reported.

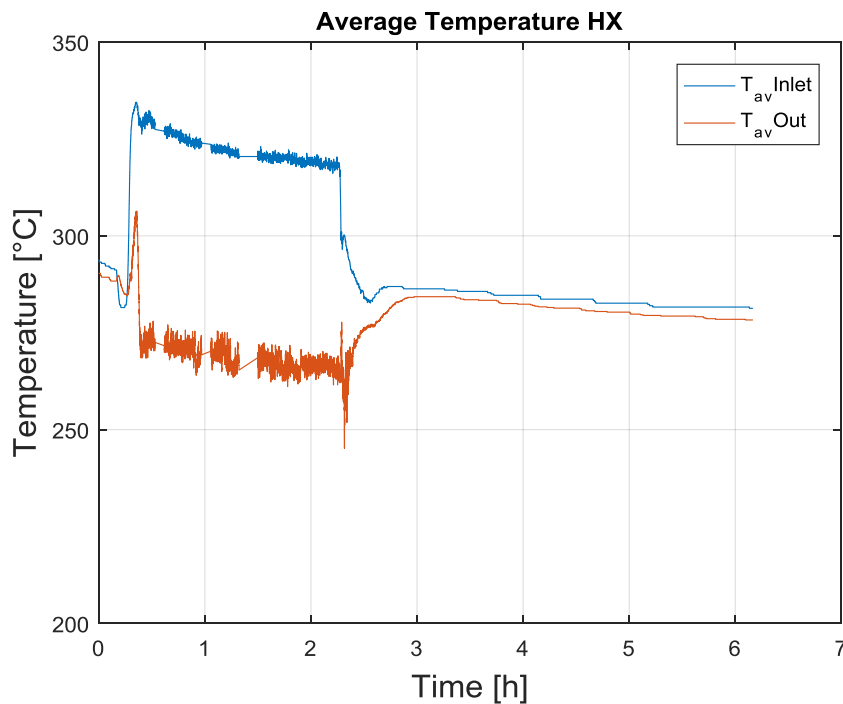


Figure 119: Inlet/Outlet average LBE temperature in the main HX

From plot Figure 120 to Figure 128 the temperature measured from each single thermocouple in the HX are reported (inlet and outlet sections and subchannels).

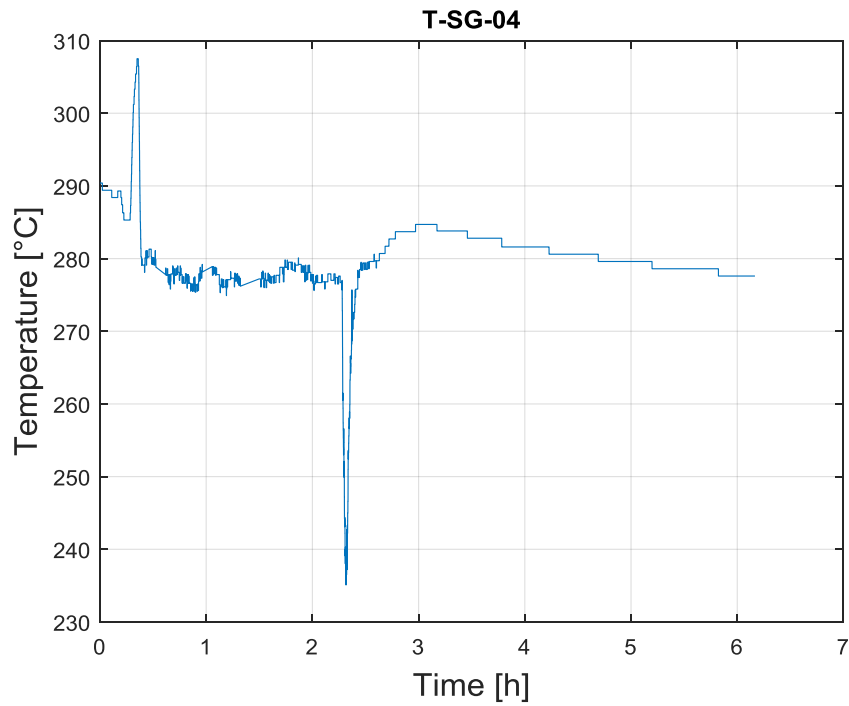


Figure 120: LBE temperature in the sub channel of the HX (T-SG-04, Test 2)

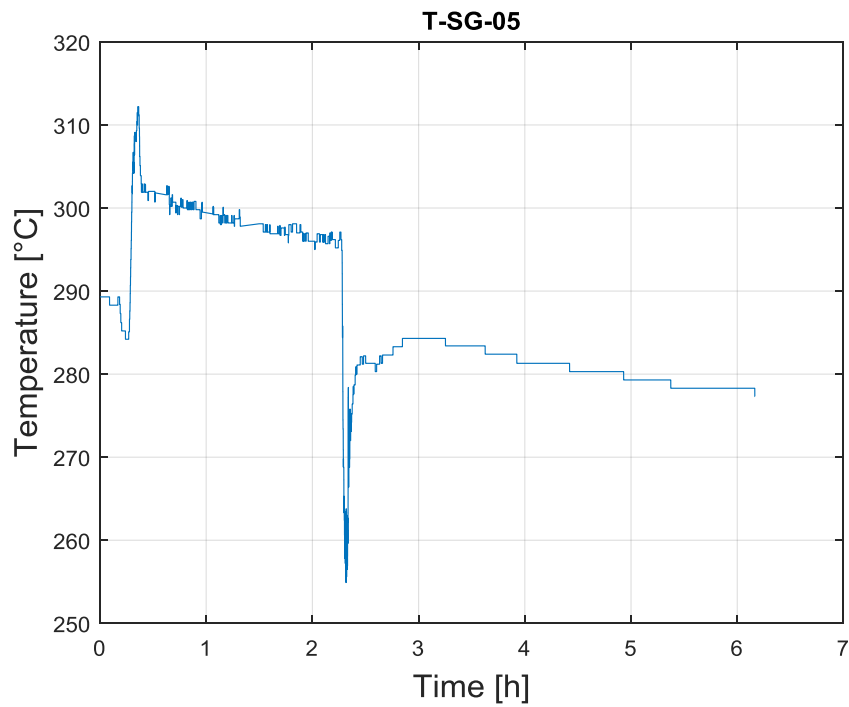



Figure 121: LBE temperature in the sub channel of the HX (T-SG-05, Test 2)

 DIVISIONE INGEGNERIA SPERIMENTALE	<u>Title</u> D3.2: CIRCE experiments: pre-test, data-set and analysis	<u>Distribution</u> PUBLIC	<u>Emission</u> 09/08/2017	<u>Pag.</u> 77 di 234
		<u>Ref.</u> CI-T-R-292	Rev. 0	

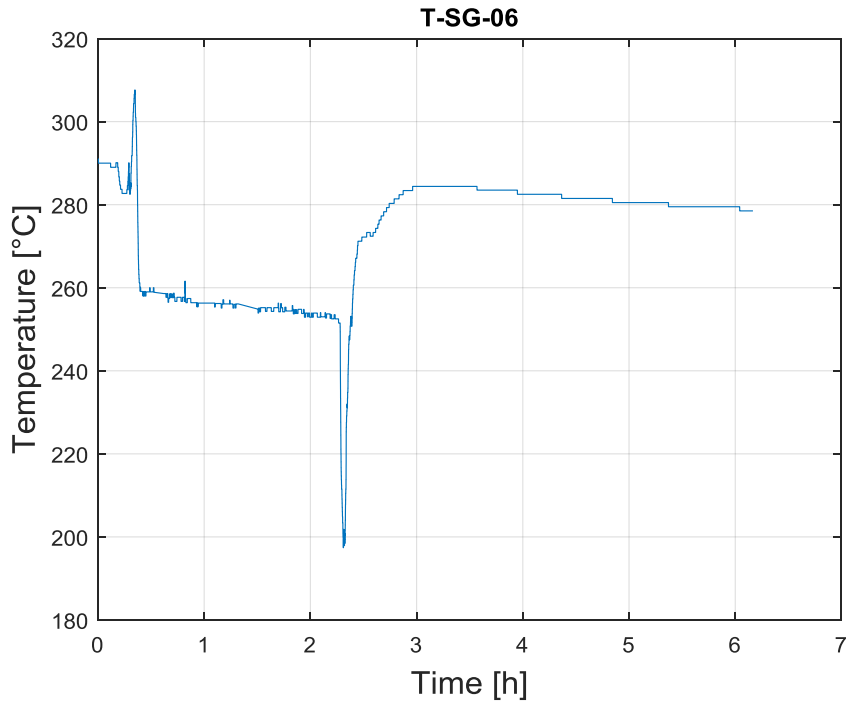


Figure 122: LBE temperature in the sub channel of the HX (T-SG-06, Test 2)

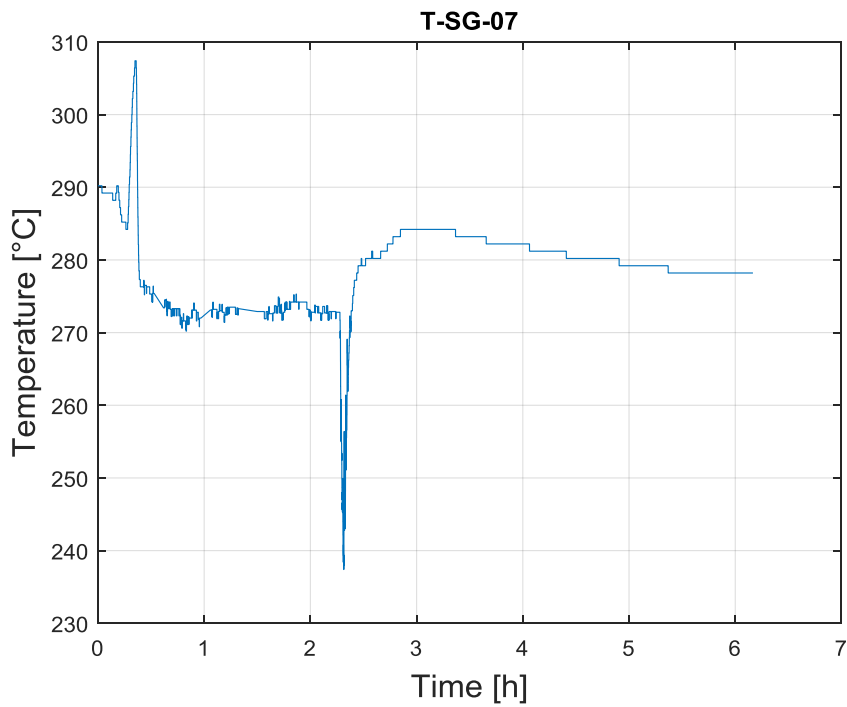



Figure 123: LBE temperature in the sub channel of the HX (T-SG-07, Test 2)

 DIVISIONE INGEGNERIA SPERIMENTALE	<u>Title</u> D3.2: CIRCE experiments: pre-test, data-set and analysis	<u>Distribution</u> PUBLIC	<u>Emission</u> 09/08/2017	<u>Pag.</u> 78 di 234
		<u>Ref.</u> CI-T-R-292	Rev. 0	

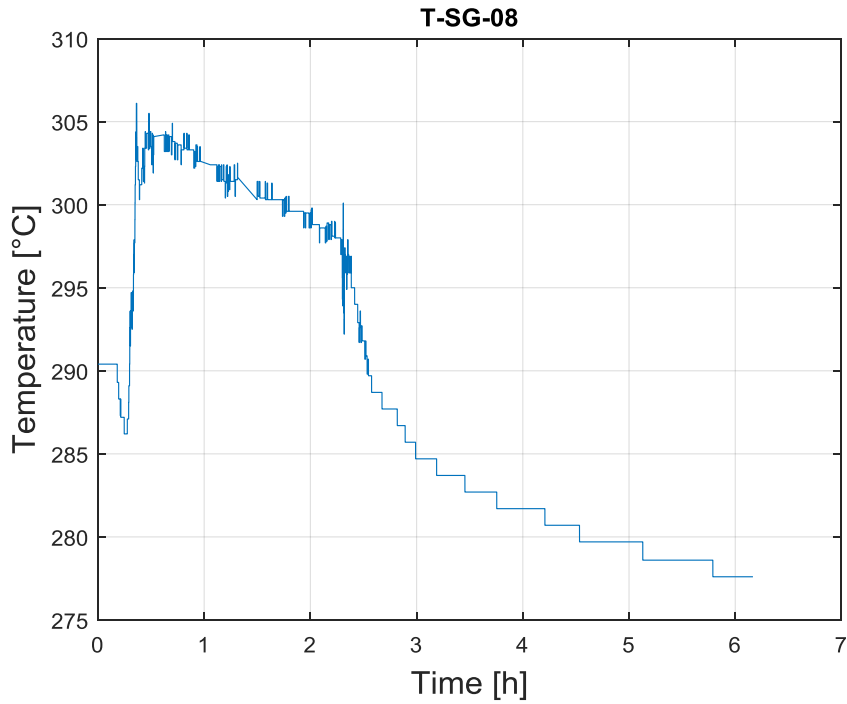


Figure 124: LBE temperature in the sub channel of the HX (T-SG-08, Test 2)

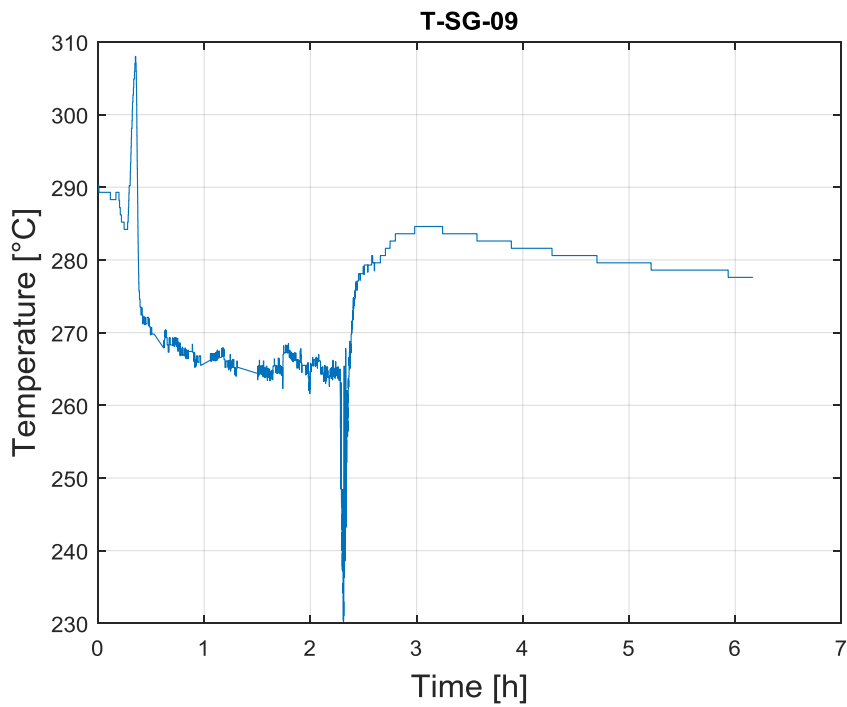


Figure 125: LBE temperature in the sub channel of the HX (T-SG-09, Test 2)

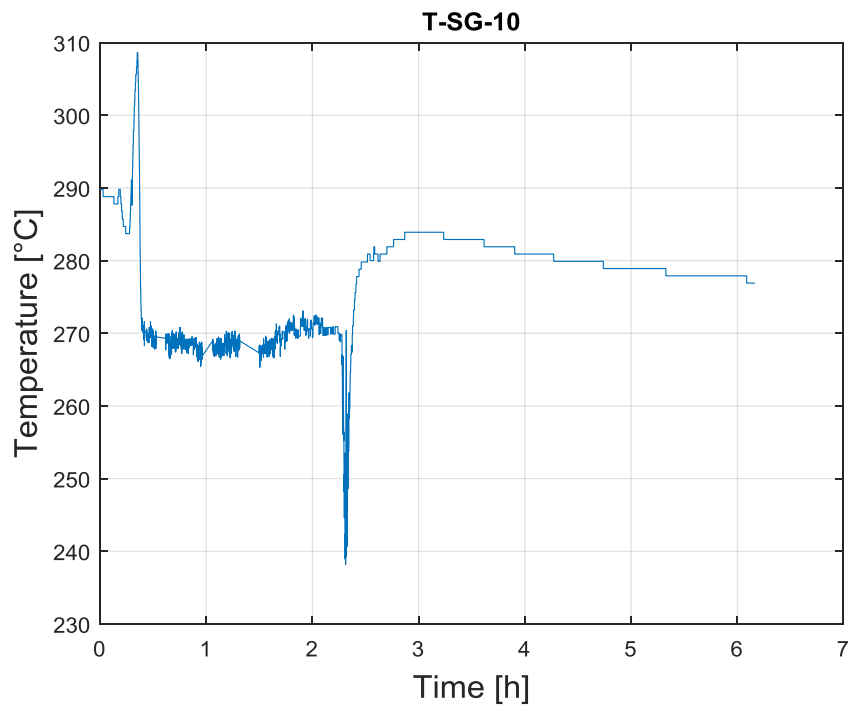


Figure 126: LBE temperature in the sub channel of the HX (T-SG-10, Test 2)

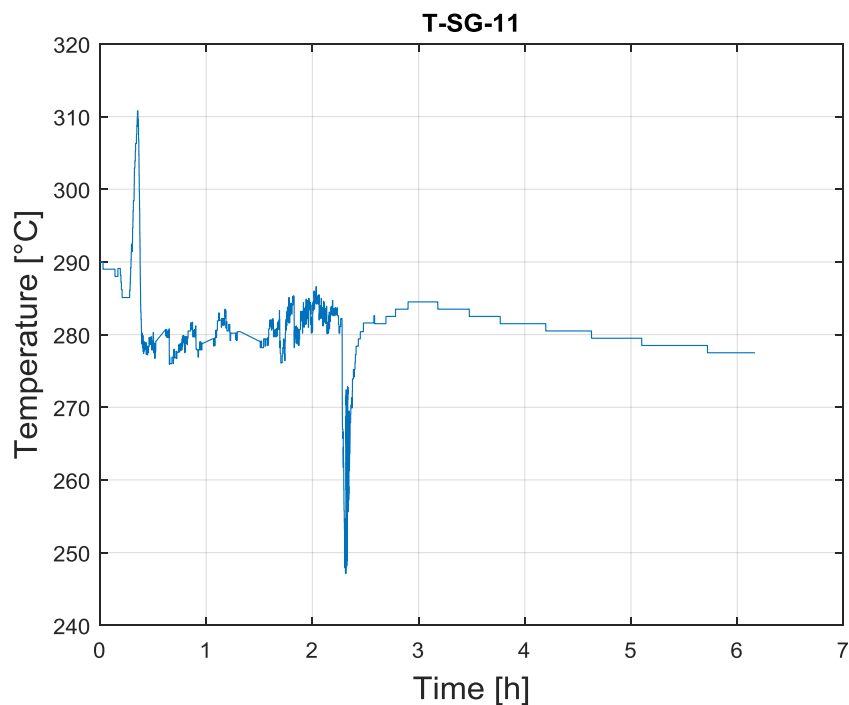



Figure 127: LBE temperature in the sub channel of the HX (T-SG-11, Test 2)

 DIVISIONE INGEGNERIA SPERIMENTALE	<u>Title</u> D3.2: CIRCE experiments: pre-test, data-set and analysis	<u>Distribution</u> PUBLIC	<u>Emission</u> 09/08/2017	<u>Pag.</u> 80 di 234
		<u>Ref.</u> CI-T-R-292	Rev. 0	

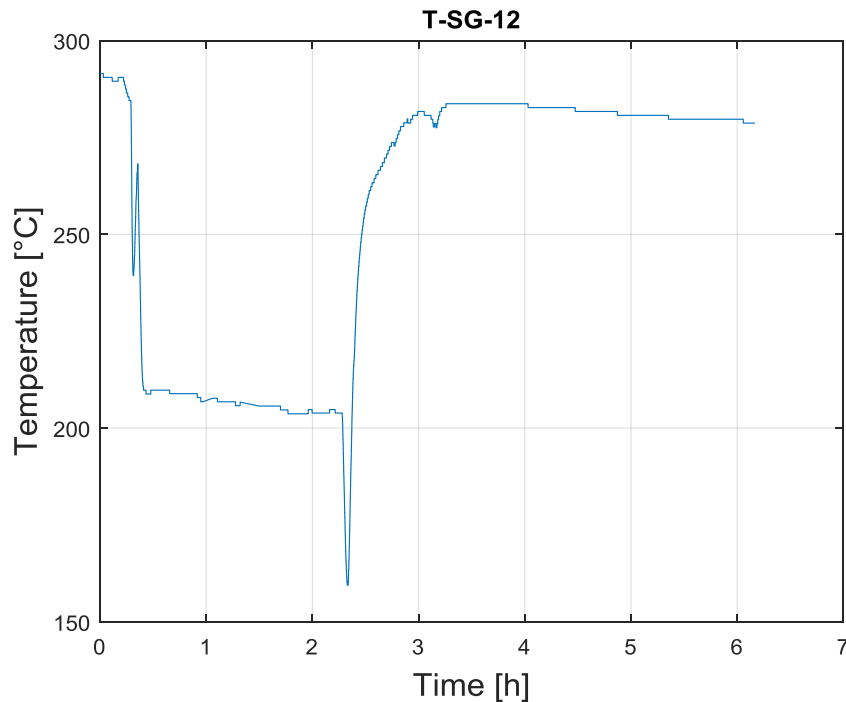


Figure 128: LBE temperature in the sub channel of the HX (T-SG-12, Test 2)

After passing through the HX, the LBE returned into the pool. Here, thermocouples for the measurements of LBE temperature were maintained in the fixed positions by vertical rods at 17 different elevations (see Annex A Fig. 13 T-MS-0101 TC per Mix&Strat.pdf) and 9 different radial position (see Annex A Fig. 14 T-MS-0100-Posizione TC Mix&Strat su piani di misura.pdf) for a total of 119 TCs with a diameter of 3 mm (T-MS-01 ... 119). In particular, with reference to Annex A Fig. 13 T-MS-0101 TC per Mix&Strat.pdf and Annex A Fig. 14 T-MS-0100-Posizione TC Mix&Strat su piani di misura.pdf, TCs on lines *A, H, I* allow measurement from the bottom side of the test section up to the FPS entrance, while TCs on lines *B, C, D, E, F, G* allow measurement up to 600 mm below the exit of the DHR.

From Figure 129 to Figure 137 the LBE temperature in the pool is reported along the vertical lines *A, B, C, D, E, F, G, H* and *I*.

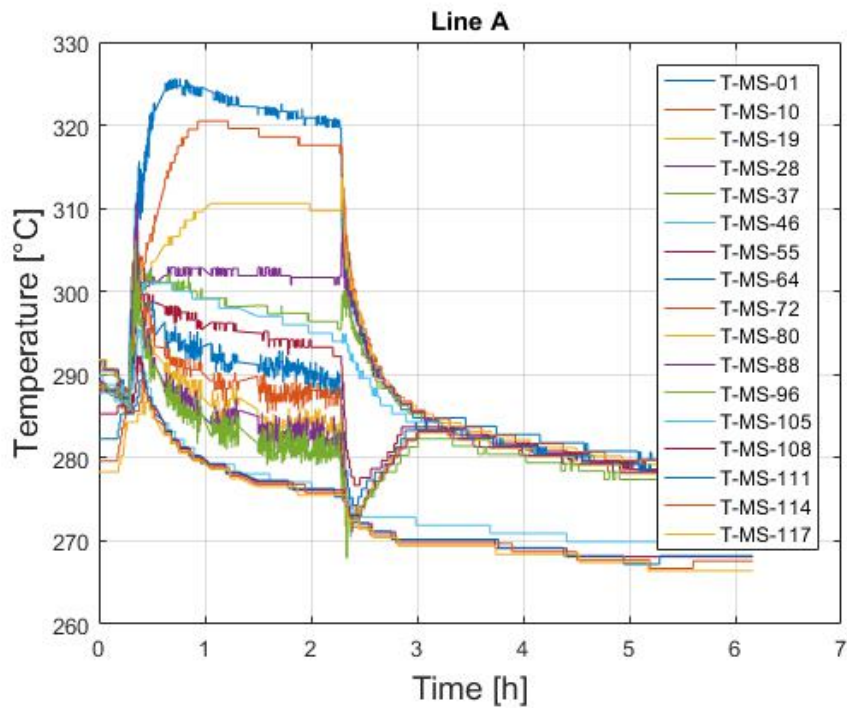


Figure 129: Temperature in the pool along Line A (Test 2)

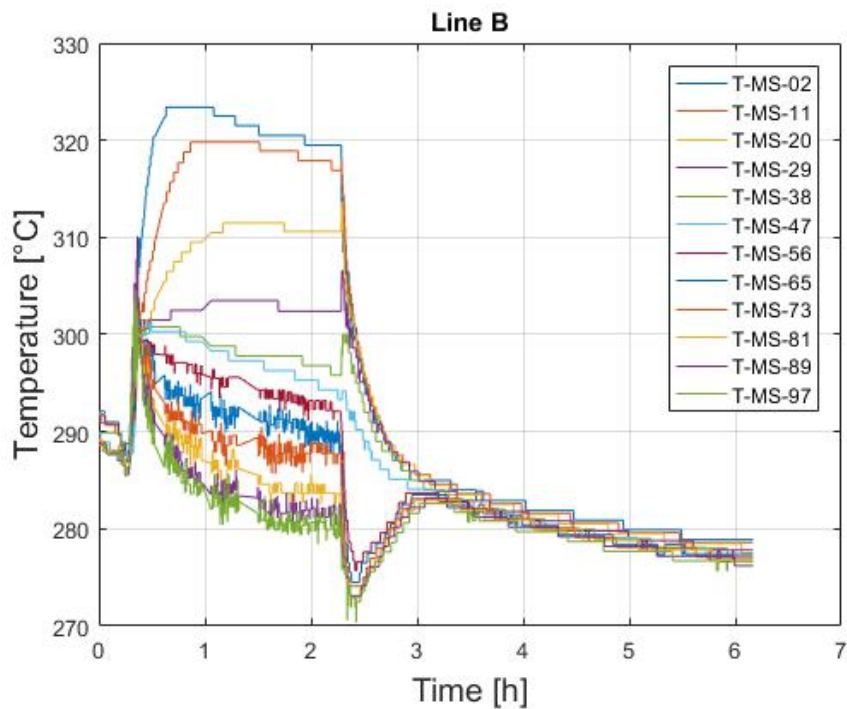


Figure 130: Temperature in the pool along Line B (Test 2)

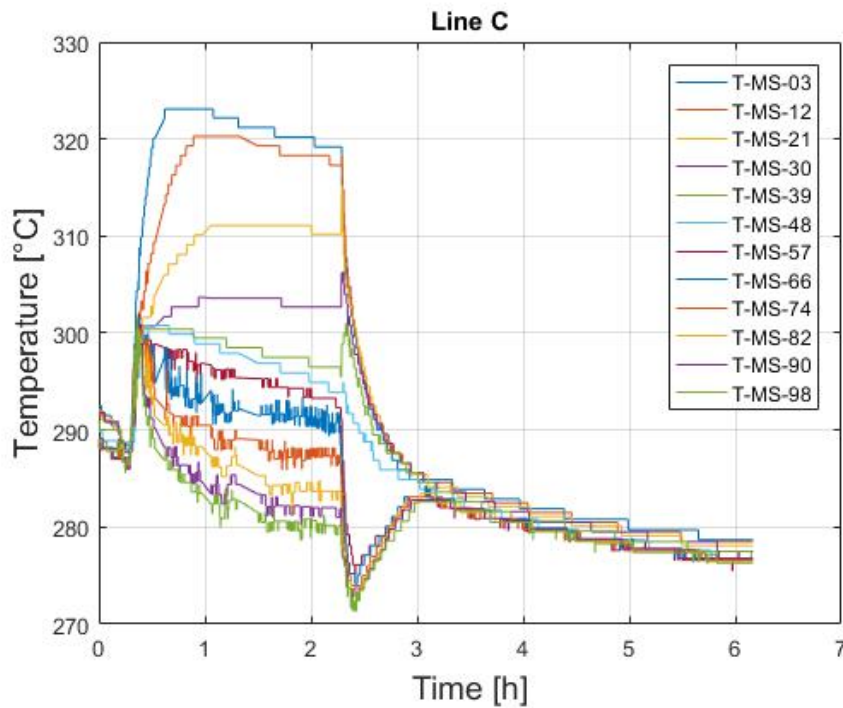


Figure 131: Temperature in the pool along Line C (Test 2)

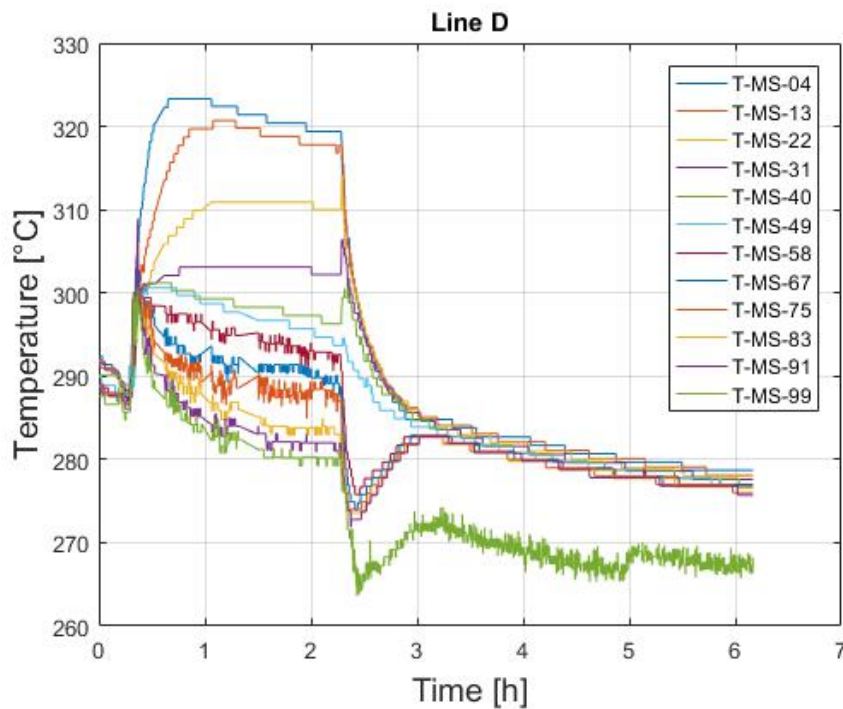


Figure 132: Temperature in the pool along Line D (Test 2)

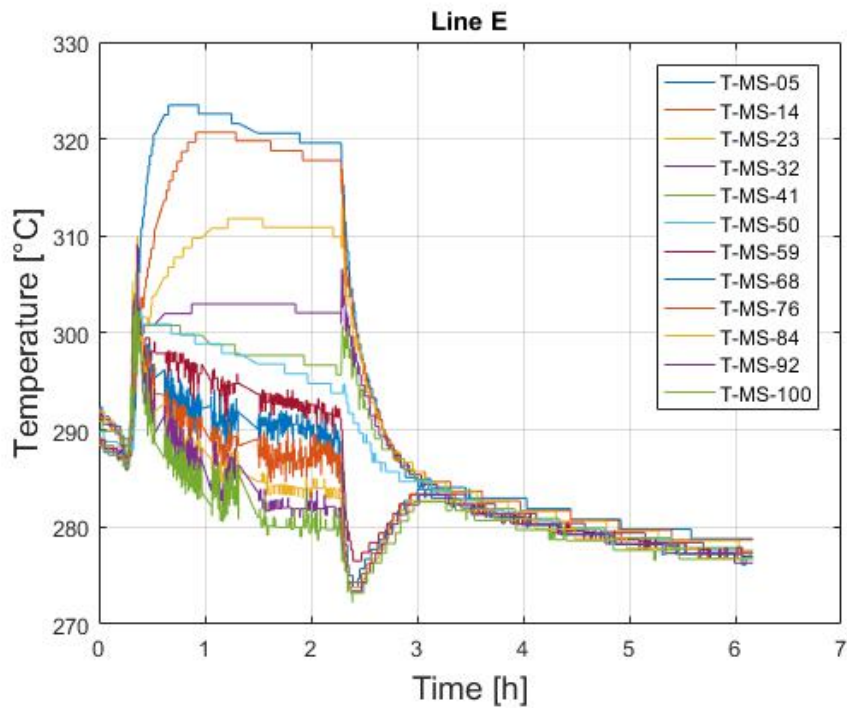


Figure 133: Temperature in the pool along Line E (Test 2)

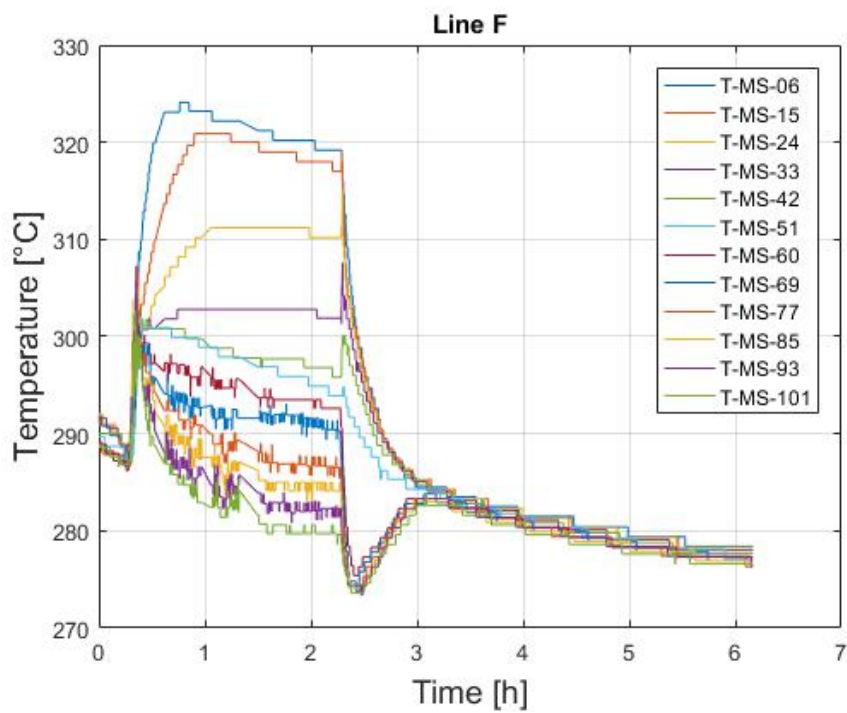


Figure 134: Temperature in the pool along Line F (Test 2)

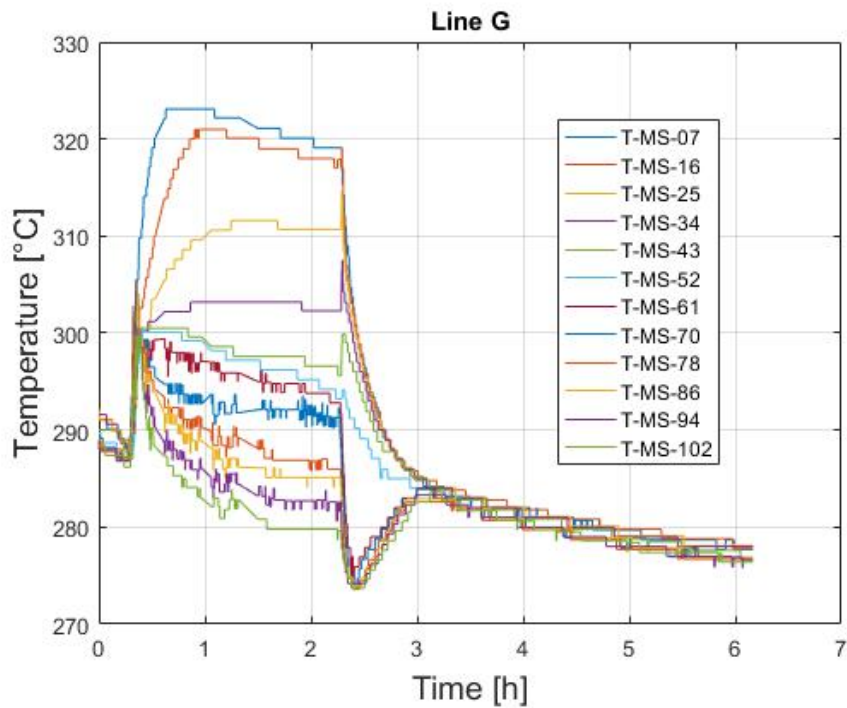


Figure 135: Temperature in the pool along Line G (Test 2)

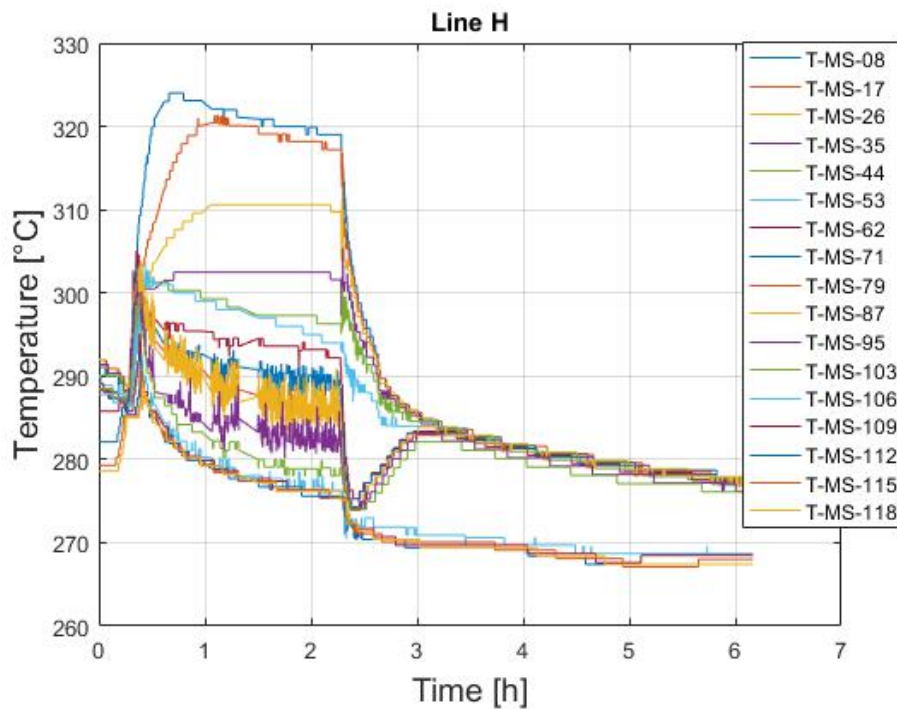



Figure 136: Temperature in the pool along Line H (Test 2)

 DIVISIONE INGEGNERIA SPERIMENTALE	<u>Title</u> D3.2: CIRCE experiments: pre-test, data-set and analysis	<u>Distribution</u> PUBLIC	<u>Emission</u> 09/08/2017	<u>Pag.</u> 85 di 234
		<u>Ref.</u> CI-T-R-292	Rev. 0	

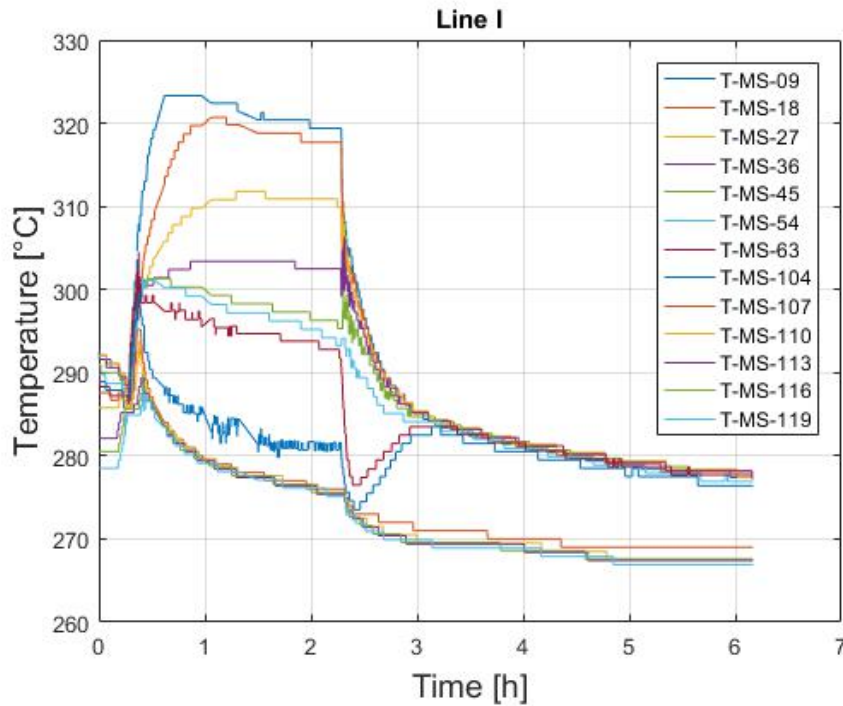



Figure 137: Temperature in the pool along Line I (Test 2)

3.3 Test 3

Test 3 is characterized by a nominal power ramp from 0 to 750 kW. The ramp starts at $t=3026$ s and stops at about 3167 s, the mean value of the power during the full power transient is about 750.3 kW with a standard deviation of 8.65 kW. The “full power” transient stops at $t=37727$ s with a descending ramp up to about 40 kW ($t\sim 37902$ s, STD ~ 0.3 kW) and then at $t=47691$ s the electrical power is reduced to about 30 kW (STD ~ 0.4). The end of the low power run is at $t=356400$ s (~ 99 h). The electric power (DC-KW) time trend is reported in Figure 138.

 DIVISIONE INGEGNERIA SPERIMENTALE	<u>Title</u> D3.2: CIRCE experiments: pre-test, data-set and analysis	<u>Distribution</u> PUBLIC	<u>Emission</u> 09/08/2017	<u>Pag.</u> 86 di 234
		<u>Ref.</u> CI-T-R-292	Rev. 0	

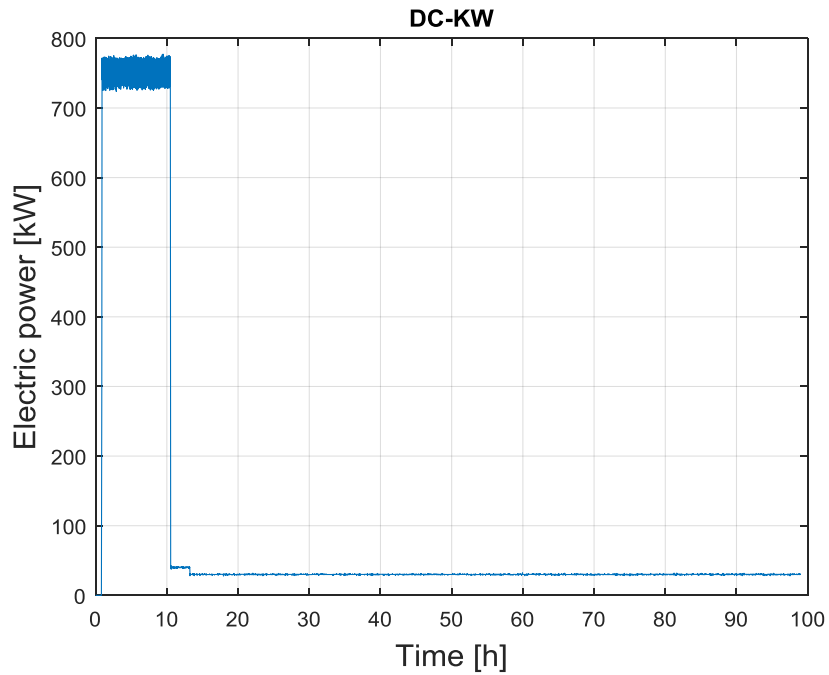



Figure 138: Electric Power [kW] (Test 3)

During the full power transient, the main heat exchanger is fed by a water mass flow rate with a mean value of 0.59 kg/s (FE501 see Figure 139) and a standard deviation 0.02 kg/s. After the simulation of the accidental scenario the water injection is stopped at about $t=37794$ s.

 DIVISIONE INGEGNERIA SPERIMENTALE	<u>Title</u> D3.2: CIRCE experiments: pre-test, data-set and analysis	<u>Distribution</u> PUBLIC	<u>Emission</u> 09/08/2017	<u>Pag.</u> 87 di 234
		<u>Ref.</u> CI-T-R-292	Rev. 0	

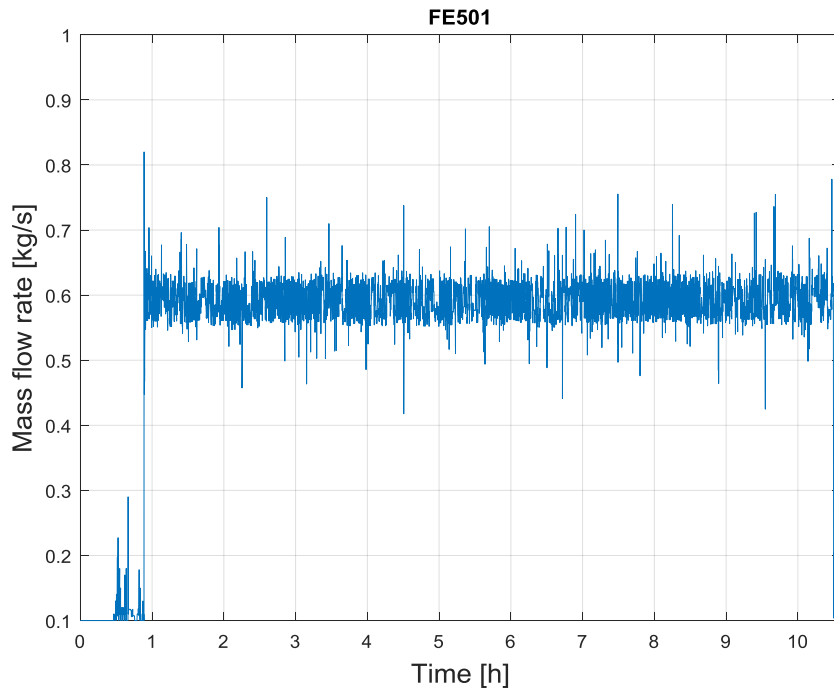


Figure 139: Water mass flow rate (Test 3)

Pressure and temperature of the water at the inlet of the HX are reported in Figure 140 and Figure 141 respectively.

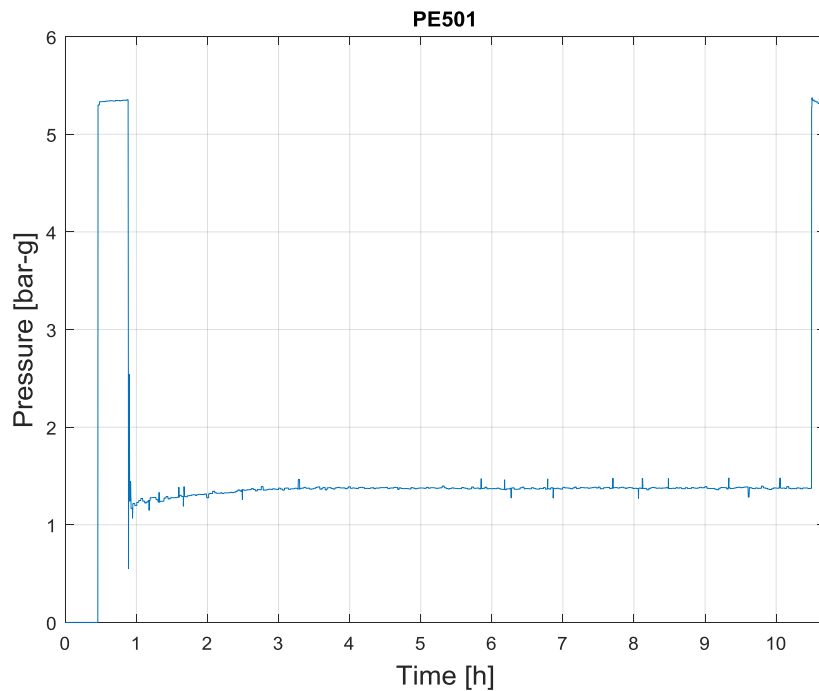



Figure 140: Water inlet pressure (Test 3)

 DIVISIONE INGEGNERIA SPERIMENTALE	<u>Title</u> D3.2: CIRCE experiments: pre-test, data-set and analysis	<u>Distribution</u> PUBLIC	<u>Emission</u> 09/08/2017	<u>Pag.</u> 88 di 234
		<u>Ref.</u> CI-T-R-292	Rev. 0	

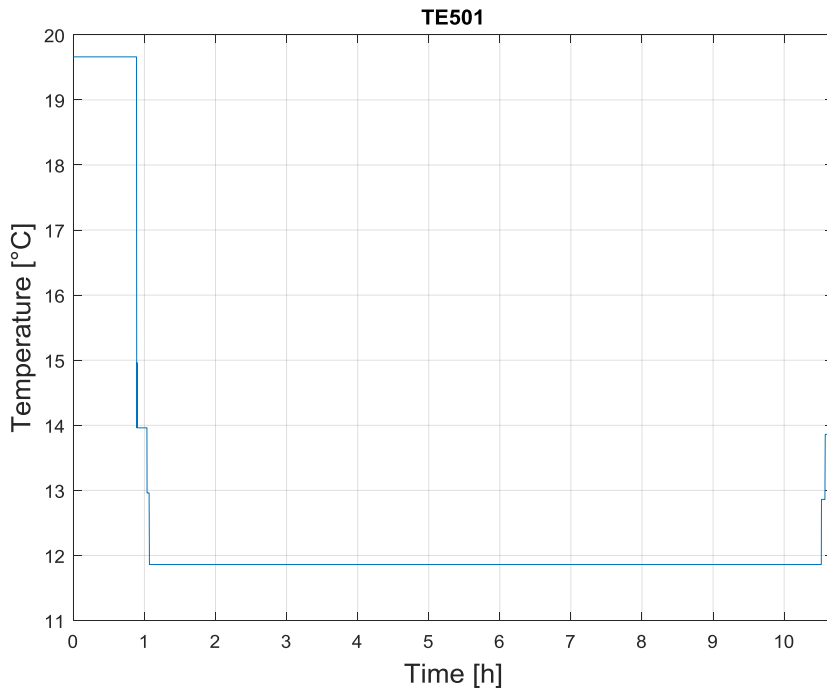


Figure 141: Water inlet temperature (Test 3)

Temperature of the steam at the outlet of the HX is reported in Figure 142.

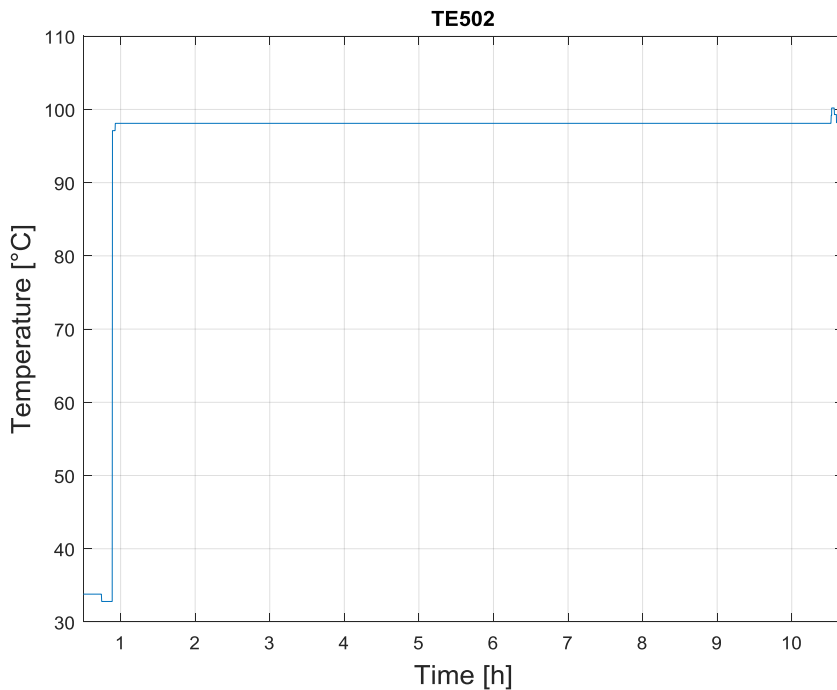



Figure 142: Steam temperature at the outlet of the HX (Test 3)

The Temperature of the helium gas entrapped in the gap between the tubes of the HX is reported in Figure 143.

 DIVISIONE INGEGNERIA SPERIMENTALE	<u>Title</u> D3.2: CIRCE experiments: pre-test, data-set and analysis	<u>Distribution</u> PUBLIC	<u>Emission</u> 09/08/2017	<u>Pag.</u> 89 di 234
		<u>Ref.</u> CI-T-R-292	Rev. 0	

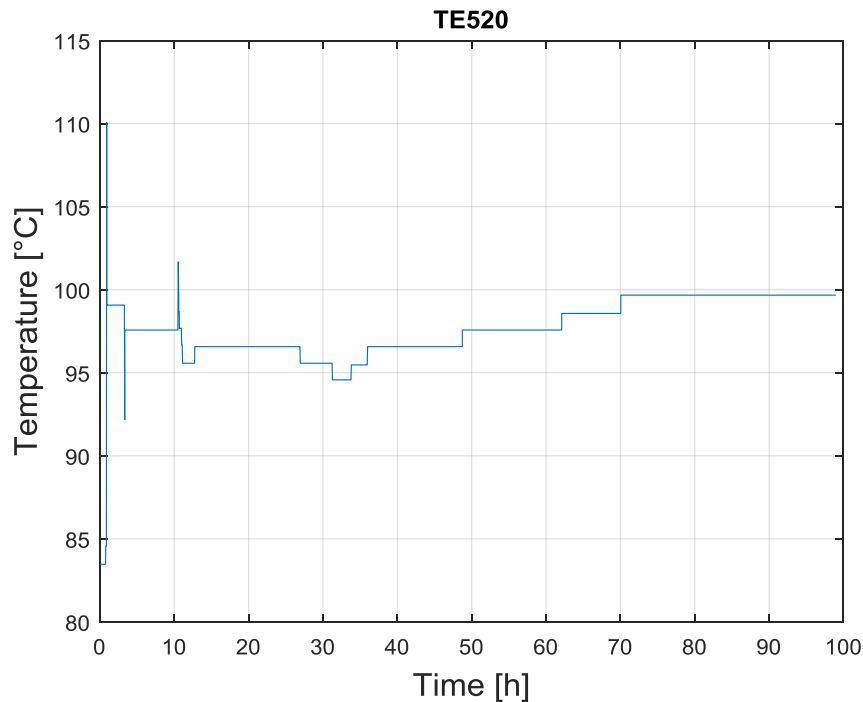


Figure 143: He temperature in the gap between the HX tubes (Test 3)

After experimental TEST 2 the argon gas circuit was upgraded with the installation of a new argon mass flow controller (FE400, see Annex B) directly operated from the control panel and connected to a new reservoir (V-400) in order to dump the mass flow rate oscillations caused by the compressors.

The gas injection, reported in Figure 144, started at $t=1588$ s and reach a value of about 2.46 NI/s at $t= 2000$ s and it is maintained at this value up to about 3297 s and then the argon flow rate is increased up to 2.76 NI/s and maintained at this value up to $t= 37792$ s.

In the low power transient the decay heat removal system (DHR) is activated injecting air in the bayonet tube of the DHR. The injection of air starts at $t=37980$ s. As shown in Figure 145, the air mass flow rate mean value is 200 g/s up to the end of the test. The standard deviation is about 0.8 g/s. Inlet and outlet air temperature in the DHR are shown in Figure 146 and Figure 147. In Figure 148 the air velocity in the DHR is plotted, the mean value is 22.9 m/s.

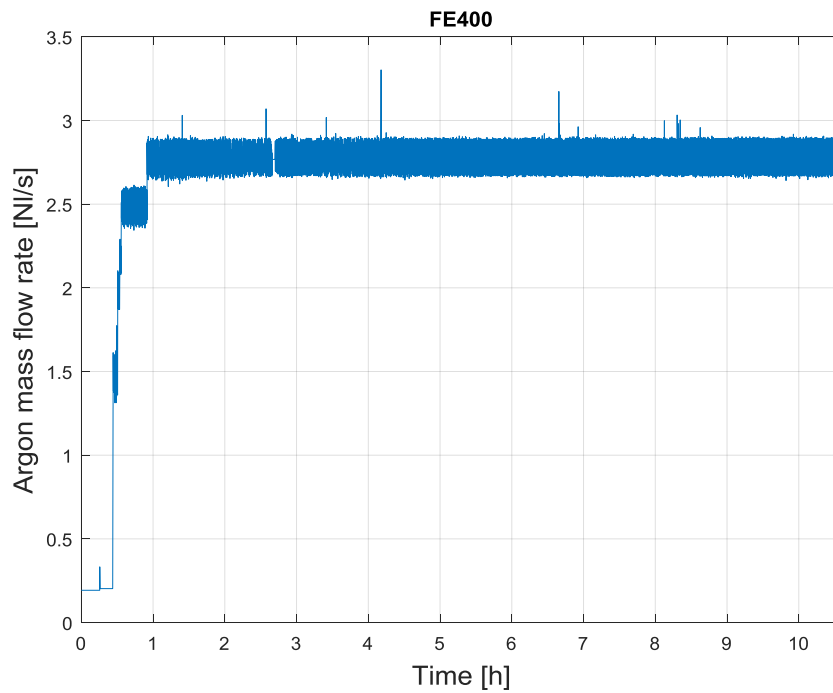


Figure 144: Argon mass flow rate (Test 3)

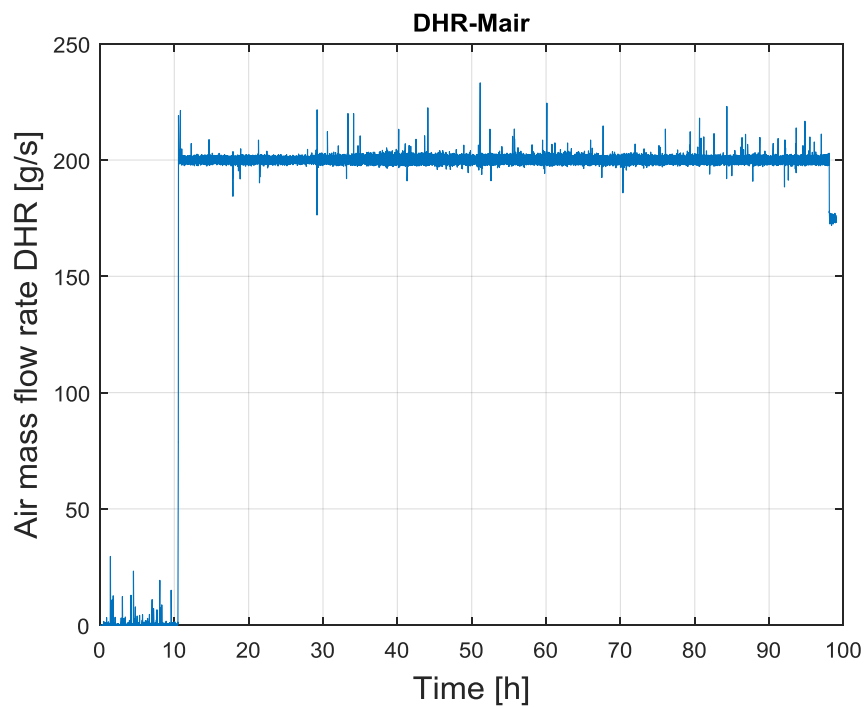


Figure 145: DHR air mass flow rate (Test 3)

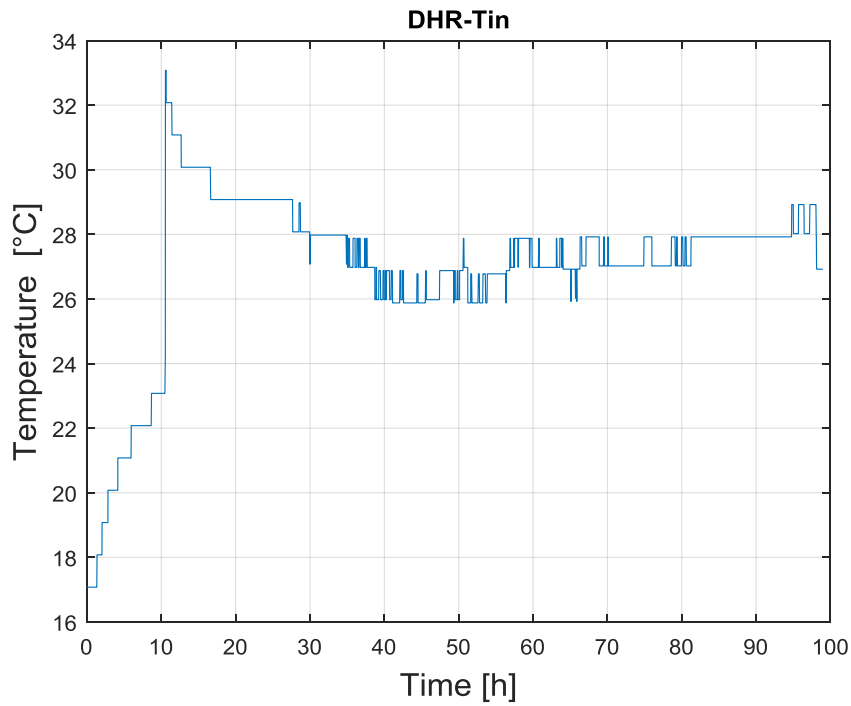


Figure 146: DHR inlet air temperature (Test3)

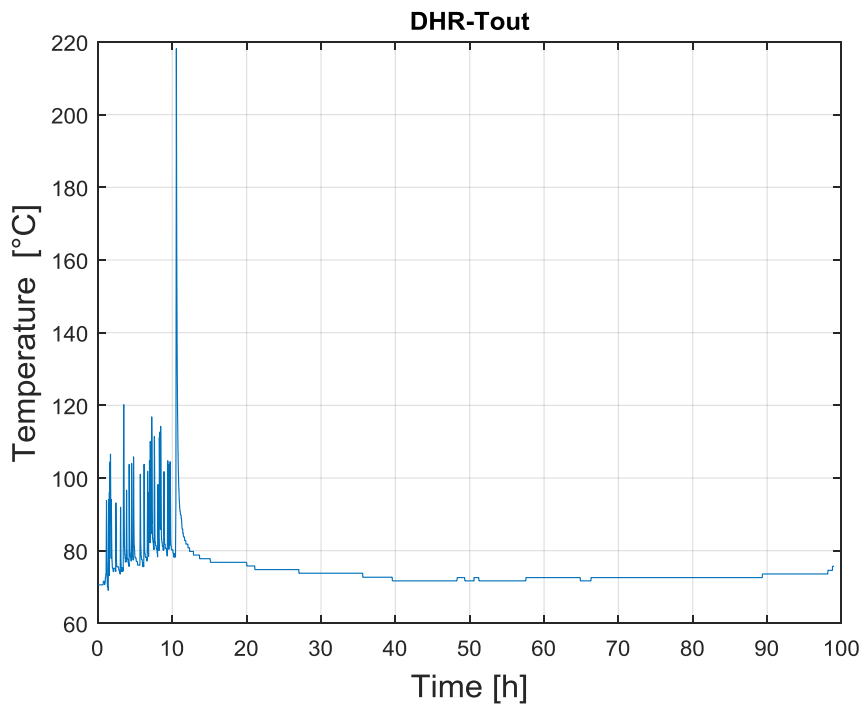



Figure 147: DHR outlet air temperature (Test3)

 DIVISIONE INGEGNERIA SPERIMENTALE	<u>Title</u> D3.2: CIRCE experiments: pre-test, data-set and analysis	<u>Distribution</u> PUBLIC	<u>Emission</u> 09/08/2017	<u>Pag.</u> 92 di 234
		<u>Ref.</u> CI-T-R-292	Rev. 0	

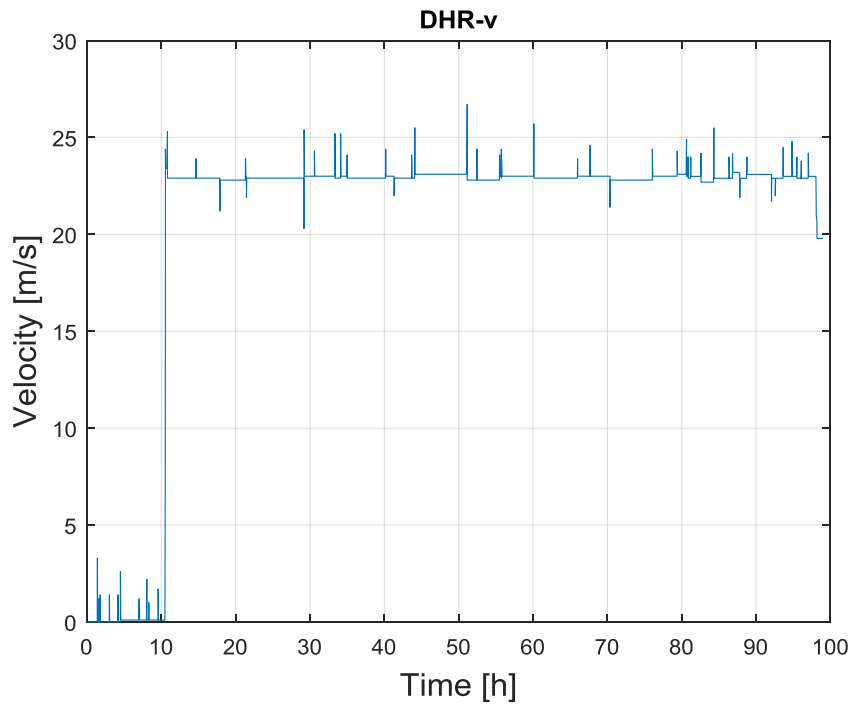



Figure 148: DHR air velocity (Test 3)

The pressure difference across the venturi flow meter (see Annex A Fig. 1 Mass flow Meter/08-384-DISEGNO.pdf) used to evaluate the LBE mass flow rate in the ICE test section is reported in Figure 149.

 DIVISIONE INGEGNERIA SPERIMENTALE	<u>Title</u> D3.2: CIRCE experiments: pre-test, data-set and analysis	<u>Distribution</u> PUBLIC	<u>Emission</u> 09/08/2017	<u>Pag.</u> 93 di 234
		<u>Ref.</u> CI-T-R-292	Rev. 0	

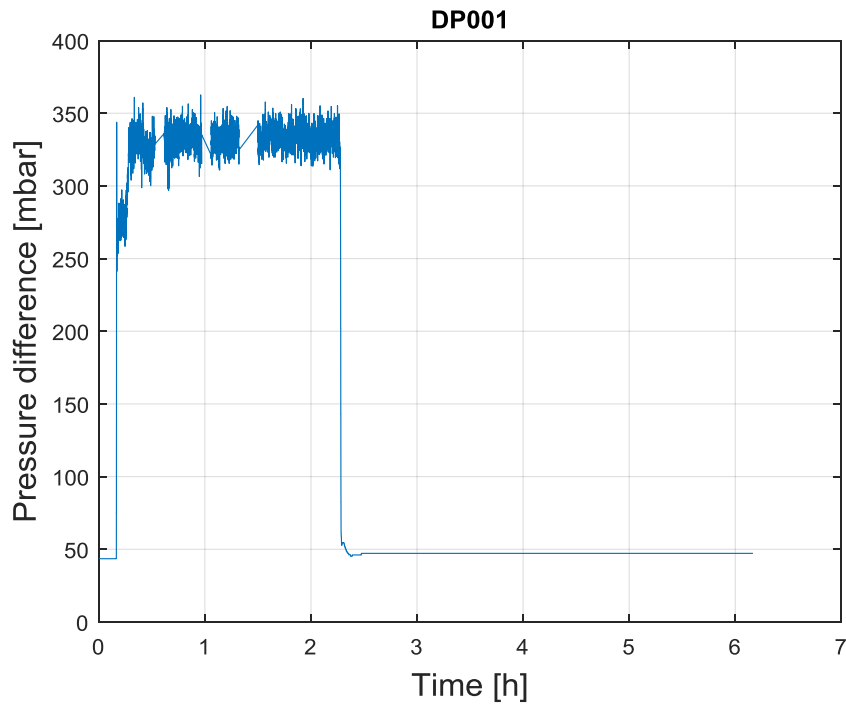



Figure 149: Pressure difference across the venturi flow meter (Test 3)

DP002 (PE009-PE010), reported in Figure 150, represents the pressure difference across the lower spacer grid (for the positioning of the bubble tubes see Annex A Fig. 2 0510 Rev 1-Fuel Pin Simulator.pdf).

PE003 represents the pressure in the fitting volume (Figure 151) while PE004 (Figure 152), PE005 (Figure 153) represent respectively the pressure in the lower and upper section of the riser. For the position of the bubble tubes PE003, PE004, PE005 see Annex A Fig. 3 0016 Instrumentation.pdf.

 DIVISIONE INGEGNERIA SPERIMENTALE	<u>Title</u> D3.2: CIRCE experiments: pre-test, data-set and analysis	<u>Distribution</u> PUBLIC	<u>Emission</u> 09/08/2017	<u>Pag.</u> 94 di 234
		<u>Ref.</u> CI-T-R-292	Rev. 0	

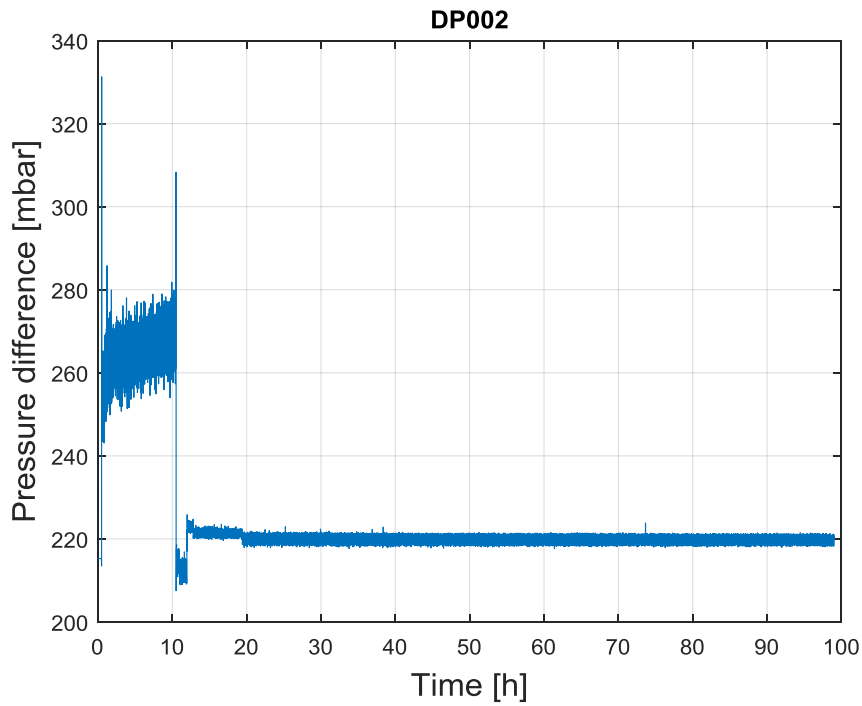


Figure 150: Pressure difference across the FPS lower spacer grid (Test 3)

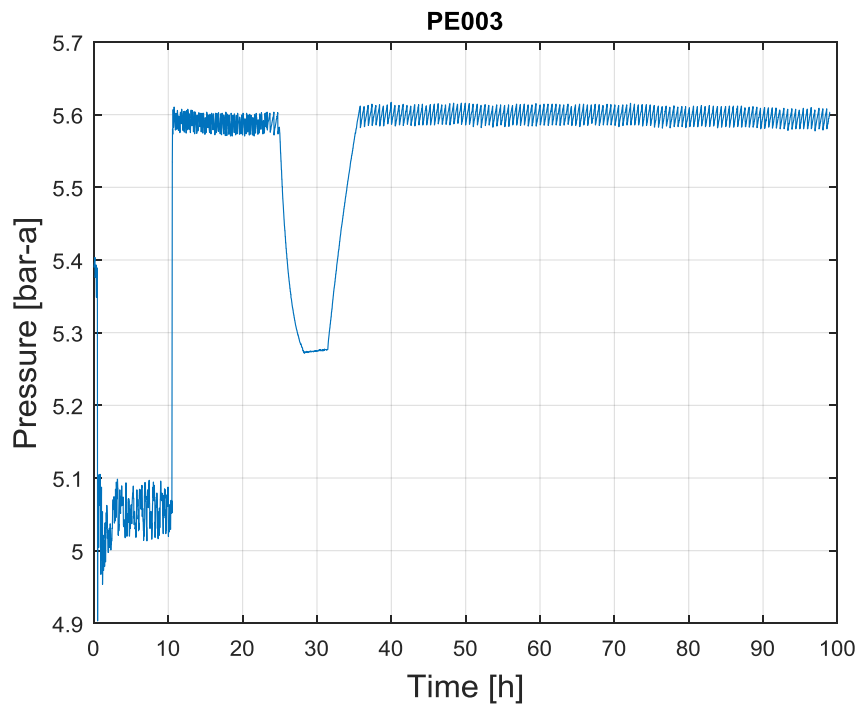


Figure 151: Pressure in the fitting volume (Test 3)

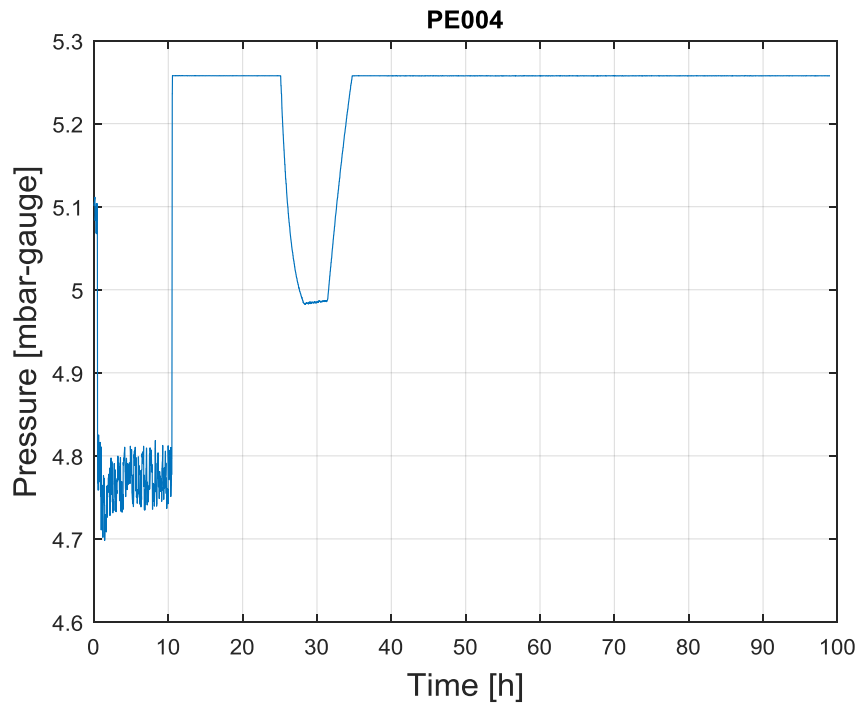


Figure 152: Pressure in the riser (lower section) (Test 3)

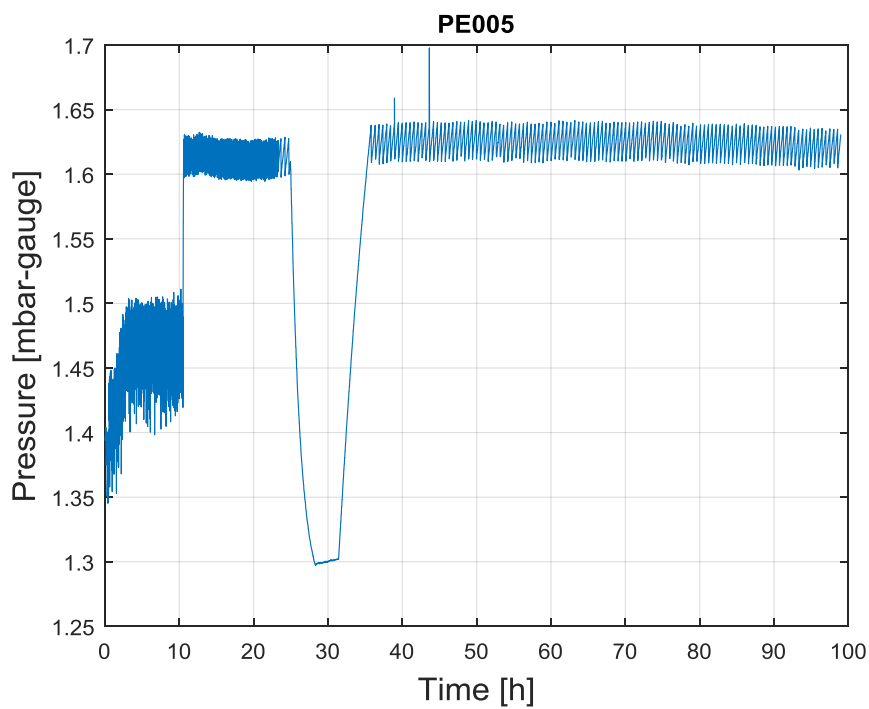



Figure 153: Pressure in the riser (upper section) (Test 3)

 DIVISIONE INGEGNERIA SPERIMENTALE	<u>Title</u> D3.2: CIRCE experiments: pre-test, data-set and analysis	<u>Distribution</u> PUBLIC	<u>Emission</u> 09/08/2017	<u>Pag.</u> 96 di 234
		<u>Ref.</u> CI-T-R-292	Rev. 0	

The LBE inside the pool is operated under a protective atmosphere of Argon gas that fill the volume from the LBE free level to the vessel head. A relative small overpressure is maintained in the gas in order to avoid oxygen contamination from the external environment. PE007 is the pressure of the argon measured in the cover gas (pressure gauge, see Figure 154), while the temperature of the cover gas is measured through a 3 mm K-type thermocouple and reported in Figure 155.

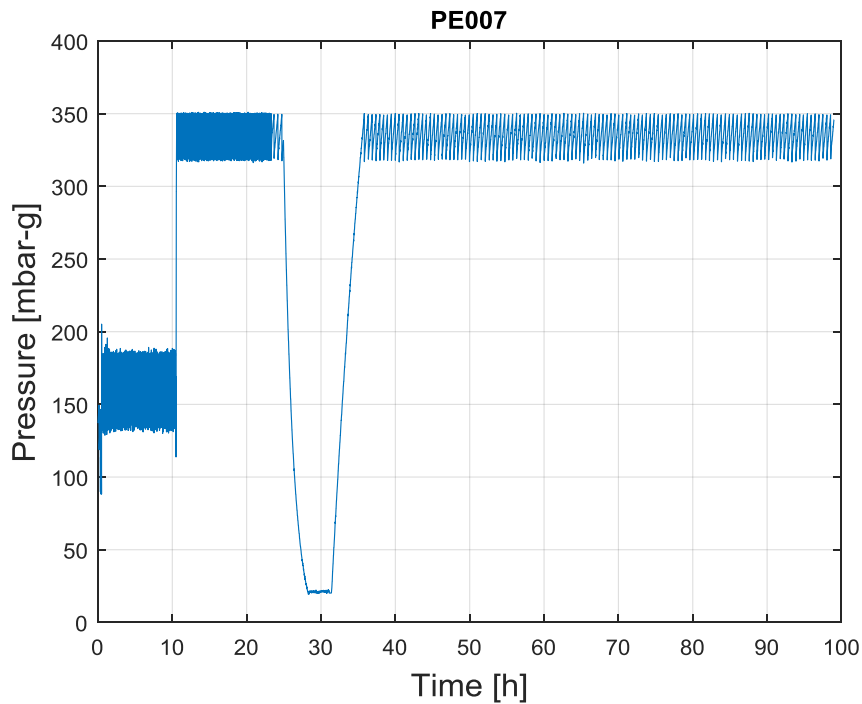



Figure 154: Pressure in the cover gas (Test 3)

 DIVISIONE INGEGNERIA SPERIMENTALE	<u>Title</u> D3.2: CIRCE experiments: pre-test, data-set and analysis	<u>Distribution</u> PUBLIC	<u>Emission</u> 09/08/2017	<u>Pag.</u> 97 di 234
		<u>Ref.</u> CI-T-R-292	Rev. 0	

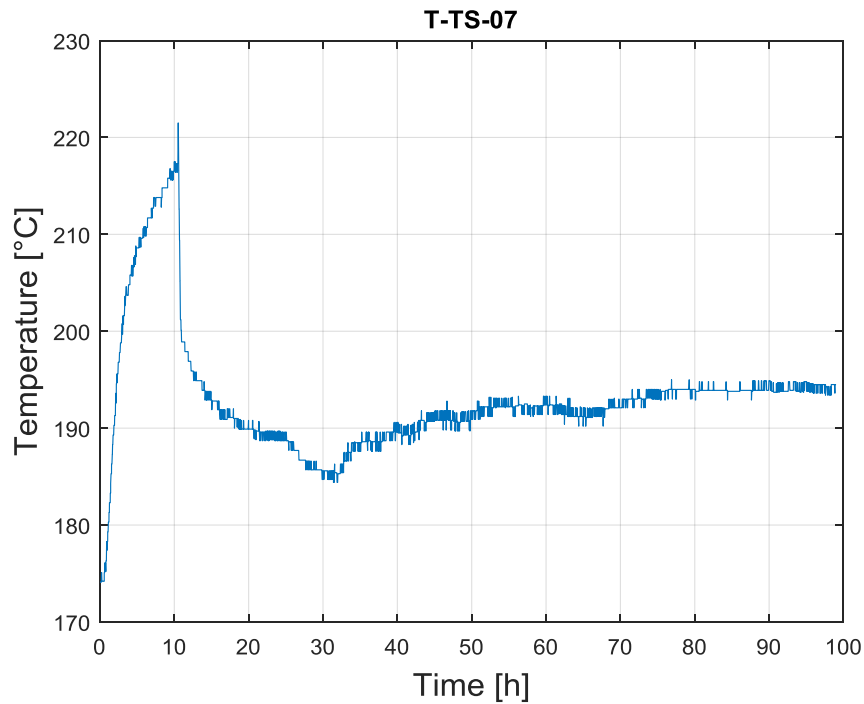



Figure 155: Temperature in the cover gas (Test 3)

For the positioning of the thermocouples in the DHR system refers to Annex A Fig. 4 THINS thermocouples arrangement.pdf and Annex A Fig. 5 T-DHR-0100-Instrumentation DHR.pdf. In Figure 156, the average temperature of the LBE at the inlet and outlet sections of the DHR is reported. In Test 3 the same phenomena encountered in Test 1 was noticed. For the whole duration of the transient at low power temperature at the intel section of the DHR shows a lower value compared to the LBE temperatures at the outlet section. for the physical interpretation refers to Annex C

 DIVISIONE INGEGNERIA SPERIMENTALE	<u>Title</u> D3.2: CIRCE experiments: pre-test, data-set and analysis	<u>Distribution</u> PUBLIC	<u>Emission</u> 09/08/2017	<u>Pag.</u> 98 di 234
		<u>Ref.</u> CI-T-R-292	Rev. 0	

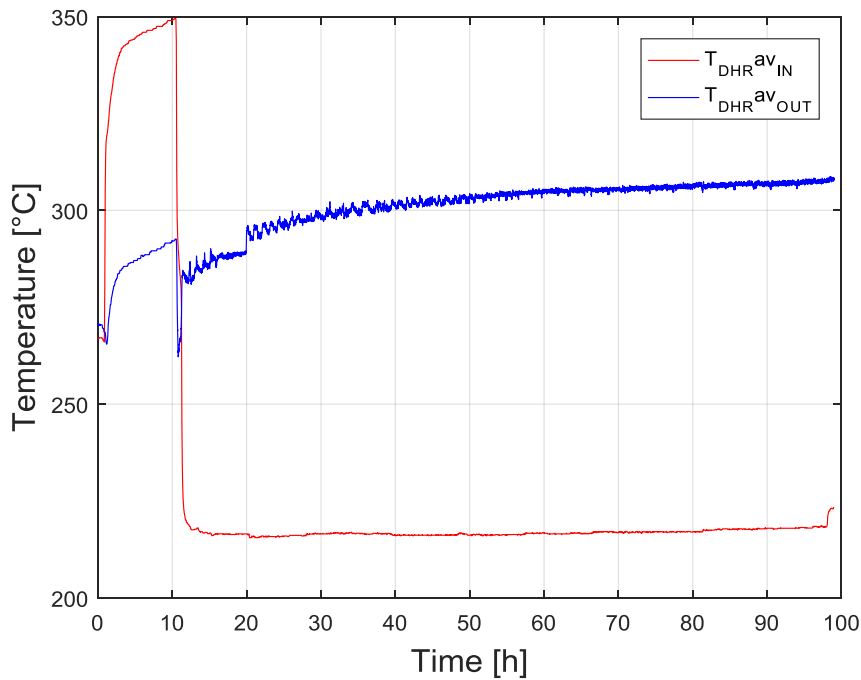



Figure 156: DHR inlet outlet average temperature (Test 3)

The LBE temperature at the FPS entrance was measured by three thermocouples with a diameter of 3 mm (T-FPS-31, 32, 33, Annex A Fig. 6 T-FPS-0100 foglio2-FPS Instrumented). The LBE temperature at the active length exit section of the FPS was measured by three thermocouples (T-FPS-34, 35, 36 Annex A Fig. 6 T-FPS-0100 foglio2-FPS Instrumented) of the same type of those at the entrance. Moreover three thermocouples T-FPS-37, 38, 39 were installed in the slot at the exit of the FPS placed at 120° (see Annex A Fig. 7 T-FPS-0100 foglio1-FPS Instrumented). For the position of the thermocouples inside the bundle refers to Annex A Fig. 8 T-FPS Instrumentation 1 of 2 and Annex A Fig. 9 T-FPS Instrumentation 2 of 2. In Figure 157, the LBE average temperature evaluated at the inlet and outlet sections of the FPS and at the outlet section of the FPS are reported (see Annex A Fig. 7 T-FPS-0100 foglio1-FPS Instrumented).

 DIVISIONE INGEGNERIA SPERIMENTALE	<u>Title</u> D3.2: CIRCE experiments: pre-test, data-set and analysis	<u>Distribution</u> PUBLIC	<u>Emission</u> 09/08/2017	<u>Pag.</u> 99 di 234
		<u>Ref.</u> CI-T-R-292	Rev. 0	

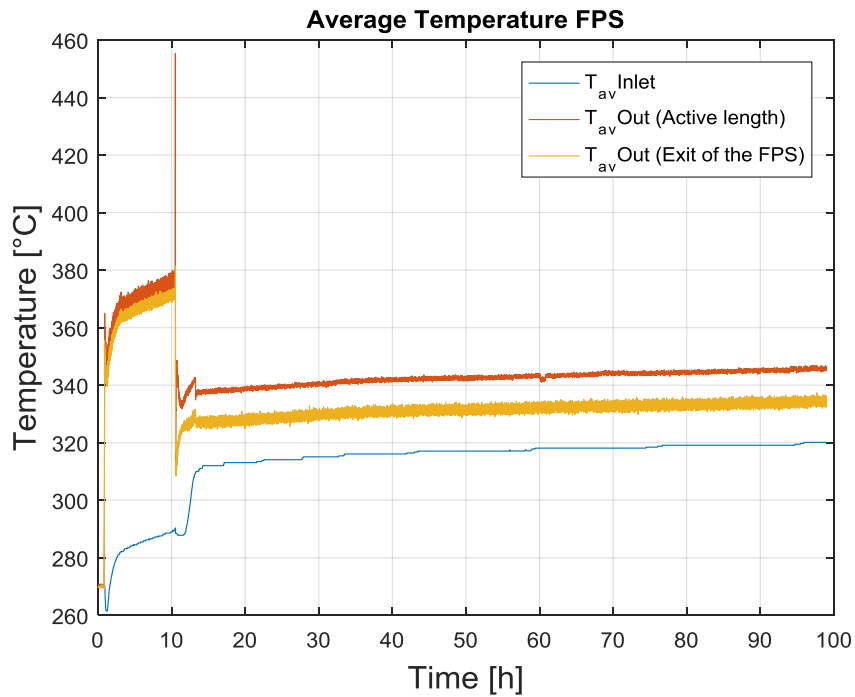


Figure 157: Active length Inlet/Outlet section and FPS Outlet LBE temperature (Test 3)

From Figure 158 to Figure 185 the single temperature in the Fuel Pin Simulator (FPS) are reported. It is worth to be mentioned that T-FPS-07 and T-FPS-013 are broken and therefore the relative plots are not reported.

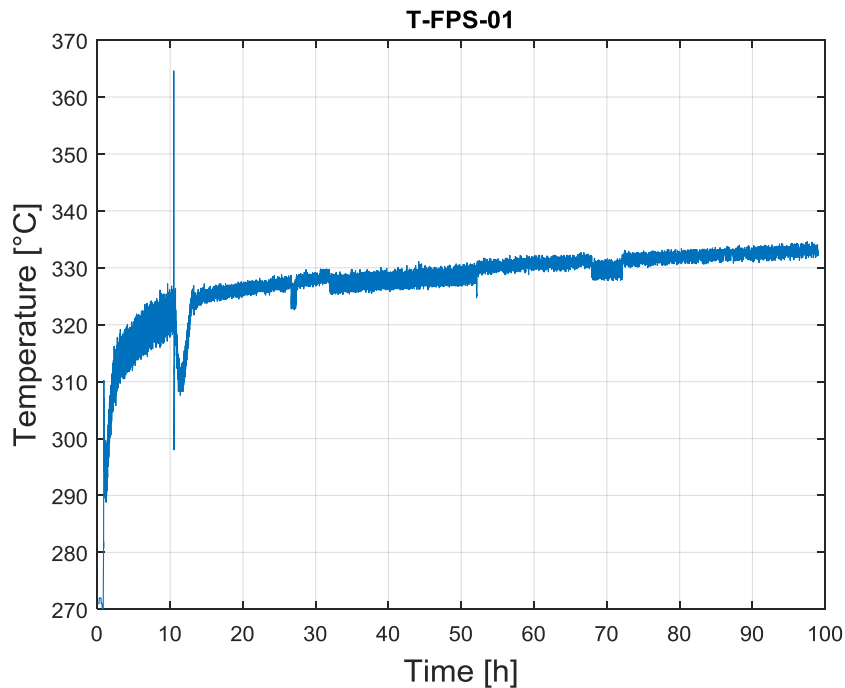


Figure 158: T-FPS-01 LBE temperature (Test 3)

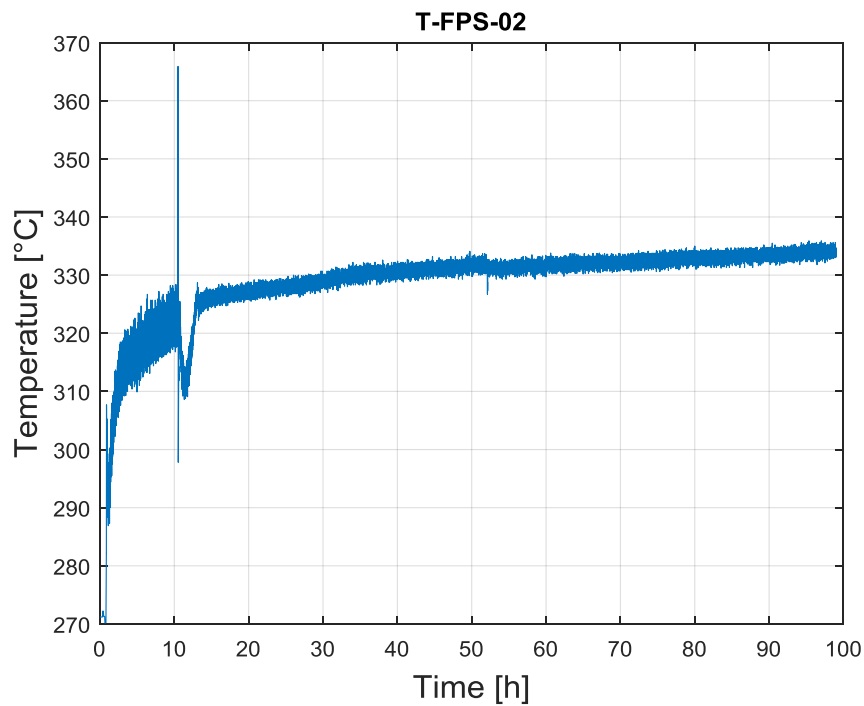


Figure 159: T-FPS-02 LBE temperature (Test 3)

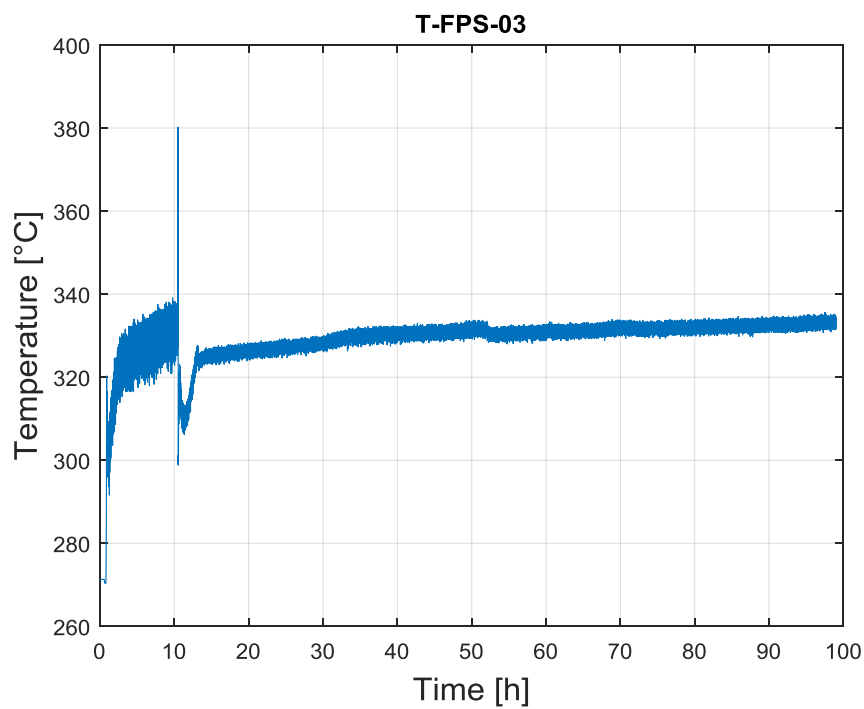


Figure 160: T-FPS-03 LBE temperature (Test 3)

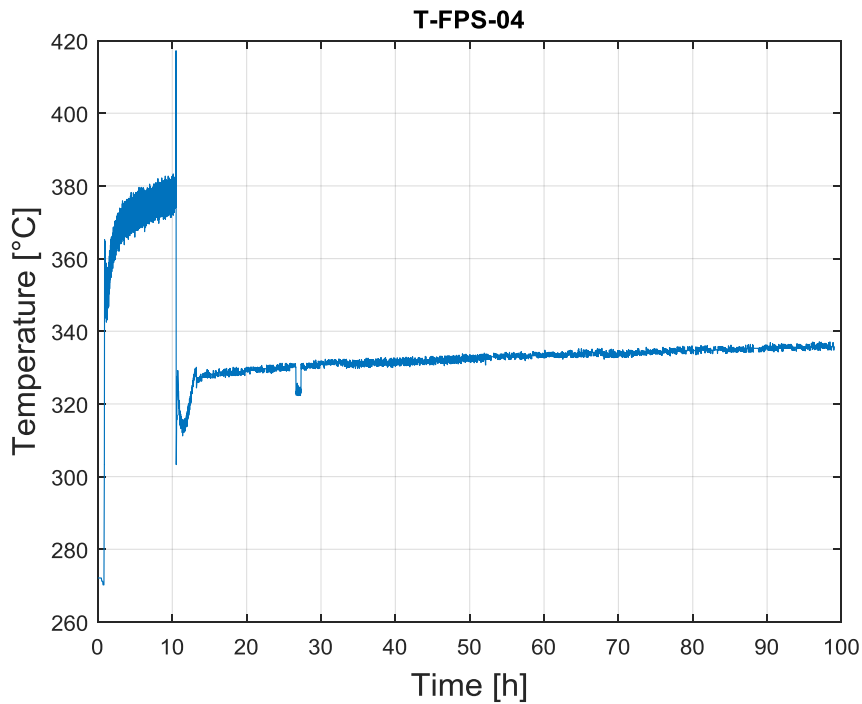


Figure 161: T-FPS-04 LBE temperature (Test 3)

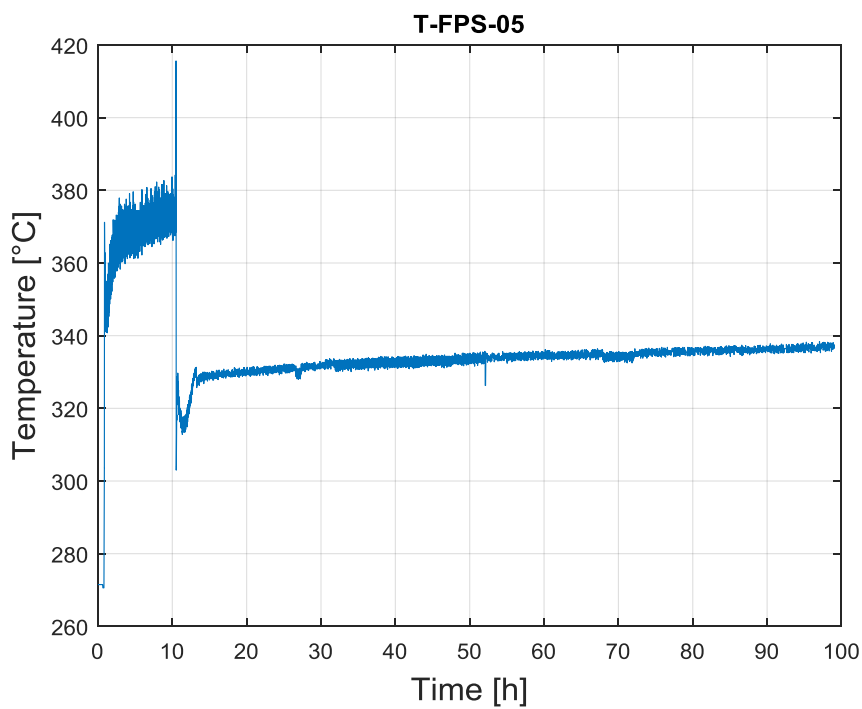


Figure 162: T-FPS-05 LBE temperature (Test 3)

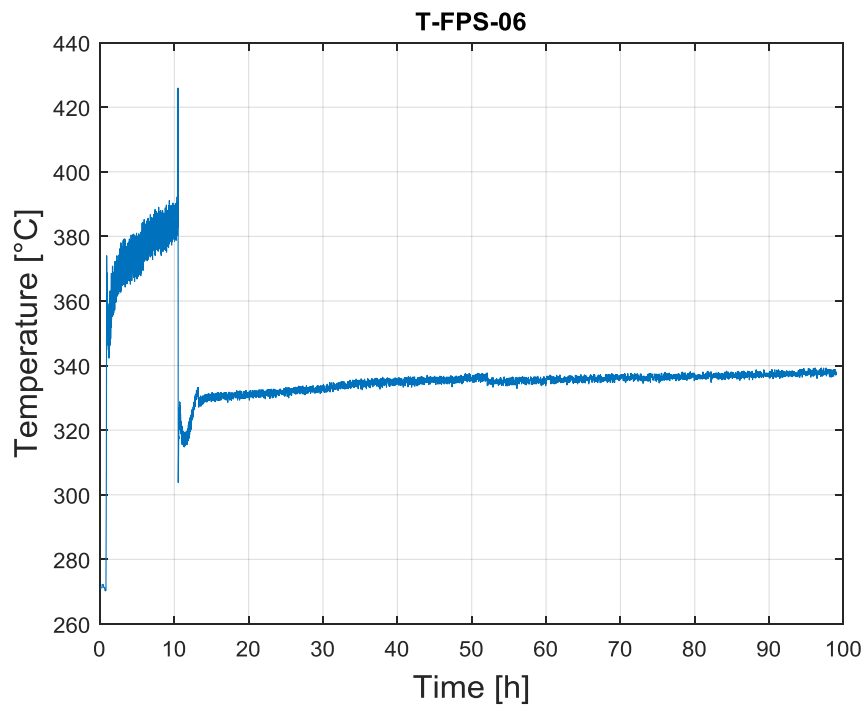


Figure 163: T-FPS-06 LBE temperature (Test 3)

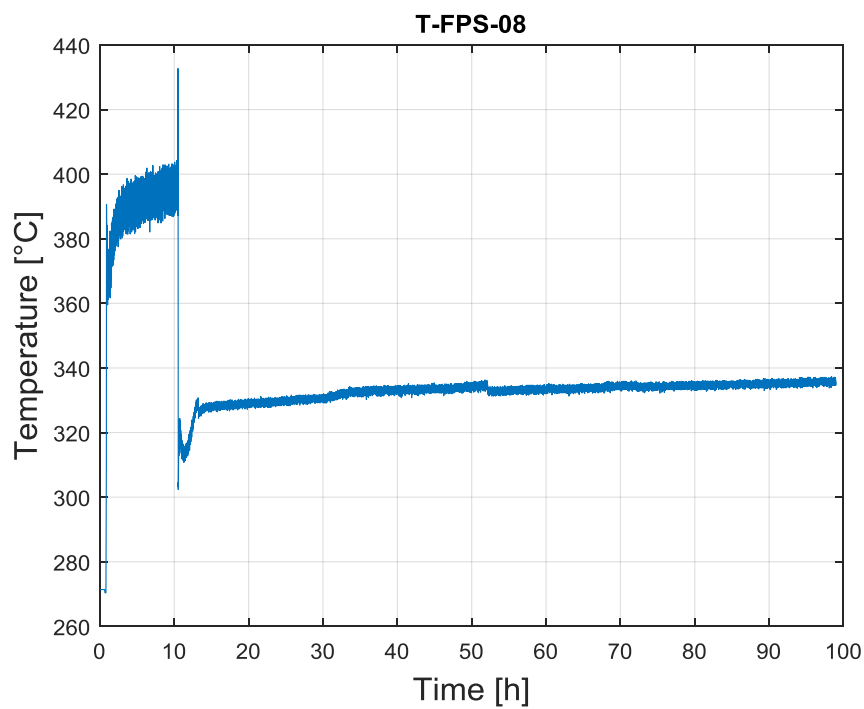


Figure 164: T-FPS-08 LBE temperature (Test 3)

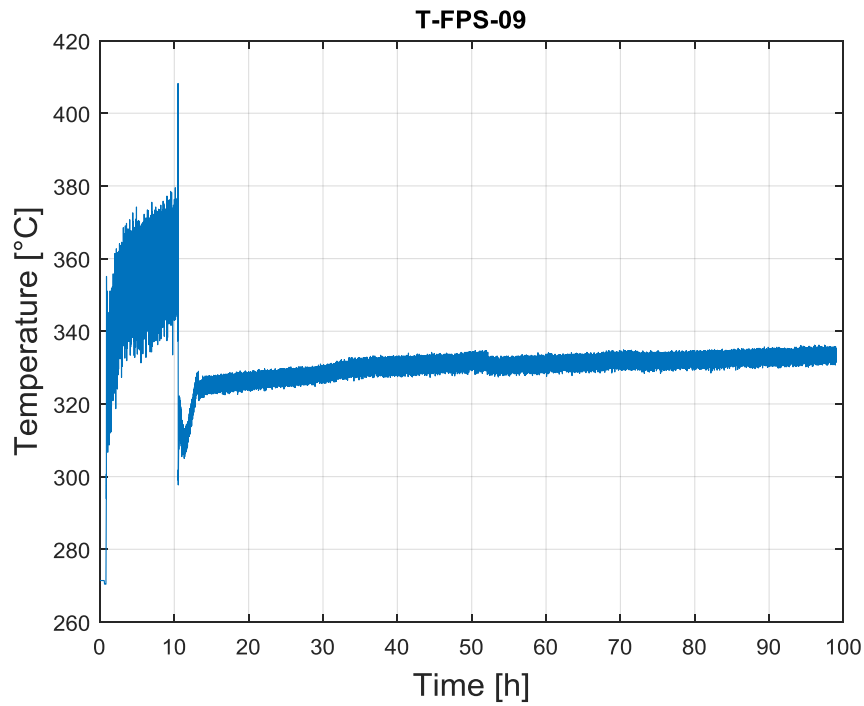


Figure 165: T-FPS-09 LBE temperature (Test 3)

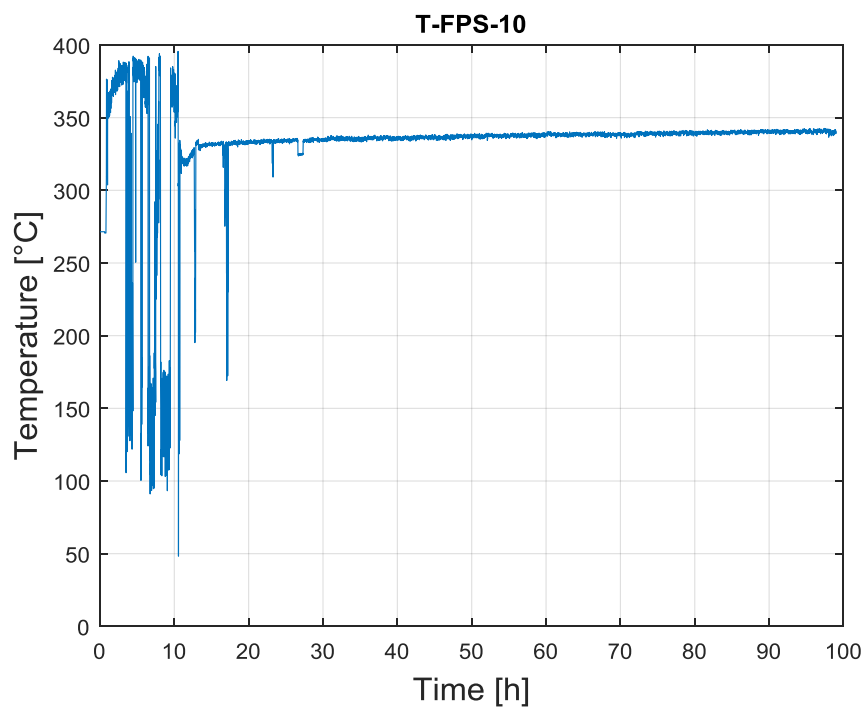


Figure 166: T-FPS-10 LBE temperature (Test 3)

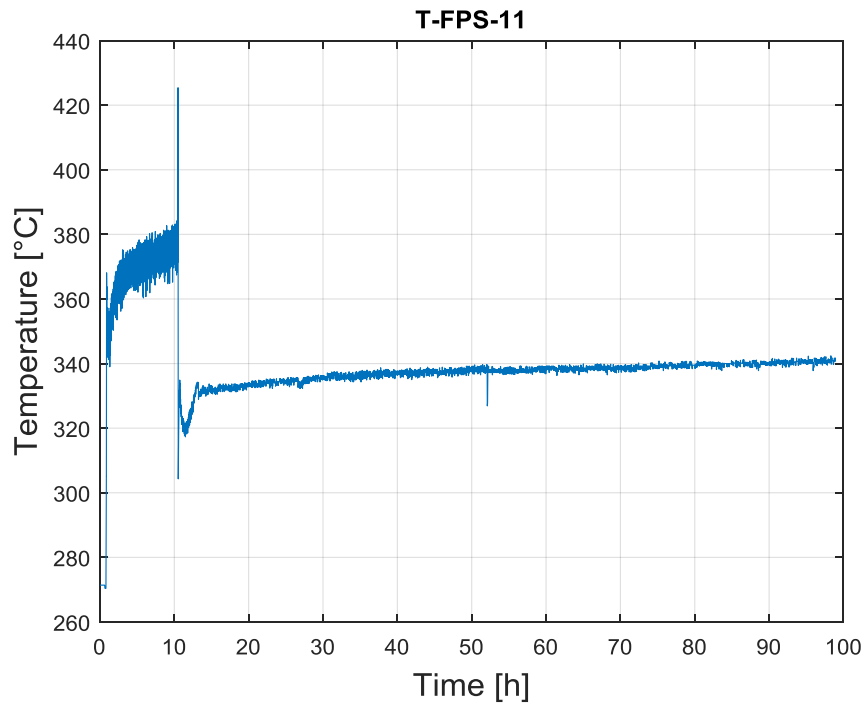


Figure 167: T-FPS-11 LBE temperature (Test 3)

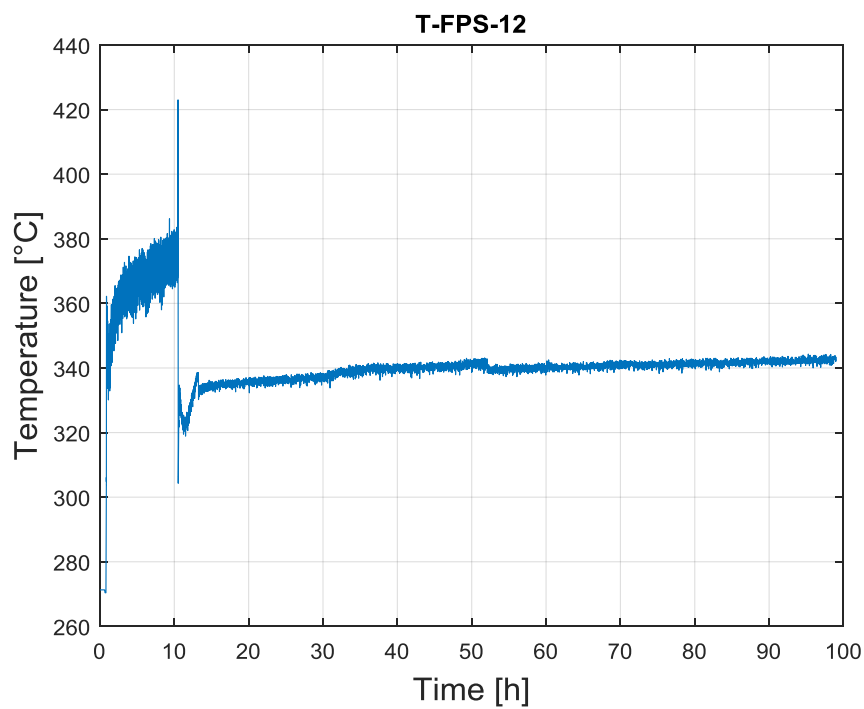


Figure 168: T-FPS-12 LBE temperature (Test 3)

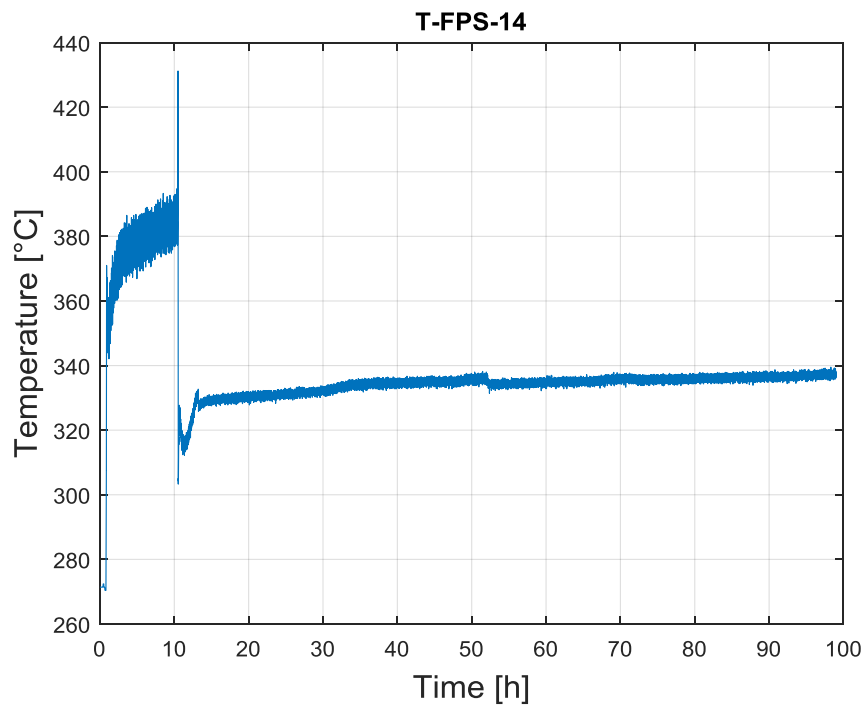


Figure 169: T-FPS-14 LBE temperature (Test 3)

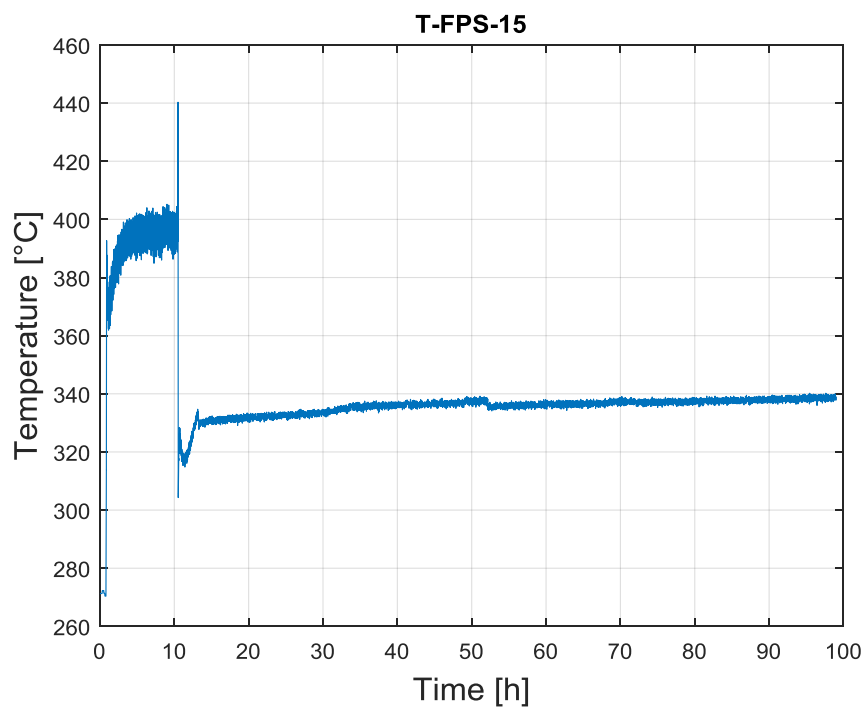


Figure 170: T-FPS-15 LBE temperature (Test 3)

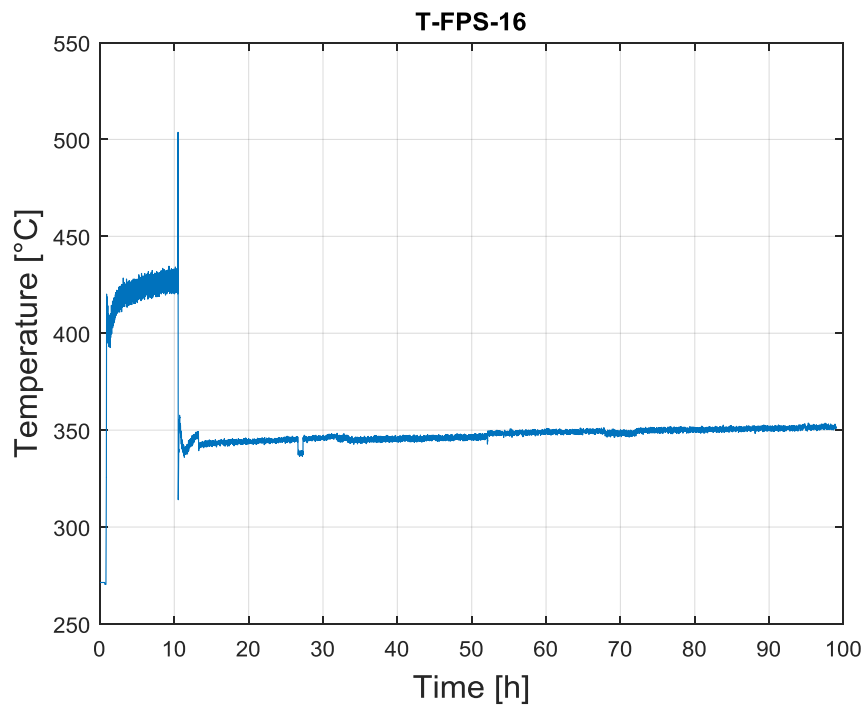


Figure 171: T-FPS-16 LBE temperature (Test 3)

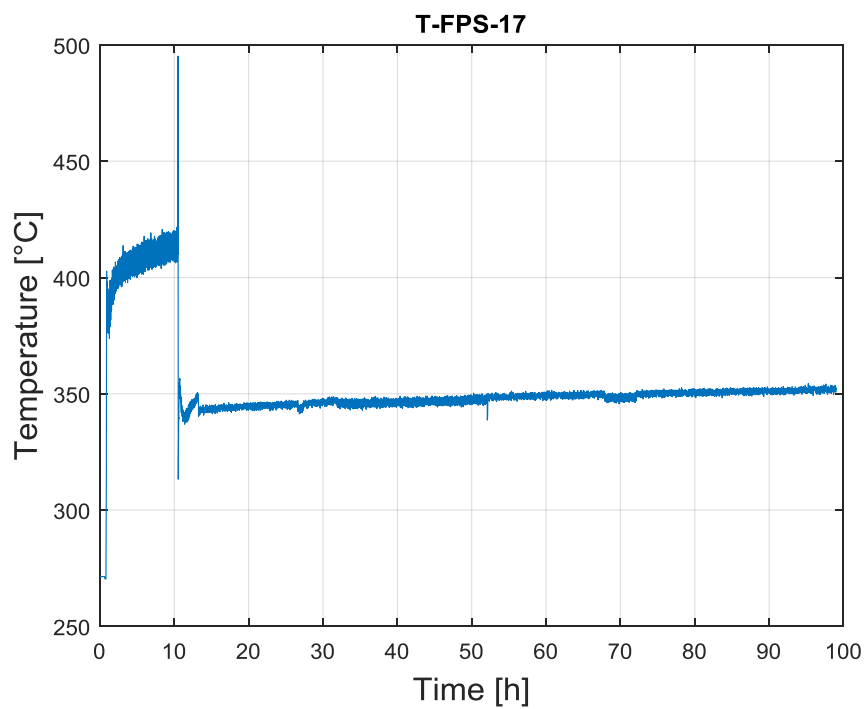


Figure 172: T-FPS-17 LBE temperature (Test 3)

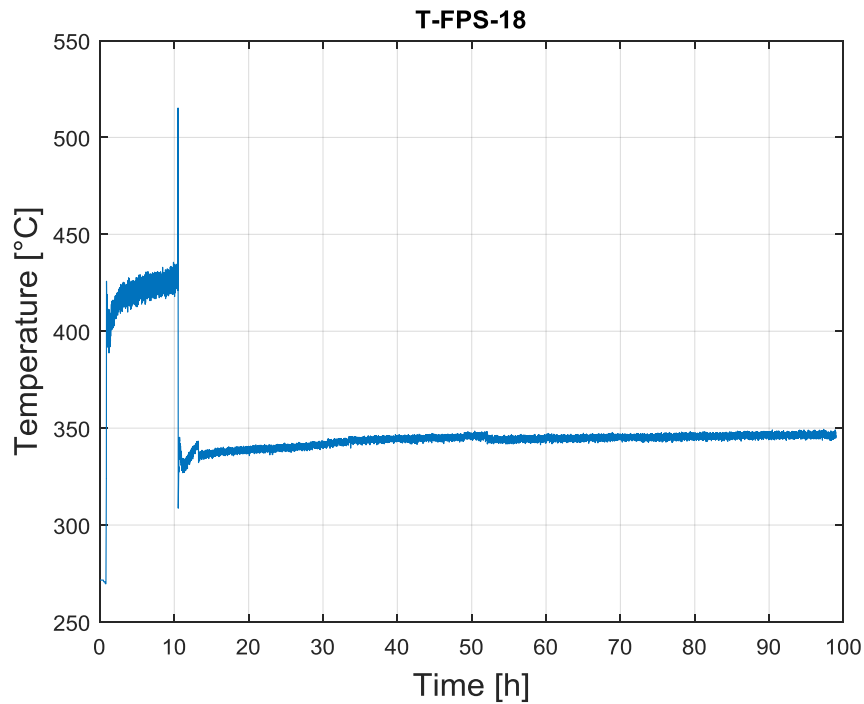


Figure 173: T-FPS-18 LBE temperature (Test 3)

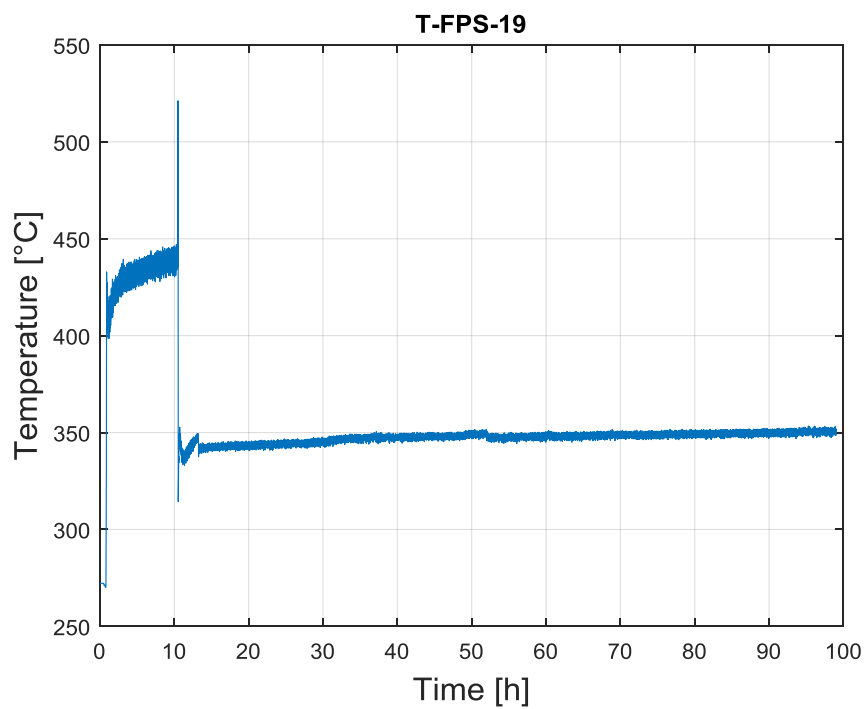


Figure 174: T-FPS-19 LBE temperature (Test 3)

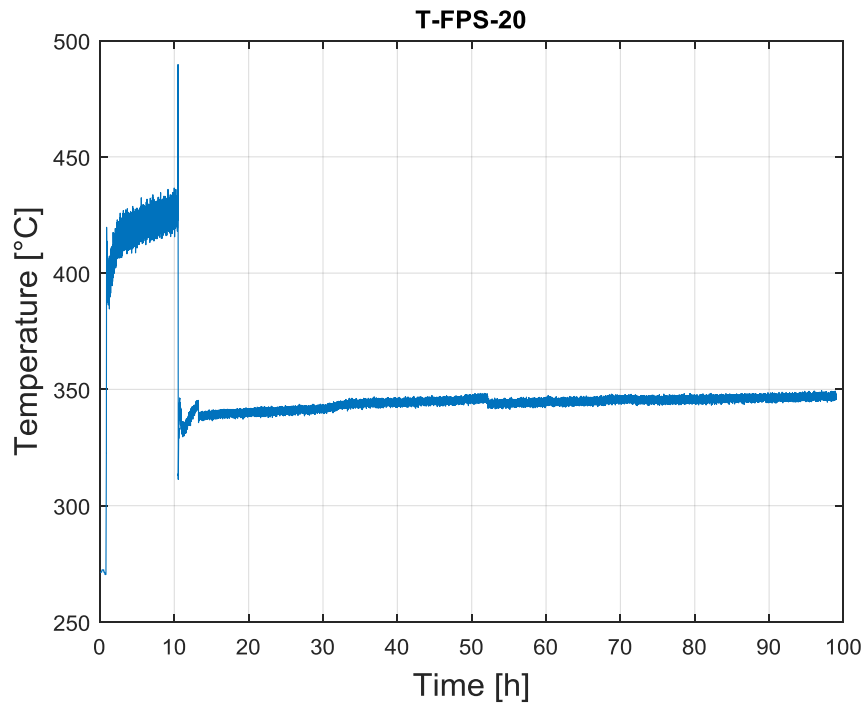


Figure 175: T-FPS-20 LBE temperature (Test 3)

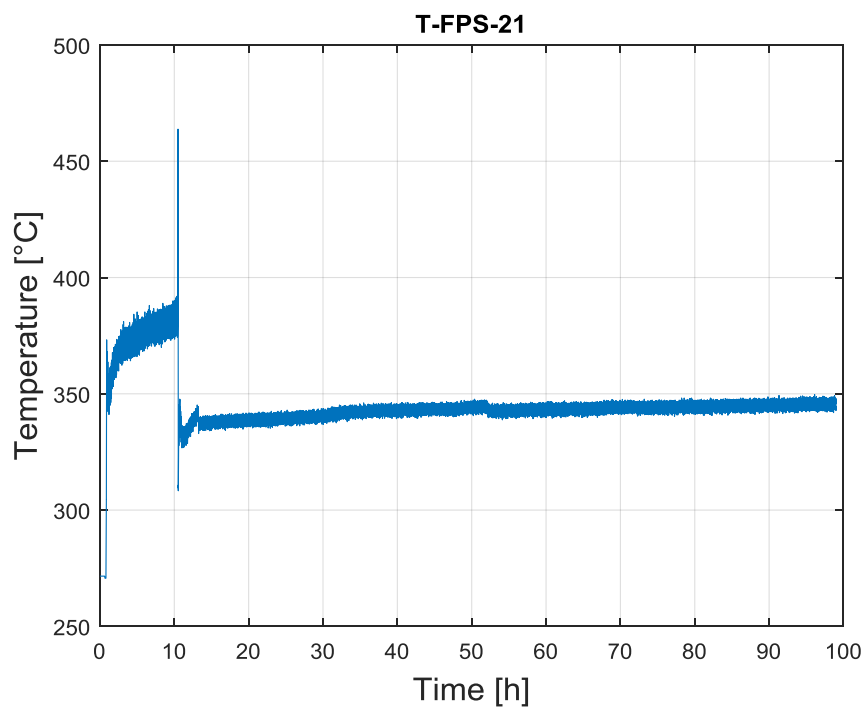


Figure 176: T-FPS-21 LBE temperature (Test 3)

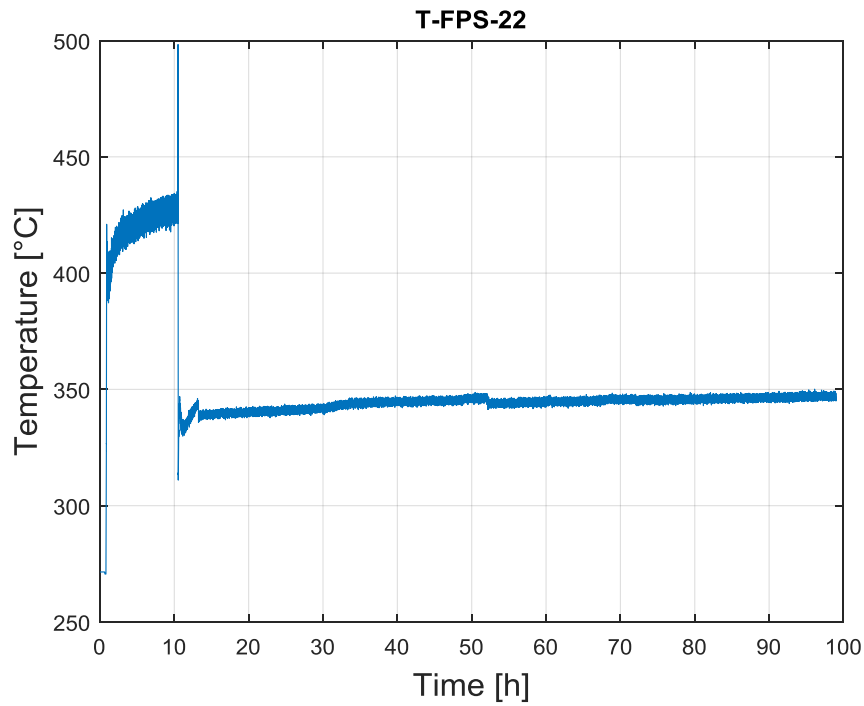


Figure 177: T-FPS-22 LBE temperature (Test 3)

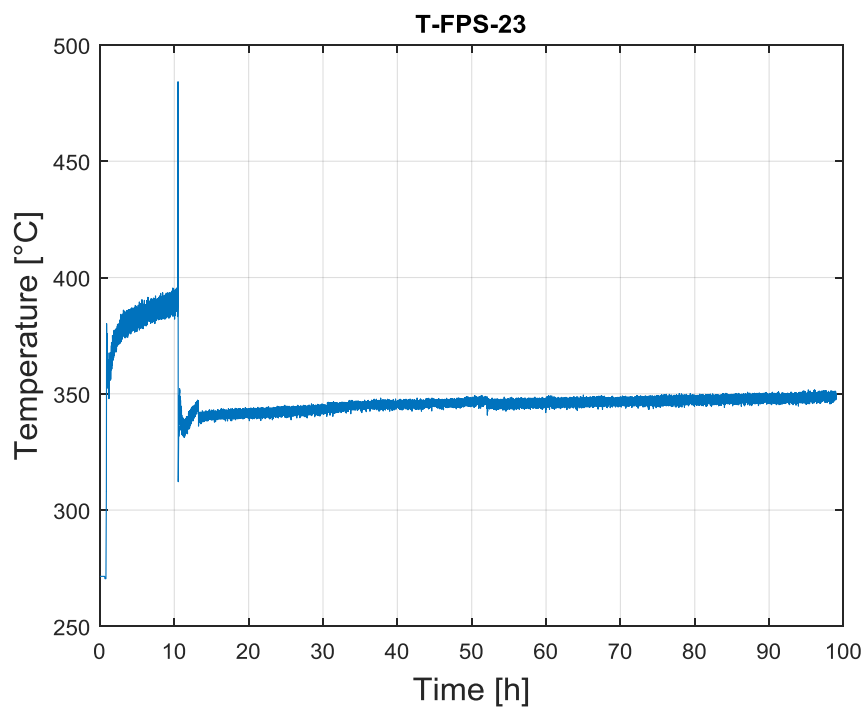


Figure 178: T-FPS-23 LBE temperature (Test 3)

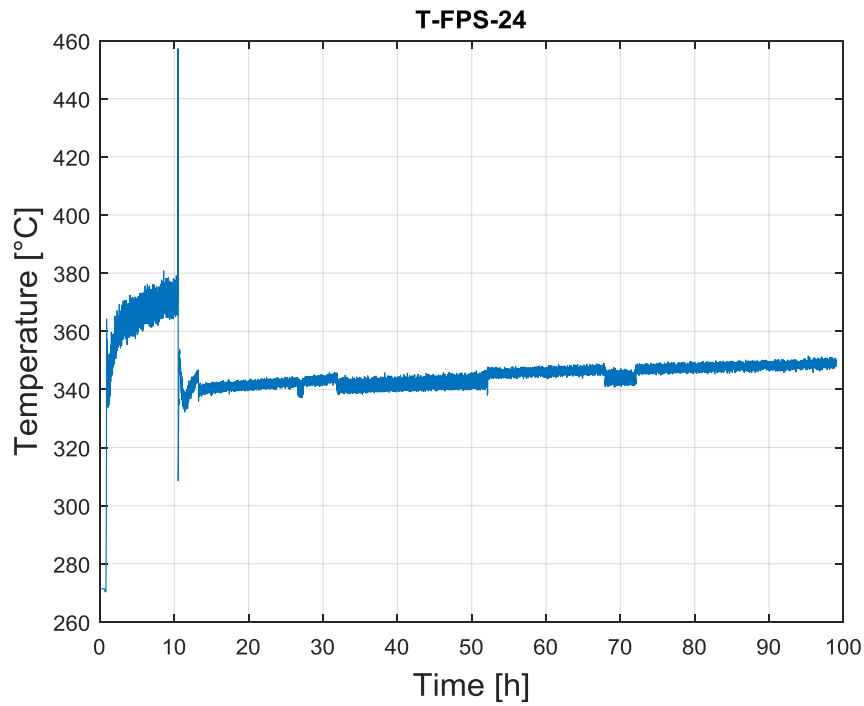


Figure 179: T-FPS-24 LBE temperature (Test 3)

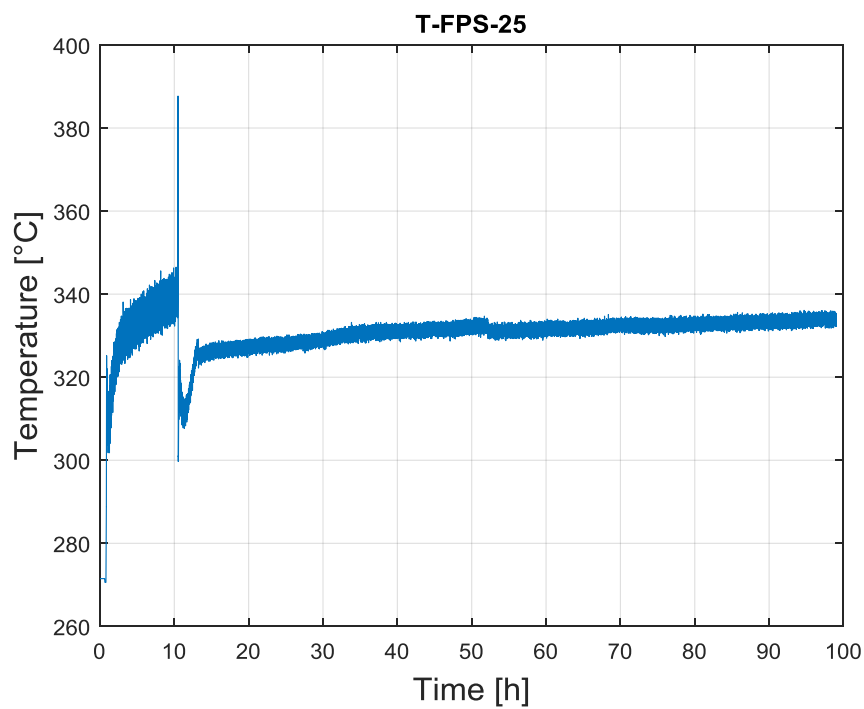


Figure 180: T-FPS-25 LBE temperature (Test 3)

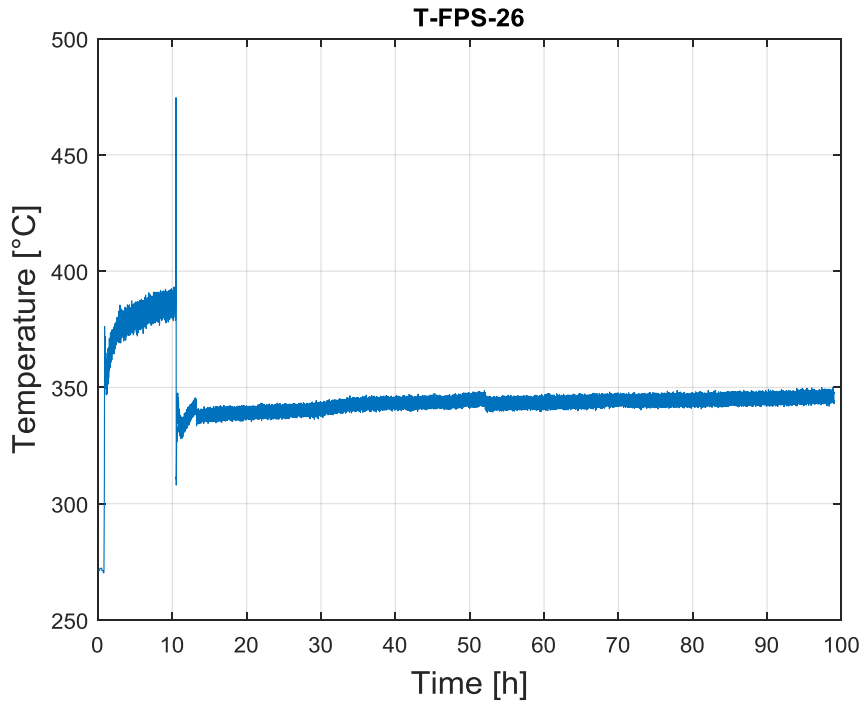


Figure 181: T-FPS-26 LBE temperature (Test 3)

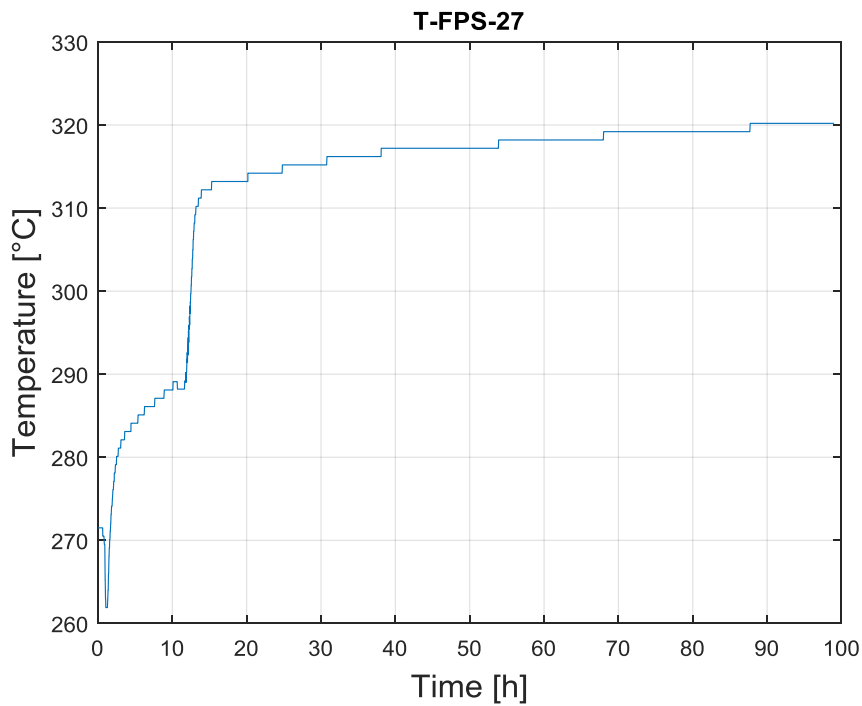


Figure 182: T-FPS-27 LBE temperature (Test 3)

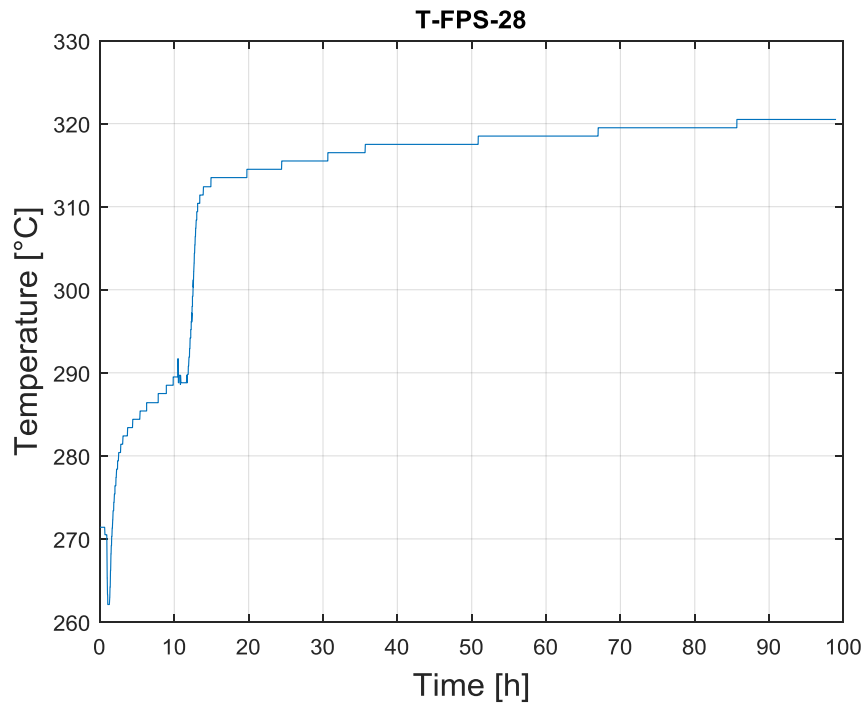


Figure 183: T-FPS-28 LBE temperature (Test 3)

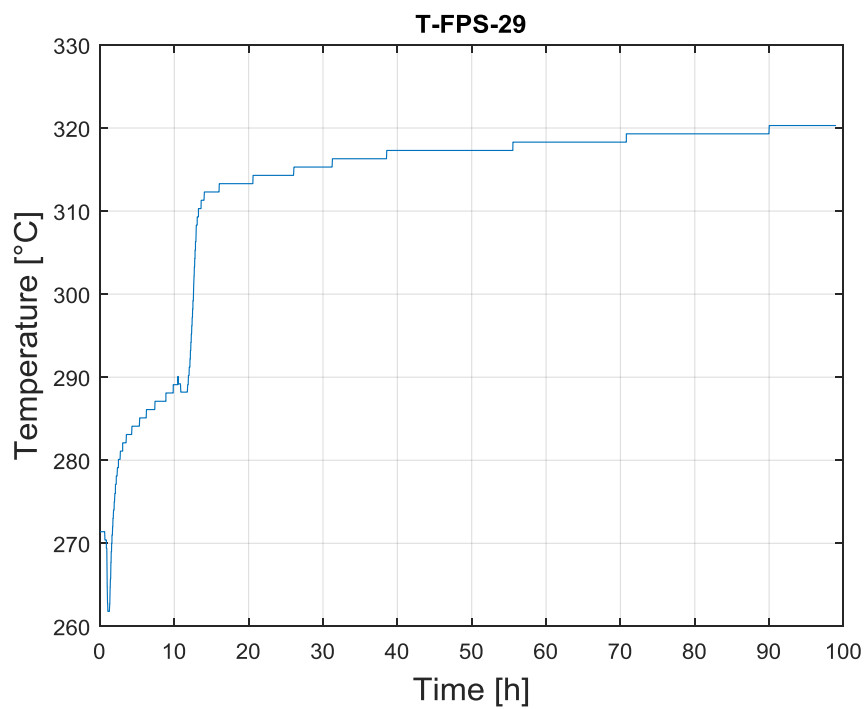



Figure 184: T-FPS-29 LBE temperature (Test 3)

 DIVISIONE INGEGNERIA SPERIMENTALE	<u>Title</u> D3.2: CIRCE experiments: pre-test, data-set and analysis	<u>Distribution</u> PUBLIC	<u>Emission</u> 09/08/2017	<u>Pag.</u> 113 di 234
		<u>Ref.</u> CI-T-R-292	Rev. 0	

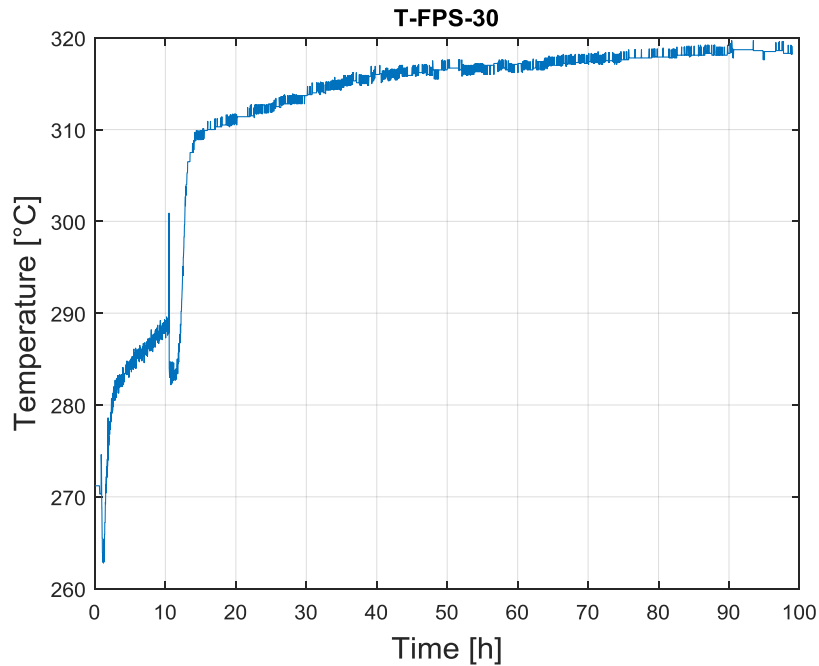


Figure 185: T-FPS-30 LBE temperature (Test 3)

The LBE heated by the FPS flows through the fitting volume into the riser (see Annex A Fig. 3 0016 Instrumentation.pdf); here temperatures are measured using TCs with a diameter of 3 mm disposed at the entrance section (T-TS-01 to 03) and at the exit section before the separator (T-TS-04 to). In Figure 186 the riser inlet/outlet average temperature is reported.

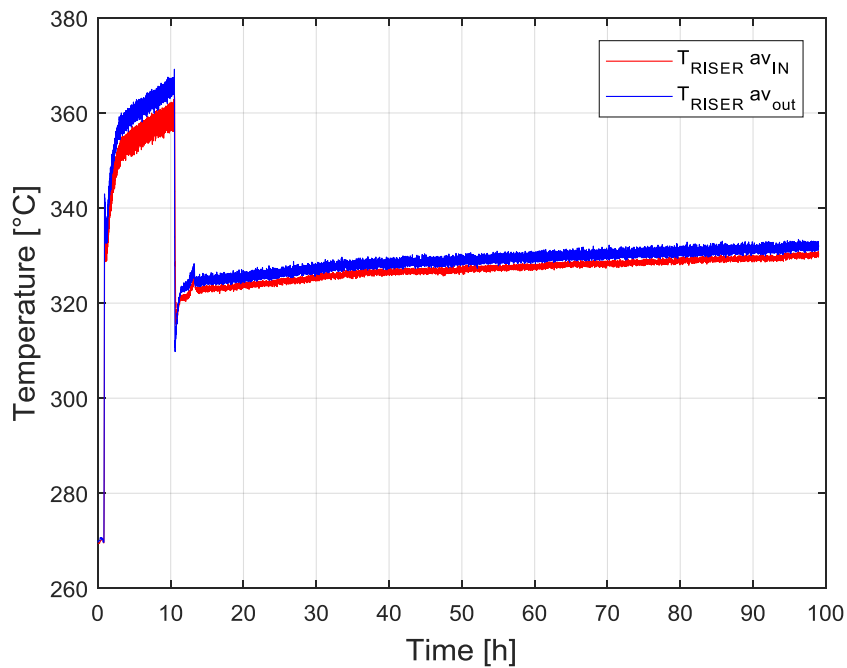



Figure 186: Inlet/Outlet average LBE temperature in the riser (Test 3)

 DIVISIONE INGEGNERIA SPERIMENTALE	<u>Title</u> D3.2: CIRCE experiments: pre-test, data-set and analysis	<u>Distribution</u> PUBLIC	<u>Emission</u> 09/08/2017	<u>Pag.</u> 114 di 234
		<u>Ref.</u> CI-T-R-292	Rev. 0	

From the riser exit, the LBE flows through the Separator into the HX shell, where the temperature at the entrance section is measured by three TCs placed at 120°, 30 mm from the bottom of the Separator (T-SG-01 ... 03, see Annex A Fig. 4 THINS thermocouples arrangement.pdf).

Sub-channel temperature measurements are measured in a plane placed 30 mm above the lower grid (see Annex A Fig. 10: 0700-Assieme-HX.pdf for the positioning of the grid), according to the scheme shown in Annex A Fig. 11: T-SG-0100-Disposizione TC Sottocanali GV.pdf (T-SG-04 ... 12).

The LBE temperature at the outlet section of the HX is measured by six thermocouples (T-SG-13 ... 18) placed at 60° each and at 100 mm before the HX skirt exit (see Annex A Fig. 12: T-SG-0101-Disposizione TC Uscita GV.pdf). In Figure 187 the LBE temperature averaged at the inlet and outlet sections of the HX is reported.

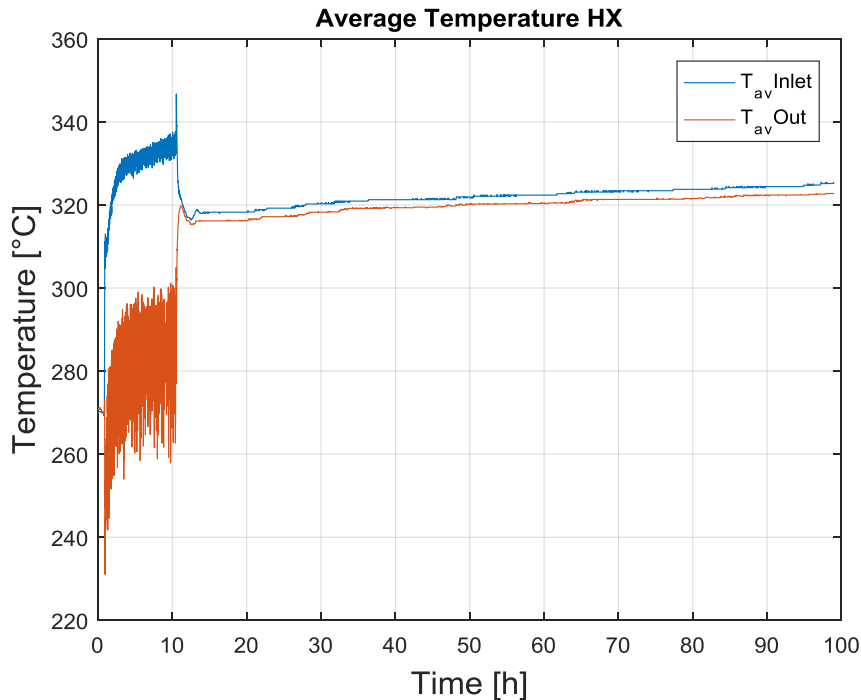


Figure 187: Inlet/Outlet average LBE temperature in the main HX (Test 3)

From Figure 188 to Figure 196 the temperature measured from each single thermocouple in the HX are reported (inlet and outlet sections and subchannels). Problems for T-SG are evidence by Figure 193.

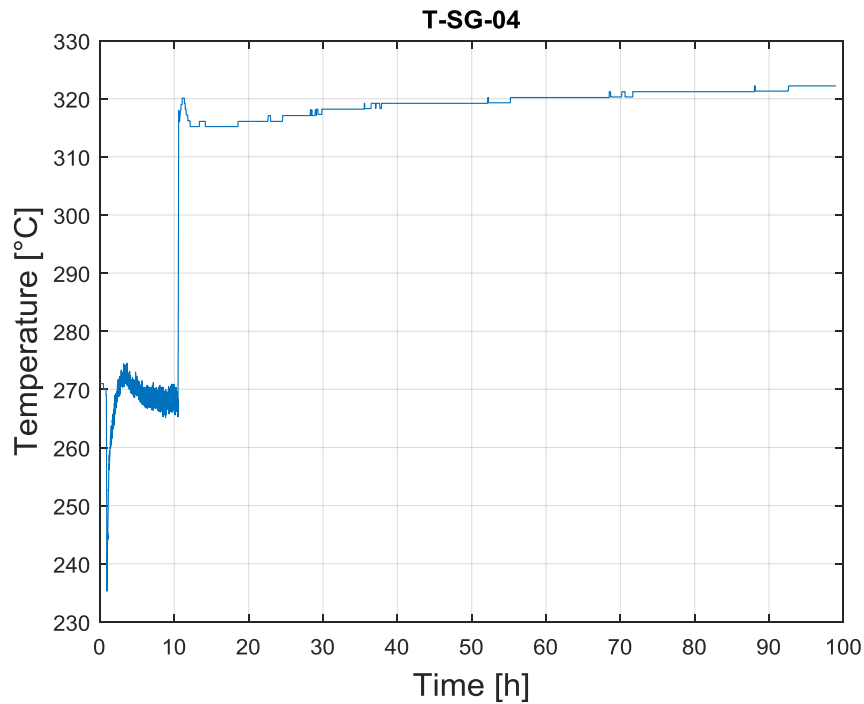


Figure 188: LBE temperature in the sub channel of the HX (T-SG-04, Test 3)

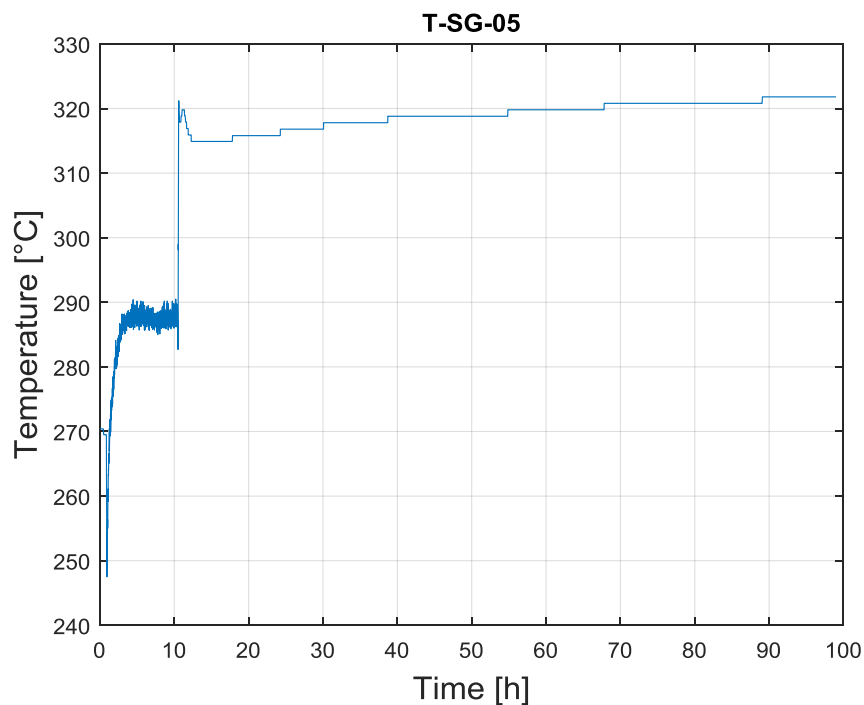


Figure 189: LBE temperature in the sub channel of the HX (T-SG-05, Test 3)

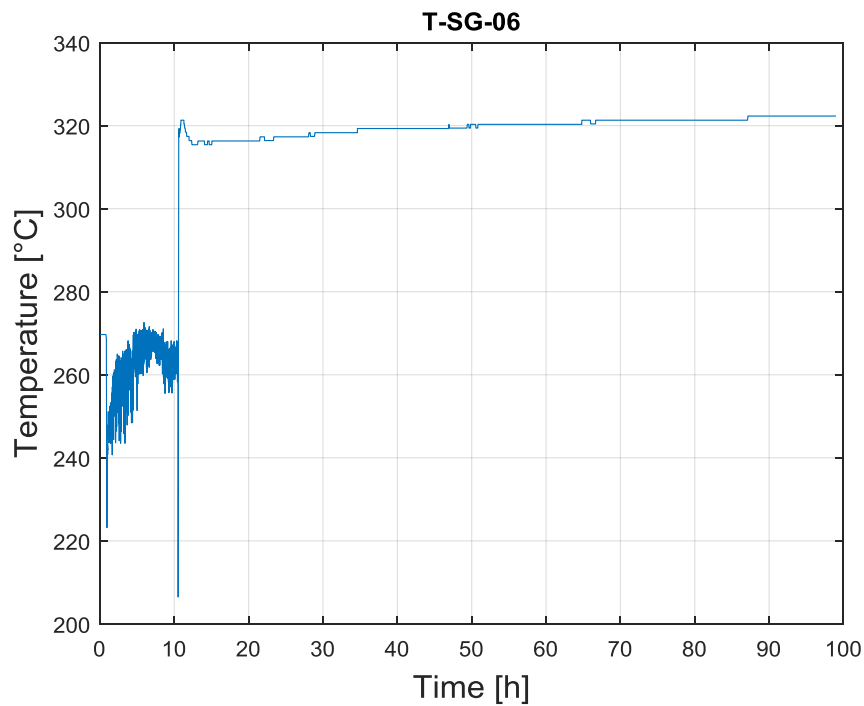


Figure 190: LBE temperature in the sub channel of the HX (T-SG-06, Test 3)

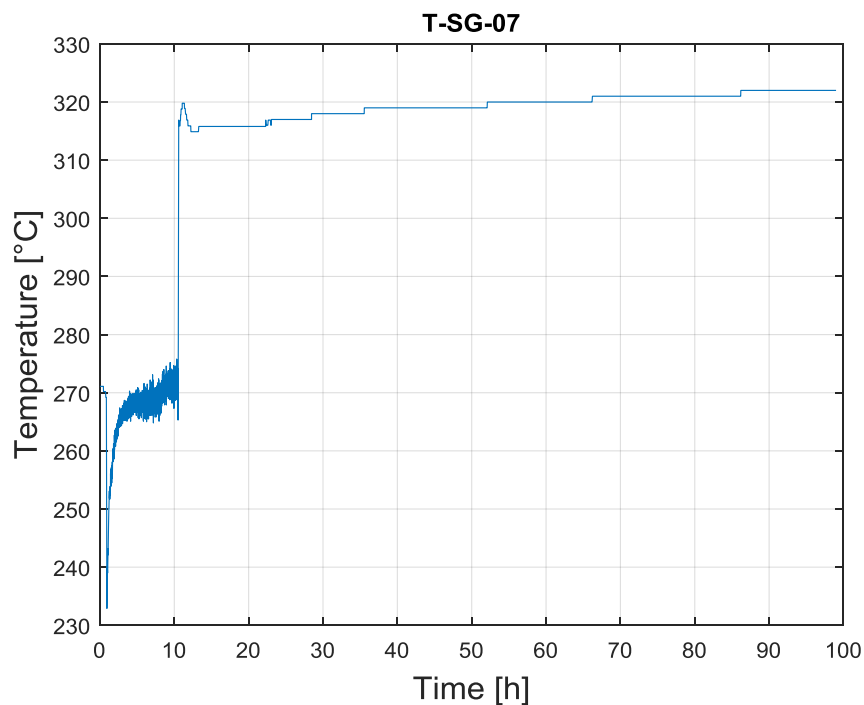


Figure 191: LBE temperature in the sub channel of the HX (T-SG-07, Test 3)

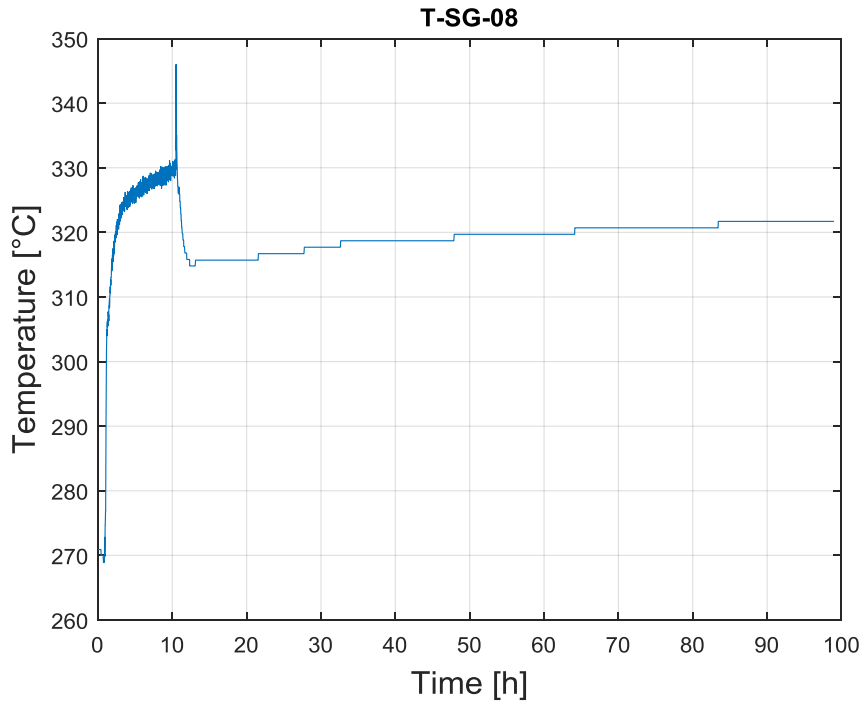


Figure 192: LBE temperature in the sub channel of the HX (T-SG-08, Test 3)

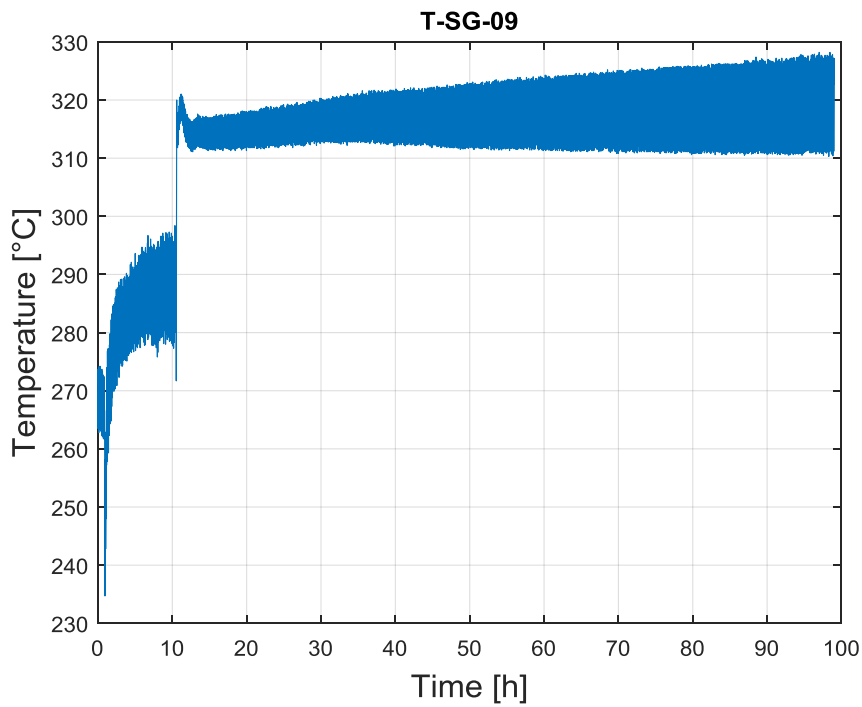


Figure 193: LBE temperature in the sub channel of the HX (T-SG-09, Test 3)

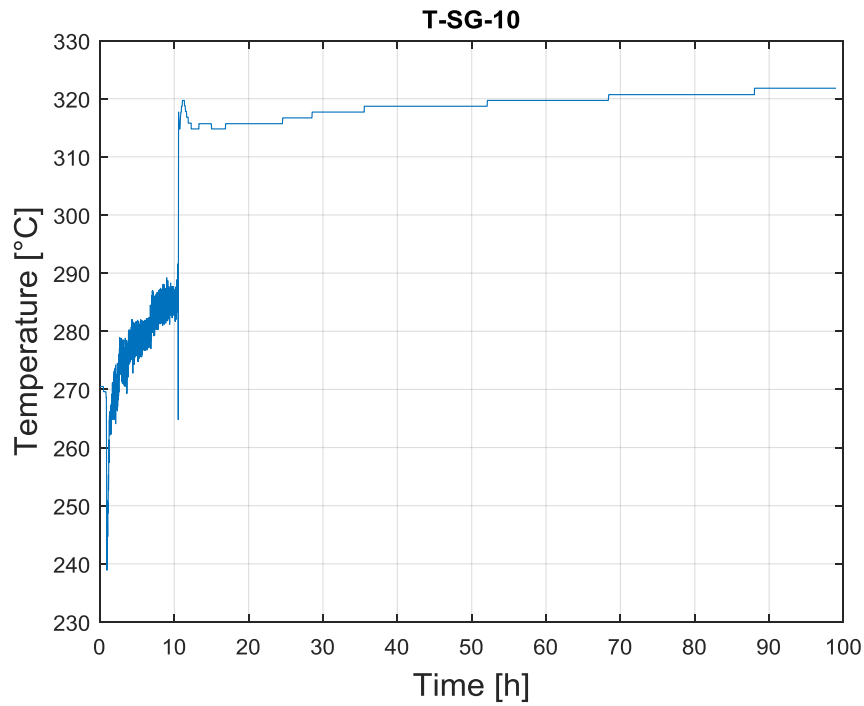


Figure 194: LBE temperature in the sub channel of the HX (T-SG-10, Test 3)

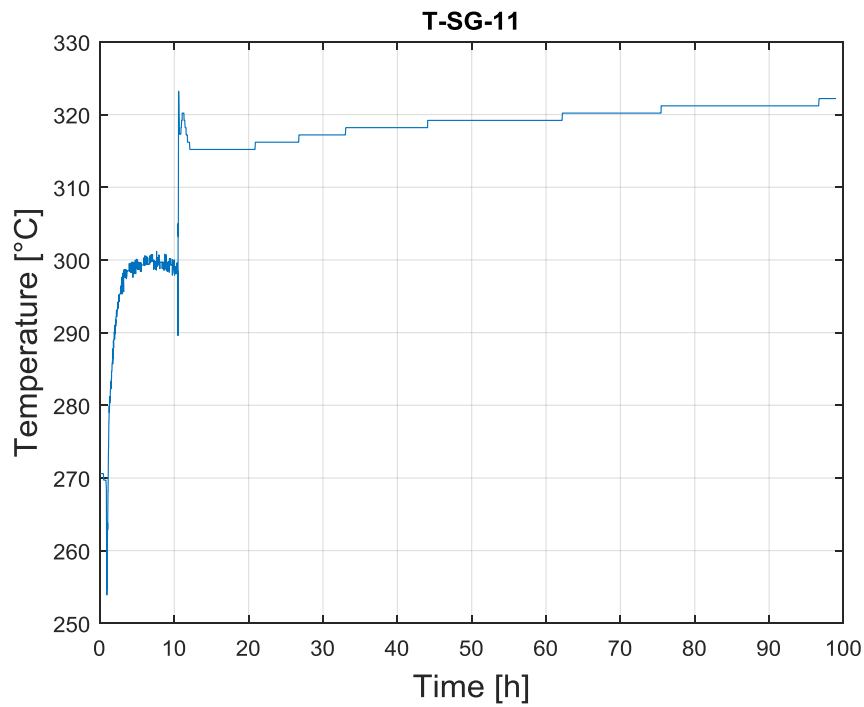



Figure 195: LBE temperature in the sub channel of the HX (T-SG-11, Test 3)

 DIVISIONE INGEGNERIA SPERIMENTALE	<u>Title</u> D3.2: CIRCE experiments: pre-test, data-set and analysis	<u>Distribution</u> PUBLIC	<u>Emission</u> 09/08/2017	<u>Pag.</u> 119 di 234
		<u>Ref.</u> CI-T-R-292	Rev. 0	

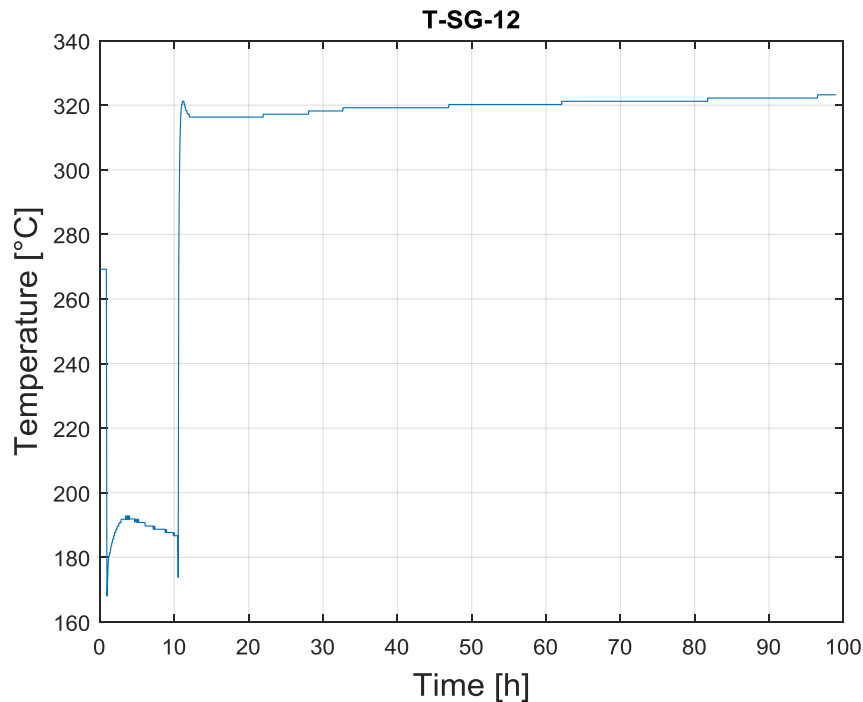


Figure 196: LBE temperature in the sub channel of the HX (T-SG-12, Test 3)

After passing through the HX, the LBE returned into the pool. Here, thermocouples for the measurements of LBE temperature were maintained in the fixed positions by vertical rods at 17 different elevations (see Annex A Fig. 13 T-MS-0101 TC per Mix&Strat.pdf) and 9 different radial position (see Annex A Fig. 14 T-MS-0100-Posizione TC Mix&Strat su piani di misura.pdf) for a total of 119 TCs with a diameter of 3 mm (T-MS-01 ... 119). In particular, with reference to Annex A Fig. 13 T-MS-0101 TC per Mix&Strat.pdf and Annex A Fig. 14 T-MS-0100-Posizione TC Mix&Strat su piani di misura.pdf, TCs on lines *A, H, I* allow measurement from the bottom side of the test section up to the FPS entrance, while TCs on lines *B, C, D, E, F, G* allow measurement up to 600 mm below the exit of the DHR.

From Figure 197 to Figure 205 the LBE temperature in the pool is reported along the vertical lines *A, B, C, D, E, F, G, H* and *I*. T-MS-118 was damaged and therefore not reported hereafter.

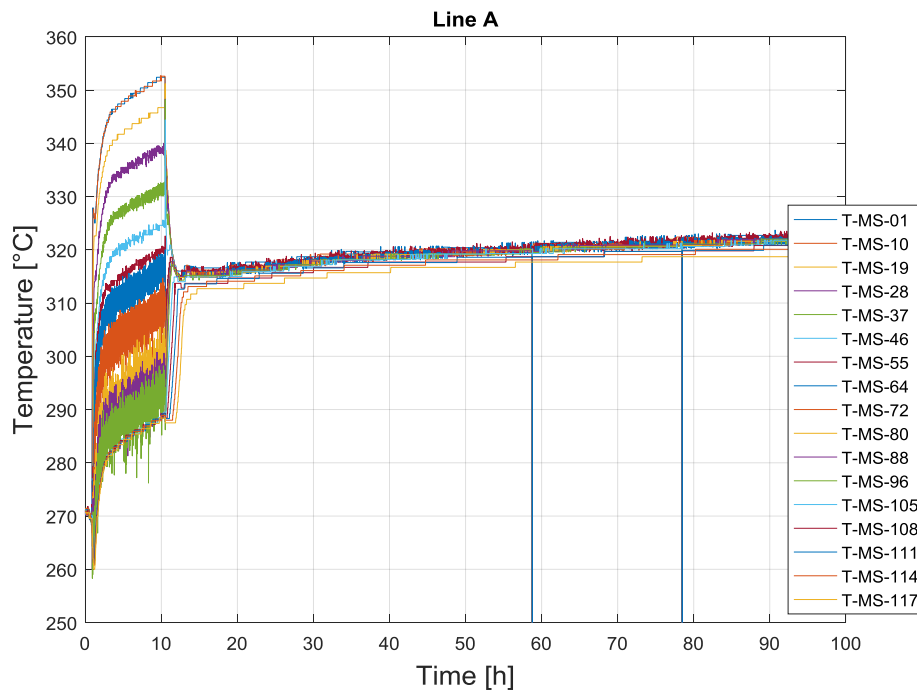


Figure 197: Temperature in the pool along Line A

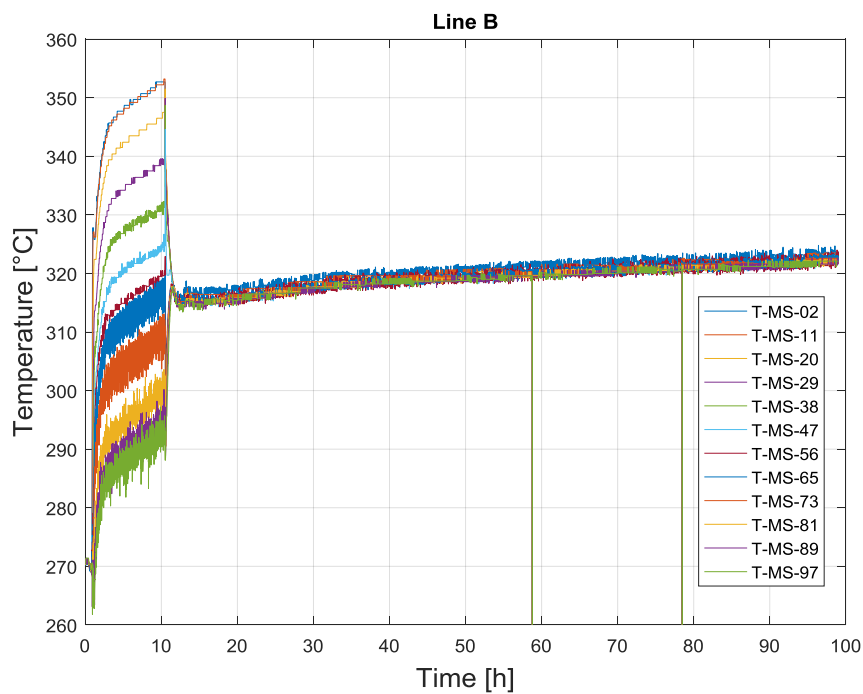


Figure 198: Temperature in the pool along Line B

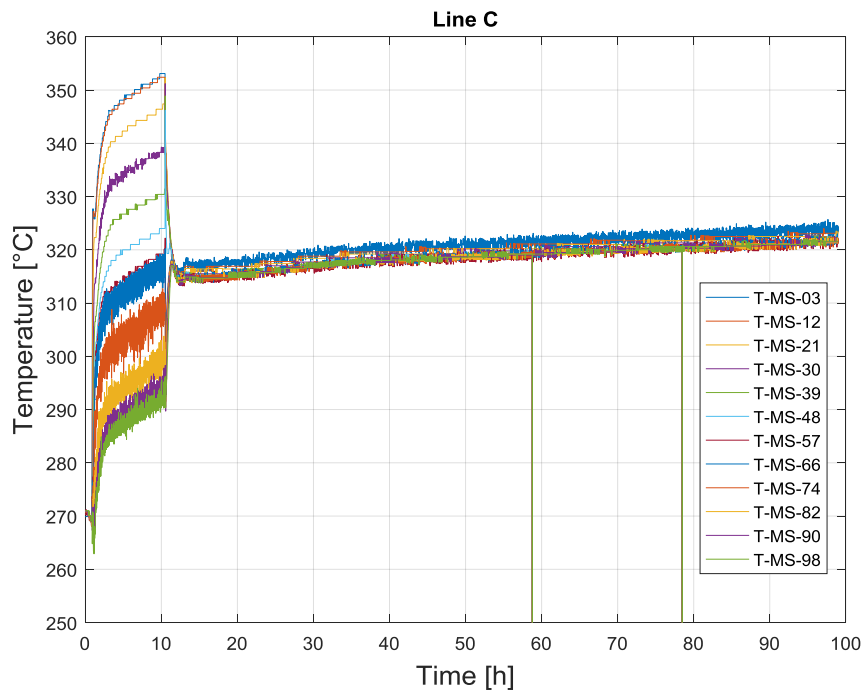


Figure 199: Temperature in the pool along Line C

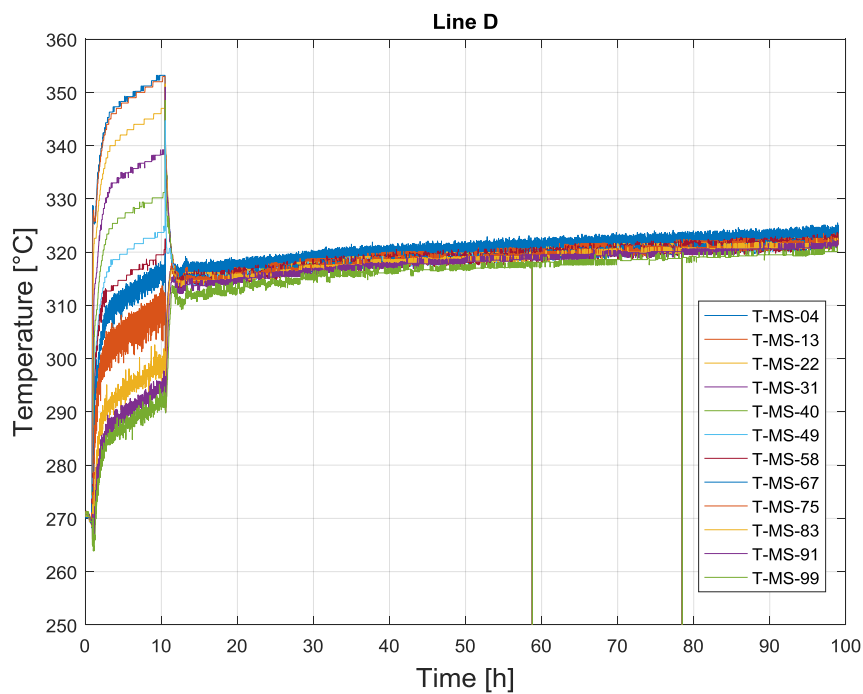


Figure 200: Temperature in the pool along Line D

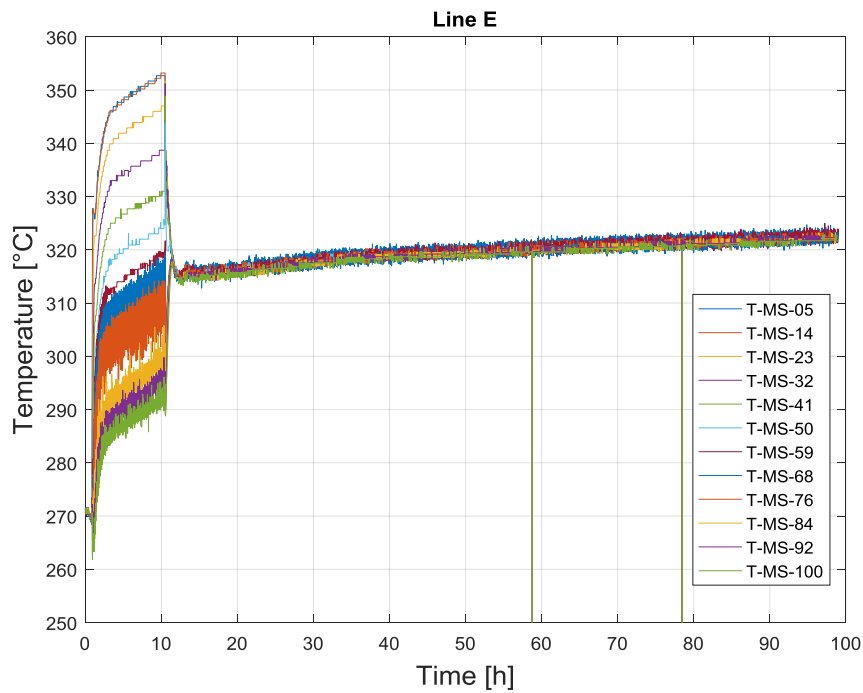


Figure 201: Temperature in the pool along Line E

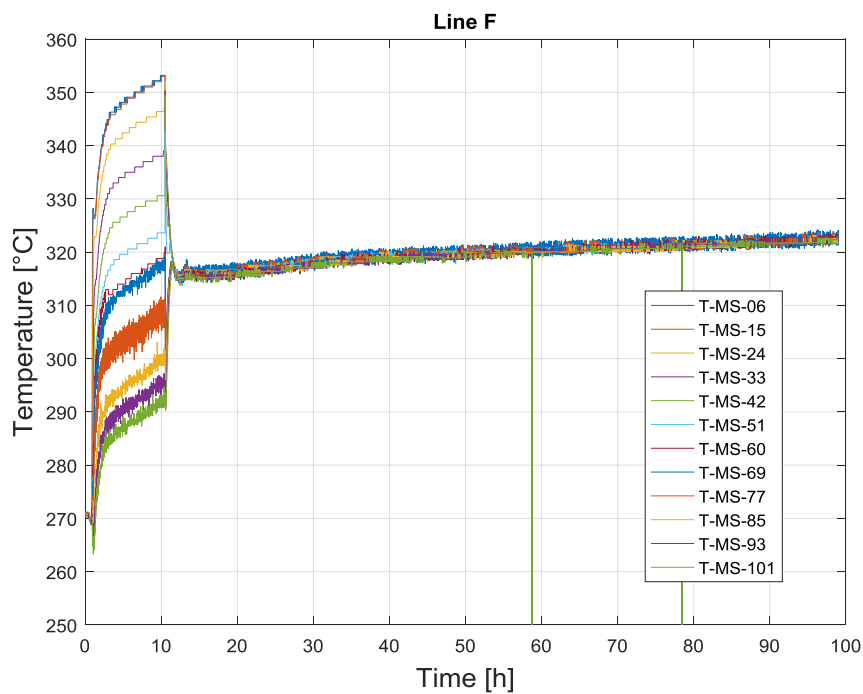


Figure 202: Temperature in the pool along Line F

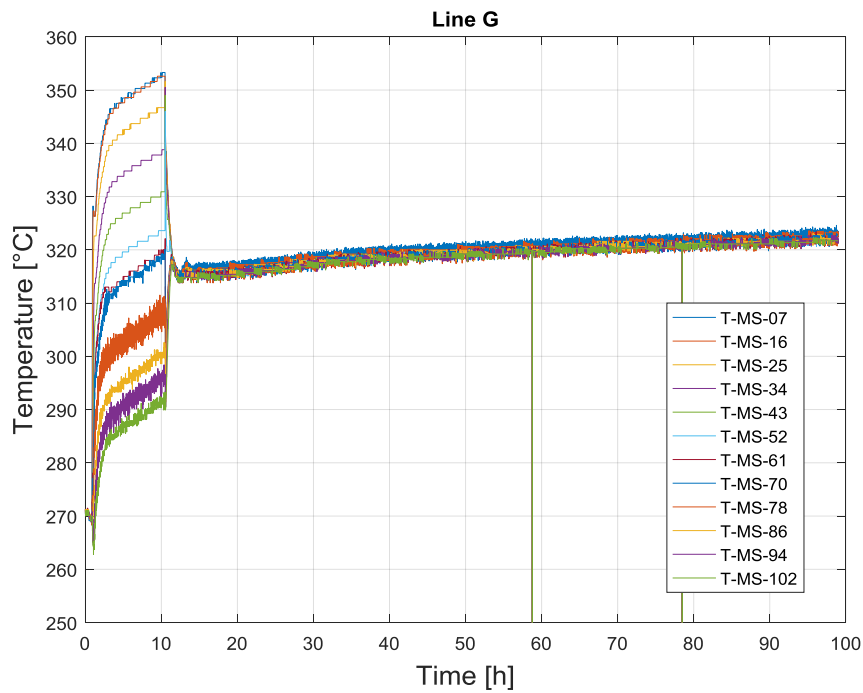


Figure 203: Temperature in the pool along Line G

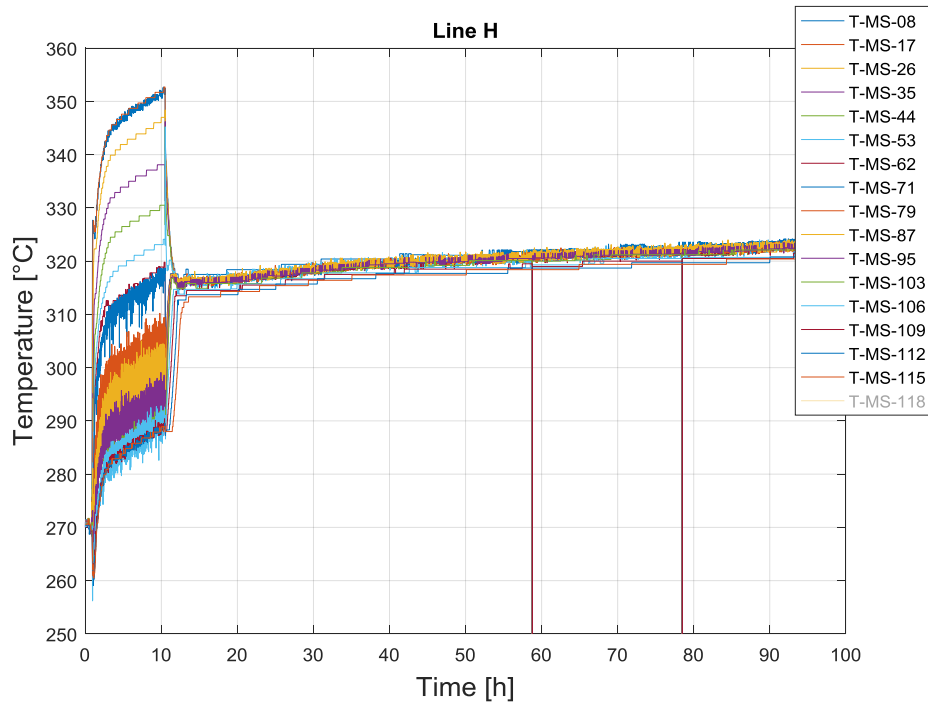



Figure 204: Temperature in the pool along Line H

 DIVISIONE INGEGNERIA SPERIMENTALE	<u>Title</u> D3.2: CIRCE experiments: pre-test, data-set and analysis	<u>Distribution</u> PUBLIC	<u>Emission</u> 09/08/2017	<u>Pag.</u> 124 di 234
		<u>Ref.</u> CI-T-R-292	Rev. 0	

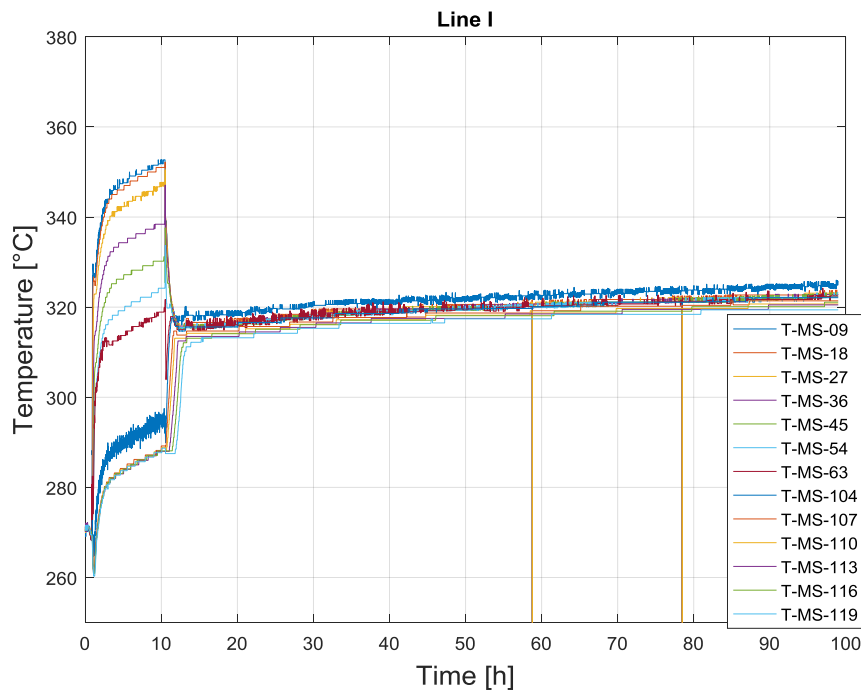



Figure 205: Temperature in the pool along Line I

3.4 Test 4

Test 4 is characterized by a nominal power ramp from 0 to 750 kW. The ramp starts at $t=1538$ s and stops at about 1681 s, the mean value of the power during the full power transient is about 750.4 kW with a standard deviation of 8.72 kW. The “full power” transient stops at about $t=40082$ s with a descending ramp up to about 31 kW ($t\sim 40204$ s, STD ~ 0.3 kW). The end of the low power run is at $t=713380$ s (~ 198 h). The electric power (DC-KW) time trend is reported in Figure 206.

 DIVISIONE INGEGNERIA SPERIMENTALE	<u>Title</u> D3.2: CIRCE experiments: pre-test, data-set and analysis	<u>Distribution</u> PUBLIC	<u>Emission</u> 09/08/2017	<u>Pag.</u> 125 di 234
		<u>Ref.</u> CI-T-R-292	Rev. 0	

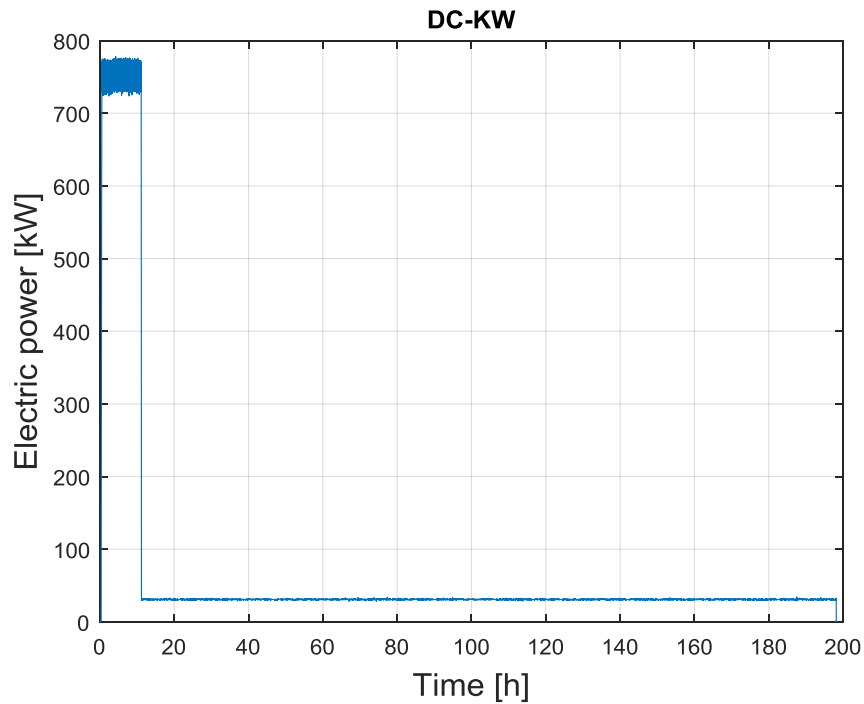



Figure 206: Electric Power [kW] (Test 4)

During the full power transient, the main heat exchanger is fed by a water mass flow rate with a mean value of 0.59 kg/s (FE501 see Figure 207) and a standard deviation 0.03 kg/s. After the simulation of the accidental scenario the water injection is stopped at about $t=37794$ s.

 DIVISIONE INGEGNERIA SPERIMENTALE	<u>Title</u> D3.2: CIRCE experiments: pre-test, data-set and analysis	<u>Distribution</u> PUBLIC	<u>Emission</u> 09/08/2017	<u>Pag.</u> 126 di 234
		<u>Ref.</u> CI-T-R-292	Rev. 0	

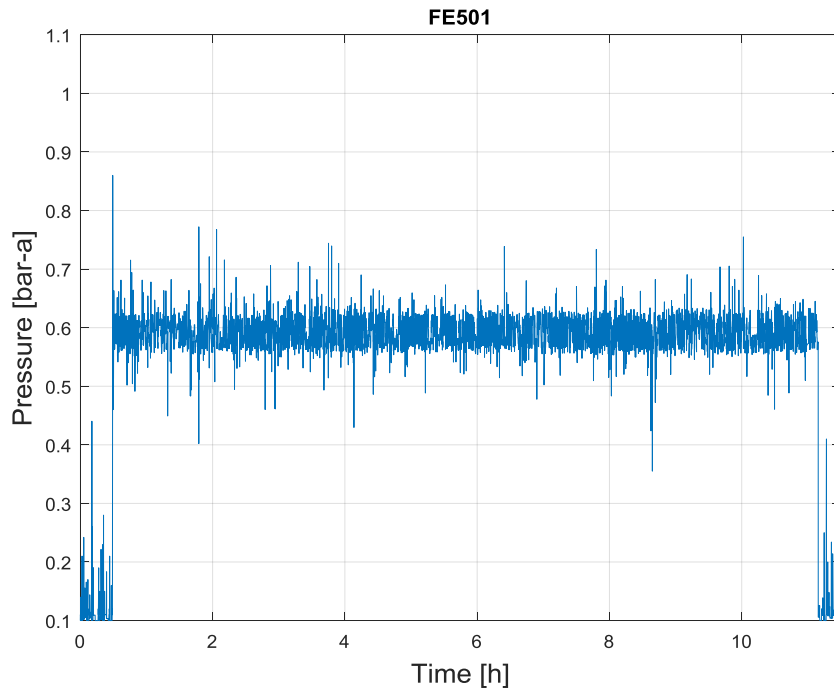


Figure 207: Water mass flow rate (Test 4)

Pressure and temperature of the water at the inlet of the HX are reported in Figure 208 and Figure 209 respectively.

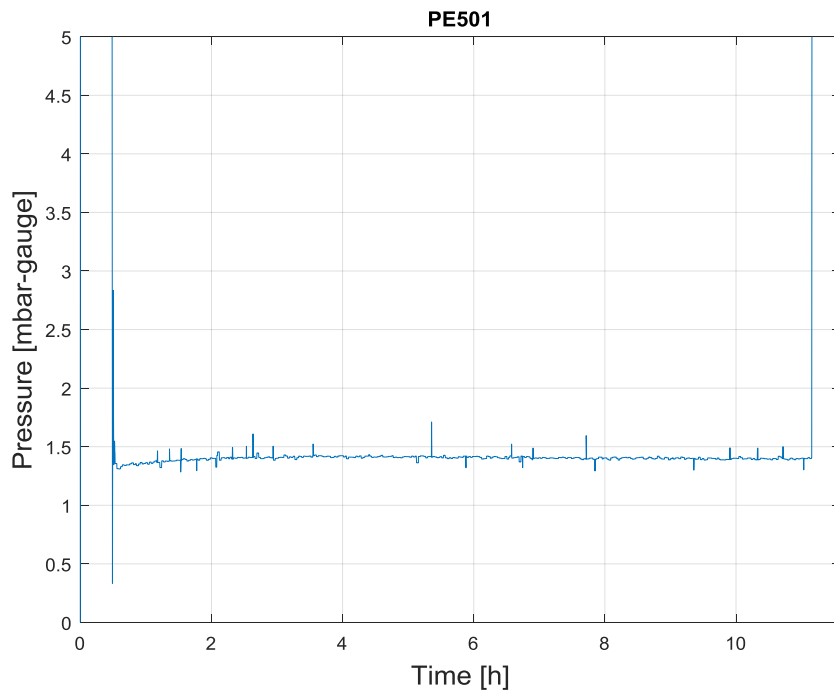



Figure 208: Water inlet pressure (Test 4)

 DIVISIONE INGEGNERIA SPERIMENTALE	<u>Title</u> D3.2: CIRCE experiments: pre-test, data-set and analysis	<u>Distribution</u> PUBLIC	<u>Emission</u> 09/08/2017	<u>Pag.</u> 127 di 234
		<u>Ref.</u> CI-T-R-292	Rev. 0	

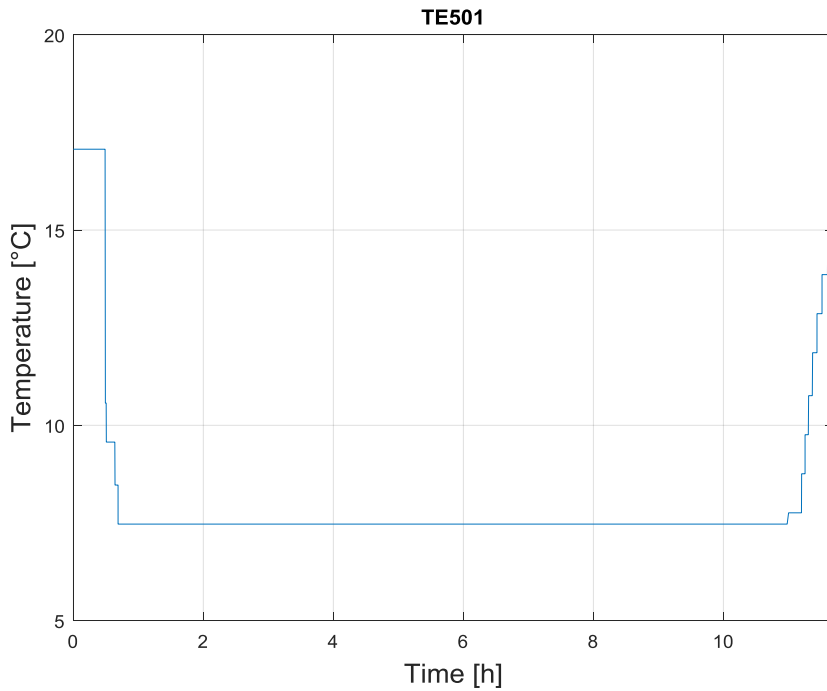


Figure 209: Water inlet temperature (Test 4)

Temperature of the steam at the outlet of the HX is reported in Figure 210.

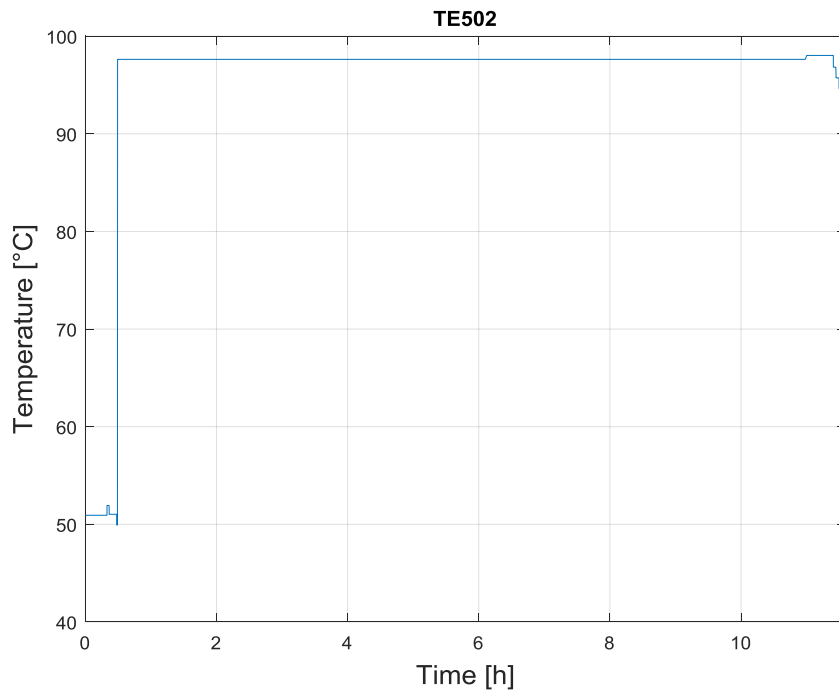



Figure 210: Steam temperature at the outlet of the HX (Test 4)

The Temperature of the helium gas entrapped in the gap between the tubes of the HX is reported in Figure 211.

 DIVISIONE INGEGNERIA SPERIMENTALE	<u>Title</u> D3.2: CIRCE experiments: pre-test, data-set and analysis	<u>Distribution</u> PUBLIC	<u>Emission</u> 09/08/2017	<u>Pag.</u> 128 di 234
		<u>Ref.</u> CI-T-R-292	Rev. 0	

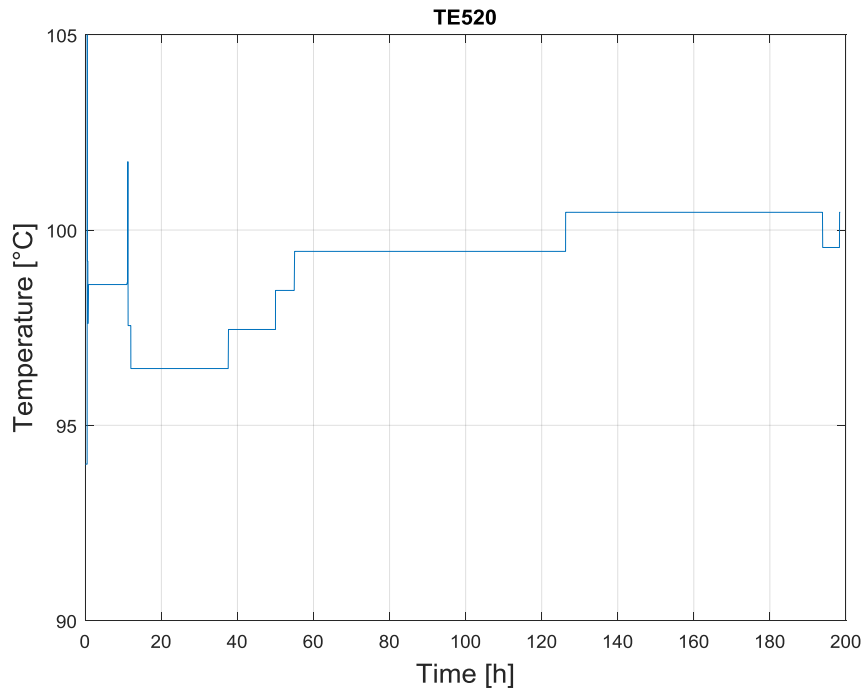



Figure 211: He temperature in the gap between the HX tubes (Test 4)

Test 4 differs from previous tests by the fact that the forced circulation is maintained also after the transition to decay heat power transient.

The gas injection, reported in Figure 212. During the full power transient, the mean value of the Argon mass flow rate is 2.75 NI/s with a standard deviation of ~0.08 NI/s, while the low power transient is operated with an argon flow rate of about 2.58 NI/s (std~ 0.3 NI/s) up to about 694400 s and then increased up to 2.75 NI/s till the end of the test.

In the low power transient the decay heat removal system (DHR) is activated injecting air in the bayonet tube of the DHR. As shown in Figure 213, the air mass flow rate mean value is 198 g/s up to the end of the test. The standard deviation is about 18.3 g/s. Inlet and outlet air temperature in the DHR are shown in Figure 214 and Figure 215. In Figure 216 the air velocity in the DHR is plotted, the mean value is 22.7 m/s.

 DIVISIONE INGEGNERIA SPERIMENTALE	<u>Title</u> D3.2: CIRCE experiments: pre-test, data-set and analysis	<u>Distribution</u> PUBLIC	<u>Emission</u> 09/08/2017	<u>Pag.</u> 129 di 234
		<u>Ref.</u> CI-T-R-292	Rev. 0	

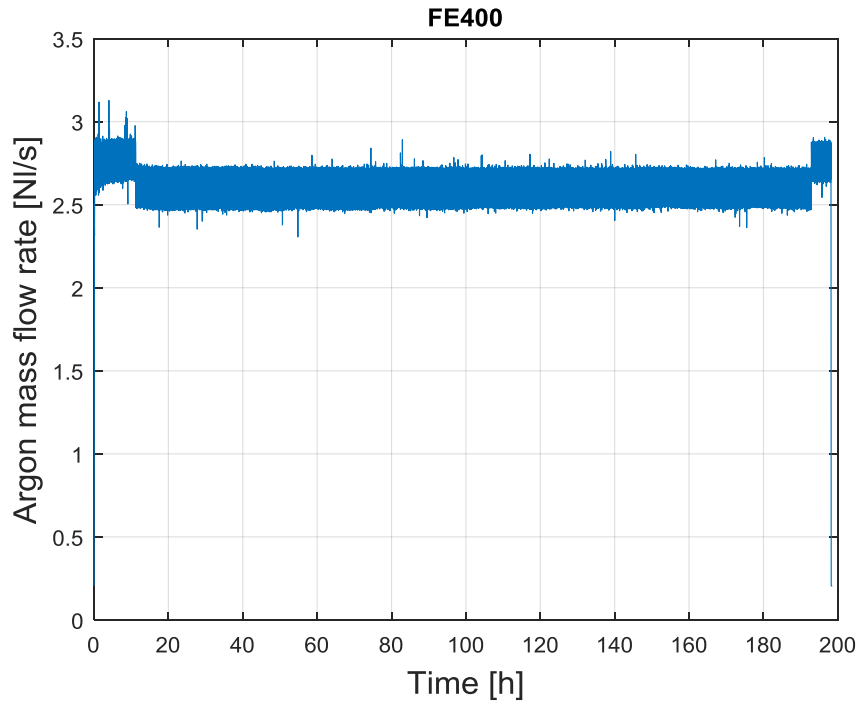


Figure 212: Argon mass flow rate (Test 4)

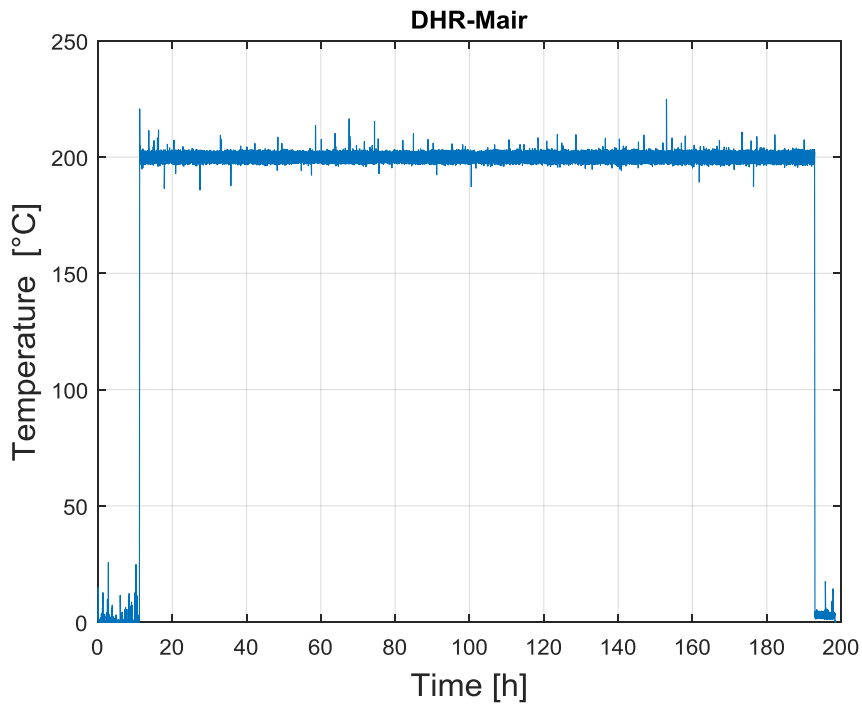


Figure 213: DHR air mass flow rate (Test 4)

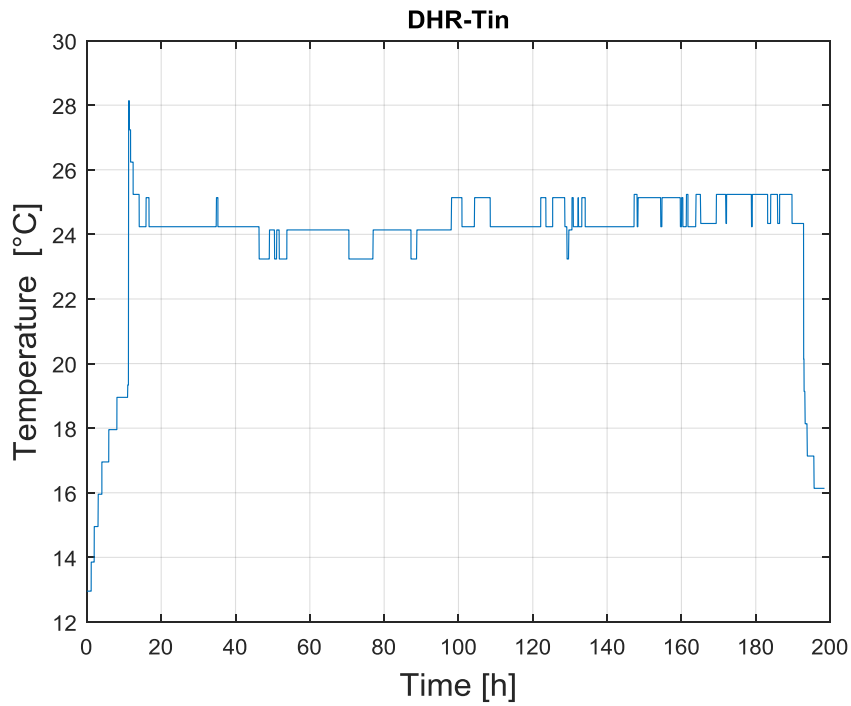


Figure 214: DHR inlet air temperature (Test3)

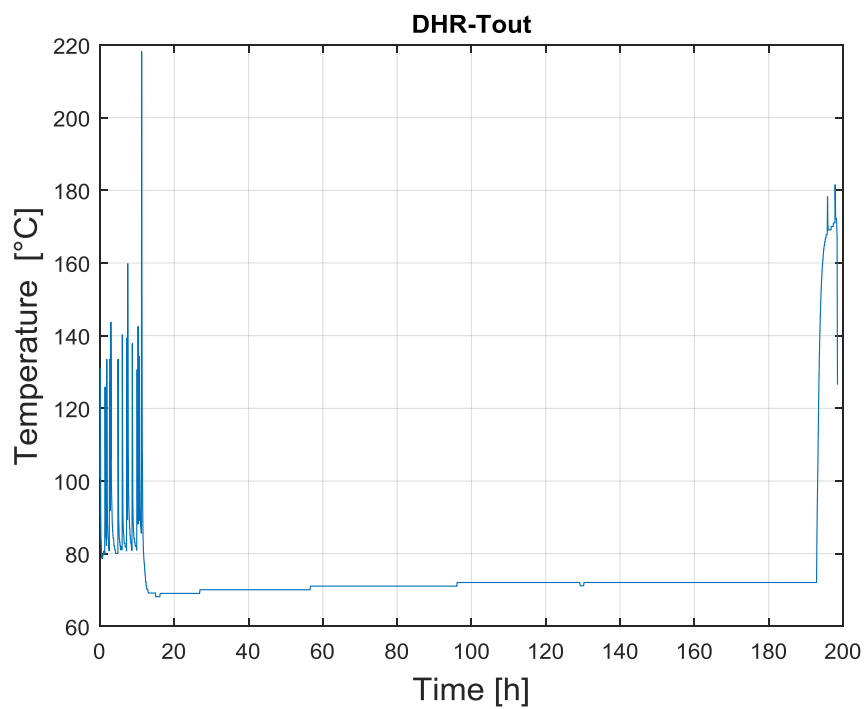



Figure 215: DHR outlet air temperature (Test3)

 DIVISIONE INGEGNERIA SPERIMENTALE	<u>Title</u> D3.2: CIRCE experiments: pre-test, data-set and analysis	<u>Distribution</u> PUBLIC	<u>Emission</u> 09/08/2017	<u>Pag.</u> 131 di 234
		<u>Ref.</u> CI-T-R-292	Rev. 0	

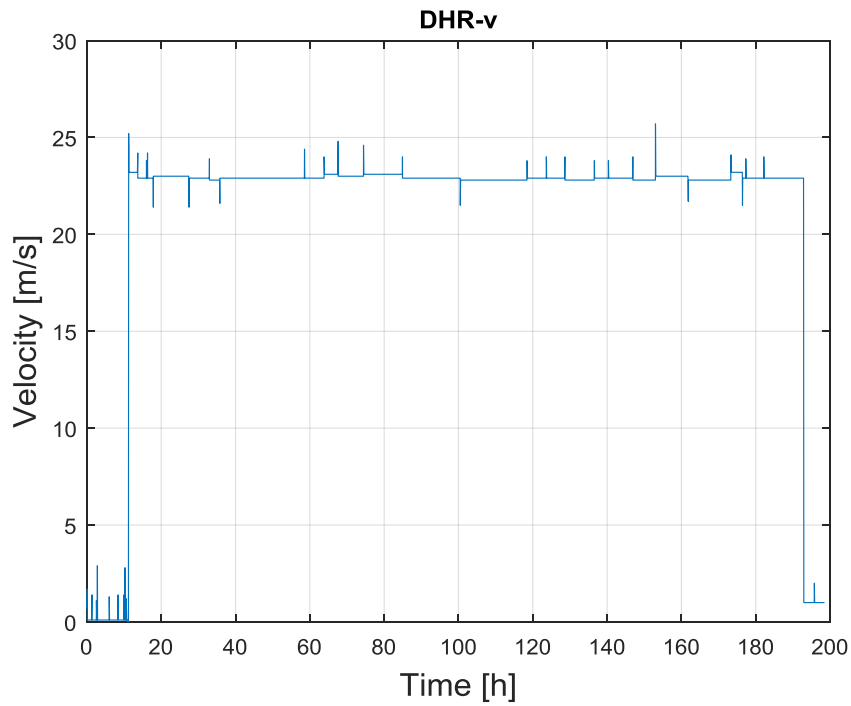



Figure 216: DHR air velocity (Test 4)

The pressure difference across the venturi flow meter (see Annex A Fig. 1 Mass flow Meter/08-384-DISEGNO.pdf) used to evaluate the LBE mass flow rate in the ICE test section is plotted in Figure 217.

 DIVISIONE INGEGNERIA SPERIMENTALE	<u>Title</u> D3.2: CIRCE experiments: pre-test, data-set and analysis	<u>Distribution</u> PUBLIC	<u>Emission</u> 09/08/2017	<u>Pag.</u> 132 di 234
		<u>Ref.</u> CI-T-R-292	Rev. 0	

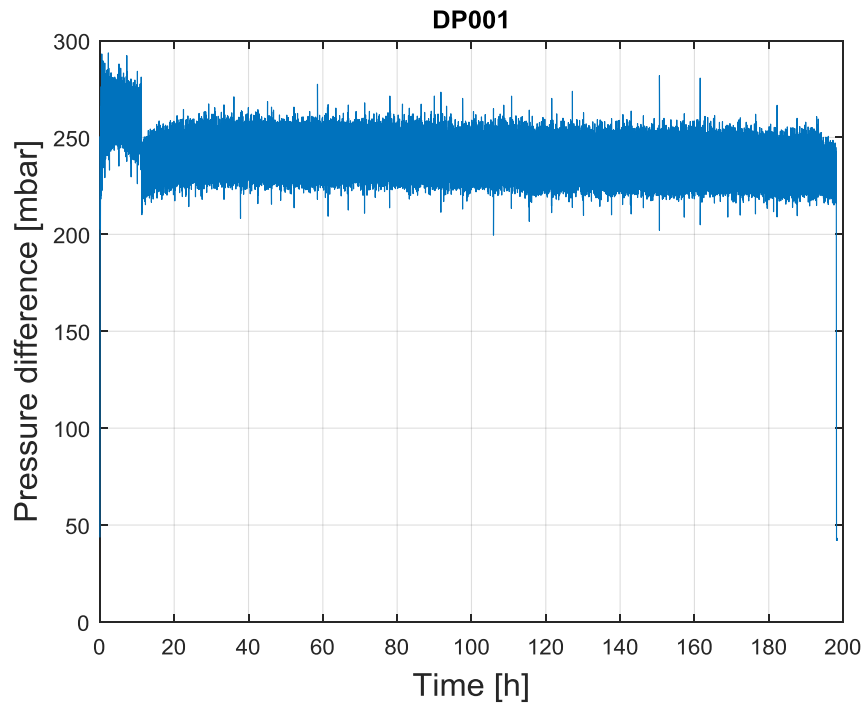



Figure 217: Pressure difference across the venturi flow meter (Test 4)

DP002 (PE009-PE010), reported in Figure 218, represents the pressure difference across the lower spacer grid (for the positioning of the bubble tubes see Annex A Fig. 2 0510 Rev 1-Fuel Pin Simulator.pdf).

PE003 represents the pressure in the fitting volume (Figure 219) while PE004 (Figure 220), PE005 (Figure 221) represent respectively the pressure in the lower and upper section of the riser. For the position of the bubble tubes PE003, PE004, PE005 see Annex A Fig. 3 0016 Instrumentation.pdf.

 DIVISIONE INGEGNERIA SPERIMENTALE	<u>Title</u> D3.2: CIRCE experiments: pre-test, data-set and analysis	<u>Distribution</u> PUBLIC	<u>Emission</u> 09/08/2017	<u>Pag.</u> 133 di 234
		<u>Ref.</u> CI-T-R-292	Rev. 0	

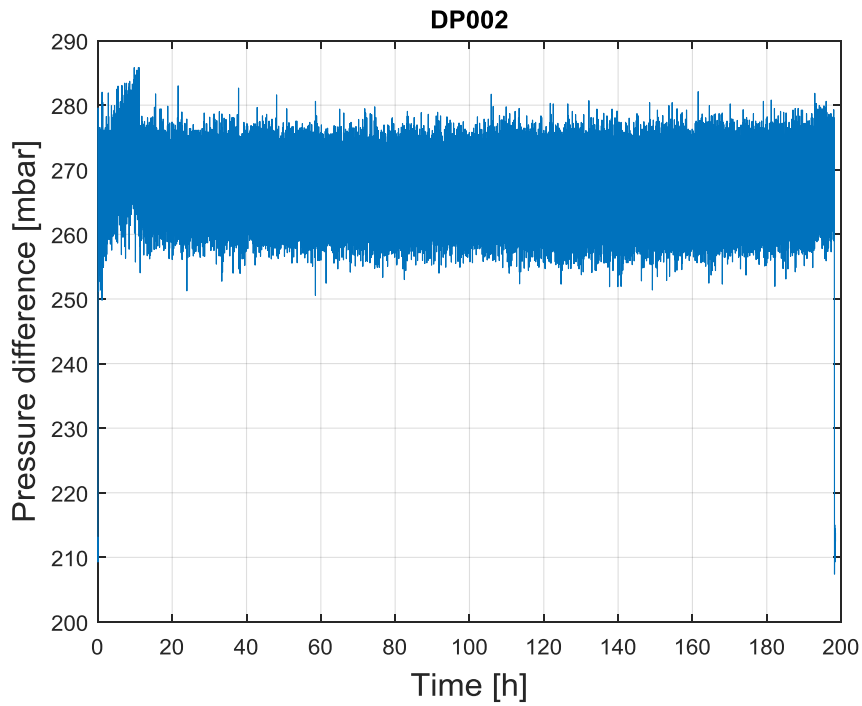


Figure 218: Pressure difference across the FPS lower spacer grid (Test 4)

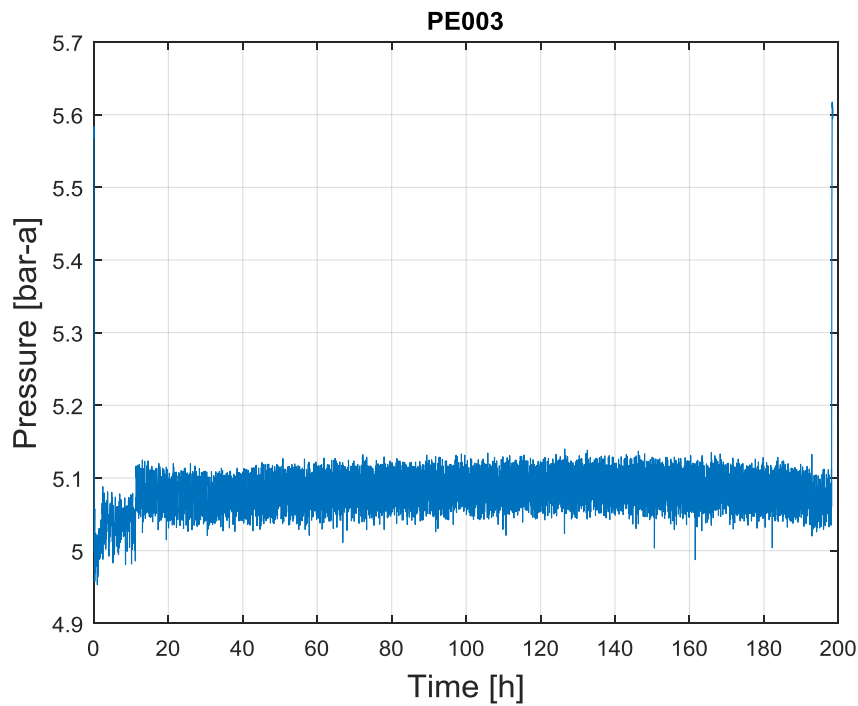



Figure 219: Pressure in the fitting volume (Test 4)

 DIVISIONE INGEGNERIA SPERIMENTALE	<u>Title</u> D3.2: CIRCE experiments: pre-test, data-set and analysis	<u>Distribution</u> PUBLIC	<u>Emission</u> 09/08/2017	<u>Pag.</u> 134 di 234
		<u>Ref.</u> CI-T-R-292	Rev. 0	

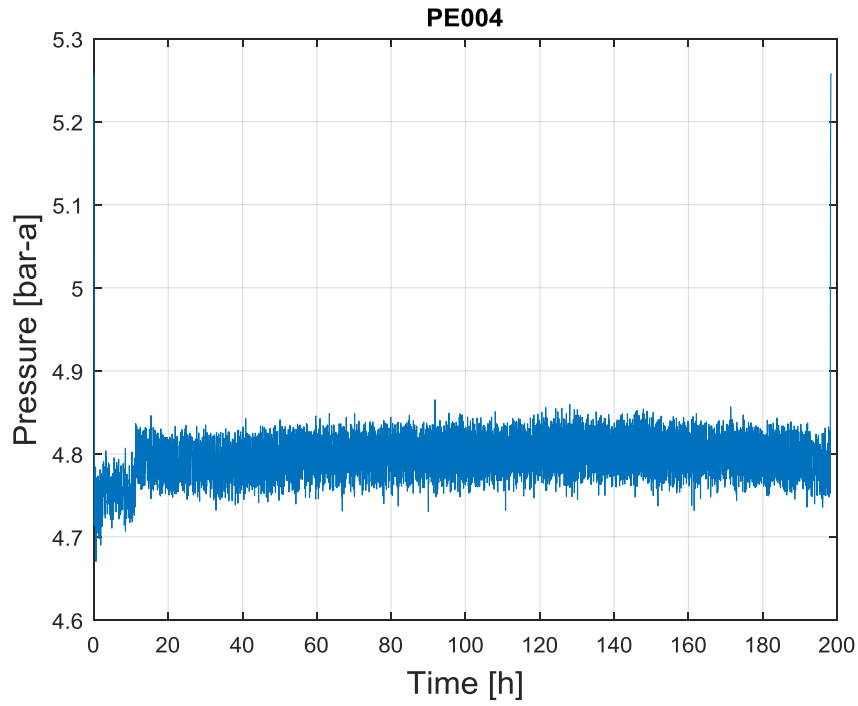


Figure 220: Pressure in the riser (lower section) (Test 4)

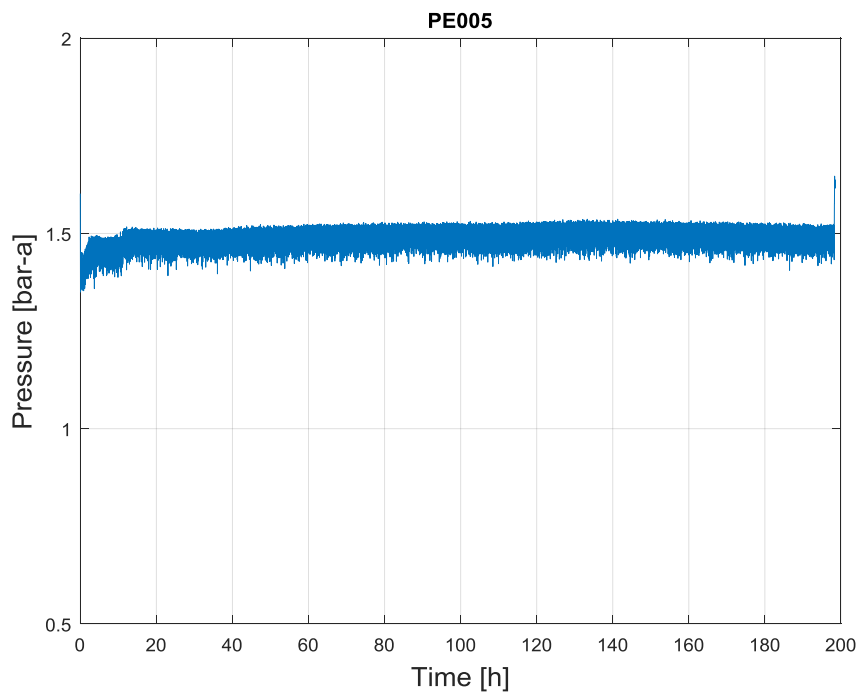



Figure 221: Pressure in the riser (upper section) (Test 4)

 DIVISIONE INGEGNERIA SPERIMENTALE	<u>Title</u> D3.2: CIRCE experiments: pre-test, data-set and analysis	<u>Distribution</u> PUBLIC	<u>Emission</u> 09/08/2017	<u>Pag.</u> 135 di 234
		<u>Ref.</u> CI-T-R-292	Rev. 0	

The LBE inside the pool is operated under a protective atmosphere of Argon gas that fill the volume from the LBE free level to the vessel head. A relative small overpressure is maintained in the gas in order to avoid oxygen contamination from the external environment. PE007 is the pressure of the argon measured in the cover gas (pressure gauge, see Figure 222), while the temperature of the cover gas is measured through a 3 mm K-type thermocouple and reported in Figure 223.

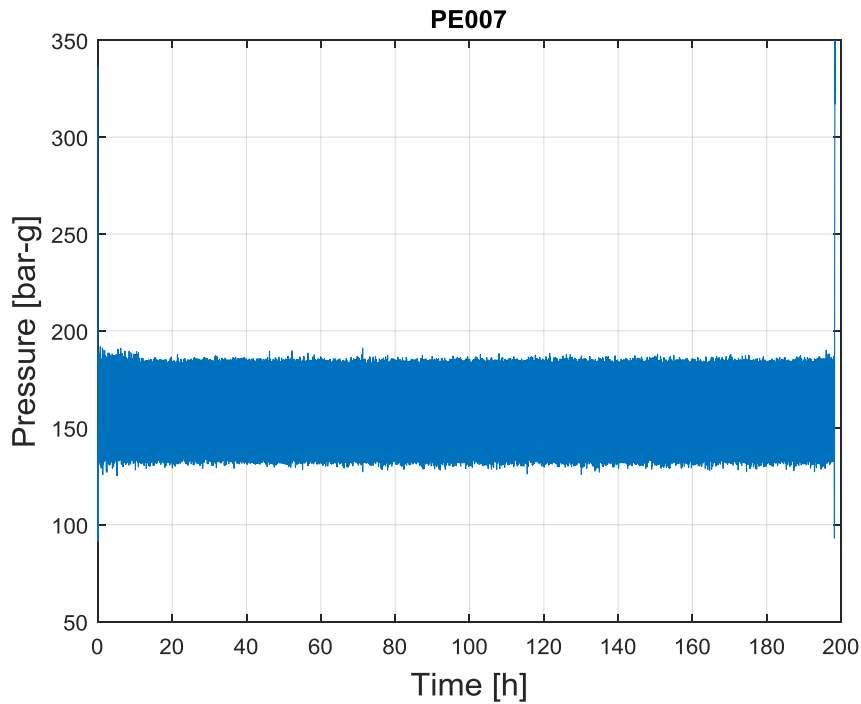



Figure 222: Pressure in the cover gas (Test 4)

 DIVISIONE INGEGNERIA SPERIMENTALE	<u>Title</u> D3.2: CIRCE experiments: pre-test, data-set and analysis	<u>Distribution</u> PUBLIC	<u>Emission</u> 09/08/2017	<u>Pag.</u> 136 di 234
		<u>Ref.</u> CI-T-R-292	Rev. 0	

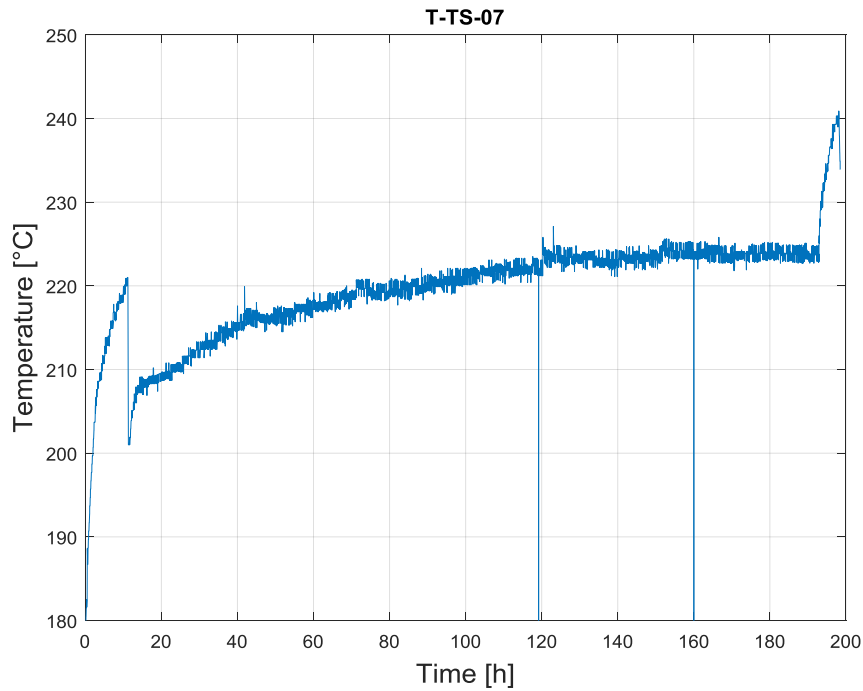



Figure 223: Temperature in the cover gas (Test 4)

For the positioning of the thermocouples in the DHR system refers to Annex A Fig. 4 THINS thermocouples arrangement.pdf and Annex A Fig. 5 T-DHR-0100-Instrumentation DHR.pdf. In Figure 224, the average temperature of the LBE at the inlet and outlet sections of the DHR is reported. In Test 4 the same phenomena encountered in Test 1 and Test 3 was observed. For the whole duration of the transient at low power temperature, the inlet section of the DHR shows a lower value compared to the LBE temperatures at the outlet section (for the physical interpretation refers to Annex C)

 DIVISIONE INGEGNERIA SPERIMENTALE	<u>Title</u> D3.2: CIRCE experiments: pre-test, data-set and analysis	<u>Distribution</u> PUBLIC	<u>Emission</u> 09/08/2017	<u>Pag.</u> 137 di 234
		<u>Ref.</u> CI-T-R-292	Rev. 0	

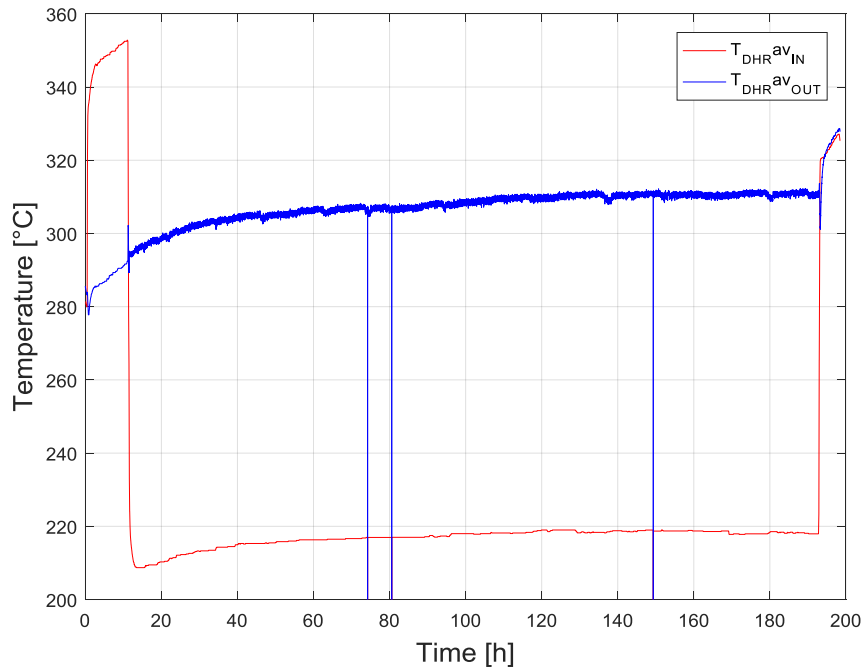



Figure 224: DHR inlet outlet average temperature (Test 4)

The LBE temperature at the FPS entrance was measured by three thermocouples with a diameter of 3 mm (T-FPS-31, 32, 33, Annex A Fig. 6 T-FPS-0100 foglio2-FPS Instrumented). The LBE temperature at the active length exit section of the FPS was measured by three thermocouples (T-FPS-34, 35, 36 Annex A Fig. 6 T-FPS-0100 foglio2-FPS Instrumented) of the same type of those at the entrance. Moreover three thermocouples T-FPS-37, 38, 39 were installed in the slot at the exit of the FPS placed at 120° (see Annex A Fig. 7 T-FPS-0100 foglio1-FPS Instrumented). For the position of the thermocouples inside the bundle refers to Annex A Fig. 8 T-FPS Instrumentation 1 of 2 and Annex A Fig. 9 T-FPS Instrumentation 2 of 2. In Figure 225 the LBE average temperature evaluated at the inlet and outlet sections of the FPS and at the outlet section of the FPS are reported (see Annex A Fig. 7 T-FPS-0100 foglio1-FPS Instrumented).

 DIVISIONE INGEGNERIA SPERIMENTALE	<u>Title</u> D3.2: CIRCE experiments: pre-test, data-set and analysis	<u>Distribution</u> PUBLIC	<u>Emission</u> 09/08/2017	<u>Pag.</u> 138 di 234
		<u>Ref.</u> CI-T-R-292	Rev. 0	

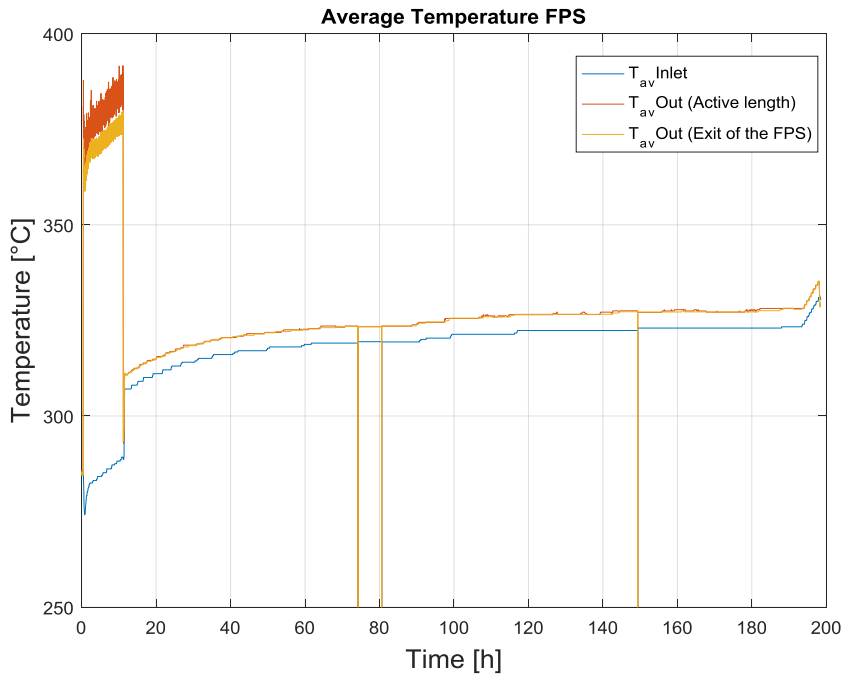


Figure 225: Active length Inlet/Outlet section and FPS Outlet LBE temperature (Test 4)

From Figure 226 to Figure 253 the single temperature in the Fuel Pin Simulator (FPS) are reported. It is worth to be mentioned that T-FPS-07 and T-FPS-013 are broken and therefore the relative plots are not reported.

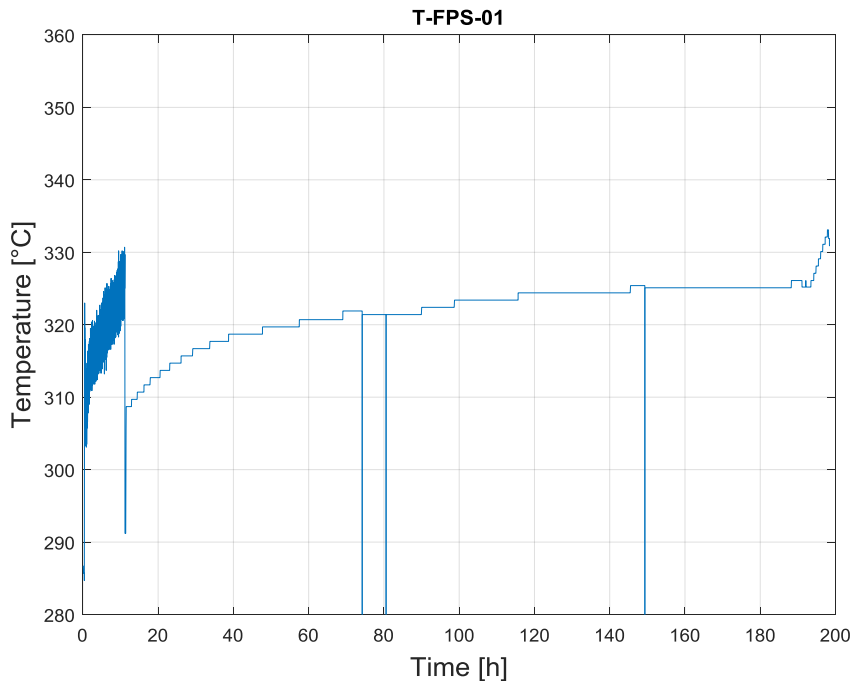


Figure 226: T-FPS-01 LBE temperature (Test 4)

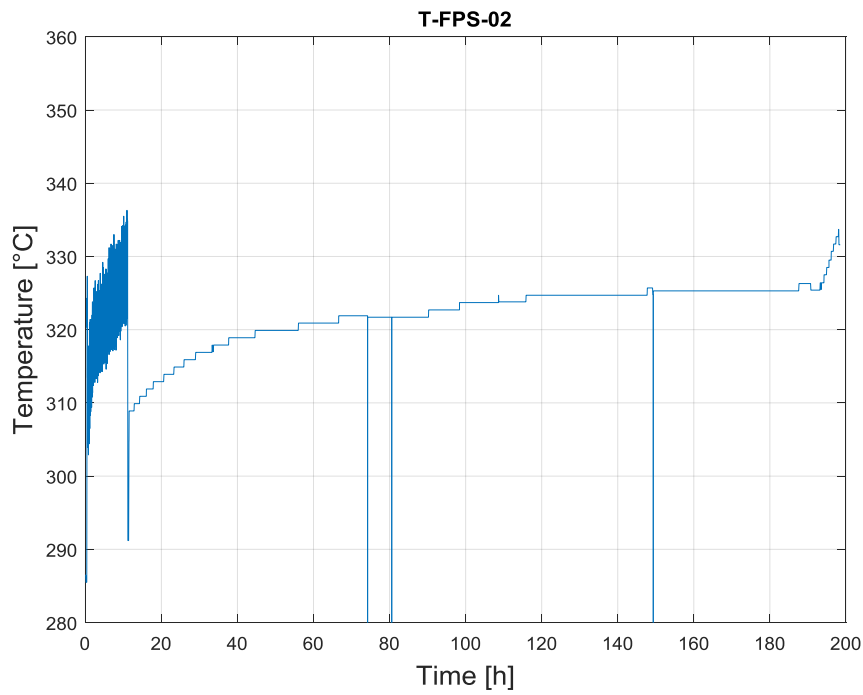


Figure 227: T-FPS-02 LBE temperature (Test 4)

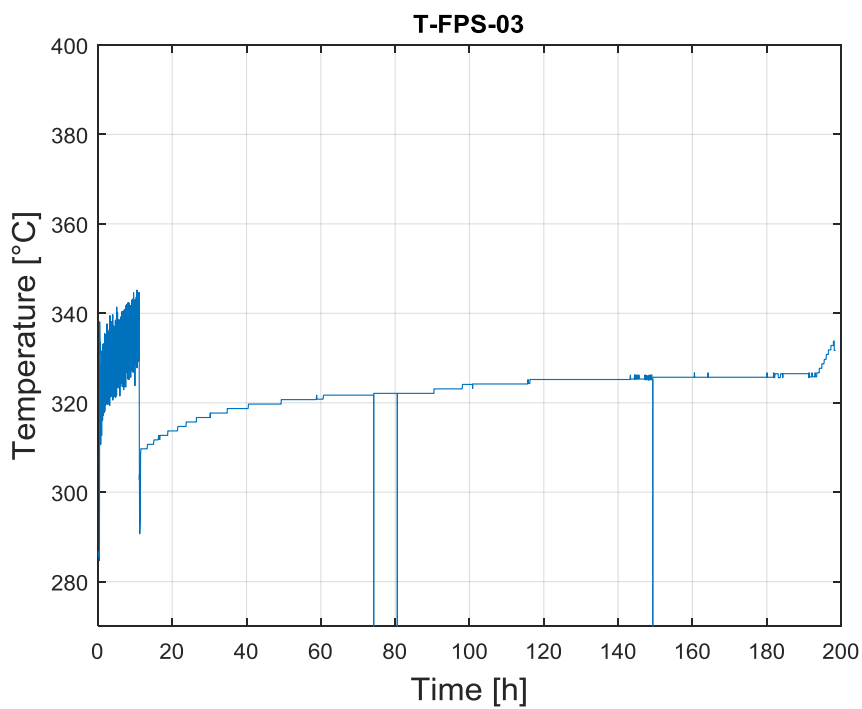


Figure 228: T-FPS-03 LBE temperature (Test 4)

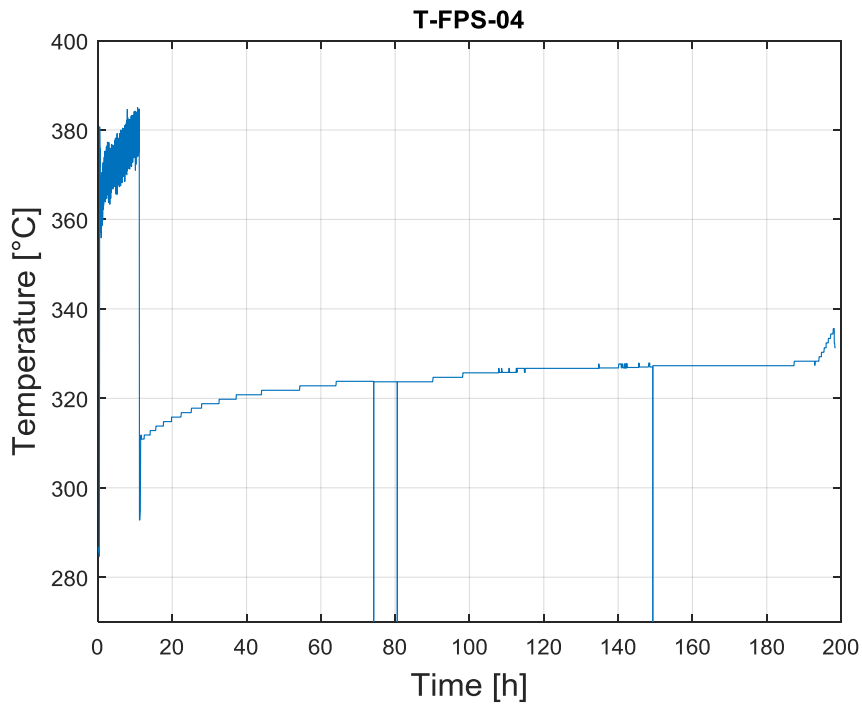


Figure 229: T-FPS-04 LBE temperature (Test 4)

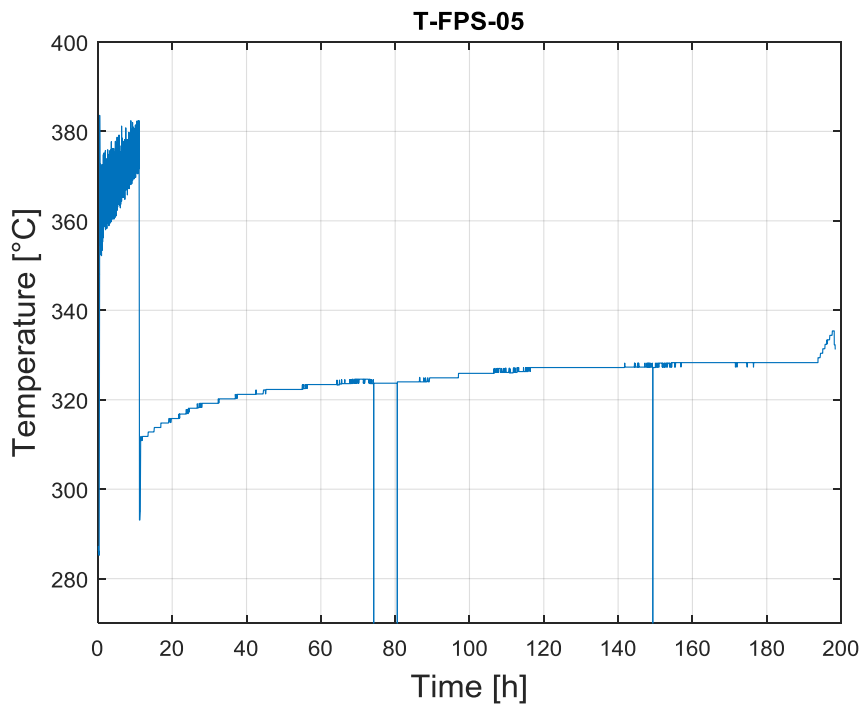


Figure 230: T-FPS-05 LBE temperature (Test 4)

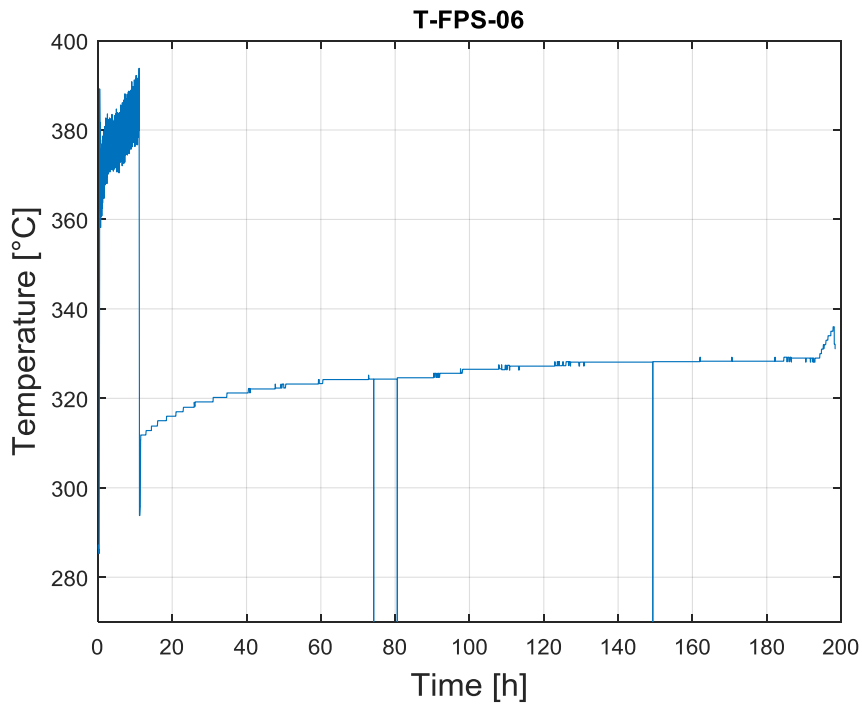


Figure 231: T-FPS-06 LBE temperature (Test 4)

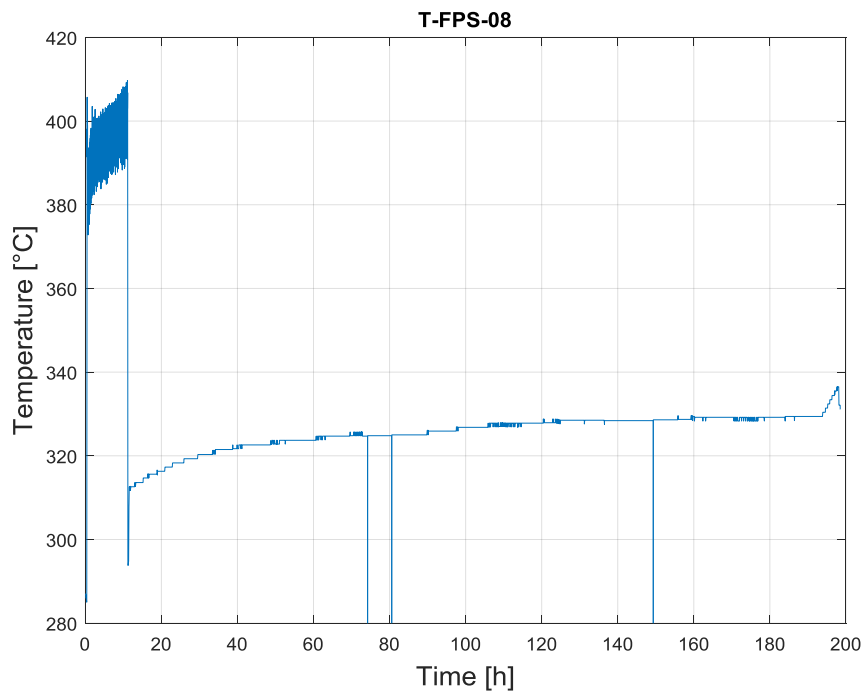


Figure 232: T-FPS-08 LBE temperature (Test 4)

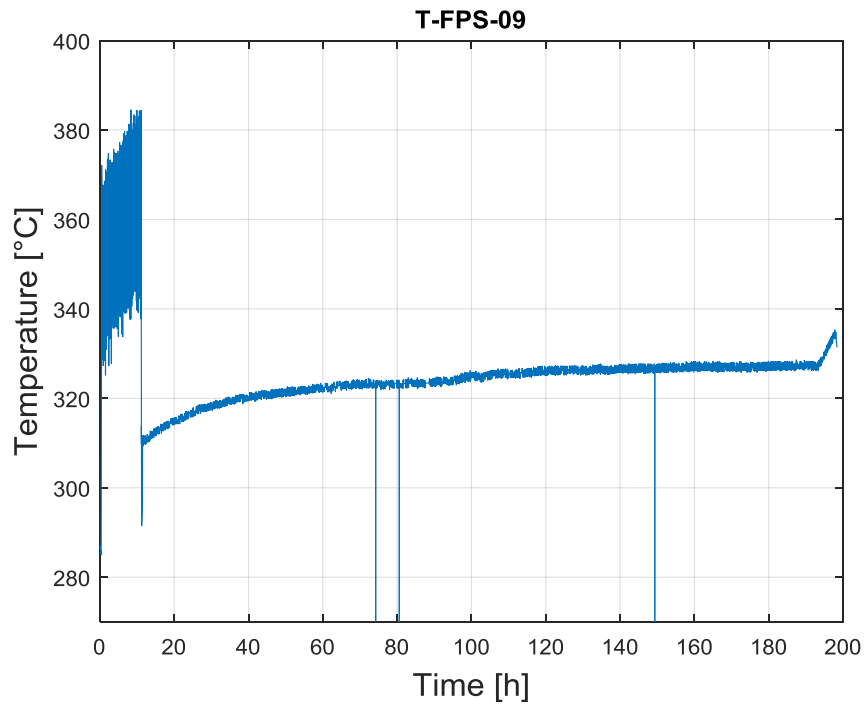


Figure 233: T-FPS-09 LBE temperature (Test 4)

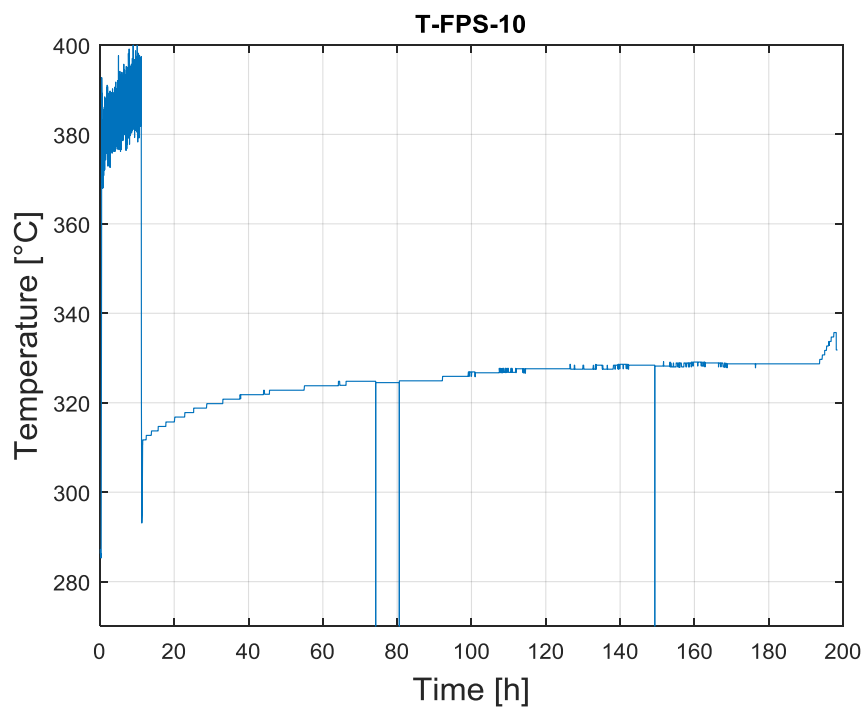


Figure 234: T-FPS-10 LBE temperature (Test 4)

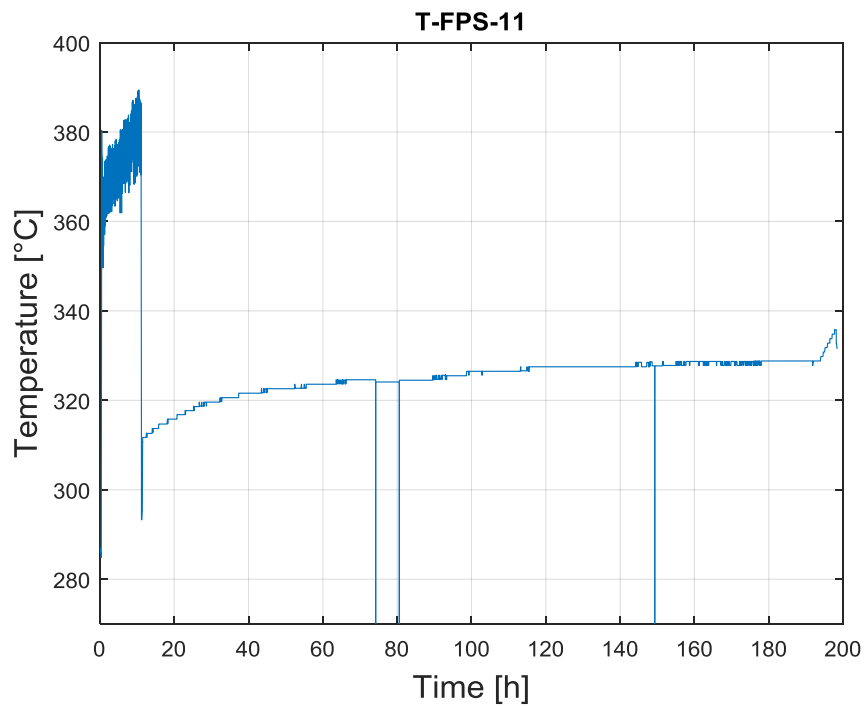


Figure 235: T-FPS-11 LBE temperature (Test 4)

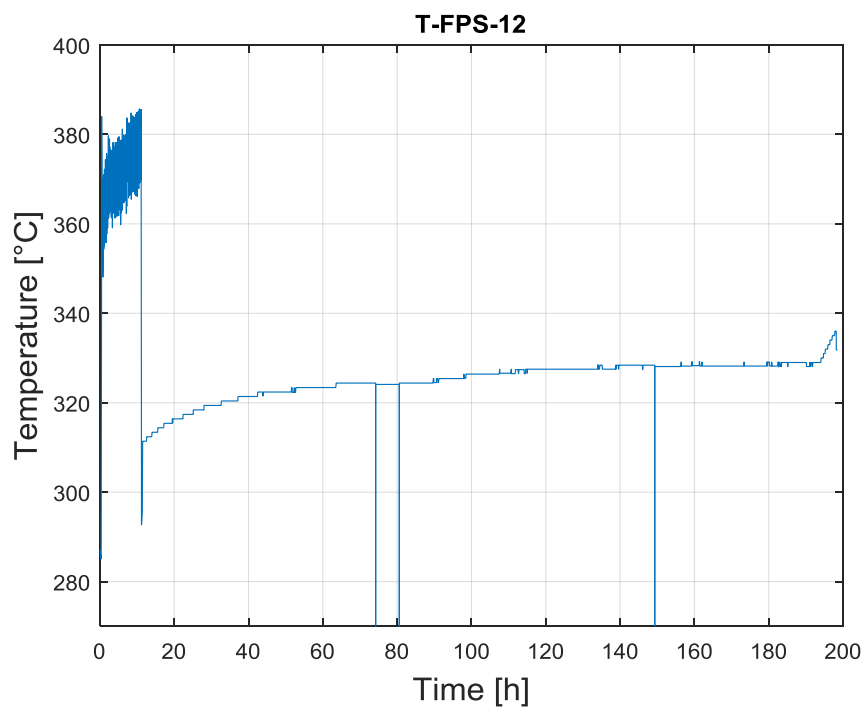


Figure 236: T-FPS-12 LBE temperature (Test 4)

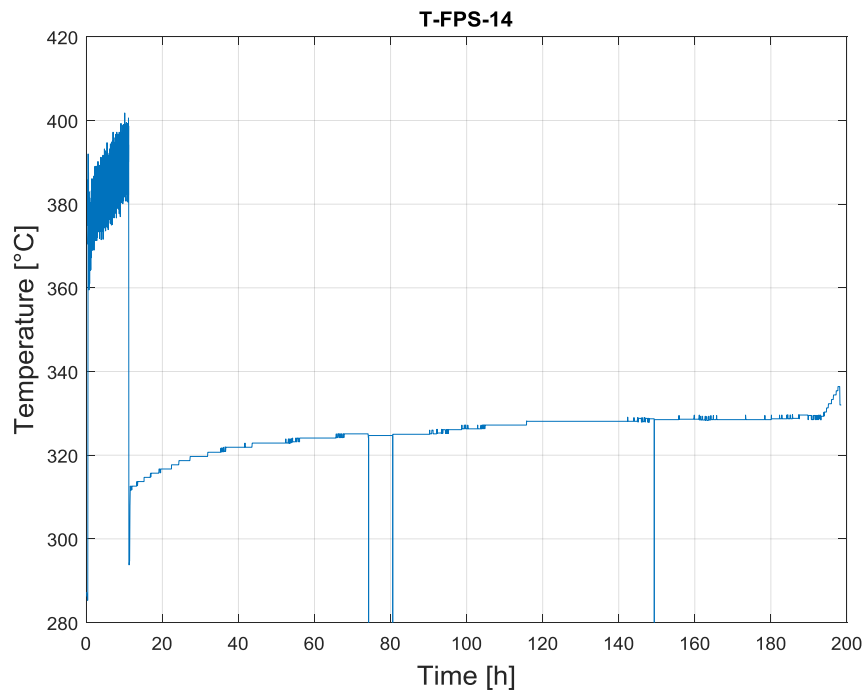


Figure 237: T-FPS-14 LBE temperature (Test 4)

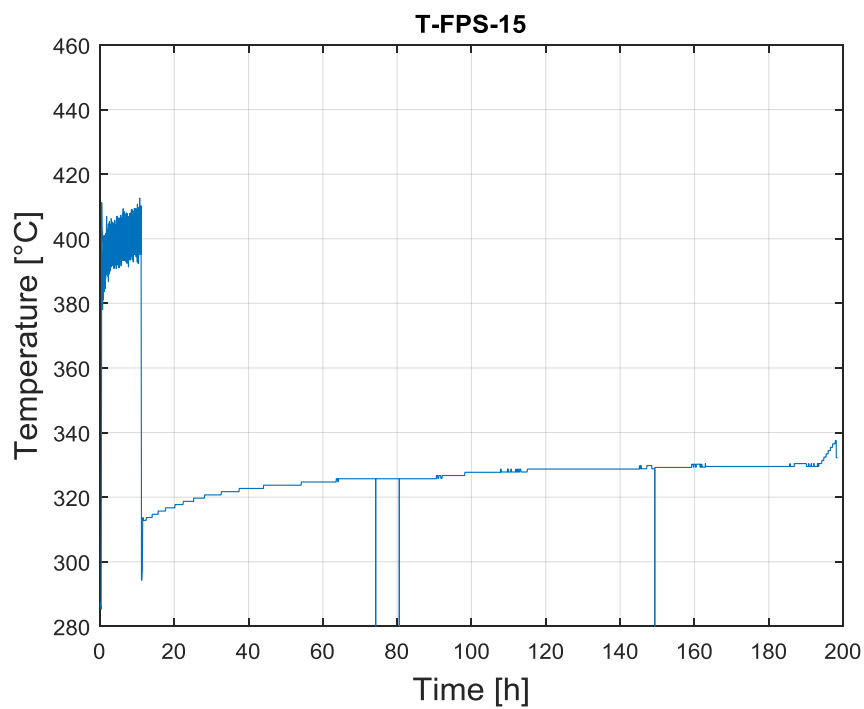


Figure 238: T-FPS-15 LBE temperature (Test 4)

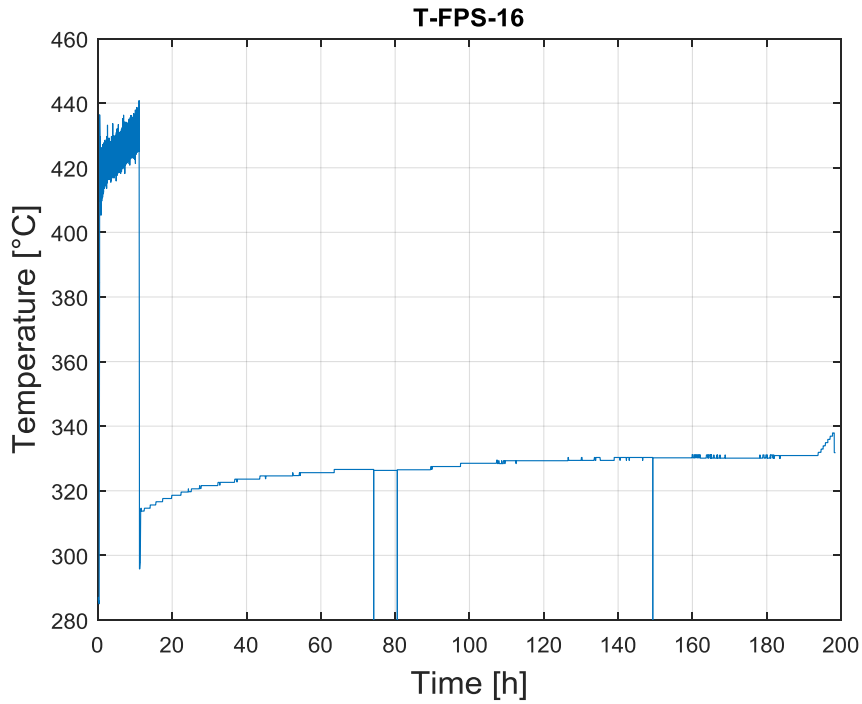


Figure 239: T-FPS-16 LBE temperature (Test 4)

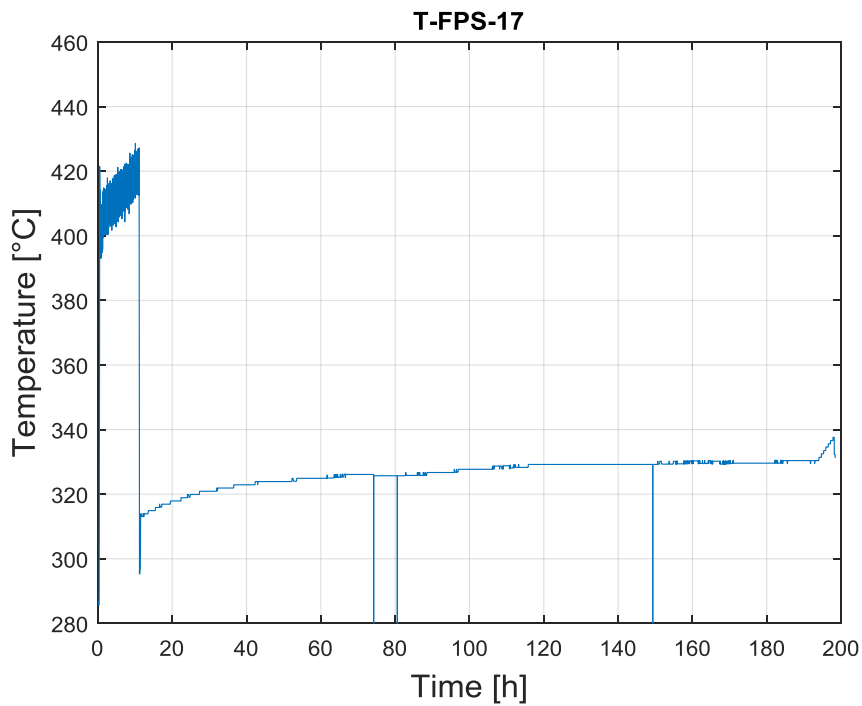


Figure 240: T-FPS-17 LBE temperature (Test 4)

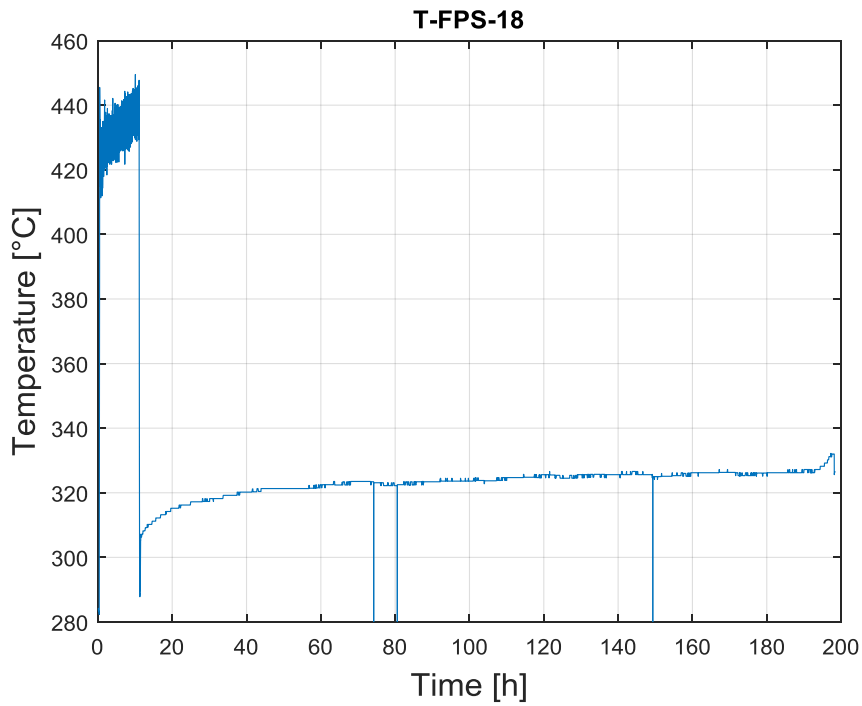


Figure 241: T-FPS-18 LBE temperature (Test 4)

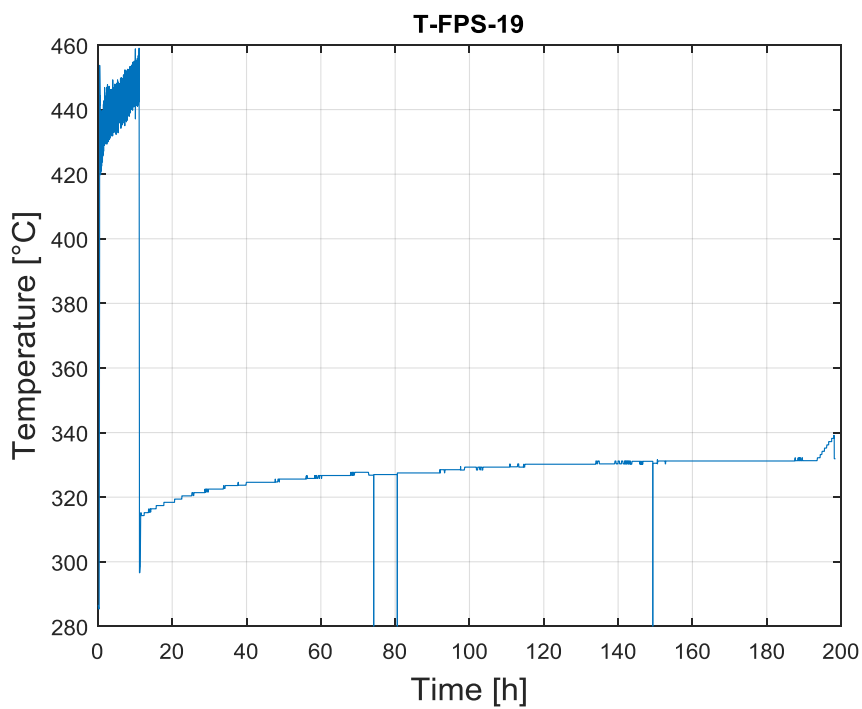


Figure 242: T-FPS-19 LBE temperature (Test 4)

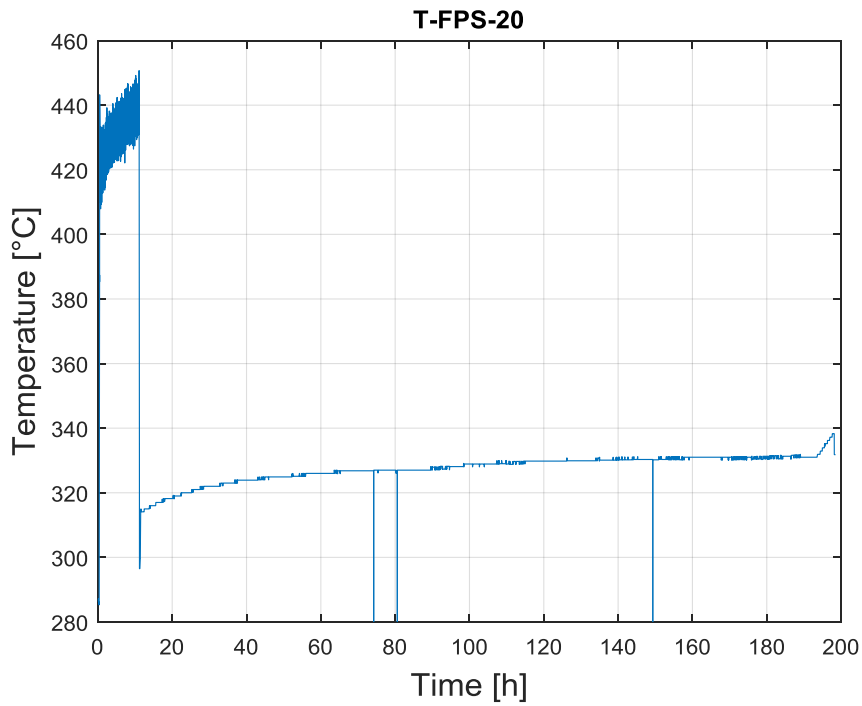


Figure 243: T-FPS-20 LBE temperature (Test 4)

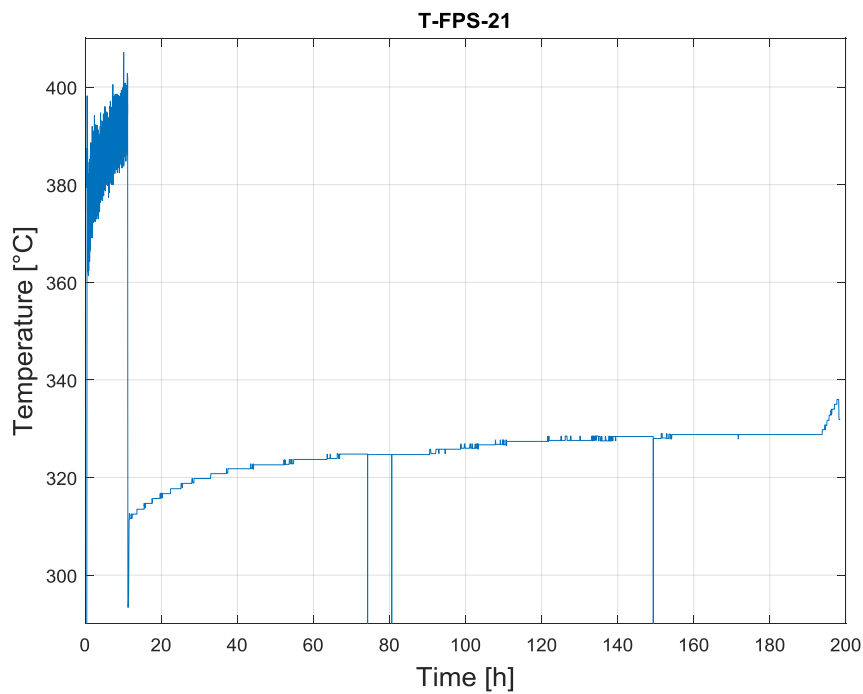


Figure 244: T-FPS-21 LBE temperature (Test 4)

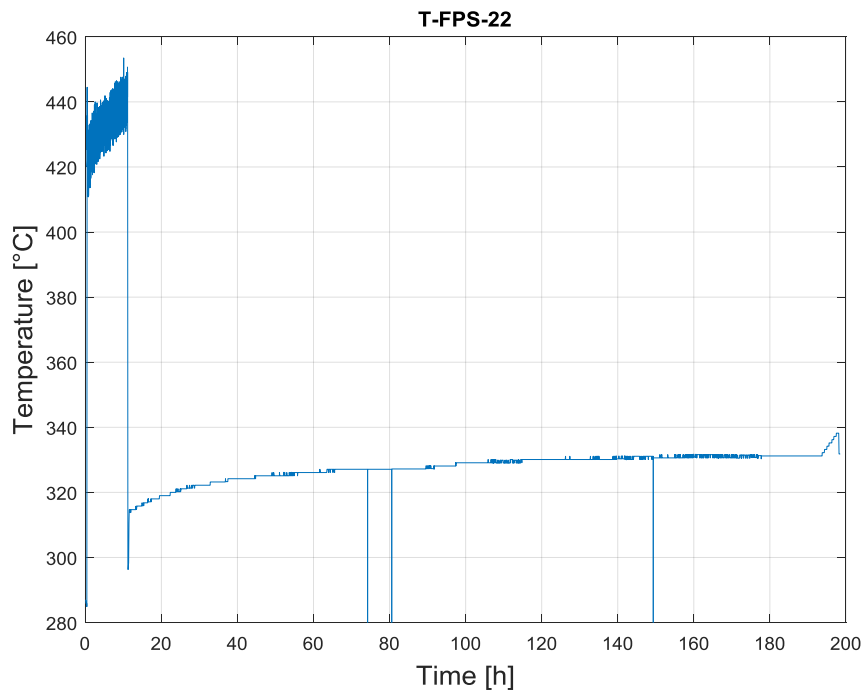


Figure 245: T-FPS-22 LBE temperature (Test 4)

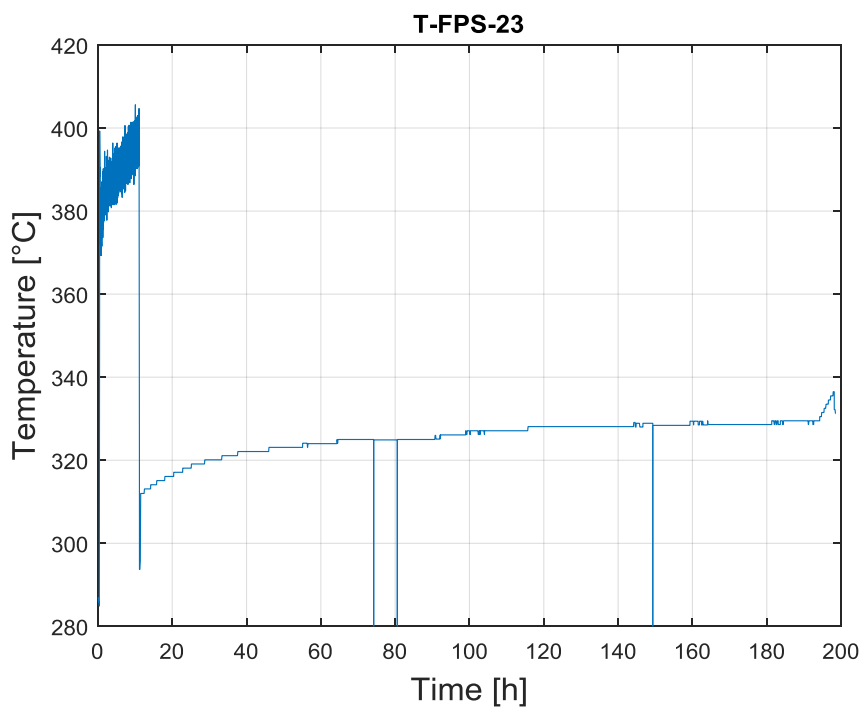


Figure 246: T-FPS-23 LBE temperature (Test 4)

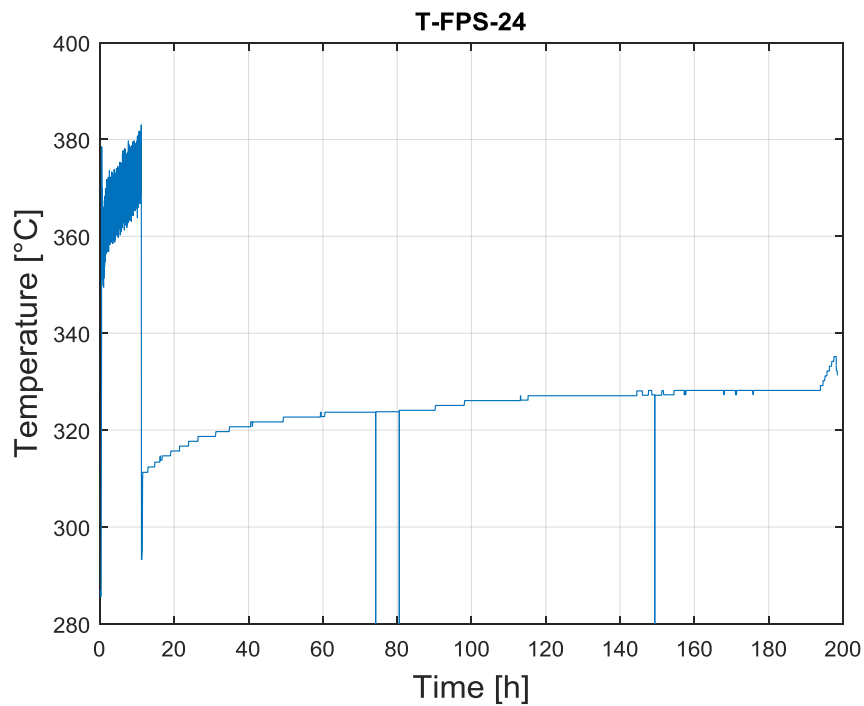


Figure 247: T-FPS-24 LBE temperature (Test 4)

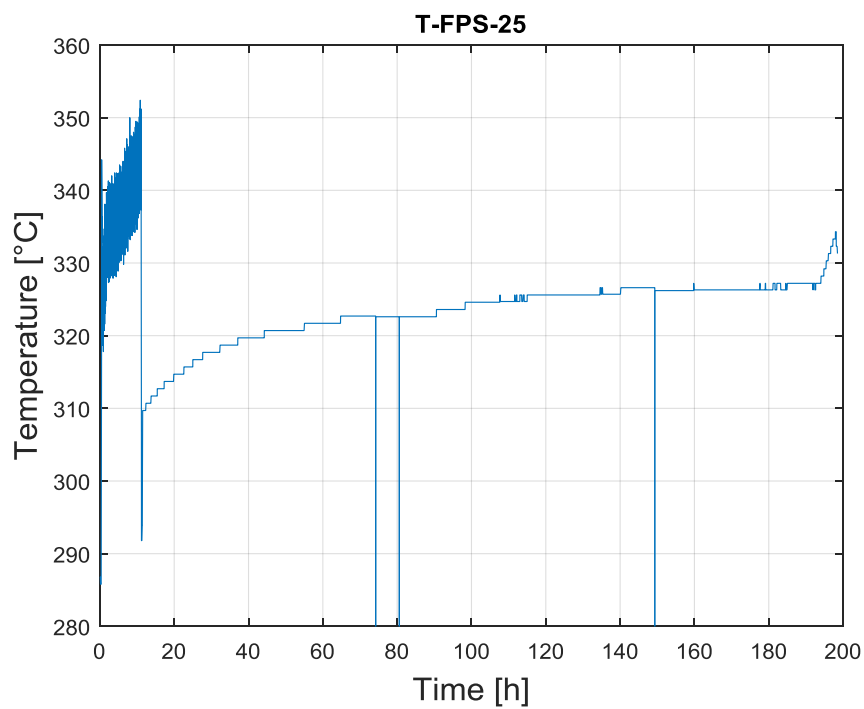


Figure 248: T-FPS-25 LBE temperature (Test 4)

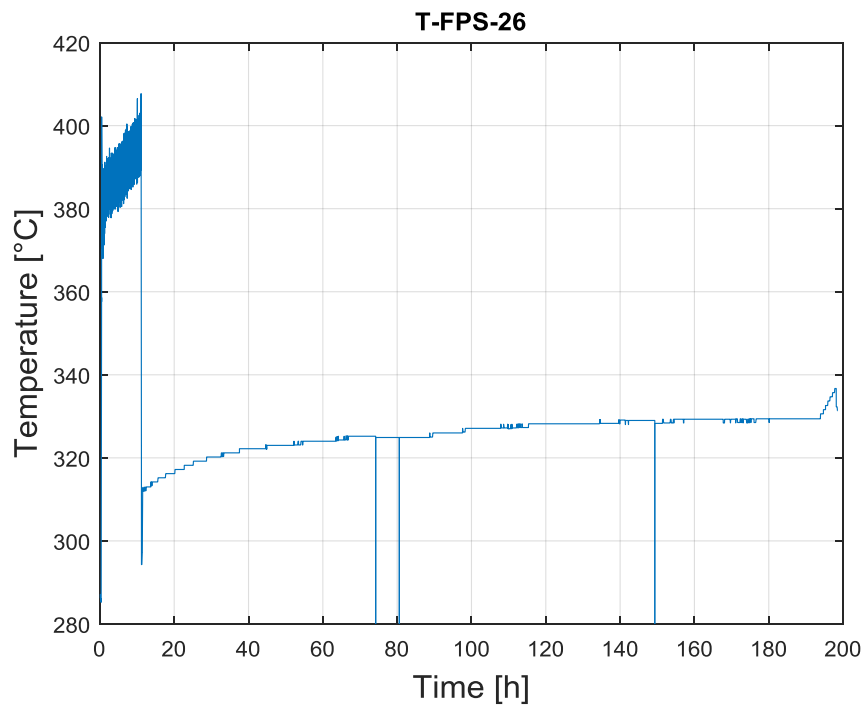


Figure 249: T-FPS-26 LBE temperature (Test 4)

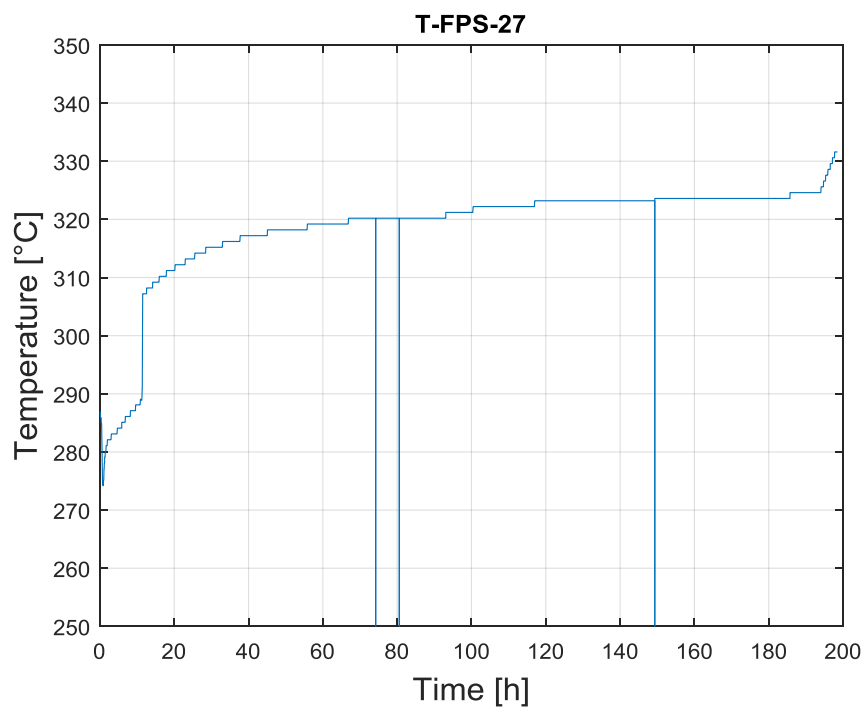


Figure 250: T-FPS-27 LBE temperature (Test 4)

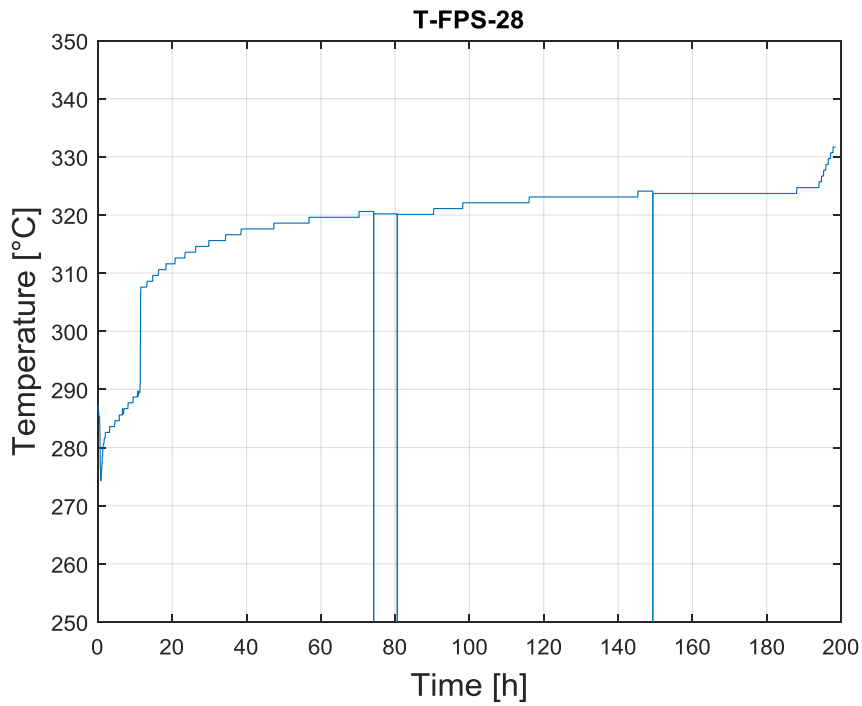


Figure 251: T-FPS-28 LBE temperature (Test 4)

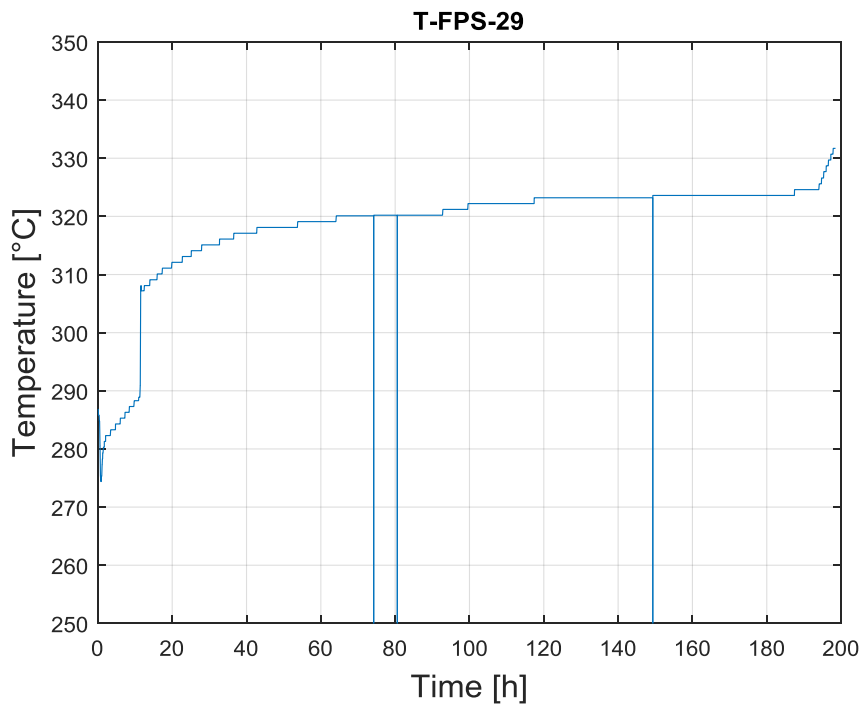



Figure 252: T-FPS-29 LBE temperature (Test 4)

 DIVISIONE INGEGNERIA SPERIMENTALE	<u>Title</u> D3.2: CIRCE experiments: pre-test, data-set and analysis	<u>Distribution</u> PUBLIC	<u>Emission</u> 09/08/2017	<u>Pag.</u> 152 di 234
		<u>Ref.</u> CI-T-R-292	Rev. 0	

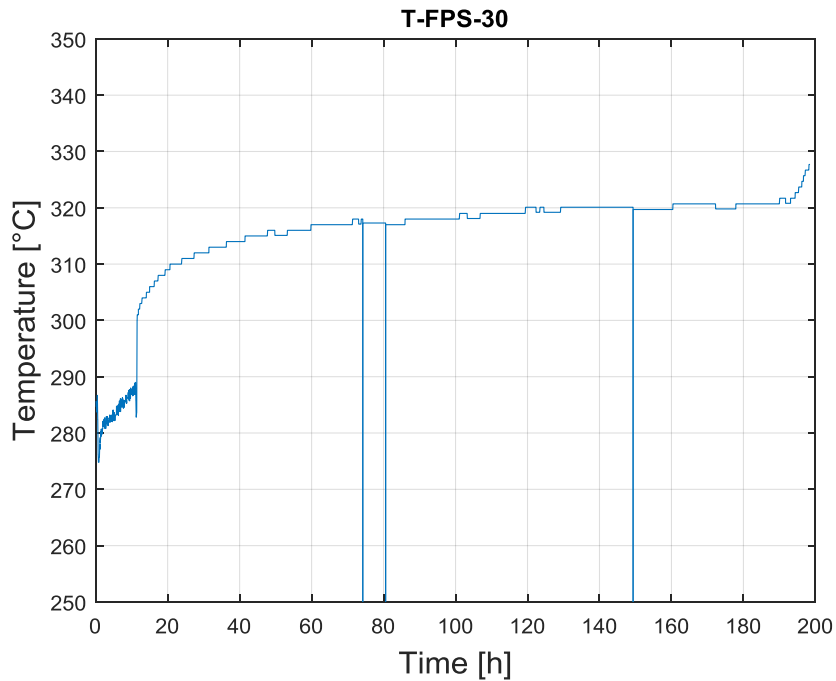


Figure 253: T-FPS-30 LBE temperature (Test 4)

The LBE heated by the FPS flows through the fitting volume into the riser (see Annex A Fig. 3 0016 Instrumentation.pdf); here temperatures are measured using TCs with a diameter of 3 mm disposed at the entrance section (T-TS-01 to 03) and at the exit section before the separator (T-TS-04 to 06). Figure 254 reports the riser inlet/outlet average temperature.

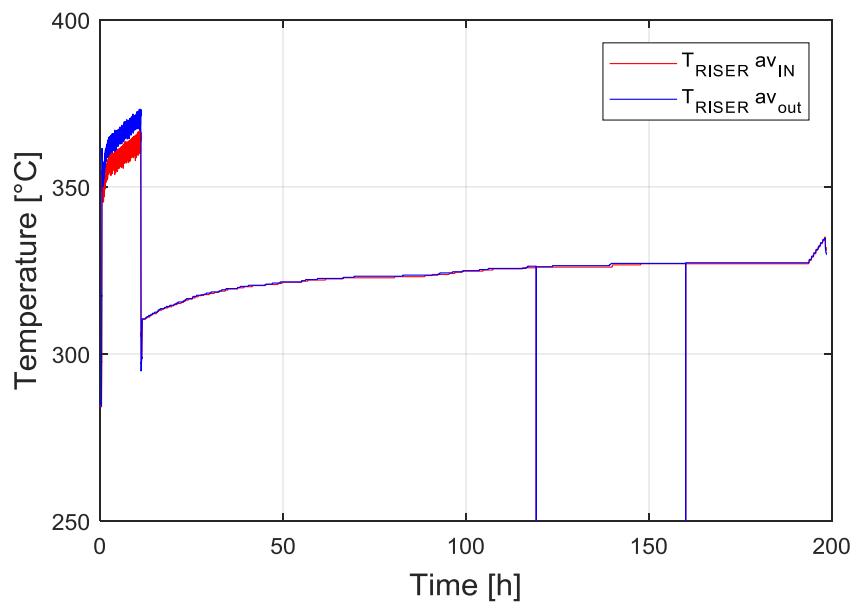



Figure 254: Inlet/Outlet average LBE temperature in the riser (Test 4)

 DIVISIONE INGEGNERIA SPERIMENTALE	<u>Title</u> D3.2: CIRCE experiments: pre-test, data-set and analysis	<u>Distribution</u> PUBLIC	<u>Emission</u> 09/08/2017	<u>Pag.</u> 153 di 234
		<u>Ref.</u> CI-T-R-292	Rev. 0	

From the riser exit, the LBE flows through the Separator into the HX shell, where the temperature at the entrance section is measured by three TCs placed at 120°, 30 mm from the bottom of the Separator (T-SG-01 ... 03, see Annex A Fig. 4 THINS thermocouples arrangement.pdf).

Sub-channel temperature are measured in a plane placed 30 mm above the lower grid (see Annex A Fig. 10: 0700-Assieme-HX.pdf for the positioning of the grid), according to the scheme shown in Annex A Fig. 11: T-SG-0100-Disposizione TC Sottocanali GV.pdf (T-SG-04 ... 12).

The LBE temperature at the outlet section of the HX is measured by six thermocouples (T-SG-13 ... 18) placed at 60° each and at 100 mm before the HX skirt exit (see Annex A Fig. 12: T-SG-0101-Disposizione TC Uscita GV.pdf). In Figure 255 the LBE temperature averaged at the inlet and outlet sections of the HX is reported.

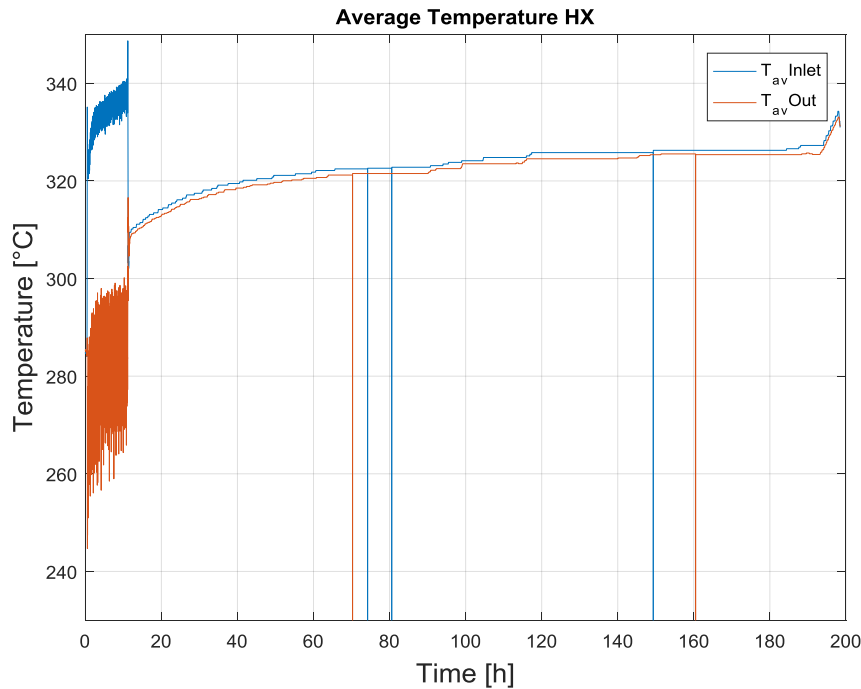


Figure 255: Inlet/Outlet average LBE temperature in the main HX (Test 4)

From Figure 256 to Figure 264 temperatures measured from each single thermocouple in the HX are reported (subchannels temperatures).

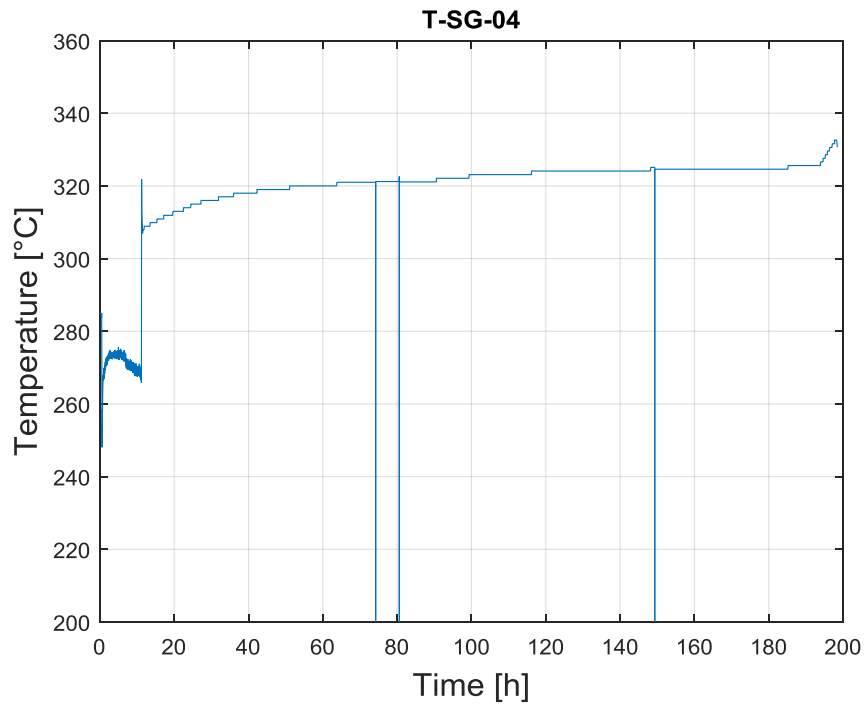


Figure 256: LBE temperature in the sub channel of the HX (T-SG-04, Test 4)

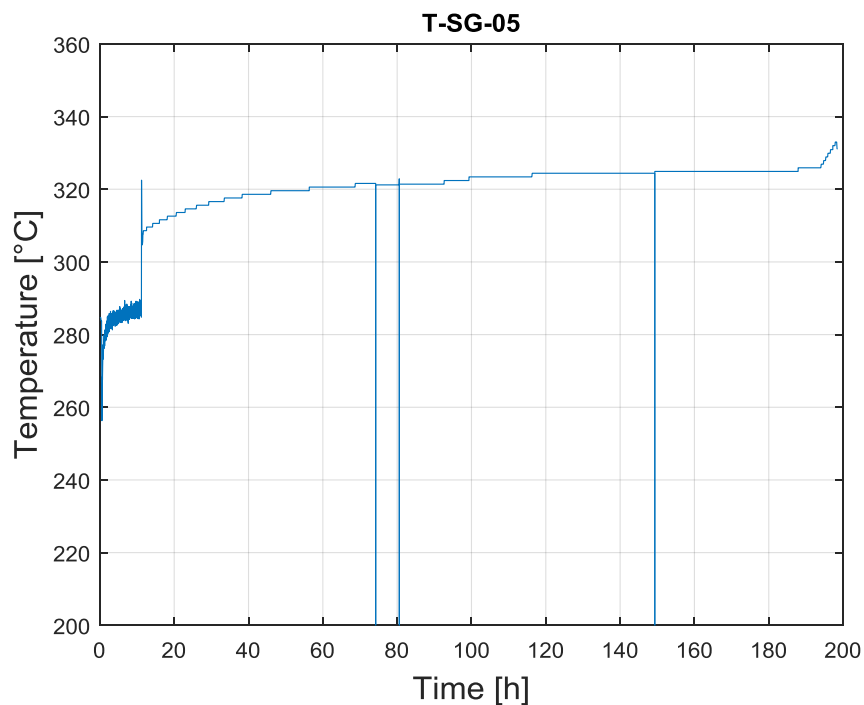


Figure 257: LBE temperature in the sub channel of the HX (T-SG-05, Test 4)

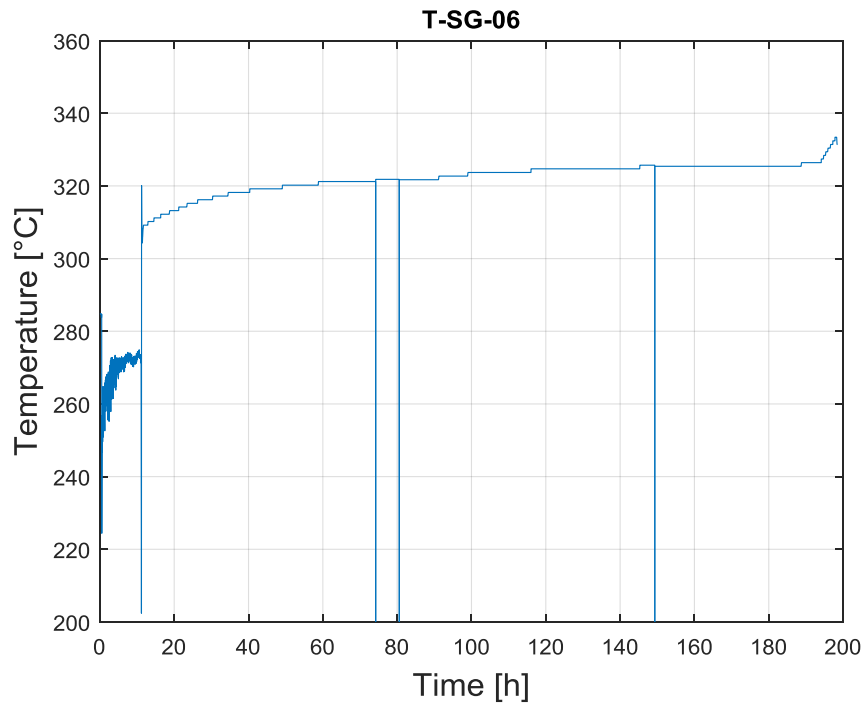


Figure 258: LBE temperature in the sub channel of the HX (T-SG-06, Test 4)

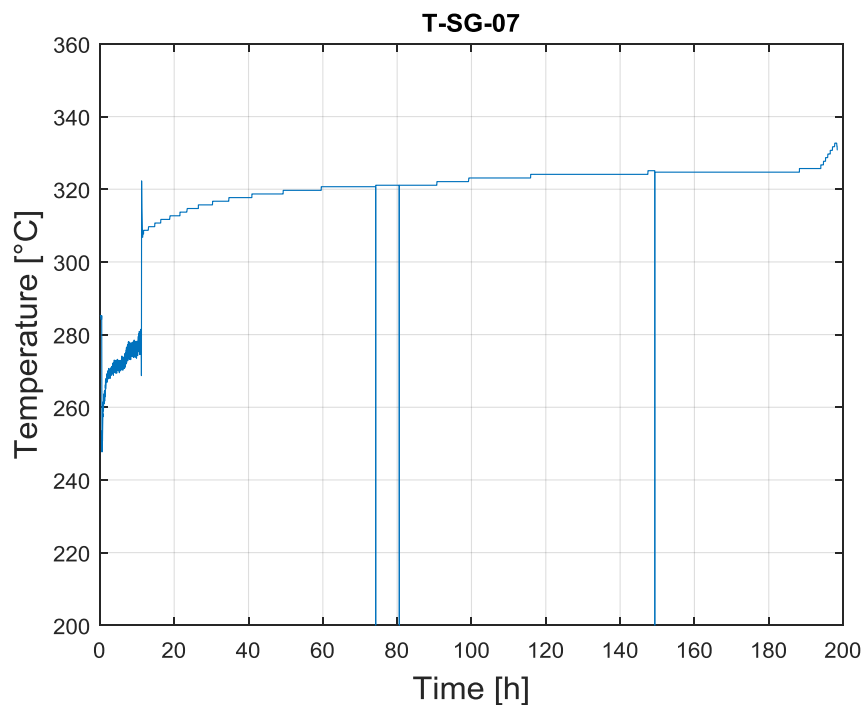



Figure 259: LBE temperature in the sub channel of the HX (T-SG-07, Test 4)

 DIVISIONE INGEGNERIA SPERIMENTALE	<u>Title</u> D3.2: CIRCE experiments: pre-test, data-set and analysis	<u>Distribution</u> PUBLIC	<u>Emission</u> 09/08/2017	<u>Pag.</u> 156 di 234
		<u>Ref.</u> CI-T-R-292	Rev. 0	

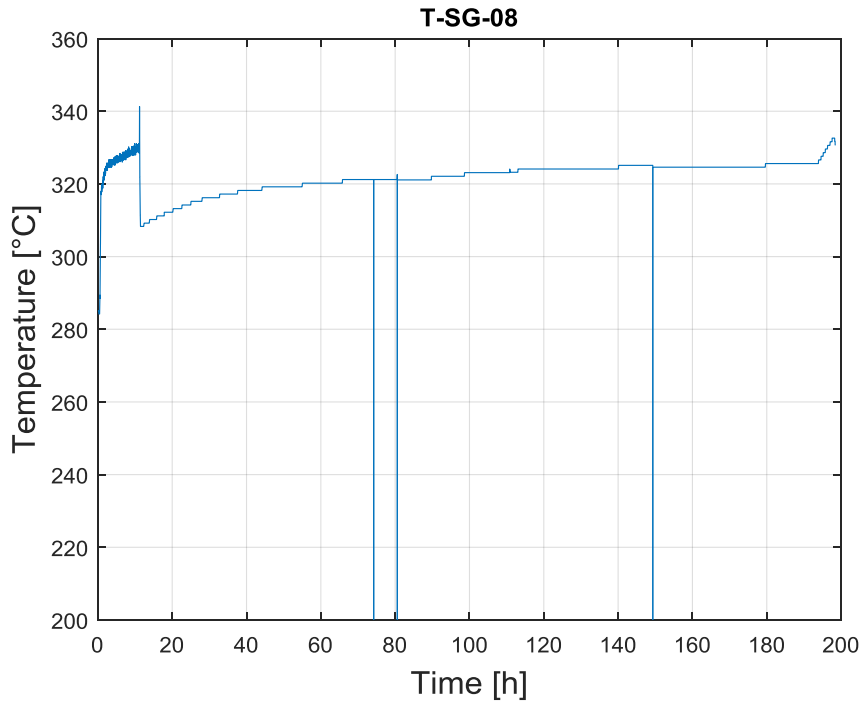


Figure 260: LBE temperature in the sub channel of the HX (T-SG-08, Test 4)

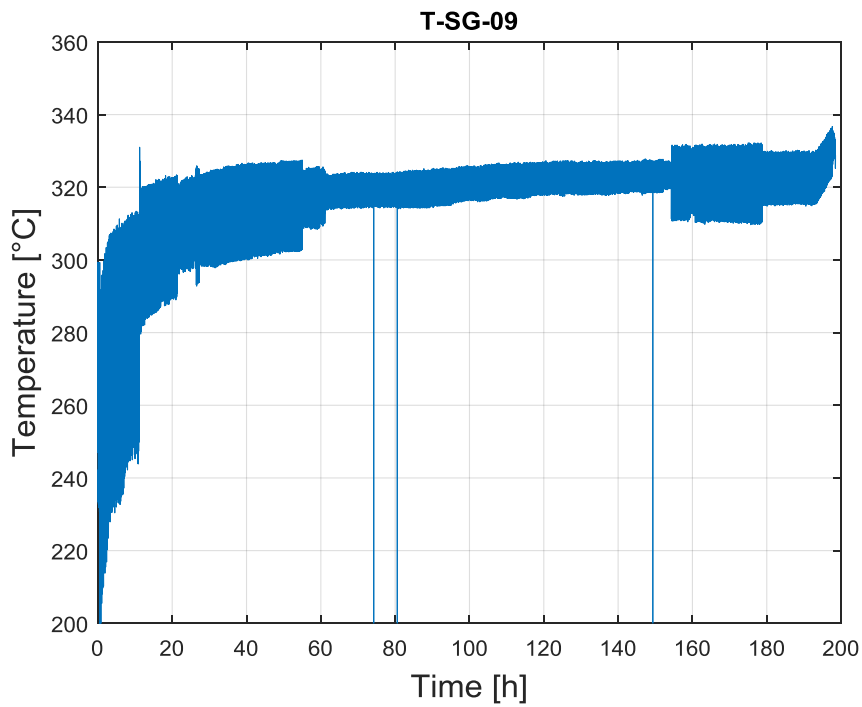


Figure 261: LBE temperature in the sub channel of the HX (T-SG-09, Test 4)

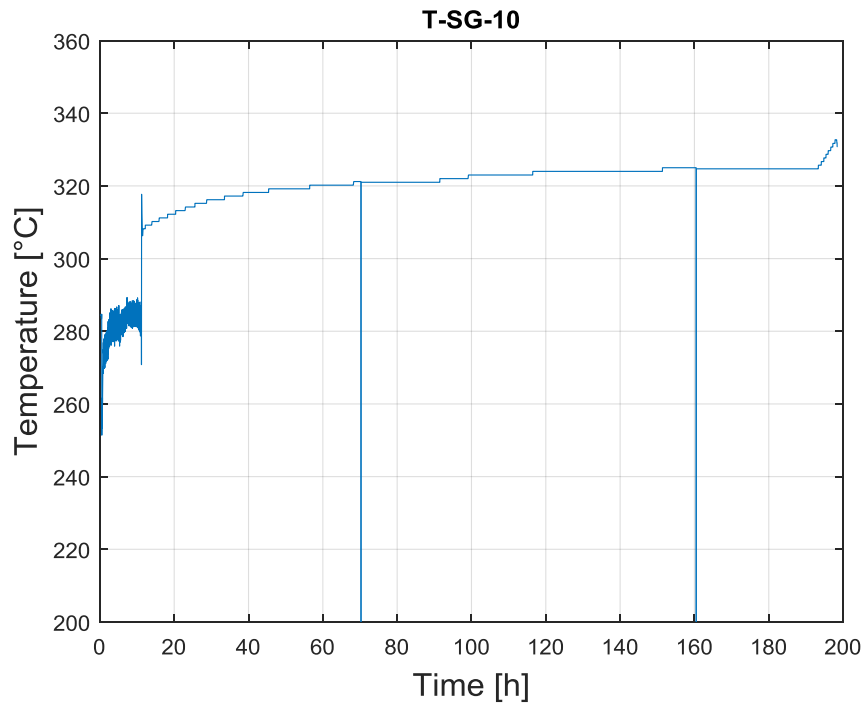


Figure 262: LBE temperature in the sub channel of the HX (T-SG-10, Test 4)

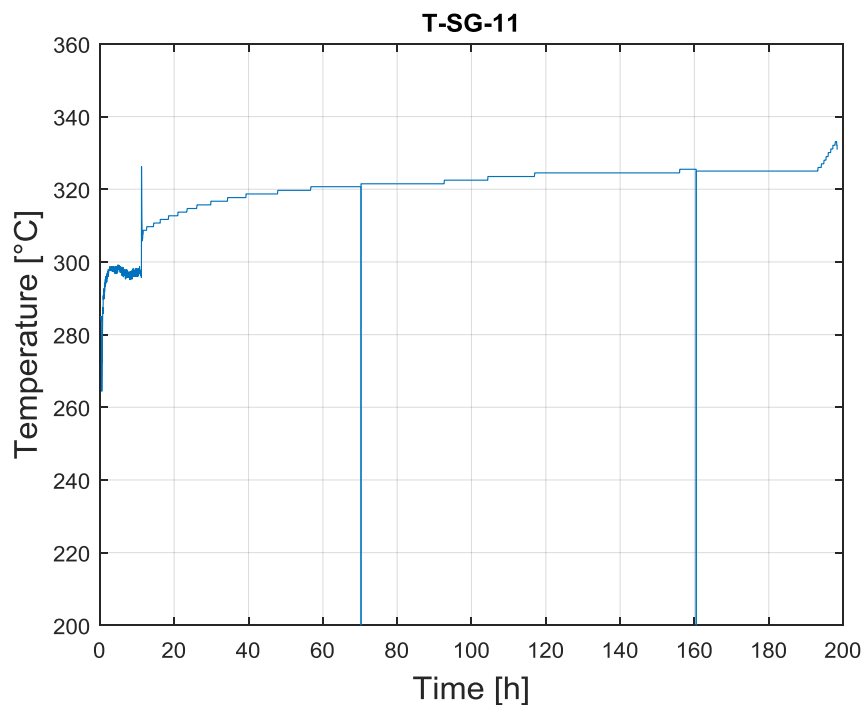



Figure 263: LBE temperature in the sub channel of the HX (T-SG-11, Test 4)

 DIVISIONE INGEGNERIA SPERIMENTALE	<u>Title</u> D3.2: CIRCE experiments: pre-test, data-set and analysis	<u>Distribution</u> PUBLIC	<u>Emission</u> 09/08/2017	<u>Pag.</u> 158 di 234
		<u>Ref.</u> CI-T-R-292	Rev. 0	

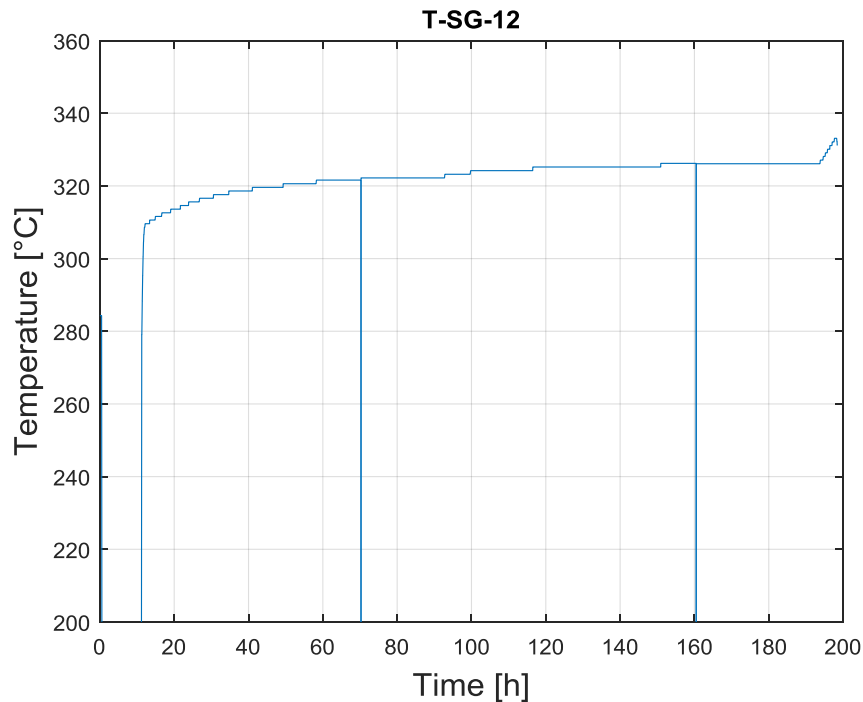


Figure 264: LBE temperature in the sub channel of the HX (T-SG-12, Test 4)

After passing through the HX, the LBE returned into the pool. Here, thermocouples for the measurements of LBE temperature were maintained in the fixed positions by vertical rods at 17 different elevations (see Annex A Fig. 13 T-MS-0101 TC per Mix&Strat.pdf) and 9 different radial position (see Annex A Fig. 14 T-MS-0100-Posizione TC Mix&Strat su piani di misura.pdf) for a total of 119 TCs with a diameter of 3 mm (T-MS-01 ... 119). In particular, with reference to Annex A Fig. 13 T-MS-0101 TC per Mix&Strat.pdf and Annex A Fig. 14 T-MS-0100-Posizione TC Mix&Strat su piani di misura.pdf, TCs on lines *A, H, I* allow measurement from the bottom side of the test section up to the FPS entrance, while TCs on lines *B, C, D, E, F, G* allow measurement up to 600 mm below the exit of the DHR.

From Figure 265 to Figure 273 the LBE temperature in the pool is reported along the vertical lines *A, B, C, D, E, F, G, H* and *I*.

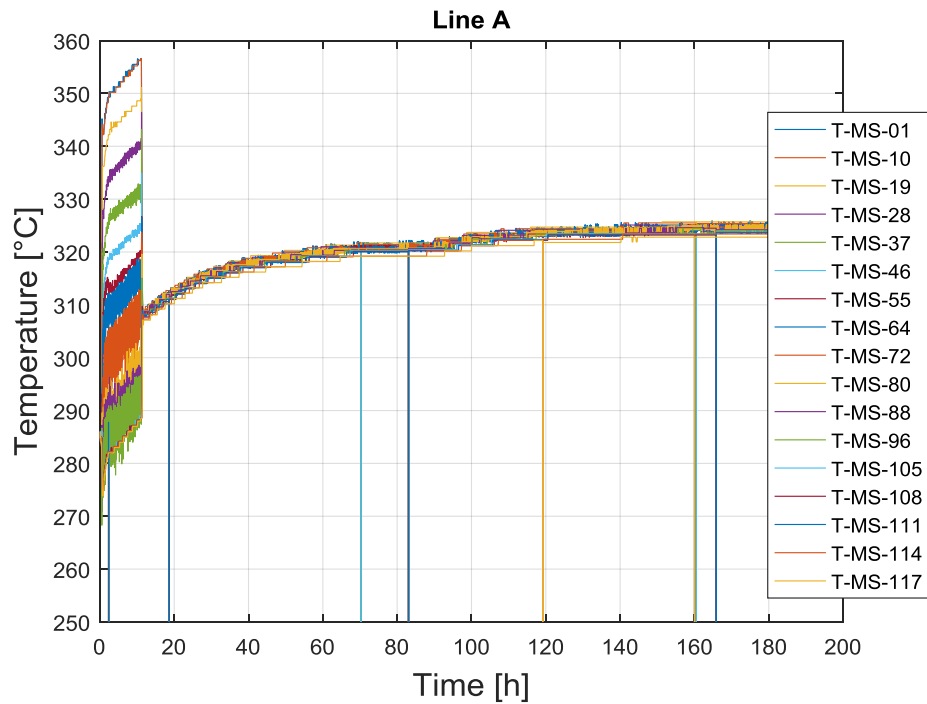


Figure 265: Temperature in the pool along Line A

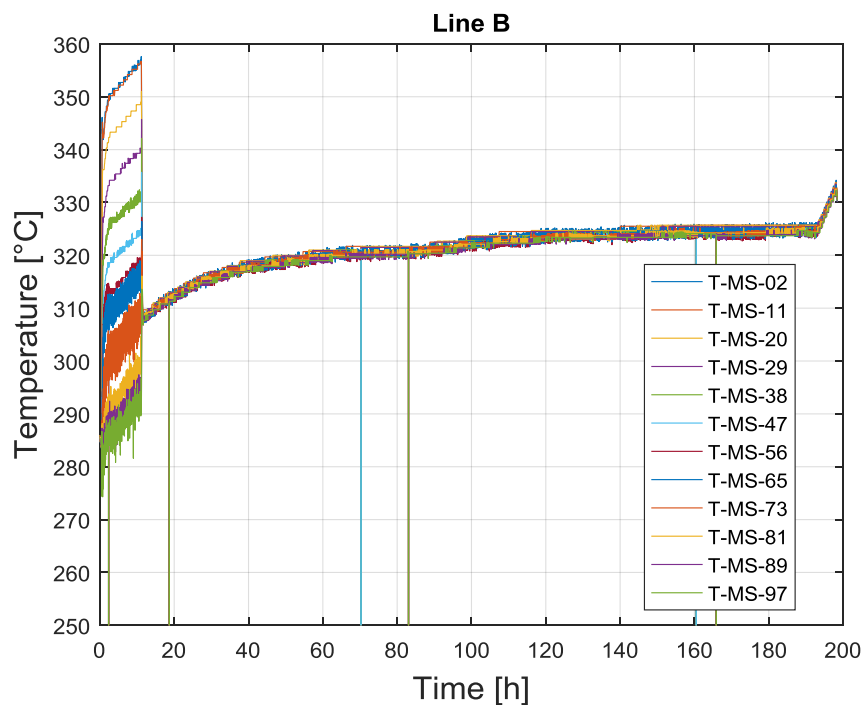


Figure 266: Temperature in the pool along Line B

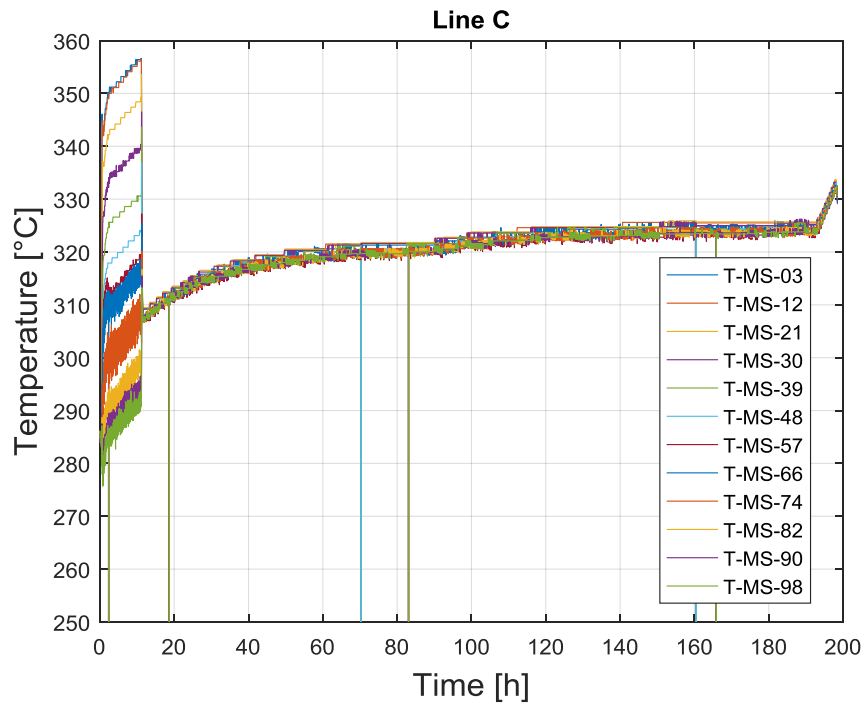


Figure 267: Temperature in the pool along Line C

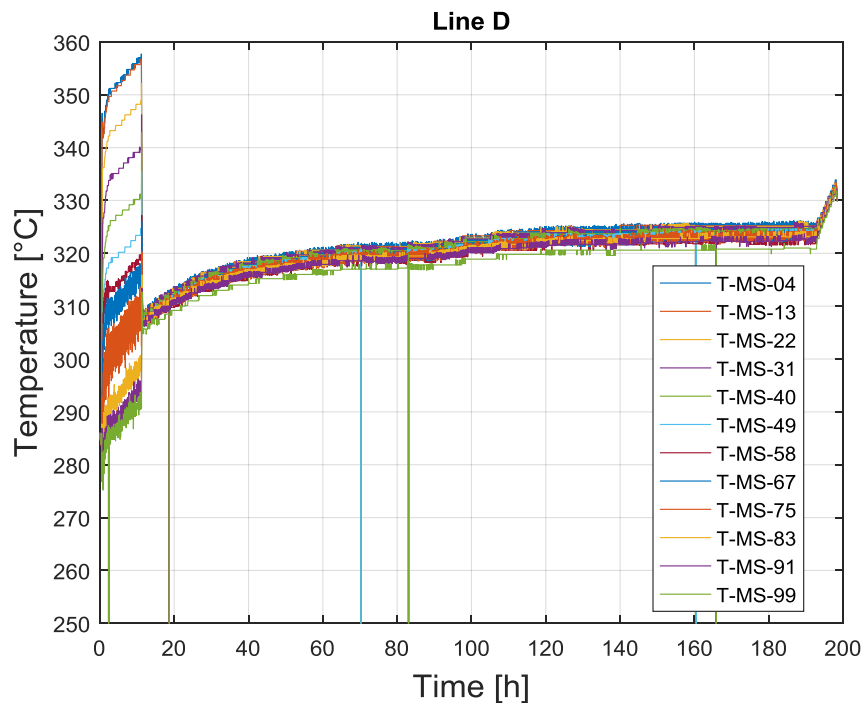


Figure 268: Temperature in the pool along Line D

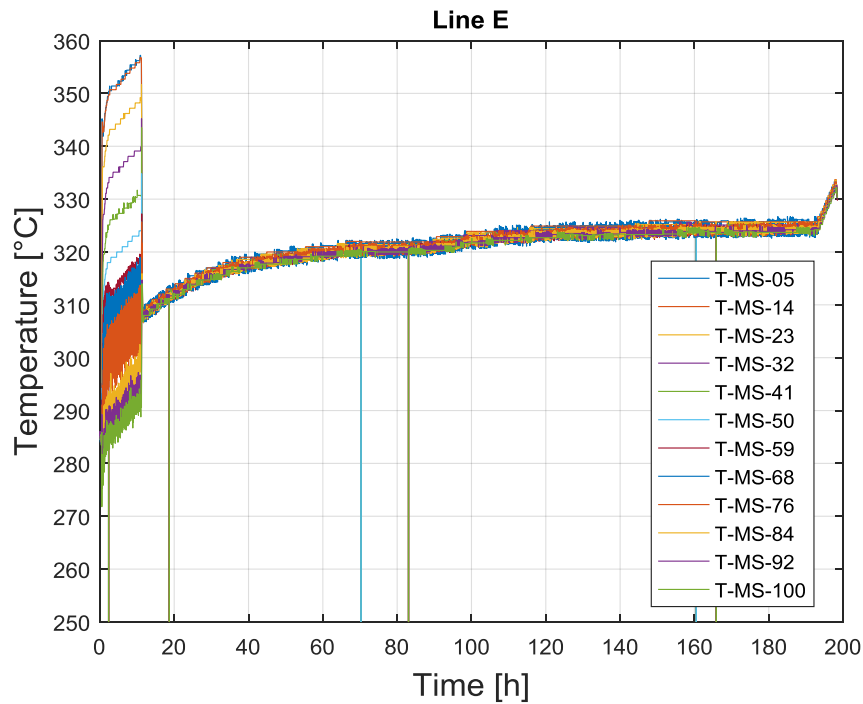


Figure 269: Temperature in the pool along Line E

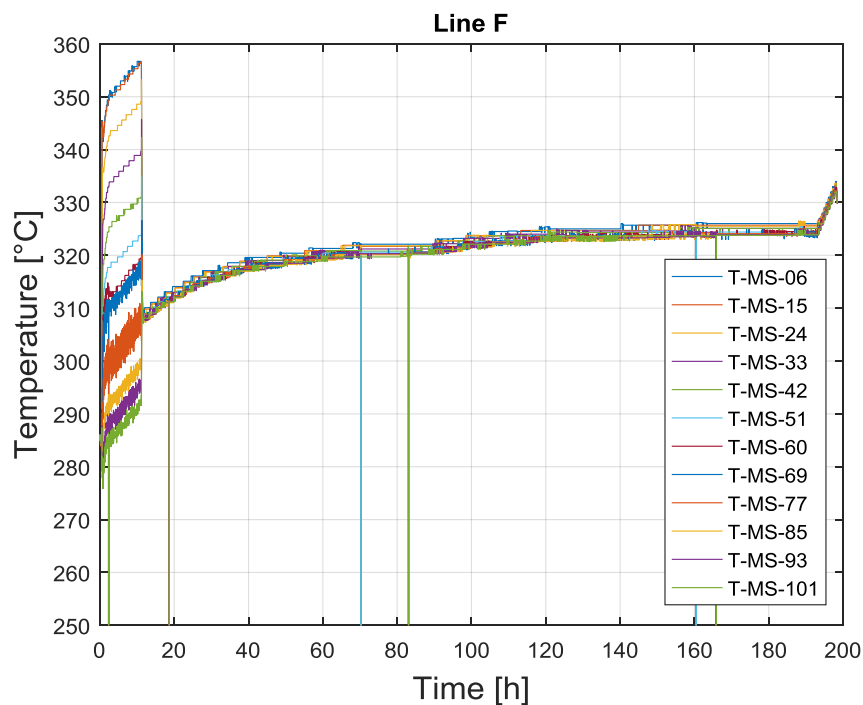


Figure 270: Temperature in the pool along Line F

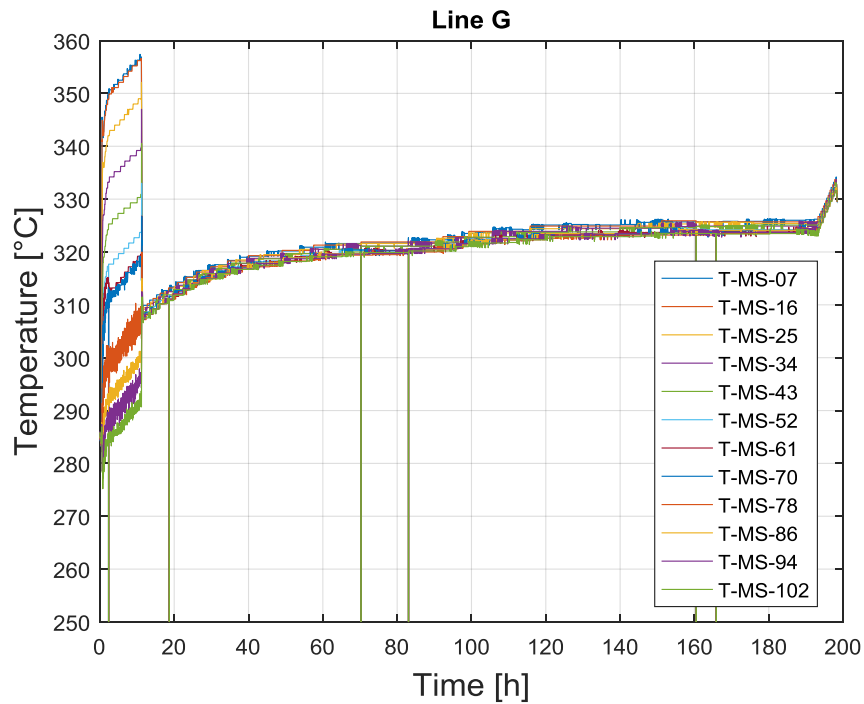


Figure 271: Temperature in the pool along Line G

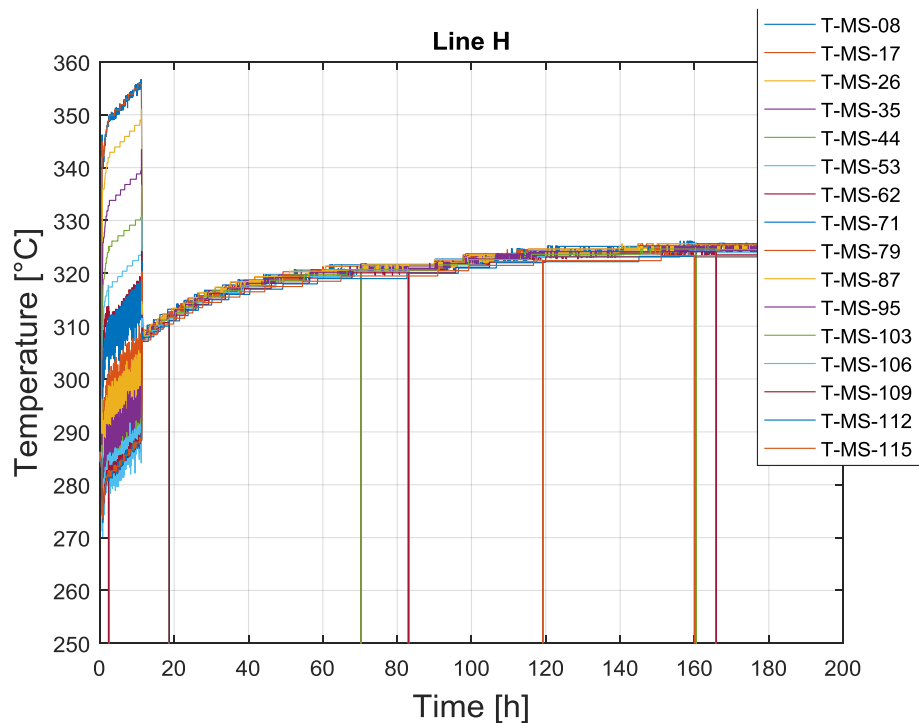


Figure 272: Temperature in the pool along Line H

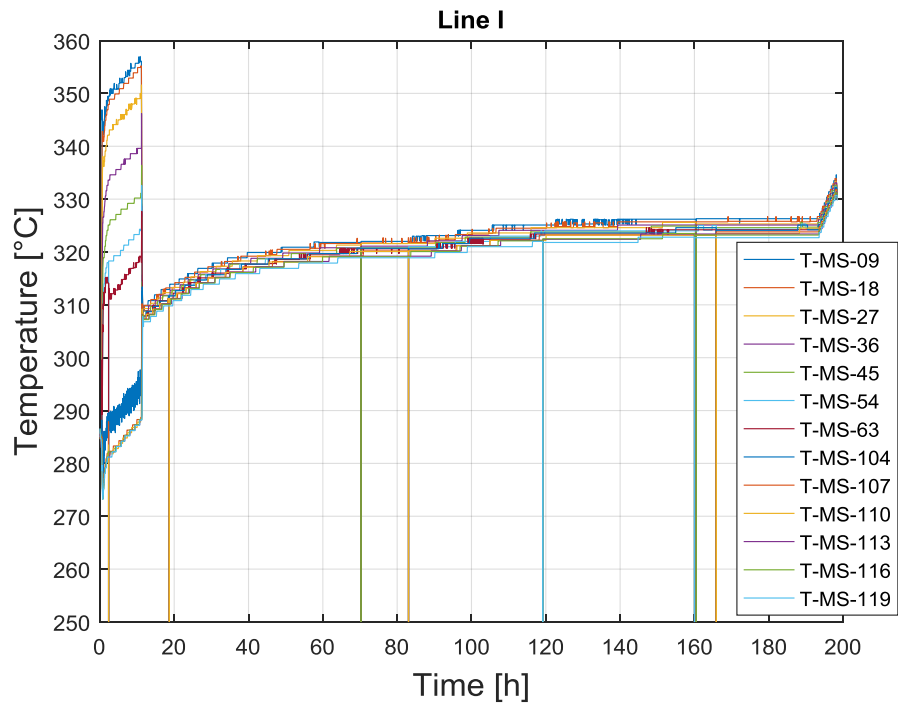



Figure 273: Temperature in the pool along Line I

 DIVISIONE INGEGNERIA SPERIMENTALE	<u>Title</u> D3.2: CIRCE experiments: pre-test, data-set and analysis	<u>Distribution</u> PUBLIC	<u>Emission</u> 09/08/2017	<u>Pag.</u> 164 di 234
		<u>Ref.</u> CI-T-R-292	Rev. 0	

Pool-Thermal hydraulics model of CIRCE-ICE (CRS4 & NRG)

This part of the document deals with description of the CFD analyses of the CIRCE-ICE experimental facility performed respectively by the “Centro di Ricerca, Sviluppo e studi superiori in Sardegna” (CRS4) and by the Nuclear Research and consultancy Group (NRG)

4 CRS4 CFD SIMULATIONS OF CIRCE-ICE

The CRS4 activity is based on the ENEA document “CIRCE Experimental Facility” Ref. CI-CI-R-162 by D. Martelli [3]. In addition, a series of drawing has been provided by ENEA, allowing to build the numerical geometry. The specific objective of this work is to be able to reproduce numerically the main features of the initial steady-state described in the ENEA document and to raise some potential issues or ambiguities.

The description of the developed “cold” CFD model consider only the fluid domain, LBE, cover gas and Argon injection. We explain why we failed to simulate the Argon in injection line and the compromise we had to accept to simulate the bubbly flow in the riser.

Taking profit of the experience gained during the first part, the second part of the work consisted in building a “hot” CFD model. Because of the foreseen entity of conductive heat exchange, the hot model must include all the structural parts, including internals, vessel and insulation.

4.1 COLD model

4.1.1 Geometry

Because it was clear from the beginning that a later hot model will be necessary, the cold geometrical model has been built first by reproducing the structural components, and then subtracting them to the volume enclosed by the containment vessel (S100). Even the vertical supports for the TCs have been given a CAD representation. However, they have not been subtracted to the fluid volume to avoid essentially useless mesh issues. See Figure 274.

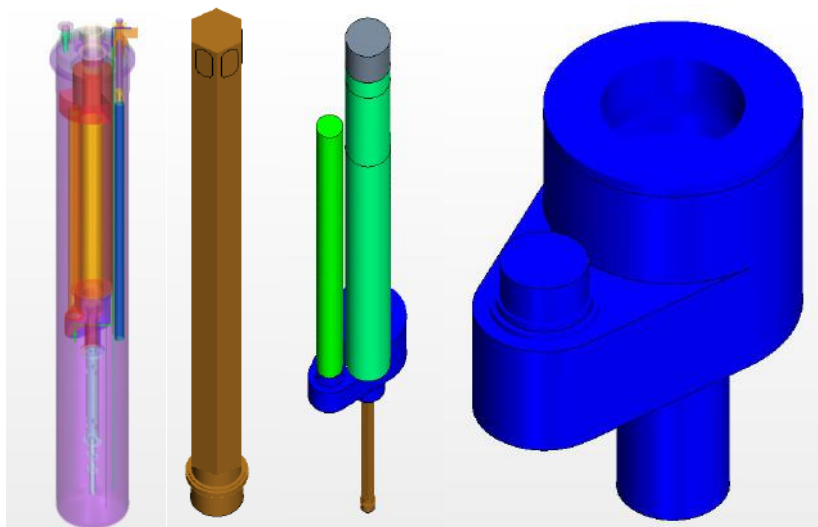



Figure 274: geometrical parts. Left, solid components. Others, fluid parts

 DIVISIONE INGEGNERIA SPERIMENTALE	<u>Title</u> D3.2: CIRCE experiments: pre-test, data-set and analysis	<u>Distribution</u> PUBLIC	<u>Emission</u> 09/08/2017	<u>Pag.</u> 165 di 234
		<u>Ref.</u> CI-T-R-292	Rev. 0	

4.1.2 Eulerian Multiphase trial

Besides the LBE, the fluid domain also contains a gas part, Argon which serve both as cover gas and for the gas lift pumping system. The first idea was to simply try to simulate both phases within the standard Eulerian two-phase flow setting and simulate the Argon injection line.

The attempt was abandoned after 48 hours of heavy calculation, as only 0.15s of physical time could be simulated, without hope for later decisive improvement. The main problem lies in the very small size of the nozzle and the very high velocity the flow should reach there. See, Figure 275 and Figure 276.

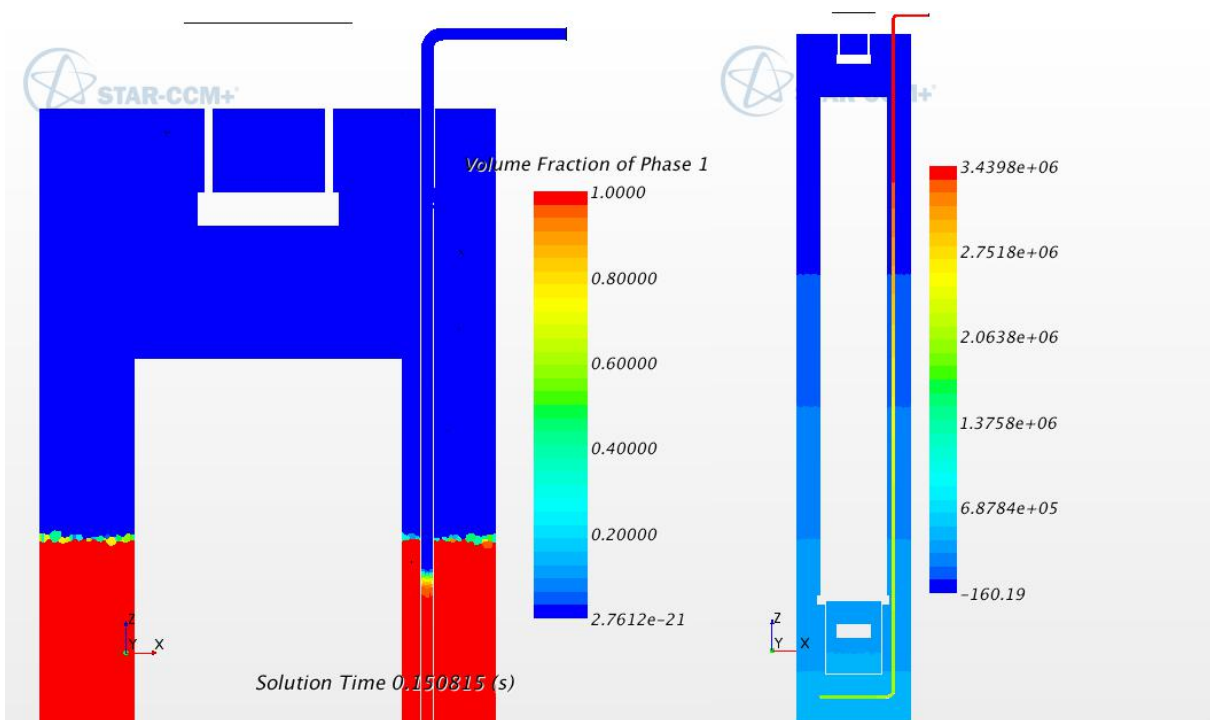



Figure 275: Eulerian two-phase trial after 0.15s. Left, LBE volume fraction. Right, pressure

 DIVISIONE INGEGNERIA SPERIMENTALE	<u>Title</u> D3.2: CIRCE experiments: pre-test, data-set and analysis	<u>Distribution</u> PUBLIC	<u>Emission</u> 09/08/2017	<u>Pag.</u> 166 di 234
		<u>Ref.</u> CI-T-R-292	Rev. 0	

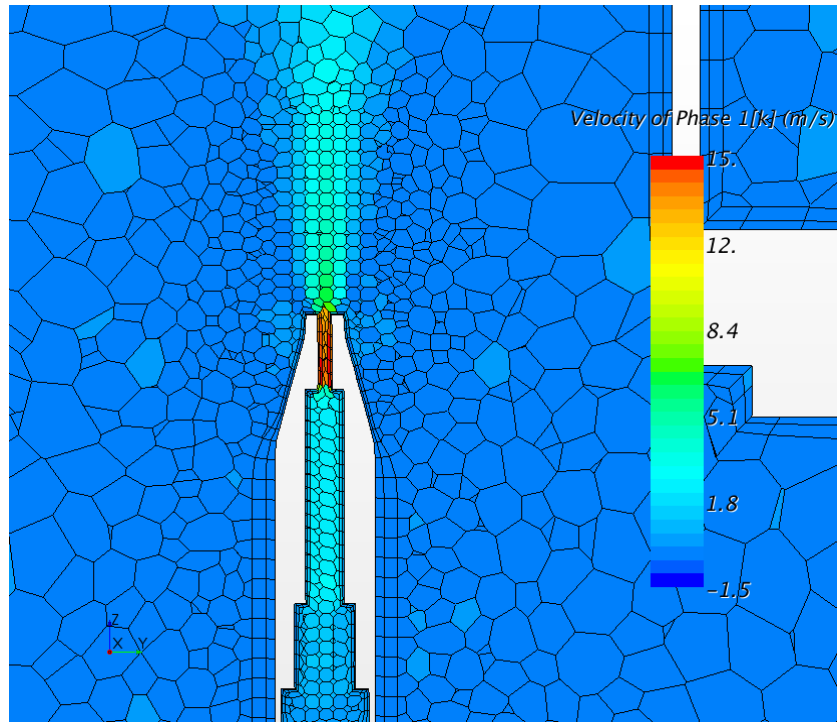


Figure 276: Eulerian two-phase trial after 0.15s. Velocity field near the nozzle

4.1.3 VoF and Lagrangian particles


An alternative approach has been followed with the following main characteristics:

- The LBE and cover gas are represented by use of the VoF setting.
- The bubbly flow in the riser is represented by incompressible buoyant Lagrangian particles.
- The Argon line flow has been eliminated.
- As the concentration of Argon bubbles at the nozzle tip would be completely unphysical, the Argon bubble numerical injector has been enlarged and located a few cm above the real nozzle tip.
- The bubbles are absorbed by the cover gas while crossing the free surface (quite recent feature of SARCCM+ in 2015)

A transient simulation with bubble injection has been performed, showing that the method is valid. A visualization of the rising bubbles after the first 5.5s and after 16.25s can be seen in Figure 277. The main issue encountered was that many computational cells had already more than 75% concentration, with some of them even more than 100% concentration, while the LBE mass flow rate was still insufficient. This was solved by performing two specific actions:

- The riser was re-meshed with larger cells
- The seed for the Lagrangian particle injection was greatly enlarged, see Figure 278

Several simulations have been performed, verifying the possibility to add some randomness to the seed points and to the diameter of the Lagrangian particles. Finally, a simulation could be

 DIVISIONE INGEGNERIA SPERIMENTALE	<u>Title</u> D3.2: CIRCE experiments: pre-test, data-set and analysis	<u>Distribution</u> PUBLIC	<u>Emission</u> 09/08/2017	<u>Pag.</u> 167 di 234
		<u>Ref.</u> CI-T-R-292	Rev. 0	

performed in which the correct LBE mass flow rate could be reached with a hydraulic resistance in the fuel pin simulator raised progressively to reach a representative pressure loss, as shown in Figure 279.

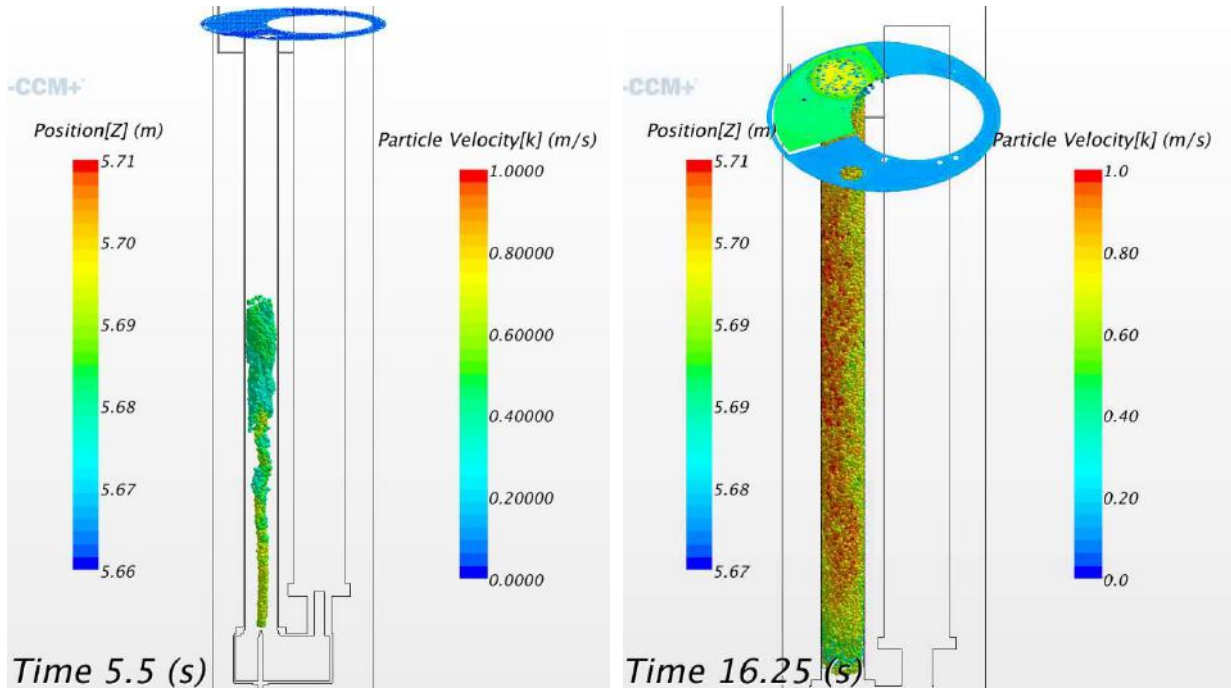


Figure 277: Rising bubbles

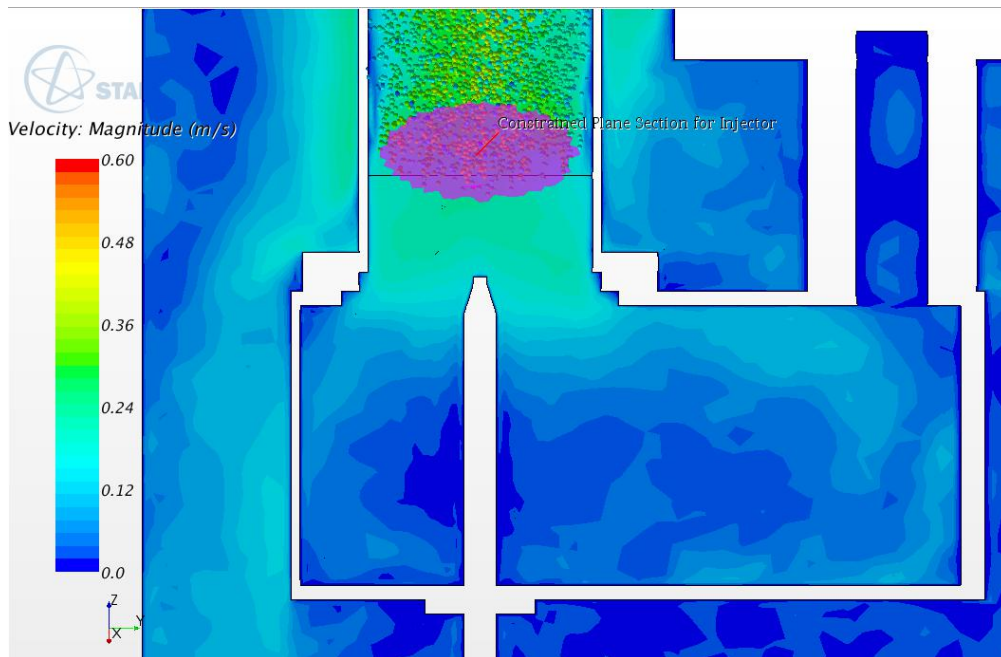



Figure 278: Enlarged seed for the Lagrangian injector

 DIVISIONE INGEGNERIA SPERIMENTALE	<u>Title</u> D3.2: CIRCE experiments: pre-test, data-set and analysis	<u>Distribution</u> PUBLIC	<u>Emission</u> 09/08/2017	<u>Pag.</u> 168 di 234
		<u>Ref.</u> CI-T-R-292	Rev. 0	

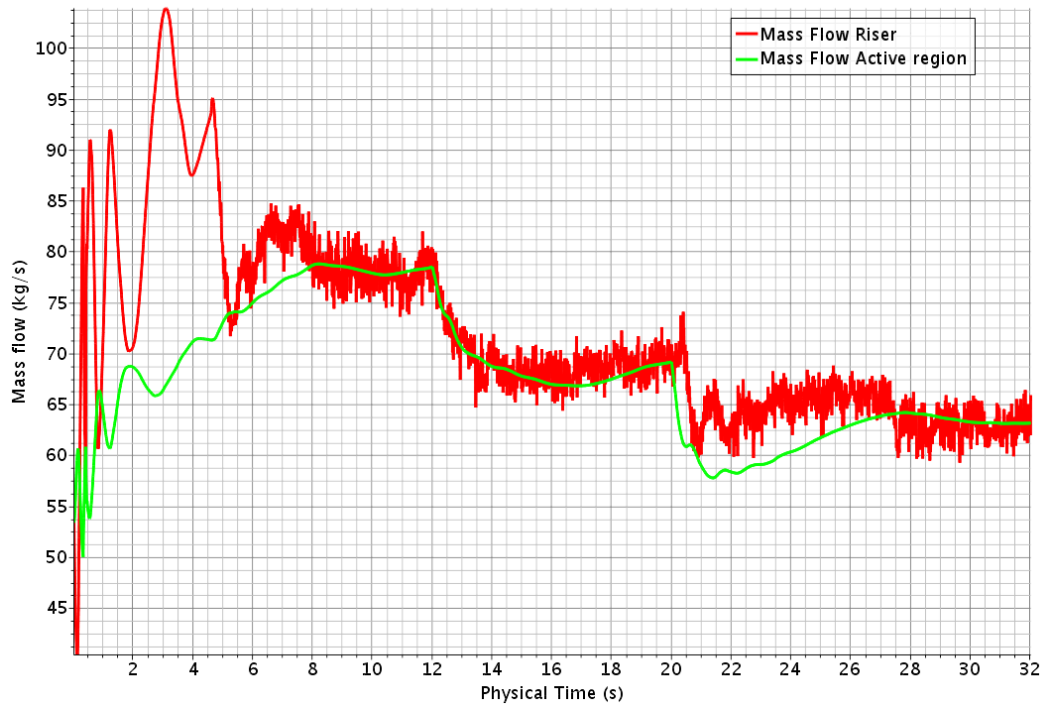



Figure 279: Cold flow final simulation. History of the mass flow in the riser and in the active region

4.1.4 Analysis

We have demonstrated that a CFD simulation can reproduce a lift force in the riser similar to the experimental one by using buoyant Lagrangian particles. However, we had to accept a very high level of approximation:

- The initial seed region is much wider than the nozzle tip. This is to avoid unphysical concentration of bubbles. This also means that the topology of the Argon at the nozzle tip is quite complex and requires some distance before a relatively stable bubbly flow is organized. Also, we have no real idea on what could be a reasonable bubble characteristic size.
- The Lagrangian particles are incompressible while there should be a volume expansion by a factor about 5 from the nozzle tip to the free-surface and a similar ratio of mean volumetric fraction, simply due to the variation of ambient pressure. Moreover, the temperature of the Argon gas at the nozzle is unknown between a quite large range and it is quite probable that its temperature evolves largely while rising, further increasing the void ratio. With a mean void fraction about 9 % inferred by ENEA from pressure measurement, we can expect more than 30% close to the free surface where a bubbly type two-phase flow becomes questionable.
- Upon closure of the injection gas valve, the feeding conduit takes some time to equilibrate its pressure, still producing a decreasing gas flow. Then the feeding conduit slowly fills up again with LBE. The time scale of this transient is unknown but most probably comparable or greater than the time required by the bubbles to perform their travel in the riser.

This very high level of approximation is such that a posteriori we cannot evaluate if and how much this approach is better than simply adding a calibrated momentum source term in the

 DIVISIONE INGEGNERIA SPERIMENTALE	<u>Title</u> D3.2: CIRCE experiments: pre-test, data-set and analysis	<u>Distribution</u> PUBLIC	<u>Emission</u> 09/08/2017	<u>Pag.</u> 169 di 234
		<u>Ref.</u> CI-T-R-292	Rev. 0	

riser. The flow however reacts very fast, at most a few seconds, to changes in Argon flow rate, as can be inferred from Figure 279. Taking into account that the change of pressure head takes also a few seconds to establish from a change of Argon flow, it means that the loop has a very small hydraulic inertia, in the order one second or less. On the other hand, the thermal inertia of the system is expected to be large, even huge. It will be necessary to have access to large transient times to reach a reasonable thermal steady-state. The time-step limitation coming from the Lagrangian bubbly flow is going to be a severe handicap.

For the reason just explained, the “hot” model will not make use of the Lagrangian particle feature, that will be replaced by a calibrated momentum source in the riser.

4.2 Hot model

Taking profit from the experience gained on the cold model, we have built a first but complete hot model. By complete hot model, we mean a model containing all the structural materials and potentially all the different fluids. All the structures are thermally coupled with the fluids they are in contact with.


Our primary objective is to reproduce a quasi steady-state with mass flow and temperature profiles comparable with experimental results from ENEA. This steady state must be obtained for a given hot nominal condition in which the pin simulator is delivering a consistent thermal source. As long as it is constant and quite high, the exact level of heat source is indifferent, so we chose to conform to the CIRCE reference configuration described in the ENEA document with the same name.

4.2.1 Geometry

The geometry is built on a high level division in separate regions whose organisation is motivated by the later ability to easily deal with issues of different natures:

- Different materials
 - Steel
 - LBE (+cover gas)
 - Insulator: external, dead volume, DHR
 - DHR fluid
 - Dead volume fluid
 - Porous media: HX, pin bundle
- Different meshers
 - Unstructured polyhedral
 - Directed (extruded)
- Specific source
 - Momentum source: riser
 - Heat source: pin bundle active part

A particular effort has been done to have quite detailed numerical geometry. The flanges have their numerical representation and the holes for instrumentation in the test section also. Screws and screw-bots that where somehow represented in the cold model, are however considered too tiny details to be considered in the hot model. It was thought that this level of

 DIVISIONE INGEGNERIA SPERIMENTALE	<u>Title</u> D3.2: CIRCE experiments: pre-test, data-set and analysis	<u>Distribution</u> PUBLIC	<u>Emission</u> 09/08/2017	<u>Pag.</u> 170 di 234
		<u>Ref.</u> CI-T-R-292	Rev. 0	

detail was necessary for the representation of the local flow patterns in the plenum that strongly influence the various walls heat flux.
 Some details of the geometry can be appreciated in the mesh section.

4.2.2 Mesh

The solid part of the numerical domain contains a lot of very thin structures. But we need to run the simulation for large times. So, the number of control volumes must be kept reasonable. This is obtained by making a quite large use of non-conform fluid-solid interfaces and by using wherever practical directed meshes. The final compromise is a mesh with 1.9 million fluid cells and 1.4 million solid cells. There are a few remaining defects, like the vessel excessive discretisation, as can be seen in Figure 280. However, it is acceptable for this stage of pre-test and must be considered as an advanced attempt before the final post-test modelling that will require some adjustment of the geometrical decomposition as result of the pre-test analysis.

Other mesh details are shown on Figure 281 and on Figure 282, also illustrating the geometrical structure of the numerical model.

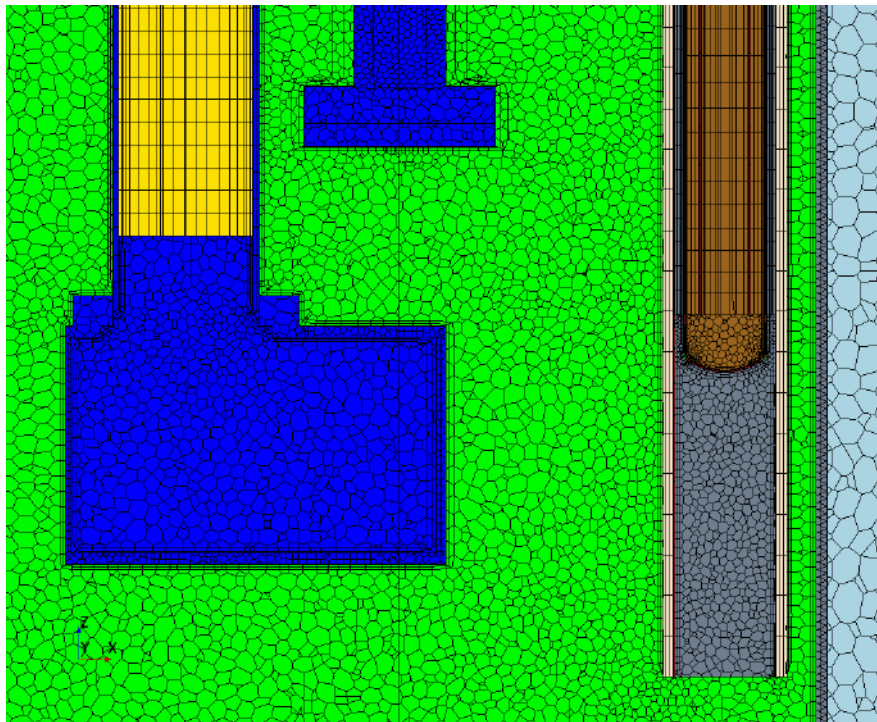


Figure 280: Mesh vertical section across the riser and the DHR


 DIVISIONE INGEGNERIA SPERIMENTALE	<u>Title</u> D3.2: CIRCE experiments: pre-test, data-set and analysis	<u>Distribution</u> PUBLIC	<u>Emission</u> 09/08/2017	<u>Pag.</u> 171 di 234
		<u>Ref.</u> CI-T-R-292	Rev. 0	



Figure 281: Mesh vertical sections across the pin simulator channel

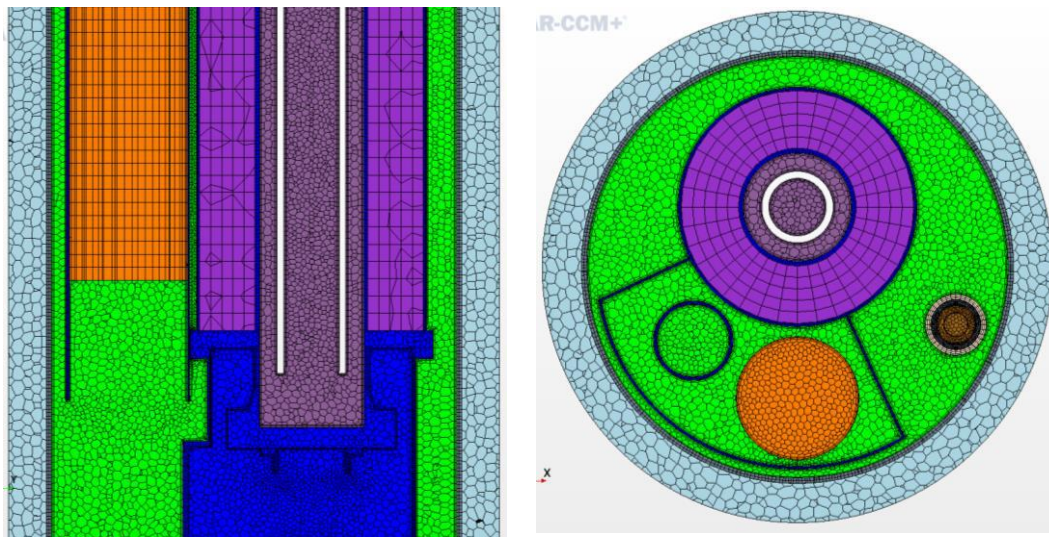



Figure 282: Left, mesh vertical section through the HX and the dead volume. Right, horizontal section across the gas flow separator

4.3 Instrumentation

The numerical model has been heavily instrumented. All the TCs on the plenum vertical supports have their numerical correspondent. The numerical vertical line probes have a constant pitch equal to the minimum pitch in the experiment, Figure 283.

With a numerical model divided in several regions, all interfaces between the regions are suited for measurements. For this reason, the main mass flow rates can be monitored and the

 DIVISIONE INGEGNERIA SPERIMENTALE	<u>Title</u> D3.2: CIRCE experiments: pre-test, data-set and analysis	<u>Distribution</u> PUBLIC	<u>Emission</u> 09/08/2017	<u>Pag.</u> 172 di 234
		<u>Ref.</u> CI-T-R-292	Rev. 0	

consistence between them is continuously checked. Fluid-solid interface are very well suited for heat flux measurement. Where necessary, the solid surface has been split so as to measure the heat flux across all relevant parts of the surface.

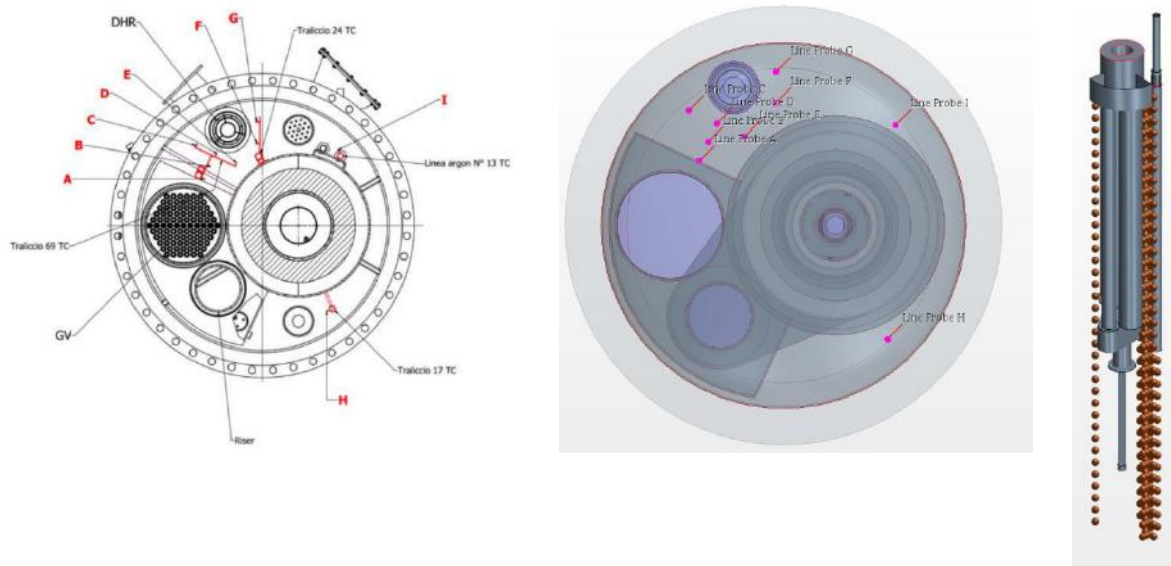



Figure 283: Left, ENEA design, arrangements of the vertical supports for the TCs. Center and right: position of the line probes in the numerical model.

4.3.1 Numerical settings

Here are the main settings of the simulation:


- K-E Realizable Two-Layer All y^+
- Time-step: 0.01s, (5 iterations)
- Starccm+ default settings
- 200 Cpu (~17 kCell/Cpu, which is quite a lower bound for a // 3D simulation)
- ~40s/hour
- Initial transient up to 2655s used for debugging and heat transfer adjustment (skipped), then restart from this initial condition for 5200s to reach a reasonable steady-state configuration
- Vertical momentum source in the riser, adjusted to get 56 kg/s: 8700 N/m^3 over 3.65 m.
- Volumetric heat source in the pin simulator active part: 707 kW for $dT \sim 88\text{K}$
- Riser insulation with a wall thermal resistance (no specific volumetric representation)
- Entrapped gas in conveyor taken into consideration by adding a local thermal resistance
- Volumetric heat sink in the HX in the form: $S = \rho C_p (T_0 - T)/\tau$, with $T_0 = 200\text{C}$.
- Turbulent Prandtl number set to $\text{Prt} = 2$

 DIVISIONE INGEGNERIA SPERIMENTALE	<u>Title</u> D3.2: CIRCE experiments: pre-test, data-set and analysis	<u>Distribution</u> PUBLIC	<u>Emission</u> 09/08/2017	<u>Pag.</u> 173 di 234
		<u>Ref.</u> CI-T-R-292	Rev. 0	

- HX and pin simulator active region simulated as porous media.

The inertial isotropic resistance coefficient in the pin simulator is close to 6/m. The vertical inertial resistance coefficient in the HX is 4/m while the radial one is 16/m. It must be stressed that a precise estimation of these coefficients as well as the driving force need not to be known for this steady-state analysis, as only their combined effect to deliver 56 kg/s is needed. However, at a later stage, and principally for a possible PLOF transient simulation, the coefficient will have to be more carefully defined. Again, as only the hydraulic integral effect is of interest in the pin simulator, it should be better for an upgraded geometry to localize in a separate region the extruded part of the current region.

There is a volume in the conveyer just below the dead volume that is probably filled with entrapped gas, at least in its upper layer. This is because, the gas present here before filling the vessel has no way to be evacuated. However, the pressure at this level is several Bar after LBE filling and the trapped gas is correspondingly compressed. There is no gas here in the simulation, but as the main effect is to create an insulating layer towards the upper wall, this property has been transferred to the upper interface with the solid wall.

 DIVISIONE INGEGNERIA SPERIMENTALE	<u>Title</u> D3.2: CIRCE experiments: pre-test, data-set and analysis	<u>Distribution</u> PUBLIC	<u>Emission</u> 09/08/2017	<u>Pag.</u> 174 di 234
		<u>Ref.</u> CI-T-R-292	Rev. 0	

4.3.2 Results

As already said, the mass flow reacts very fast (at the 5200s time scale) to changes in the numerical rising force. The flow in the riser and in the pin simulator are flat and equal, as it should be from mass conservation. The flow in the heat exchanger show tiny oscillations (less than 1kg/s) which are in turn both caused and absorbed by the free surfaces. With a last numerical issue regarding a spurious flow in the DHR solved, the flow in the DHR remains about zero. These aspects can be appreciated in Figure 284.

Some adjustments have been performed during the first 2600s of the transients in an attempt to reach a configuration similar to the experimental one. Some thermal resistance has been added where it is quite probable that some gas is trapped, below the dead volume as already mentioned, but also at the top part between the hexagonal pin simulator shell and its cylindrical surrounding skirt. The Prandtl number has also been raised to 2. This will be discussed later.

The last adjustment has been done about time 2600s and the simulation has been continued for another 2600s. The temperature evolution in several significant position is shown Figure 285. We can see what is essentially a parallel slow drift of all temperatures with a rate of change slowly vanishing. It must be noted that the system is only marginally sensible to a global variation of the temperature as the HX power is only slightly dependant on the LBE inlet temperature and that the high global thermal inertia make these small changes quite long to equilibrate. The thermal energy removed increased from 675 to 695 kW, as shown in Figure 286

Unlike in the experimental setup, it is quite easy to measure the heat flux through the solid components. The principal heat flux have been monitored and are shown in Figure 289.

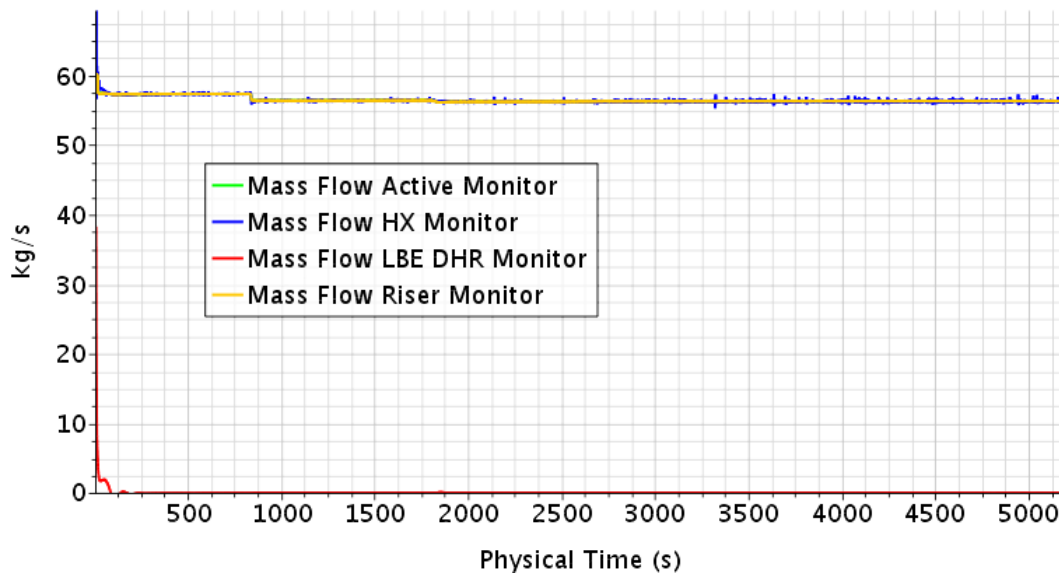



Figure 284: Main mass flows during the hot model simulation

 DIVISIONE INGEGNERIA SPERIMENTALE	<u>Title</u> D3.2: CIRCE experiments: pre-test, data-set and analysis	<u>Distribution</u> PUBLIC	<u>Emission</u> 09/08/2017	<u>Pag.</u> 175 di 234
		<u>Ref.</u> CI-T-R-292	Rev. 0	

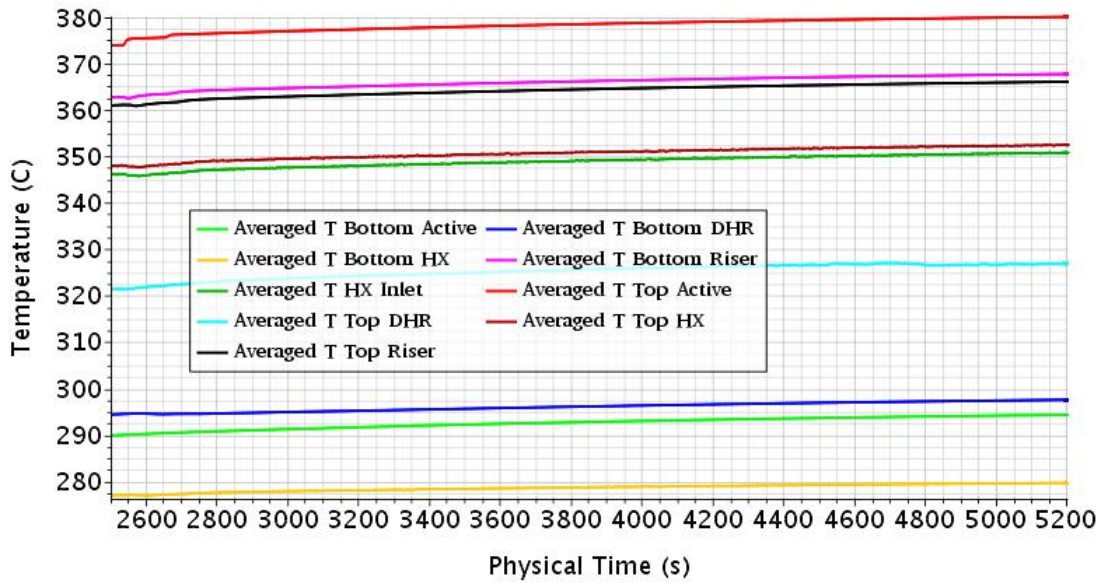


Figure 285: Hot model simulation after final thermal adjustments. Temperature evolution at several locations

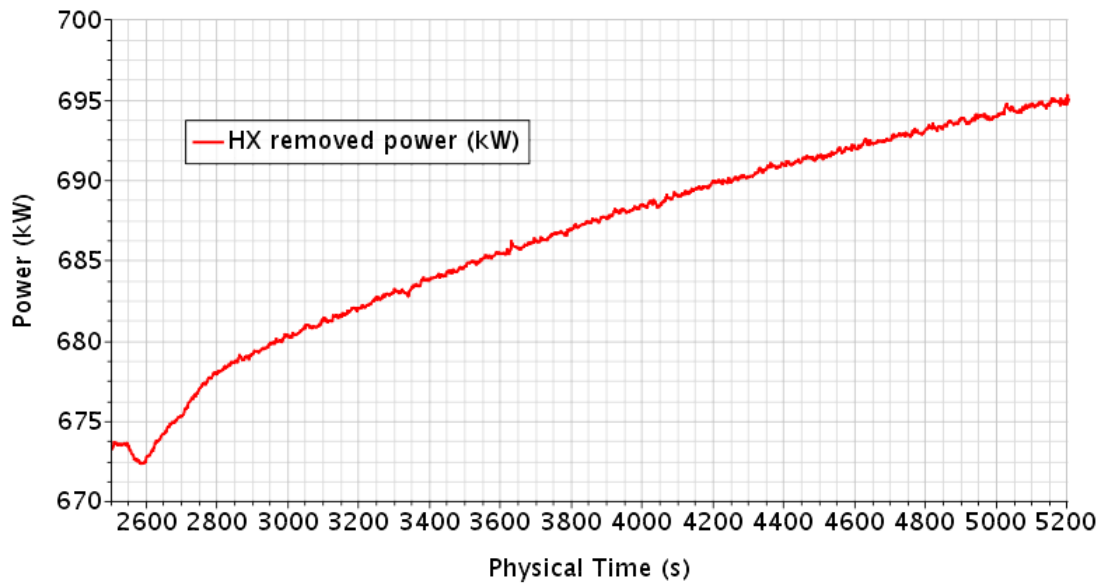



Figure 286: Time evolution during the last 2600s of the power removed by the HX

 DIVISIONE INGEGNERIA SPERIMENTALE	<u>Title</u> D3.2: CIRCE experiments: pre-test, data-set and analysis	<u>Distribution</u> PUBLIC	<u>Emission</u> 09/08/2017	<u>Pag.</u> 176 di 234
		<u>Ref.</u> CI-T-R-292	Rev. 0	

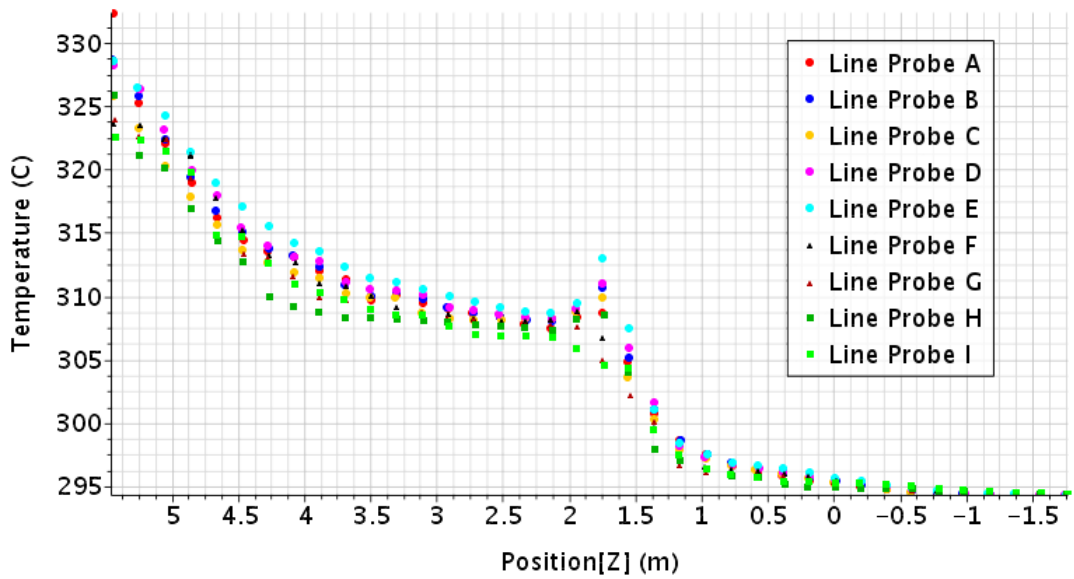


Figure 287: Temperature at the line probe points at time 5200s

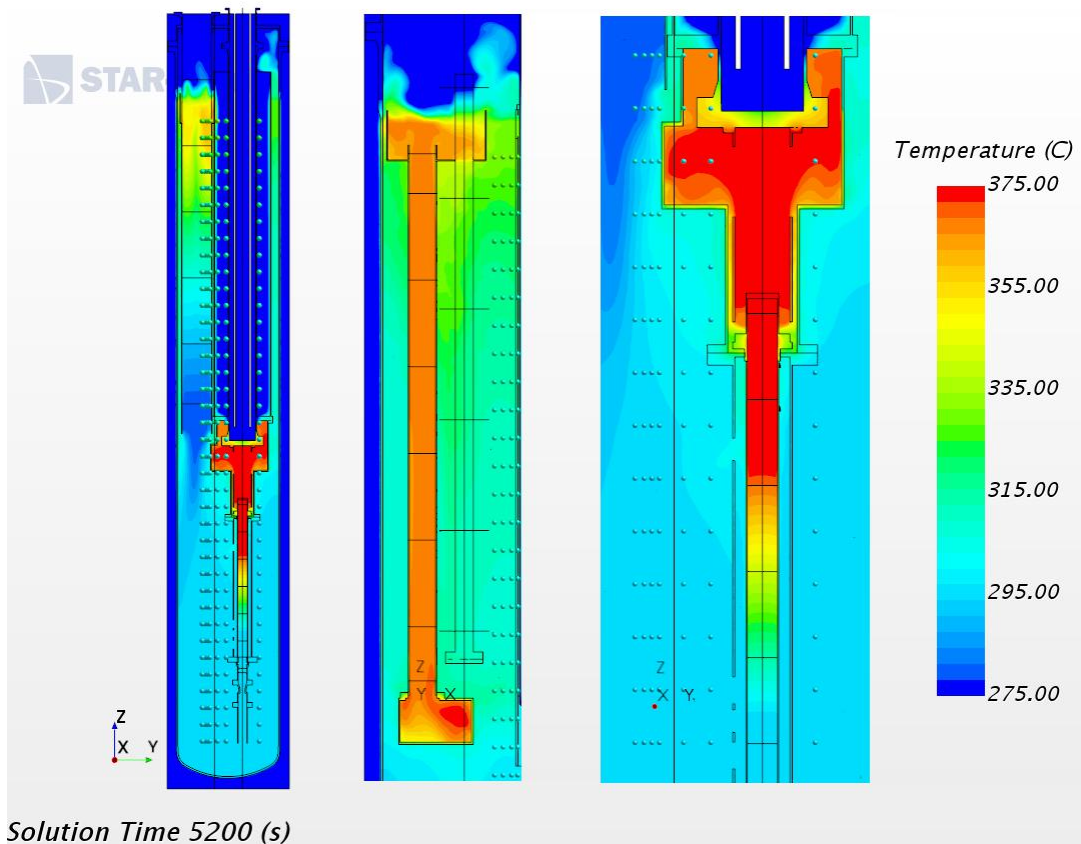



Figure 288: Temperature field across the main components at time 5200s.

 DIVISIONE INGEGNERIA SPERIMENTALE	<u>Title</u> D3.2: CIRCE experiments: pre-test, data-set and analysis	<u>Distribution</u> PUBLIC	<u>Emission</u> 09/08/2017	<u>Pag.</u> 177 di 234
		<u>Ref.</u> CI-T-R-292	Rev. 0	

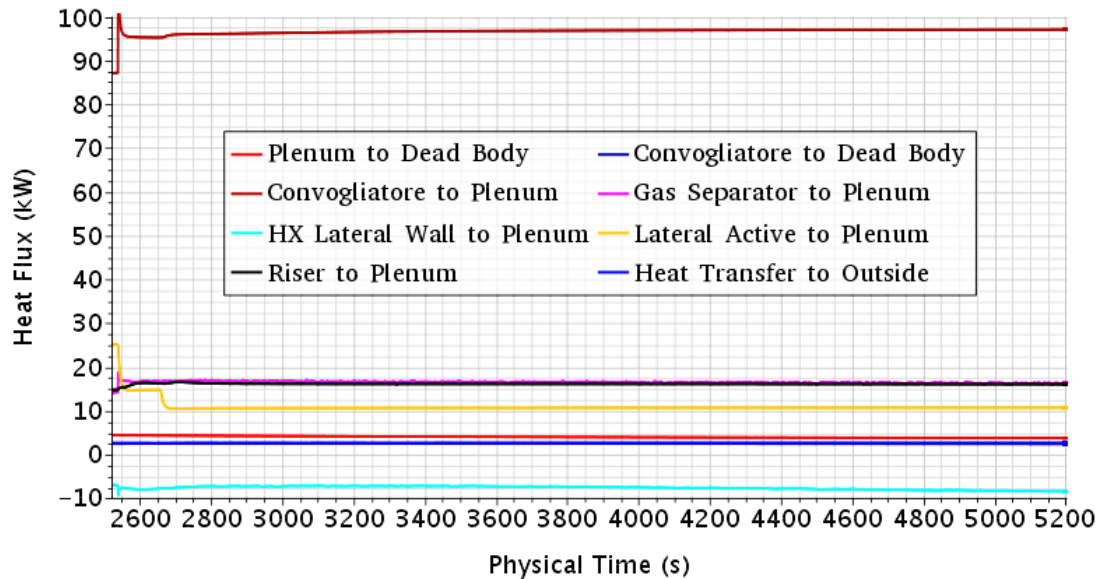


Figure 289: history of the main conductive heat transfers.


4.3.3 Analysis

We first look at the internal coherence of the numerical solution, check how far we are from an effective steady state configuration. From Figure 285, we can see that the temperature in the most strategic positions seem to be quite close to some asymptotic value. We cannot however neglect the possibility of a slow drift at a larger time scale. We thus give a look at the global thermal balance at time 5200s:

- Heat source in pin simulator: 707.5 kW
- HX heat sink: 695.1 kW
- Heat flux Plenum to Dead Body: 3.8 kW
- Heat flux Conveyor to Dead Body: 2.7 kW
- Heat flux External insulator to outside: 2.5 kW
- Total heat losses: 704.1 kW
- Discrepancy: 3.4 kW or ~ 0.5%

The total LBE inventory is 68.3 ton, while the model has 7200 kg of steel giving a thermal inertia of 13.2 MJ/K and a possible temperature drift of 0.9K/h. However, by looking at Figure 286, we can infer that the 3.4 kW discrepancy is likely to strongly reduce during the next few tens of minutes. We can thus conclude that we are most likely very close to a global steady-state and there is little hope to see a further heat profile neat evolution. In other words, discrepancies with the experiment (other than a mere global drift of the temperature) cannot be justified by an incomplete steady-state operation.

We first make a confront between the experiment and the simulation by looking at the temperature evolution along the hot line. Given the mass flow rate, it can be convenient to keep in mind the conversion 1K is roughly equivalent to 8 kW, meaning that a side wall heat

 DIVISIONE INGEGNERIA SPERIMENTALE	<u>Title</u> D3.2: CIRCE experiments: pre-test, data-set and analysis	<u>Distribution</u> PUBLIC	<u>Emission</u> 09/08/2017	<u>Pag.</u> 178 di 234
		<u>Ref.</u> CI-T-R-292	Rev. 0	

flux of 8 kW induces a bulk flow temperature drop by 1K. In Table 5, we show the experimental and numerical temperatures at critical sections together with the temperature change from the previous section and the equivalent heat loss. First of all, we see a difference of 9.3K at the pin simulator bottom. This is not really relevant as the numerical model would work almost the same at 9.3K above, on the condition that the reference temperature T_0 in the HX approximate heat exchange law is also shifted by the same amount. Then, we can see that the temperature rise between the HX outlet and the Pin simulator inlet is quite large 15K and almost identical for the experiment and the simulation. This is the change of LBE temperature while flowing in the middle and lower part of the plenum. This added enthalpy content is clearly identified in the simulation as coming from heat losses of the rising line which is as high as 120 kW. In conformity with , the relevant heat losses in the rising line are as follows:


- 97 kW from the ConveyorFigure 289
- 11 kW from the Pin Simulator
- 16 kW from the riser (as some part is not insulated)
- 16 kW from the gas separator.

Only the first two items and part of the third one participate to the flow heating between the HX outlet and the Pin Simulator inlet. Interestingly, we the HX flow is heated through its walls by the amount of 7.2 kW.

Table 5: Experimental and numerical temperatures at critical sections. Also, temperature change from the previous section and equivalent heat loss.

Position	Experimental T(C) / dT (K)	Simulation T (C) / dT (K)	Equivalent power experiment (kW)	Equivalent power simulation (kW)
Bottom Active	285 / 15	294.3 / 14.7	117.6	120
Top Active	362 / 77	380.0 / 85.7	616 (HS=735-7% kW)	685.6 (HS=707 kW)
Bottom Riser	357 / -5	367.7 / -12.3	-40	-98.4
Top riser	357 / 0	366.1 / -1.6	0	-12.8
HX inlet (plane section)	348 / -9	350.8 / -15.3	-72	-122.4
HX outlet	270 / -78	279.6 / -71.2	-624	-569.6

The main issue regards what happens between the Pin Simulator bottom and the Riser bottom, passing through the Pin Simulator top. In the experiment, the Pin heat source, is estimated to 735-7%=685 kW. The 7% missing being supposed to be lost in the wire connections inside the dead volume. From the measured temperature difference between the top and the bottom, we see only 616 kW of net heating. This would mean about 70 kW heat losses where the simulation “sees” only ~21 kW. On the other hand, the experimental measure gives only 5K (or 40 kW) through the conveyor walls while the simulation predicts 98 kW. While the simulation results should not be taken as granted, it is very unlikely to have such a large underestimation for the Pin simulator heat losses together with such a large overestimation for the conveyor. Some explanation must be found somewhere else.

 DIVISIONE INGEGNERIA SPERIMENTALE	<u>Title</u> D3.2: CIRCE experiments: pre-test, data-set and analysis	<u>Distribution</u> PUBLIC	<u>Emission</u> 09/08/2017	<u>Pag.</u> 179 di 234
		<u>Ref.</u> CI-T-R-292	Rev. 0	

A flow bypass between at the junction at the bottom of the conveyor would bring additional cold LBE in the rising line and a colder temperature at the Riser bottom and is therefore not a plausible explanation. On the other hand, if we suppose that the heat release of the pin has not exactly the foreseen vertical distribution, more precisely, if we suppose that about 50 kW are released between the measure at the top of the active part and the bottom of the Dead Volume, then all the measures become quite consistent and in line with the numerical simulation. In effect, the head release in the pin active part would then be about 635 kW and about 20 kW heat loss quite acceptable. Moreover, the 5k of temperature decrease through the conveyor would correspond to the balance of ~90 kW heat losses and 50 kW heat source.

This explanation fits so well with both the experimental and numerical data what we will make it ours.

Following the hot line, the difference between the numerical and experimental heat losses through the riser walls is simply due to the difference of temperature in the plenum at the other side of the wall.

The difference at the HX inlet plane section is probably due to a combination of effects. First, we compare the mean of three point-wise temperature value with a mass flow averaged one. Second, the HX is modelled as a porous medium and the local flow arrangement is quite approximate. Note that the incoming flow comes laterally from a bubbly flow in course of separation and its reasonably accurate numerical simulation is far beyond our actual capabilities, as explained in the cold model evaluation. Third, the heat exchange model of the HX is extremely approximated. Even in the given setup, the choice of 200 C for the reference temperature while the secondary flow coolant between 10 and 110 C is motivated by the need to stabilize the global enthalpy content of the system. In effect, a smaller temperature difference with the LBE increases the negative thermal reactivity feedback and promotes a faster global thermal convergence. The temperature change from the Riser top to the HX bottom is the same, -89 K, in the experiment and in the simulation.

The main objective of this exercise is to reproduce (up to a global shift) the vertical temperature profile in the LBE plenum of the reference experiment. For this reason, we plot side by side the experimental and numerical curves, in Figure 290.

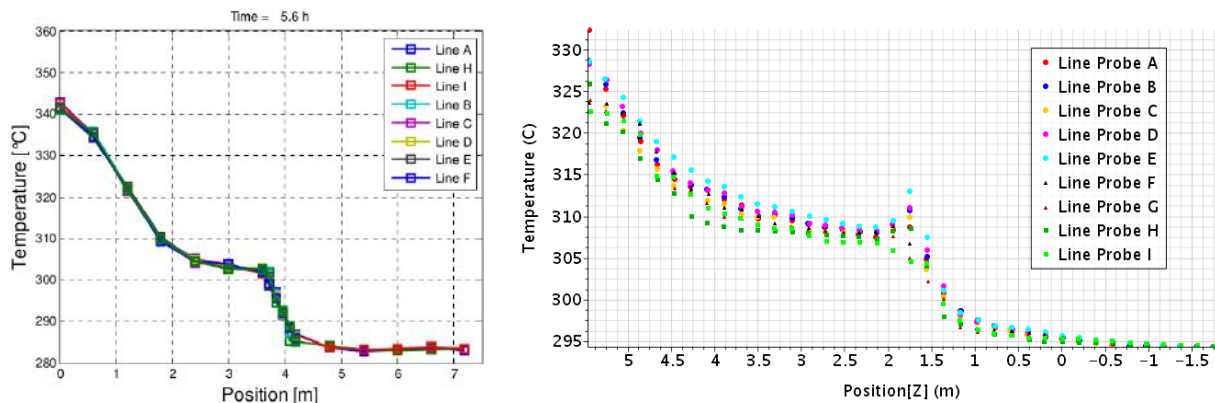



Figure 290: side by side experimental and numerical temperature profile at the plenum TCs.

We can see that that the simulation reproduces qualitatively some global features of the vertical thermal profiles. From top to bottom we have for 2m a decreasing temperature with a

 DIVISIONE INGEGNERIA SPERIMENTALE	<u>Title</u> D3.2: CIRCE experiments: pre-test, data-set and analysis	<u>Distribution</u> PUBLIC	<u>Emission</u> 09/08/2017	<u>Pag.</u> 180 di 234
		<u>Ref.</u> CI-T-R-292	Rev. 0	

quite constant slope, then a plateau for 1.5m, then a sharp temperature decrease for 0.5 m then a plateau again.

Some other features are however absolutely not satisfying:

- The global temperature variation is 30K in the simulations, vs. 55 K experimental.
- The numerical TC probes show a horizontal spread while the experimental one show a tight stratification
- The simulation exhibit a temperature peak before the sharp decrease. This peak is not present in the experiment (it may be but it is quite unlikely that TC probes are lacking at the right position).


The key discrepancy appears to be the temperature vertical gradient in the top 2m of LBE. It is tempting to give the culpability to an excessive effective conductivity of the molten LBE. To reduce this effective conductivity, the turbulent Prandtl number has been artificially increased from the default 0.9 to the value of 2. This value, while promoted in the literature, is completely unjustified here because the characteristic length scales greatly exceed the millimeter range. However, this value has been implemented in this simulation (from the last 2600s), but did not brought any substantial improvement. The reason for the discrepancy of the temperature slope has to be found elsewhere.

The dispersion of the numerical temperatures at a given height is an indication that small buoyancy induced flows, typically along the heat exchanging walls, are able to slightly disturb the otherwise quiescent LBE. In the experiment, the stratification is very homogeneous and the tiny flow just described do not influence the temperature profile. It is very difficult to understand how this can be true, unless we can suppose a small stabilizing downward flow. There are good reason to believe that such a flow exists and comes from the hot LBE at the top of the riser, even if its quantification is not yet possible. Two sources are possible:

- LBE ejected above the gas separator lateral walls by the greatly agitated two phase flow near the free surface, the void fraction there being possibly as high as 30 %.
- A bypass flow between the riser and the gas separator bottom.

Both explanations are not mutually exclusive and would explain such a hot LBE free surface temperature. Note that traces of LBE splashes have been found while refurbishing the experimental facility.

A last point regards the use of the VoF setting. It was chosen in continuity with the analysis on the MYRRHA numerical model in which the hot and cold plenum free surfaces are at two different heights with a gap about 2m and large LBE volume transfer in case of transients involving changes of the pumps head. This is not really the case in CIRCE because the pumping system is aligned with the most resistive parts of the loop in such a way that the change of free-surface level is only a couple of centimetres, as shown on Figure 277 right. The main drawback of the VoF setting is the incompatibility with the steady-state numerical setup. While the transient setup was probably better suited to understand the general CIRCE flow pattern in a first preliminary step for pre-test calculation, the VoF setting may result unnecessary if not useless for the later stage of the modelling. The cover gas still needs to be in some way simulated, but in a separate volume and fluid continuum.

 DIVISIONE INGEGNERIA SPERIMENTALE	<u>Title</u> D3.2: CIRCE experiments: pre-test, data-set and analysis	<u>Distribution</u> PUBLIC	<u>Emission</u> 09/08/2017	<u>Pag.</u> 181 di 234
		<u>Ref.</u> CI-T-R-292	Rev. 0	


5 NRG SIMULATION OF CIRCE-ICE

Within the frame of WP3 of the SESAME project, NRG focuses its activity on building a full CFD model of the CIRCE facility in its Integral Circulation Experiments (ICE, [4], [5]) set-up using ANSYS Fluent [6]. This model includes both the inner loop, which consists of, among others, the heat source, heat sink and “pump” of the system, as well as the main pool, representing the plenum of the test facility. Heat losses from the inner loop to the main pool and from the main pool to the environment will also be included. Results obtained with the model will subsequently be compared with the experimental campaign of WP3. This will be done for several steady-state cases representing experiments at full power, as well as various Protected Loss Of Heat sink and Loss Of Flow (PLOH + LOF) accident scenarios.

One of the four test runs to be performed within WP3 is here reported, viz., test 1 reported in §3.1. This represents an experiment in which the steady-state thermal forced convection flow receives a heat input from the Fuel Pin Simulator (FPS) of 800kW and the LBE flows through the inner loop at a mass flow rate of 65 kg/s. About 750kW of the 800kW heat input is removed through the primary heat exchanger. After 10 hours of physical run time, the test will go into its PLOH+LOF accident-scenario mode: power input is reduced to 30kW representing decay heat. The secondary side of the primary heat exchanger stops working so that the decay heat will be removed by the emergence heat exchanger, the Decay Heat Removal (DHR) system. Furthermore, the pumps (simulated by the gas enhanced circulation) stop working so that the flows goes from its forced convection mode to natural convection.

5.1 Model description

The CIRCE facility and the ICE test section have been described extensively in previous reports [2], [3], [4], [5]. The geometrical model (CAD geometry) developed at NRG for the simulations is reported in Figure 291 along with arrows indicating how various parts of the actual test facility. One of the major simplifications made is modelling the test section between the feeding conduit and the fitting volume, which also includes the flow meter, FPS, the upstream and downstream mixing zones and the release pipe, as one long cylinder with a constant radius. Furthermore, no bolts, flanges, etc. are included in the CAD geometry, and almost all walls have zero thickness, the exception being the heat exchanger wall. Also, the top lid is not included in the geometry. As a matter of fact, the CAD geometry only extends up till the free surface, so no cover gas is present in the model. In the sections below, several parts will be discussed in detail.

 DIVISIONE INGEGNERIA SPERIMENTALE	<u>Title</u> D3.2: CIRCE experiments: pre-test, data-set and analysis	<u>Distribution</u> PUBLIC	<u>Emission</u> 09/08/2017	<u>Pag.</u> 182 di 234
		<u>Ref.</u> CI-T-R-292	Rev. 0	

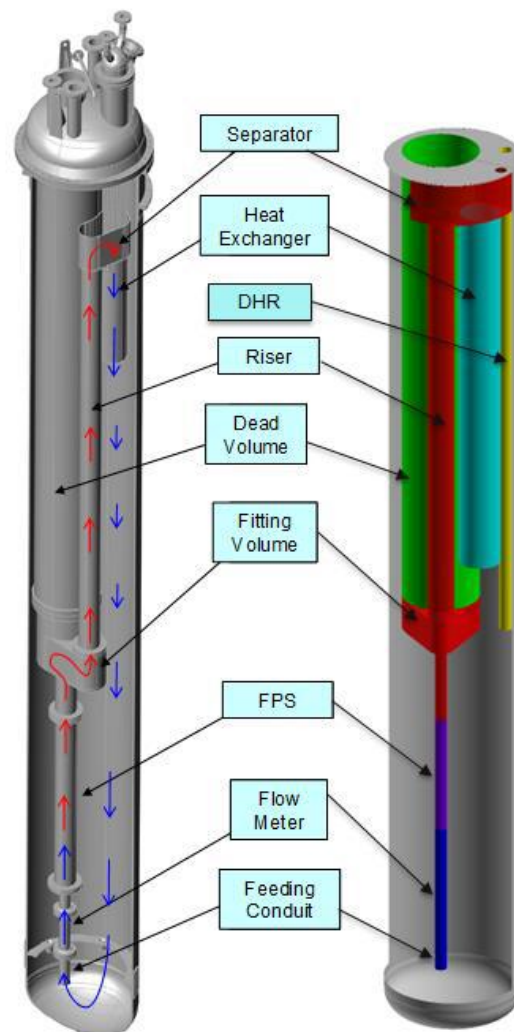



Figure 291: CAD geometry alongside test-facility.

5.1.1 Fuel Pin Simulator

5.1.1.1 FPS geometry

As mentioned before, the part of the inner loop from the feeding conduit till the fitting volume has been modelled as a single cylinder. This cylinder has a radius of 102,3mm, equal to the radius of the feeding conduit of the test facility. 37 electrical pins serve as heat source of the system, with an active length of 1m. These pins extend all the way through the mixing zones, release pipe (a cylindrical pipe after the FPS) and the fitting volume into the dead volume, where they are attached to electrical wires. A schematic of a cross-cut through the FPS is shown in Figure 292. As can be seen in the figure, the pins are actually located in a hexagonal tube, while the model contains a cylindrical tube. The difference in flow resistance between the two shapes has to be accounted for. Furthermore, the pins aren't physically included in the CAD geometry. Their influence on the flow will be modelled as a porous medium, which will be discussed in more detail in the next section. Modelling of the heat input is discussed further in this document.

 DIVISIONE INGEGNERIA SPERIMENTALE	<u>Title</u> D3.2: CIRCE experiments: pre-test, data-set and analysis	<u>Distribution</u> PUBLIC	<u>Emission</u> 09/08/2017	<u>Pag.</u> 183 di 234
		<u>Ref.</u> CI-T-R-292	Rev. 0	

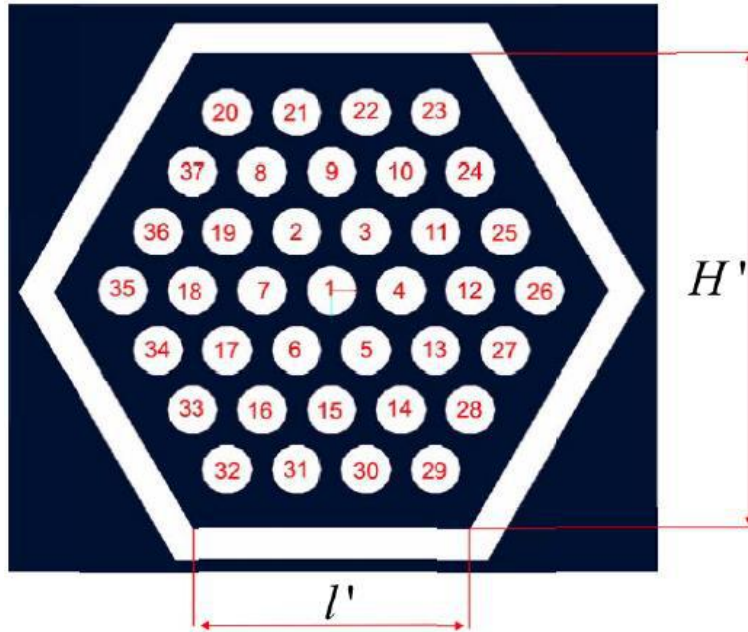


Figure 292: Schematic of the FPS cross section ($l' = 55.4\text{mm}$, $H' = 96\text{mm}$).

5.1.1.2 Porous Medium Approach


Since the electrical pins aren't physically present in the model, their flow resistance will be modelled by means of a porous medium zone. Porous media are modelled by the addition of a momentum source term to the standard fluid flow equations. The source term is composed of two parts: a viscous loss term (Darcy, the first term on the right-hand side of the following equation), and an inertial loss term (the second term on the right-hand side of the following equation):

$$S_i = - \left(\sum_{j=1}^3 D_{ij} \mu v_j + \sum_{j=1}^3 C_{ij} \frac{1}{2} \rho |v| v_j \right)$$

where S_i is the source term for the i -th (x , y or z) momentum equation, $|v|$ is the magnitude of the velocity and D and C are prescribed matrices. This momentum sink contributes to the pressure gradient in the porous cell, creating a pressure drop that is proportional to the fluid velocity (or velocity squared) in the cell. For the case of simple homogeneous porous media, which is applicable here, the source term reads:

$$S_i = - \left(\frac{\mu}{\alpha} v_i + C_2 \frac{1}{2} \rho |v| v_i \right) = \nabla p_{porous} = \frac{\Delta p_{porous}}{L_{ref}}$$

where α is the permeability (with dimensions m^2) and C_2 is the inertial resistance factor (dimensions $1/m$), i.e., D and C are diagonal matrices with $1/\alpha$ and C_2 , respectively, on the diagonals (and zero for the other elements). Note that here $\alpha = [m^2]$ and $C_2 = [1/m]$, which can easily be verified when realizing that S_i is the change of momentum with time, i.e., $S_i = \frac{\partial(\rho u_i)}{\partial t} = \left[\frac{kg}{m^2 s^2} \right]$ and $p = [Pa] = \left[\frac{N}{m^2} \right] = \left[\frac{kg}{m \cdot s^2} \right]$.

 DIVISIONE INGEGNERIA SPERIMENTALE	<u>Title</u> D3.2: CIRCE experiments: pre-test, data-set and analysis	<u>Distribution</u> PUBLIC	<u>Emission</u> 09/08/2017	<u>Pag.</u> 184 di 234
		<u>Ref.</u> CI-T-R-292	Rev. 0	

In the current simulation, the viscous losses are neglected and thus only the inertial resistance term is considered. If the pressure losses Δp_{porous} over the reference length L_{ref} are known, the inertial resistance factor at a particular flow rate can be determined by:

$$C_2 = \frac{\Delta p_{porous}}{L_{ref} \frac{\rho}{2} \tilde{u}^2}$$

In the above equation, the superficial velocity \tilde{u}^2 needs to be considered, which is the velocity of the fluid if the medium was fully open. It is related to the physical velocity by:

$$\vec{v}_{superficial} = \gamma \vec{v}_{physical}$$

where γ is the porosity of the medium defined as the ratio of the volume occupied by the fluid to the total volume. To determine the inertial resistance factor, the total pressure loss needs to be known. Since the model uses a uniform cylinder to represent the inlet and heating part of the inner loop, all pressure losses over the separate parts contained in this uniform cylinder and not directly resolved need to be accounted for. These pressure losses are due to: 1. Venturi-Bocaglio flow meter, 2. heat source, 3. inlet hexagonal wrapper, 4. lower grid assembly, and 5. spacer grids (three in total).

The method used to determine the pressure losses over these various part is similar to the one outlined in [2], i.e., local pressure drop coefficients are determined for each part, which are subsequently combined into an effective pressure drop coefficient. The total pressure drop based on a particular mass flow rate \dot{m} can then be determined using:

$$\Delta p_{fric} = \frac{1}{2} \frac{\dot{m}^2}{\rho_{eff} A_{eff}^2} K_{eff}$$

Table 1 summarizes the contributions to the effective pressure drop coefficients of the various parts for a mass flow rate of 65kg/s. To come to these values, a porosity

$$\gamma = \frac{flow\ volume}{actual\ volume} = \frac{0.5H'l' - 37\pi r_{pin}^2}{\pi r_{FPS}^2} = 0.733$$

was used, as well as a reference temperature of 350°C, which is needed to determine material properties. For a mass flow rate of 65kg/s, the total pressure drop $\Delta p_{fric} \approx 40kPa$. The inertial resistance factor in axial direction $C_2 \approx 9.1/m$. This value was obtained using a reference length $L_{ref} = 1.45m$, i.e., longer than just the active part of the Fuel Pin Simulator, reason being that the pins also obstruct the flow in the downstream mixing zone similar to inside the FPS. Beyond the DMZ, the LBE flows into the Release Pipe, which has a larger diameter. There, the flow area taking into account the pins is similar than the flow area in the model without the pins.

As for the inertial resistance factors in the two directions perpendicular to the axial directions, in a Cartesian coordinate frame, they were set at a factor of 1000 larger than the one in axial direction. The reason for such large resistance factors is that, in reality, the flow is blocked in radial direction due to the pins.


 DIVISIONE INGEGNERIA SPERIMENTALE	<u>Title</u> D3.2: CIRCE experiments: pre-test, data-set and analysis	<u>Distribution</u> PUBLIC	<u>Emission</u> 09/08/2017	<u>Pag.</u> 185 di 234
		<u>Ref.</u> CI-T-R-292	Rev. 0	

Table 6: Local pressure drop coefficients in various parts of the FPS cylinder.

Relevant part	Local pressure drop coefficient [-]
Flow Meter	1.593
Heat Source	1.578
Inlet Hexagonal Wrapper	0.19
Lower Grid Assembly	2.277
Spacer Grids (3x)	1.431
Total	7.068

5.1.1.3 Heat source model

The power input of the test facility is modelled using a Volumetric Heat Source (VHS) with units W/m^3 :

$$Q_{FPS} = \frac{P_{FPS}}{V_{FPS}},$$

Where P_{FPS} is the power supplied to the electric pins in the FPS and V_{FPS} is the volume of the FPS in the model. This kind of model allows for a very accurate control over the amount of heat added to the system, and the CFD model automatically adds the right amount of heat to a particular cell based on its volumetric size. Since the velocity of the LBE inside the FPS is nearly uniform, it results in a nearly linear temperature profile.

5.1.2 Argon Injection


To avoid the computational cost of a two-phase flow approach, the argon injection to force the flow, which basically is a mock-up of a pump, is not included explicitly, but accounted for through a Volumetric Momentum Source (VMS, $[N/m^3]$) in the riser, much like what was used to model the heat input in the FPS. Such a model adds a source term to the momentum equations. However, there isn't a clear one-on-one relation between the desired mass flow rate and the value to be used for the VMS due to the presence of buoyancy. Hence, trial-and-error is used to come to the correct input value based on a targeted mass flow rate. E.g., for $P_{FPS} = 800kW$ and a desired $\dot{m} = 65 kg/s$, a value of $VMS_{Riser} = 12.250 N/m^3$ is needed. This is valid for LBE temperatures in the 300 - 400°C range.

5.1.3 Cover gas & free surface

The same assumption made for the argon injection is used in terms of the cover gas in the CFD model. Thus the CAD geometry only extends up till the free surface. This free surface is modelled as an impenetrable wall with free-slip condition and is maintained at a fixed height. The fixed height assumption is very reasonable for Steady-State simulations, however, it is expected to change during transient runs. To estimate this change in height, let's assume a decrease in overall average temperature of 300°C, which is quite reasonable for a switch from forced convection to natural convection. This temperature decrease results in a density increase of about 0.4% (see § 5.2.2). On a total vessel height of about 7.5m, that's a drop in free surface of 3cm. The aforementioned assumption is hence reasonable.

5.1.4 Heat exchanger

The primary heat exchanger in the CIRCE-ICE test facility is a low-pressure boiling water shell heat exchanger consisting of 91 bayonet tubes. More details can be found in [4] and

 DIVISIONE INGEGNERIA SPERIMENTALE	<u>Title</u> D3.2: CIRCE experiments: pre-test, data-set and analysis	<u>Distribution</u> PUBLIC	<u>Emission</u> 09/08/2017	<u>Pag.</u> 186 di 234
		<u>Ref.</u> CI-T-R-292	Rev. 0	

[5]. Since the main interest is the heat being removed by the heat exchanger and the resulting temperature profile, and not so much the flow field inside the heat exchanger, the tubes are not explicitly included in the geometry. To compensate for the friction losses due to the bayonet tubes, the heat exchanger will be modelled as a porous medium as discussed in the next section.

5.1.4.1 Porous Medium Model for the HX

An identical porous medium model as used for the FPS will be used for the HX. Thus the main task is to estimate the pressure losses due to the bayonet tubes at a particular mass flow rate and subsequently determine the inertial resistance factor. The pressure loss due to friction can be estimated using the following equation:

$$\Delta p_{fric} = \frac{1}{2} \frac{\dot{m}^2}{\rho_{HX} A_{HX}^2} K_{HX} = \frac{1}{2} \frac{\dot{m}^2}{\rho_{HX} A_{HX}^2} f_{HX} \frac{L_{HX}}{D_{h,HX}},$$

here, $L_{HX} = 3205\text{mm}$ is the length of the heat exchanger, $D_{h,HX} = 22\text{mm}$ its hydraulic diameter and f_{HX} the Darcy-Weisback factor. To determine the latter, the Churchill Correlation [15] has been adopted. This correlation applies to a wide range of Reynolds number, spanning the laminar, transition and turbulent regimes:

$$f = 8 \left[\left(\frac{8}{Re} \right)^{12} + \frac{1}{(A+B)^{3/2}} \right]^{1/12}, \quad A = \left[2.457 \ln \left(\frac{1}{(7/Re)^{0.9} + 0.27(\epsilon/D_h)} \right) \right]^{16}, \quad B = \left[\frac{37530}{Re} \right]^{16},$$

where ϵ is the average roughness of the components, assumed to be zero here. Table 7 summarizes the relevant parameters, assuming an average temperature of 350°C and a mass flow rate of 65 kg/s :

Table 7: HX porous medium input parameters for a mass flow rate of 65 kg/s.


Parameter	Model input
f_{HX}	0.026 [-]
Δp_{fric}	371 [Pa]
$C_{2,HX} - \text{axial}$	4.76 [1/m]
$C_{2,HX} - \text{transversal}$	4760 [1/m]
γ_{HX}	0.499

5.1.4.2 Heat sink model

Consistent with the FPS, Volumetric Heat Source is used. However, this time it's negative, as it's supposed to be a sink, and it won't have a constant value. Instead, the following model is used:

$$Q_{HX} = \frac{\rho c_p}{\tau} (T_0 - T),$$

here, ρ is the density of the LBE, c_p the specific heat, T the actual, current, temperature of the LBE, T_0 a target temperature and τ is a relaxation time. Such a model introduces two additional degrees of freedom, T_0 and τ , which allows for a better control over the temperature in the simulation. Thus, if for example the temperature suddenly rises, the heat removed through such a model will also increase, thereby suppressing fluctuations. The target temperature T_0 is somewhat representative of the water/steam temperature on the secondary

 DIVISIONE INGEGNERIA SPERIMENTALE	<u>Title</u> D3.2: CIRCE experiments: pre-test, data-set and analysis	<u>Distribution</u> PUBLIC	<u>Emission</u> 09/08/2017	<u>Pag.</u> 187 di 234
		<u>Ref.</u> CI-T-R-292	Rev. 0	

side of the heat exchanger, while τ is similar to a residence time of the LBE inside the heat exchanger. These parameters are tuned such to get the desired heat removed by the heat exchanger for a particular test.

5.1.5 Decay heat removal system

In case of accident scenarios in which the primary heat exchanger is no longer operational, the DHR serves as the heat sink of the system. It consists of a single bayonet tube, with LBE flowing in through slots from the top and leaving at the bottom, and cold air coming in from the top, flowing downwards before turning around and getting heated while flowing upwards and finally leaving at the top. A schematic is shown in Figure 293. The air component of the DHR will not be included in the CFD model; only the LBE part. Therefore, only the annular cylinder through with the LBE flows is incorporated in the model, while the air side is represented as an empty cylinder. Also, the slots have been replaced by a simple opening at the top.

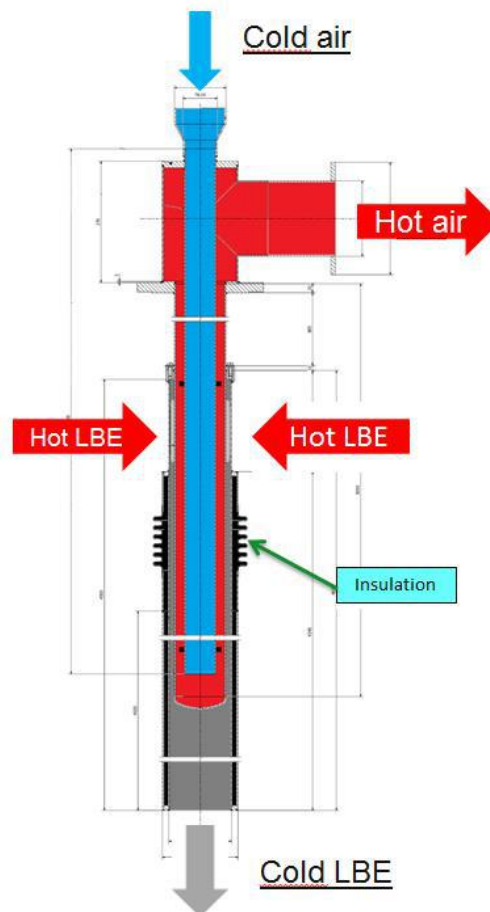



Figure 293: Schematic of the DHR.

Regarding the heat being removed from the system, this is modelled as a Volumetric Heat Sink. Similar to the FPS, it assumes a constant value, though since it is a sink it is negative:

 DIVISIONE INGEGNERIA SPERIMENTALE	<u>Title</u> D3.2: CIRCE experiments: pre-test, data-set and analysis	<u>Distribution</u> PUBLIC	<u>Emission</u> 09/08/2017	<u>Pag.</u> 188 di 234
		<u>Ref.</u> CI-T-R-292	Rev. 0	

$$Q_{DHR} = -\frac{P_{DHR}}{V_{DHR}}$$

5.1.6 Coniugate heat transfer

One of the more important phenomena taking place during the operation of the test facility is Conjugate Heat Transfer (CHT). This contributes to the heat balance of the system in two ways: 1) heat transfer from the hot inner loop to the colder main pool through the inner structures, e.g., through the fitting volume walls, and 2) heat transferred from the main pool to the environment through the vessel walls, and, to a lesser degree, through the dead volume walls. In order to get an accurate model, and to get a proper stratification in the pool, CHT should not be neglected.

In the current model, in which almost all the walls have zero physical thickness, the Shell Conduction option of Fluent [6] is used. This option allows to create additional layers of cells in walls, in which, during the simulation, the heat equation in the following form is solved:


$$\frac{\partial T}{\partial t} = \frac{k}{\rho c_p} \left(\frac{\partial^2 T}{\partial x^2} + \frac{\partial^2 T}{\partial y^2} + \frac{\partial^2 T}{\partial z^2} \right),$$

where T is the temperature, k the thermal conductivity of the material, ρ its density and c_p its specific heat. This Shell Conduction option requires the specification of the thickness of the layer as well as the material, and takes into account heat transfer through the walls, as well as in-wall heat transfer and thermal inertia of the walls. The latter is important during transient runs, when heat contained in the walls slows down the cooling of the system. Finally, it allows for the creation of multiple layers. For example, around the riser of the test facility, an additional cylinder is placed that contains air. This means there are three layers of material needed to represent the CHT from the riser to the main pool: 1) the riser tube itself, 2) the layer of air, and 3) the cylinder in which the air is contained.

5.2 Mesh generation

To create the mesh of the model, the mesh generation software GAMBIT [8] is used. This software is quite flexible in its use and allows for a large control over the cell sizes and cell growth. The whole geometry is subdivided into various volumes such that most of the computational domain contains hexahedral cells using the Cooper Scheme. Only two parts have tetrahedral cells, viz. a part of the Main Pool just above the fitting volume and in the very bottom of the main vessel. However, in both these parts the LBE is rather stagnant, so it is expected to not adversely affect the numerical simulations.

Boundary layers are used in the Fuel Pin Simulator, the riser and the heat exchanger, where the first layer thickness was chosen such that $y^+ > 30$ everywhere in the inner loop. Figure 294 and Figure 295 illustrate what the mesh looks like at two different levels of the geometry. As can be seen, smaller cells are used in the inner loop, where velocities and gradients are larger. In the more stagnant main pool, cells are grown to larger sizes. A summary of the mesh statistics is introduced in Table 8.

 DIVISIONE INGEGNERIA SPERIMENTALE	<u>Title</u> D3.2: CIRCE experiments: pre-test, data-set and analysis	<u>Distribution</u> PUBLIC	<u>Emission</u> 09/08/2017	<u>Pag.</u> 189 di 234
		<u>Ref.</u> CI-T-R-292	Rev. 0	

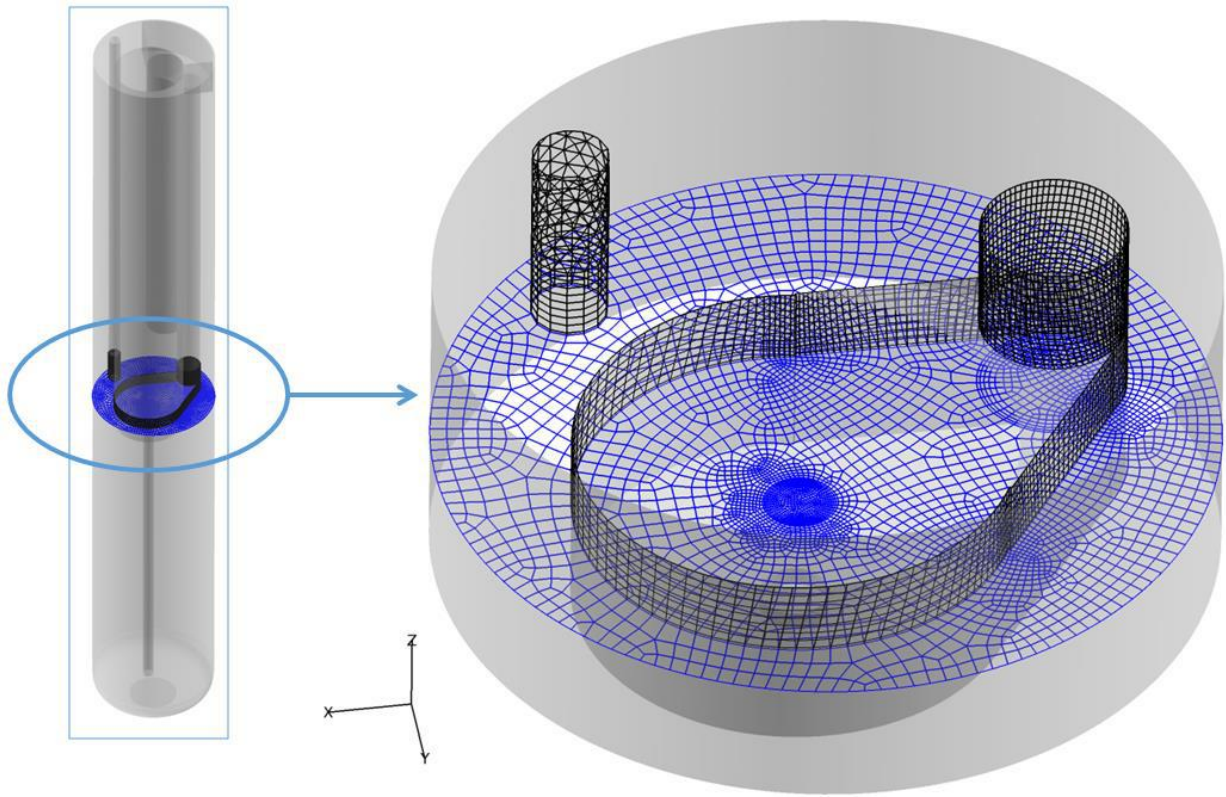


Figure 294: Cross-cut through Fitting Volume showing the mesh. Also shown are various wall meshes.

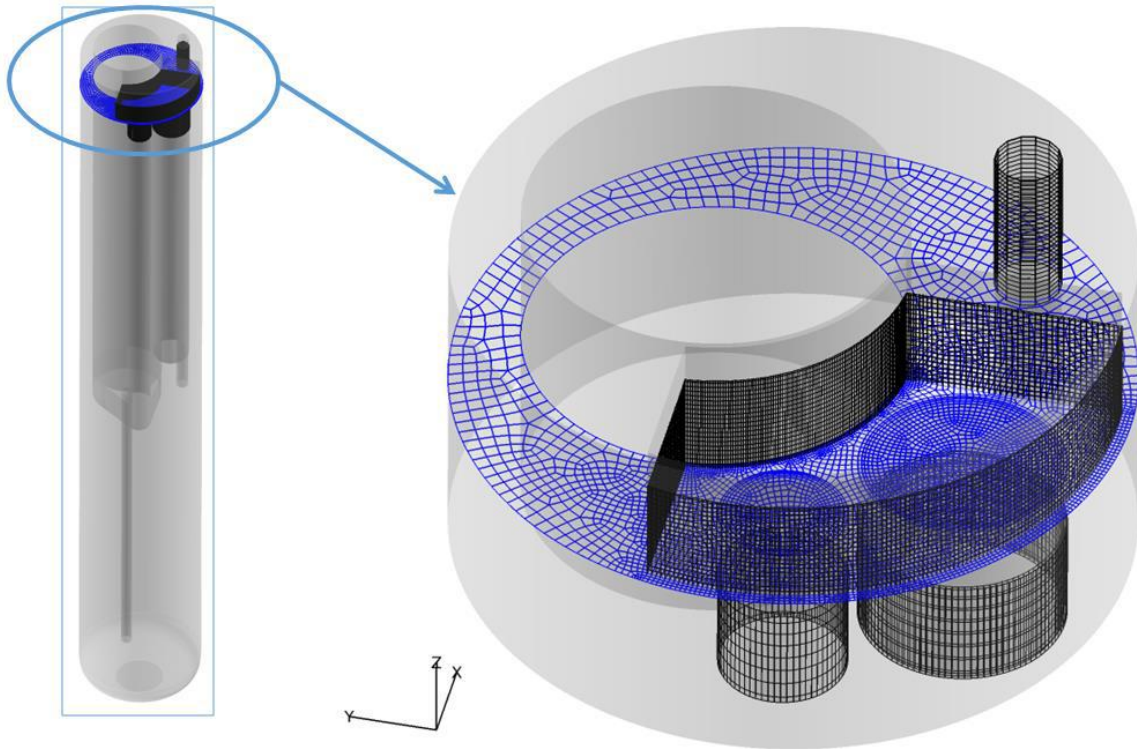


Figure 295: Cross-cut through the Separator showing the mesh. Also shown are various wall meshes.


 DIVISIONE INGEGNERIA SPERIMENTALE	<u>Title</u> D3.2: CIRCE experiments: pre-test, data-set and analysis	<u>Distribution</u> PUBLIC	<u>Emission</u> 09/08/2017	<u>Pag.</u> 190 di 234
		<u>Ref.</u> CI-T-R-292	Rev. 0	

Table 8: Various mesh statistics.

Mesh parameter/statistic	Value
Number of volumes	40
Total number of cells	2.285.220
Total number of tetrahedral cells	238.222
Total number of hexahedral cells	2.046.998
Maximum skewness	0.94
Number of cells with skewness > 0.9	4
Largest aspect ratio	61

5.2.1 Simulation Settings

To obtain the flow and temperature fields, the Navier-Stokes and energy equations are solved numerically in the RANS context. The corresponding settings are summarized in Table 9.

Table 9: Relevant simulation settings


Settings	
CFD code	ANSYS Fluent 17.2
Turbulence model	Realizable κ - ϵ model
Wall treatment option	Enhanced Wall Treatment
Liquid metal heat transfer	Turbulent Prandtl number = 2.0 [9]
Velocity-pressure coupling	SIMPLE algorithm
Gradient discretization	Least squares cell based
Spatial discretization	2 nd order
Linear system iterative method	Gauss-Seidel
Boundary conditions - flow	No-slip (except for free surface)
Boundary conditions - temperature	Conjugate Heat Transfer

Regarding the initial conditions used to get to a steady-state flow, the flow field starts from rest. The temperature in the main pool is initialized at a reasonable low temperature, while the inner loop has a corresponding high temperature. Inside the FPS and HX, the temperature varies linearly between these two temperature. This initial temperature field gives faster convergence than initializing at one fixed temperature.

5.2.2 Material Properties

The following temperature dependent equations for the density ρ_{LBE} [kg/m^3], dynamic viscosity μ_{LBE} [$Pa \cdot s$], thermal conductivity k_{LBE} [W/mK] and specific heat c_{pLBE} [J/kgK] of Lead-Bismuth Eutectic, taken from the LBE handbook [10] are, are implemented in the CFD code:

$$\begin{aligned}
 \rho_{LBE} &= 11065 - 1.293T, \\
 \mu_{LBE} &= 4.94 \cdot 10^{-4} e^{(754.1/T)}, \\
 k_{LBE} &= 3.284 + 1.617 \cdot 10^{-2}T - 2.305 \cdot 10^{-6}T^2, \\
 c_{pLBE} &= 164.8 - 3.94 \cdot 10^{-2}T + 1.25 \cdot 10^{-5}T^2 - 4.56 \cdot 10^5/T^2,
 \end{aligned}$$

 DIVISIONE INGEGNERIA SPERIMENTALE	<u>Title</u> D3.2: CIRCE experiments: pre-test, data-set and analysis	<u>Distribution</u> PUBLIC	<u>Emission</u> 09/08/2017	<u>Pag.</u> 191 di 234
		<u>Ref.</u> CI-T-R-292	Rev. 0	

here, temperatures are always in Kelvin. Material properties are also needed for the walls. These are made either of Stainless Steel grade AISI 304 or AISI 316L. Their properties are quite similar, and therefore it was chosen to use the properties of SS AISI 316L for all walls. These are given by [11]:

$$\rho_{SS} = 8110.5 - 0.44476T$$

$$c_{pSS} = 306.682 + 0.74277T - 7.5148 \cdot 10^{-4}T^2 + 3.10023 \cdot 10^{-7}T^3$$

$$k_{SS} = 10.145 + 0.01253T + 2.1927 \cdot 10^{-6}T^2$$

Furthermore, material properties of ceramic fibre, air and argon gas are needed. The former is used as an insulator to prevent heat losses to the environment. Air is used to minimize heat transfer from the inner loop to the main pool and argon is the cover gas. Values of the properties for these materials are summarized in Table 10. Piecewise-linear indicates that values for these properties are specified at particular temperatures, as provided by the references, and linear interpolation is used to obtain values at intermediate temperatures.

Table 10: Material properties for various materials

	Density [kg/m^3]	Thermal conductivity [W/mK]	Specific heat [J/kgK]
Air [12]	0.566	Piecewise-linear	Piecewise-linear
Ceramic fibre [manufacturer]	130.0	Piecewise-linear	1130.0
Argon [Fluent database]	1.6228	0.0158	520.64

Densities of all these materials are kept constant, with values corresponding to a temperature of 350°C. The reason for this is that we don't take into account thermal expansion of any wall or insulation material. This also applies to the steel walls. Argon properties are kept constant since it's being re-circulated and maintained at a nearly fixed temperature.

5.3 Results of the CFD Simulation

5.3.1 Description of SESAME WP3 Test 1

A thorough overview of SESAME WP3 Test 1 can be seen in Table 11. It consists of an initial ramp-up to a steady-state flow with a total heat input of about 800kW and an LBE mass flow rate $\dot{m} = 60 - 70 \text{ kg/s}$. Furthermore, heat is removed by the main heat exchanger at a rate of 750 kJ per second. After having reached steady-state and running in steady-state, a Protected Loss Of Heat and Loss Of Flow (PLOH + LOW) accident scenario is mimicked. During such an accident scenario, the pumps stop working and the fuel operates at a decay heat, with is about 3-5% of its nominal power. Furthermore, the main heat exchanger is isolated from the system and the DHR serves as the heat sink of the system. In practise, the system goes from forced convection mode into natural convection at a much lower power.


 DIVISIONE INGEGNERIA SPERIMENTALE	<u>Title</u> D3.2: CIRCE experiments: pre-test, data-set and analysis	<u>Distribution</u> PUBLIC	<u>Emission</u> 09/08/2017	<u>Pag.</u> 192 di 234
		<u>Ref.</u> CI-T-R-292	Rev. 0	

Table 11: Description of accident scenario Test 1

Nominal Steady State	PLOH+LOF Transient
FPS nominal power $\approx 800\text{kW}$	Core “scram” at about 30 kW (decay power)
LBE $\dot{m} = 60 - 70 \text{ kg/s}$ (by gas lift)	LBE circulation through natural convection.
Argon mass flow rate $\approx 3 \text{ NI/s}$	No forced circulation
Average velocity into the HS $\approx 1\text{m/s}$	Natural circulation due to decay heat.
Pool LBE initial temperature $\approx 314^\circ\text{C}$	Pool temperature to be determined.
Vessel heating system: not active	Vessel heating system: not active
HX water flow rate $\approx 0.6 \text{ kg/s}$	Isolation of the feed water
HX inlet water at room temperature	Isolation of the feed water.
HX thermal power removed $\approx 750\text{kW}$	Isolation of the main HX (not operational)
DHR: not active	DHR:active

The time evolution of the experiment is described in Table 7. The total test consists of about 20hrs, of which the approximately first 10 hours are used to reach a steady-state and the second half of the experiment is allocated to the transient.


Table 12: Time evolution of SESAME WP3 Test 1.

FULL POWER RUN	
Event	Time
Power ramp (0-800kW)	0.3h \rightarrow 0.35h
Full power (800kW)	0.35h \rightarrow 10.3h
Water injection (main HX)	0.35h \rightarrow 10.35h
Argon injection	0.17h \rightarrow 10.35h
TRANSITION	
Event	Time
Power Ramp (800-30 kW)	10.3h \rightarrow 10.35h
Air injection (DHR)	10.35h \rightarrow 20.09h

5.3.2 Steady-State results.

Before performing the transient part of the test, the proper steady-state flow has to be reached. As outlined in the previous section, this can be obtained by a simulation in which the LBE initially is at rest with a temperature of about 314°C . It is subsequently forced to flow by means of argon injection, resulting in a mass flow rate of around 65 kg/s . The nominal heat input by the FPS is about 800kW . This part of the experiment lasts for $\sim 10.3\text{hrs}$ before the transient starts. We want to reproduce the flow and temperature conditions of the LBE before the transient is started.

In the simulation, the flow is started from rest, with an initial pool temperature of about 300°C . The initial temperature of the inner loop was set at 380°C , with a linear variation between these two temperatures inside the FPS and HX. This way of initializing the temperature is done to reach convergence faster. The Volumetric Momentum Source inside

 DIVISIONE INGEGNERIA SPERIMENTALE	<u>Title</u> D3.2: CIRCE experiments: pre-test, data-set and analysis	<u>Distribution</u> PUBLIC	<u>Emission</u> 09/08/2017	<u>Pag.</u> 193 di 234
		<u>Ref.</u> CI-T-R-292	Rev. 0	

the riser is tuned in order to get the proper mass flow rate. Table 13 gives an overview of some relevant values of the simulation once it reaches a steady-state condition, along with experimental values right before the transient starts.


As can be seen, there's some discrepancy between the power input; 790kW for the simulation and 813kW for the experiment. A lower heat input in the model was used because some of the power supplied to the electrical cables in the experiment is lost due to Joule heating inside the Dead Volume [3]. This means less power is available for heating of the LBE, with an estimated loss of about 3-5%. Heat removed by the heat exchanger in the model is very close to what is removed in the experiment. Also, the mass flow rate inside the inner loop agrees very well due to the tuning of the VMS in the riser.

The inlet and outlet temperatures of the inner loop, i.e., $T_{in,FPS}$ and $T_{out,HX}$ agree very well, being off by only $\sim 2^{\circ}\text{C}$ and $\sim 5^{\circ}\text{C}$, respectively. This is very important because it means LBE flows out of and into the main pool at approximately the correct temperatures. Other inner loop temperatures differ more, but are still reasonably close.

Table 13: Steady-state conditions comparison between simulation and experiment.

	Simulation	Experiment
Thermal Power in the FPS	790kW	813kW
\dot{m} LBE in the FPS	65.2 kg/s	~ 65 kg/s
\dot{m} LBE in the DHR	0.0 kg/s	0.0 kg/s
$T_{inlet,av}$ FPS	323.8 $^{\circ}\text{C}$	325 $^{\circ}\text{C}$
$T_{outlet,av}$ FPS (Fitting Volume)	410.1 $^{\circ}\text{C}$	402 $^{\circ}\text{C}$
$T_{inlet,av}$ Riser	404.6 $^{\circ}\text{C}$	395 $^{\circ}\text{C}$
$T_{outlet,av}$ Riser	403.5 $^{\circ}\text{C}$	395 $^{\circ}\text{C}$
$T_{inlet,av}$ HX	402.0 $^{\circ}\text{C}$	389 $^{\circ}\text{C}$
$T_{outlet,av}$ HX	319.0 $^{\circ}\text{C}$	314 $^{\circ}\text{C}$
$T_{inlet,av}$ DHR	392.6 $^{\circ}\text{C}$	384 $^{\circ}\text{C}$
$T_{outlet,av}$ DHR	328.4 $^{\circ}\text{C}$	326 $^{\circ}\text{C}$
\dot{Q}_{water} removed by the HX	743kW	750 kW

An important goal of the project is to reproduce the stratification of the Lead-Bismuth Eutectic inside the main pool. This stratification is caused by heat losses from the inner loop, through the structure walls, to the main pool. Figure 296 shows a comparison between the simulation and experiment of the stratification for the steady-state flow. Here, a depth of 0m corresponds to the bottom of the separator and a depth of 7m to a level slightly below the inlet of the inner loop. Overall, a very good agreement is found, especially in the lower part of the vessel. The steep temperature gradient around a depth of 4m, which corresponds to the fitting volume level, is also properly captured. This steep temperature gradient is caused by large heat losses from the fitting volume to the main pool, where the walls consist of single-layered steel of about 10mm thick. This in comparison to the FPS and riser, which are much better insulated due to a double layer of steel with either air or stagnant LBE in between.

 DIVISIONE INGEGNERIA SPERIMENTALE	<u>Title</u> D3.2: CIRCE experiments: pre-test, data-set and analysis	<u>Distribution</u> PUBLIC	<u>Emission</u> 09/08/2017	<u>Pag.</u> 194 di 234
		<u>Ref.</u> CI-T-R-292	Rev. 0	

Pool Stratification Simulation vs. Experiment

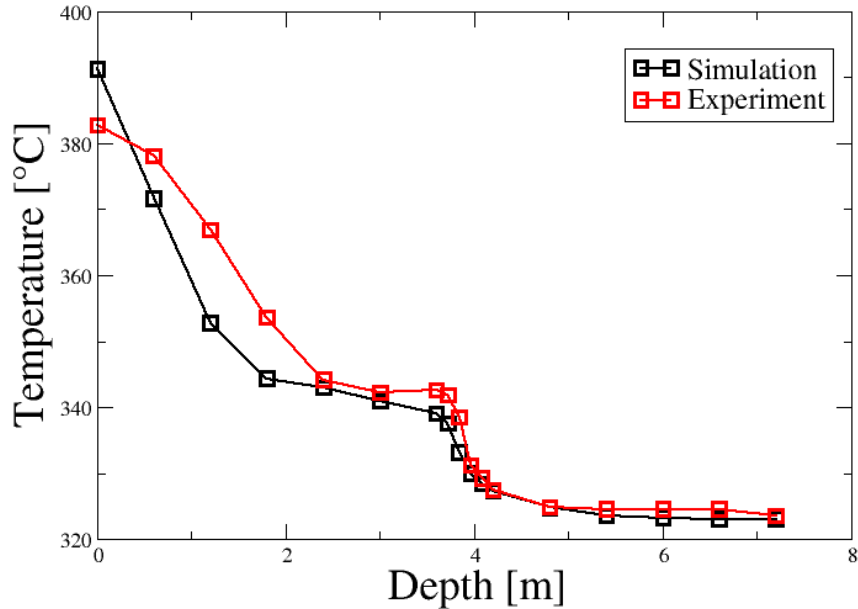



Figure 296: Stratification comparison inside the Main Pool.

A larger discrepancy is found in the upper two meters of the vessel. This is probably caused by an inaccurate representation of the conjugate heat transfer between the riser and the main vessel. However, more investigation here is needed.

The stratification present inside the main pool is clearly visible in Figure 297, which shows the temperature and vertical velocity profiles on a vertical cross cut through the centre of the heat exchanger. Temperatures in the bottom half of the pool are fairly uniform, but increase strongly going upwards. Explanation for this can partly be found in Figure 298, which shows the temperature profile on a vertical plane through the centres of the heat source and the riser. The zoom clearly shows there's quite a large amount of heat lost from the fitting volume to the main pool, resulting in heating of the LBE at that level. This phenomenon can also be observed in the stratification plot of Figure 296.

Finally, Figure 299 shows temperature profiles at four different values of the y-coordinate. By comparing these four profiles, it results that there isn't much of a horizontal temperature gradient.

 DIVISIONE INGEGNERIA SPERIMENTALE	<u>Title</u> D3.2: CIRCE experiments: pre-test, data-set and analysis	<u>Distribution</u> PUBLIC	<u>Emission</u> 09/08/2017	<u>Pag.</u> 195 di 234
		<u>Ref.</u> CI-T-R-292	Rev. 0	

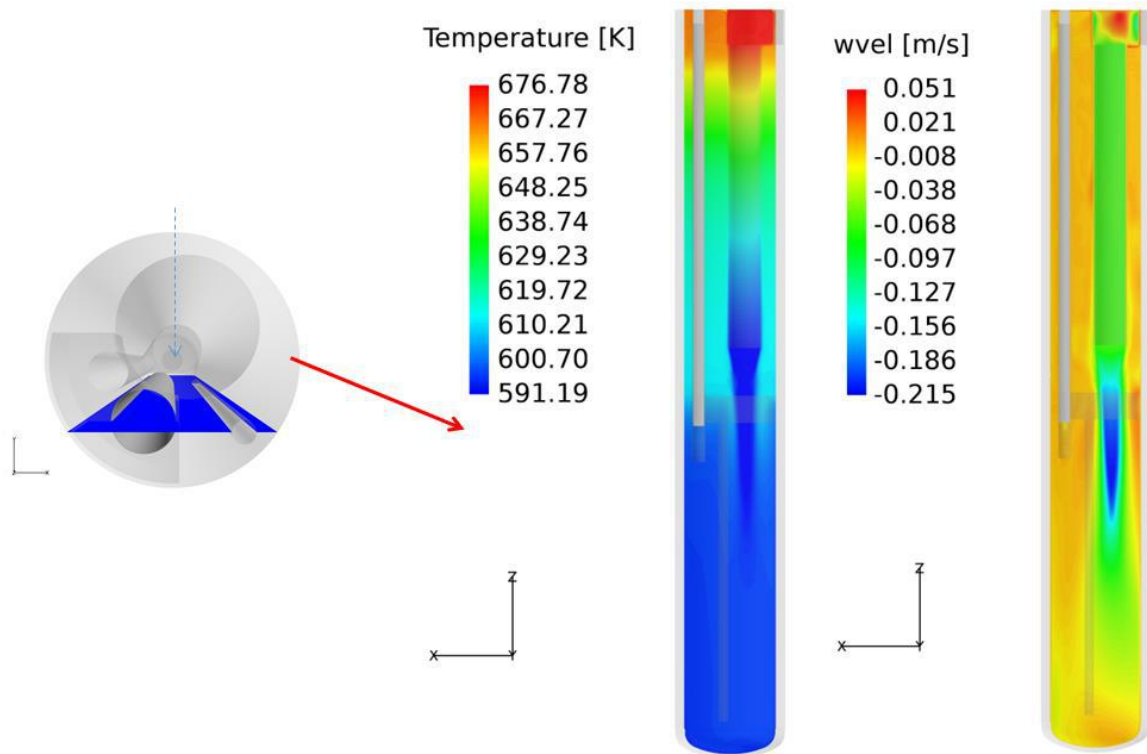


Figure 297: Temperature (middle) and vertical velocity (right) profiles on a vertical plane through the centre of the Heat Exchanger.

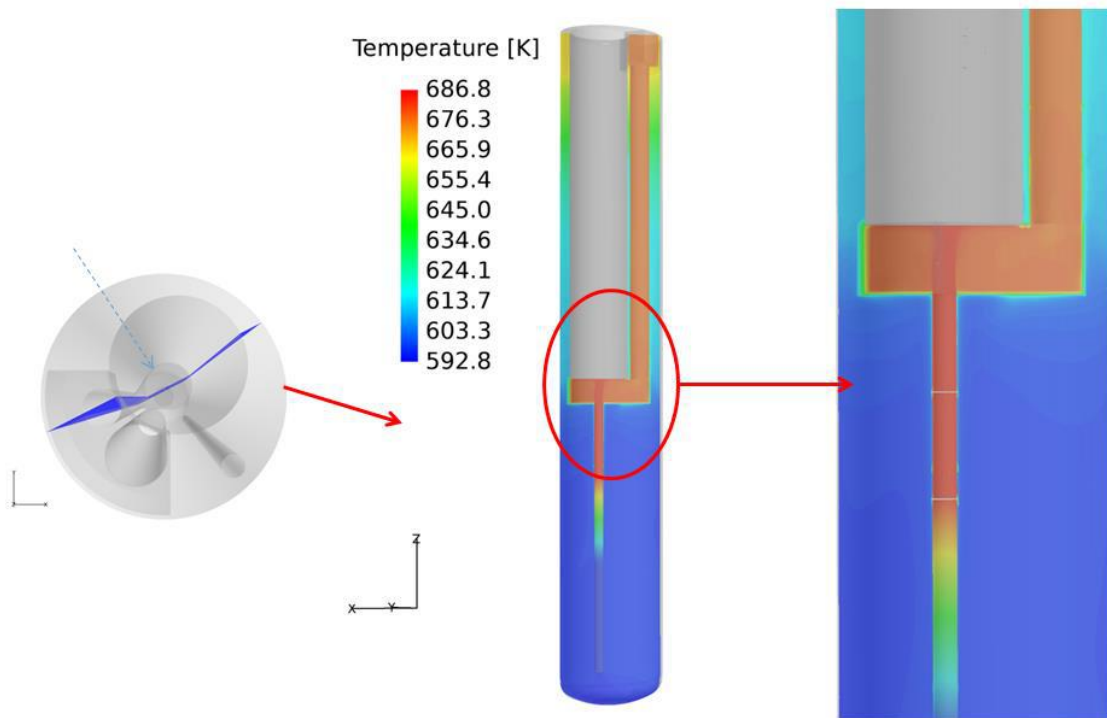



Figure 298: Temperature profile on a vertical plane through the centres of the FPS and Riser (middle), along with a zoom around the Fitting Volume (right).

 DIVISIONE INGEGNERIA SPERIMENTALE	<u>Title</u> D3.2: CIRCE experiments: pre-test, data-set and analysis	<u>Distribution</u> PUBLIC	<u>Emission</u> 09/08/2017	<u>Pag.</u> 196 di 234
		<u>Ref.</u> CI-T-R-292	Rev. 0	

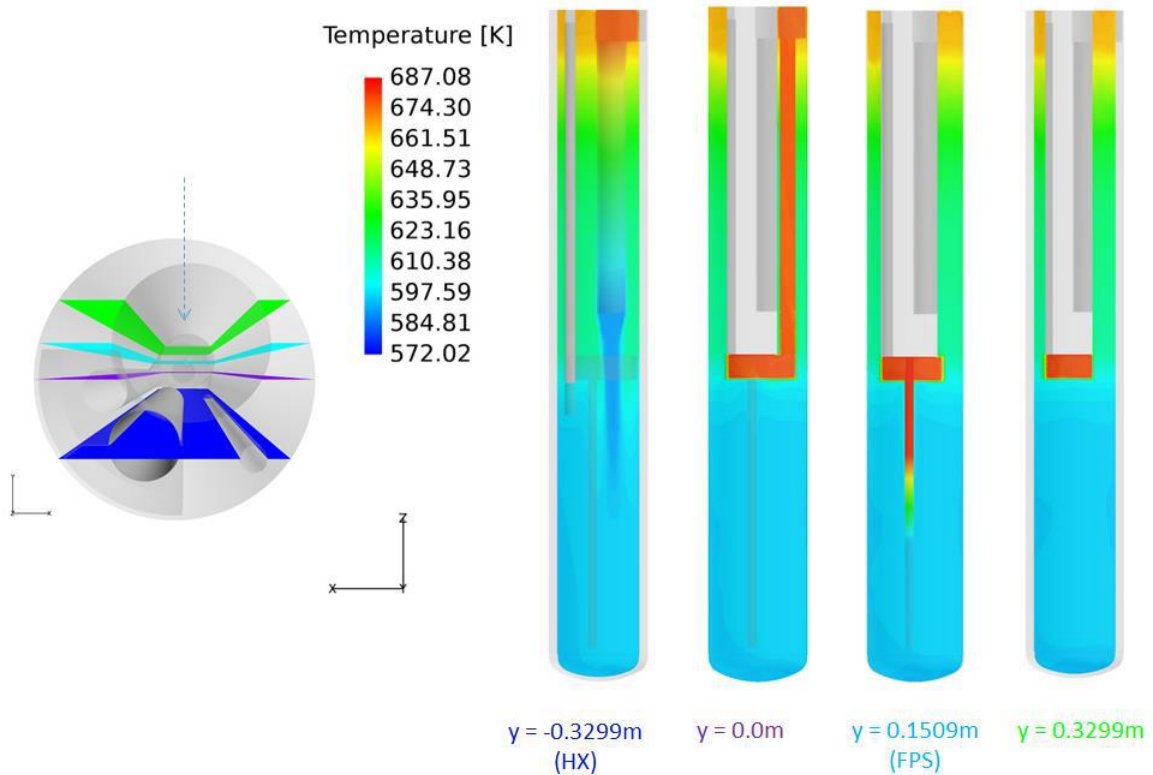


Figure 299: Vertical temperature profiles at, from left to right, $y = -0.1509\text{m}$ (Heat Exchanger), $y = 0.0\text{m}$ (centre Vessel), $y = 0.1509\text{m}$ (FPS) and $y = 0.3299\text{m}$.

5.3.3 Transient simulation

As mentioned in §5.3.1, after approximately 10hrs of operating at 800kW, the FPS is switched to decay heat mode, with a power input of ~30kW. The flow is no longer driven by the argon, resulting in a transition from forced convection to natural convection. Furthermore, the decay heat is removed by the DHR, as the HX is no longer operational as well. Figure 300 shows the power added to the system by the FPS on the left and the heat removed by the DHR on the right as function of time. As can be seen, the FPS delivers about 30kW in the decay heat mode, while the thermal power removed by the DHR initially is about 30kW when the transient sets in. It then drops rapidly to about 18.5kw, with a slow decrease over about 6 hours to a value of 16.5kw, at which point it drops again rapidly to its final value of ~8kW, before the experiment comes to an end.

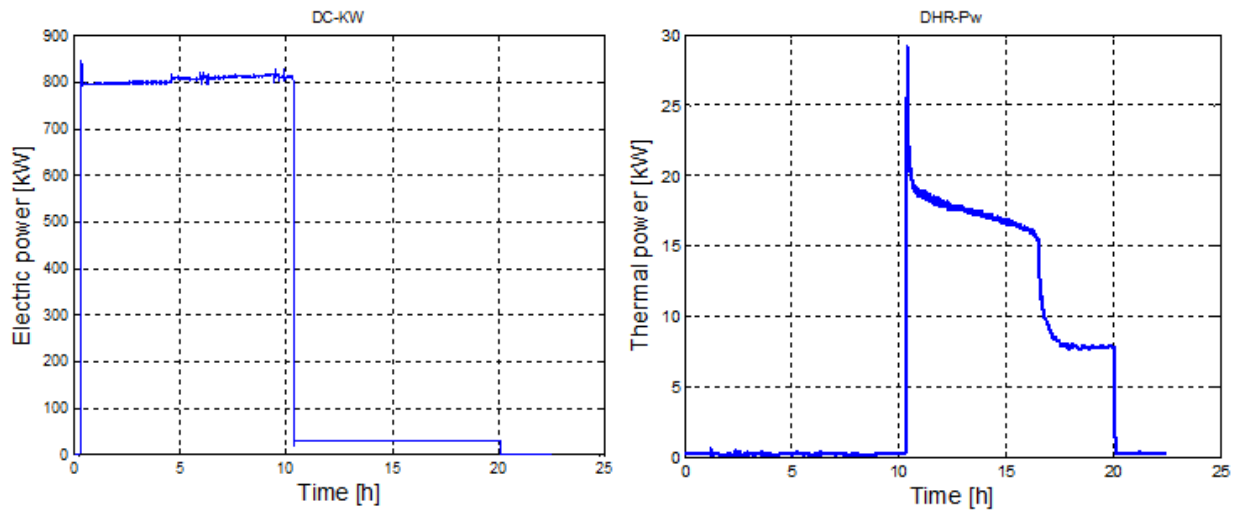



Figure 300: FPS input power and DHR heat removed as function of time for the experiment.

To model the transition from forced to natural convection, the simulation is divided into three parts. The first 10.35hrs represent the steady-state, forced convection, flow. It starts from when the simulation has reached a steady-state, so it does **not** represent or include the spin up from rest to the steady-state condition. After 10.35hrs, the simulation switches to transient 1 conditions: a volumetric heat source of 30kW in the FPS and a volumetric heat sink of 17.5kW in the DHR. The riser and heat exchanger are turned off. This transient 1 part runs for 6.15hrs, from $t = 10.35\text{hrs}$ to $t = 16.5\text{hrs}$, at which time the thermal heat removed by the DHR is reduced to 8.0kW. This represents transient 2. The power input remains unaltered during this transition. An overview of the three parts is given in Table 14.

Table 14: Simulation set-up of the steady-state and transient parts

Event	Time
Full power: 800kW	0h-10.35h \approx 37.300sec
Transient 1: FPS = 30kW, DHR = 17.5kW	10.35h – 16,5h = 59.400s
Transient 2: FPS = 30kW, DHR = 8.0kW	16,5h – 20h = 72.000s

 DIVISIONE INGEGNERIA SPERIMENTALE	<u>Title</u> D3.2: CIRCE experiments: pre-test, data-set and analysis	<u>Distribution</u> PUBLIC	<u>Emission</u> 09/08/2017	<u>Pag.</u> 198 di 234
		<u>Ref.</u> CI-T-R-292	Rev. 0	

Mass flow rate through inner loop. experiment vs. simulation

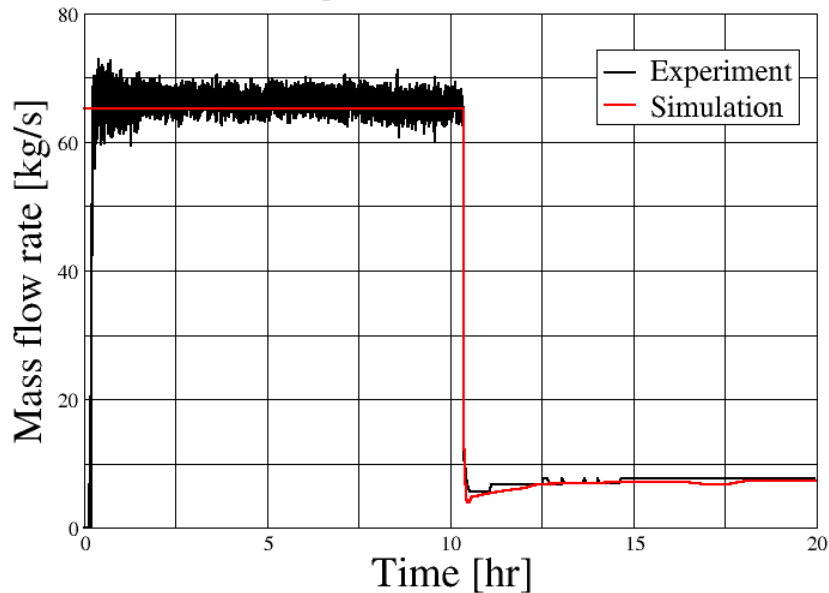



Figure 301: Mass flow rate through the inner loop as function of time.

A comparison between the LBE mass flow rates in the inner loop for the experiment and numerical simulation is depicted in Figure 301. There is quite a good agreement between the two contours, especially considering that, during the transient part, the LBE circulates through natural convection, i.e., it is no longer an input but a result of the simulation. In the simulation, a small decrease in mass flow rate is found during the transition from transient 1 to transient 2 (at $t \sim 16.5$ hrs), while in the experiment the mass flow rate remains unaltered. Looking at the stepwise increases in mass flow rate of the experiment, it is very plausible the flow meter wasn't able to pick up in this small change in mass flow rate. Overall, the simulation resolves quite well the pattern of the mass flow rate found in the experiment, with a strong initial decrease when the forcing is turned off, followed by a slow, small increase to a steady value of about 7.8kg/s.

Figure 302 shows the inlet and outlet temperatures of the FPS for both the experiment and the numerical simulation. The initial flat temperatures found in the CFD analyses (from $t = 10$ hrs to $t = 10.35$ hrs), are due to the fact that, as mentioned before, the simulation doesn't include the start up from rest but has constant conditions throughout the steady-state part. The temperature evolution during the PLOH+LOF accident scenario is quite different between the experiment and simulation. For the outlet temperature of the FPS, a strong initial drop is found in both cases that agrees quite well quantitatively, followed by a slight increase. However, the increase is much larger in the simulation than in the experiment. Furthermore, the temperature in the simulation keeps decreasing steadily, while during the experiment it seems to have reached a steady value after about 16 hours. A similar tendency is seen for the inlet temperature of the FPS. An explanation for this difference could be the assumption of a constant volumetric heat sink used for the DHR, as such a model removes a constant amount of heat during the simulation. Perhaps a heat sink model as used for the heat exchanger, see §5.1.4.2., might improve the numerical predictions.

 DIVISIONE INGEGNERIA SPERIMENTALE	<u>Title</u> D3.2: CIRCE experiments: pre-test, data-set and analysis	<u>Distribution</u> PUBLIC	<u>Emission</u> 09/08/2017	<u>Pag.</u> 199 di 234
		<u>Ref.</u> CI-T-R-292	Rev. 0	

The change in time of the inlet and outlet temperatures of the heat exchanger during the experiment and simulation is shown in Figure 303. They seem to agree reasonably for the initial two-to-three hours of the transient; the inlet temperature in both cases shows an initial strong drop followed by a slower decrease, while the outlet temperature initially increases and subsequently decreases. Though just as what was observed for the FPS temperatures, they keep decreasing in the simulation while a levelling off is seen in the experiment.

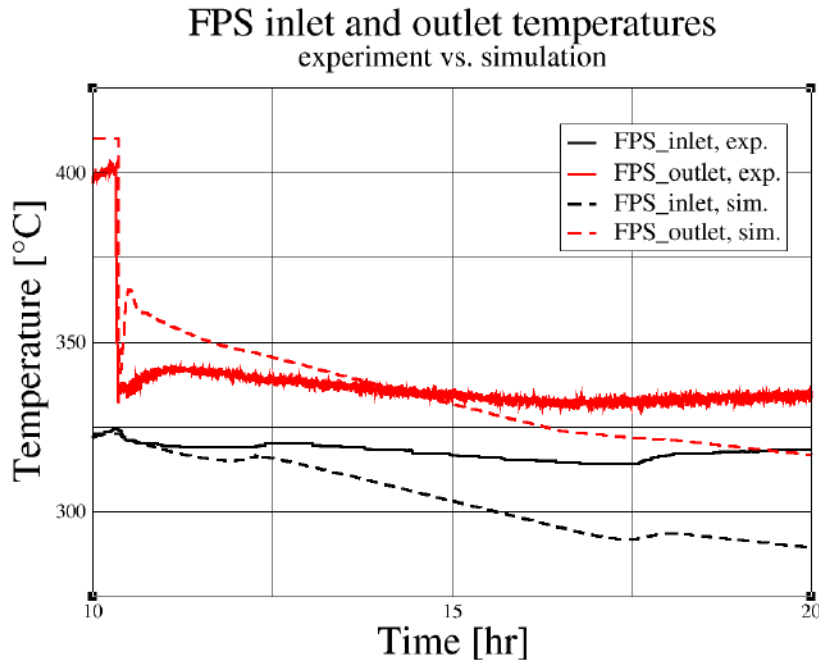



Figure 302: Comparison between inlet and outlet temperatures of the FPS between the experiment and simulation.

Finally, a comparison of the stratification in the main pool between the experiment and numerical findings is presented in Figure 304. The best agreement between the two profiles is found after 12 hours, where the temperatures in the top part of the main vessel are off by only a few degrees, while those in the bottom match nearly perfectly. Only in the very bottom part there is a difference. Furthermore, the location of the temperature drop is predicted correctly. However, as time increases, the differences between the experiment and simulation become more pronounced. The location of the temperature drop is still correct, but the temperature differences become larger. Furthermore, in the experiment the stratification becomes less pronounced, while the same isn't found in the CFD analyses. Also the temperature in the bottom of the main pool increases in the experiment during the second half of the accident scenario, while in the simulation it keeps decreasing. More investigation is needed to understand the cause(s) of these discrepancies.

 DIVISIONE INGEGNERIA SPERIMENTALE	<u>Title</u> D3.2: CIRCE experiments: pre-test, data-set and analysis	<u>Distribution</u> PUBLIC	<u>Emission</u> 09/08/2017	<u>Pag.</u> 200 di 234
		<u>Ref.</u> CI-T-R-292	Rev. 0	

HX inlet and outlet temperatures experiment vs. simulation

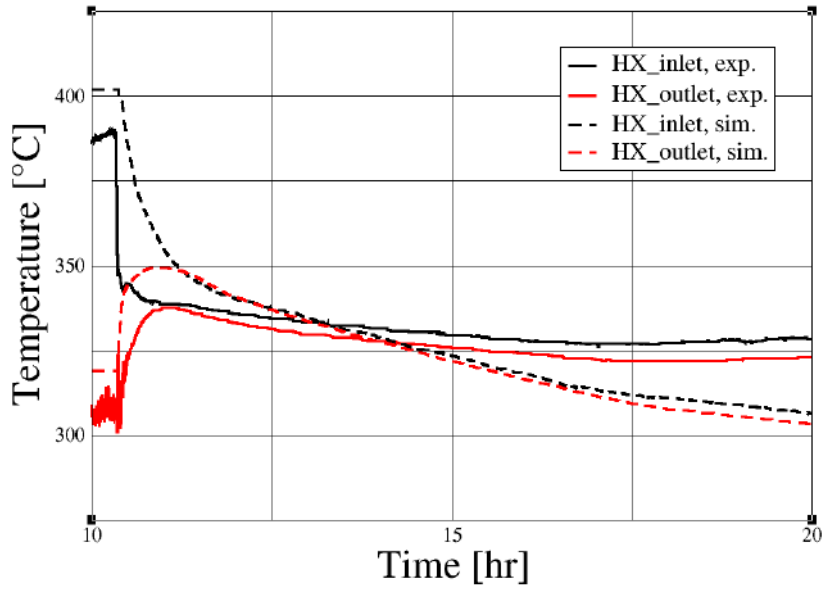


Figure 303: Comparison between inlet and outlet temperatures of the HX between the experiment and simulation.

Main pool stratification. experiment vs. simulation

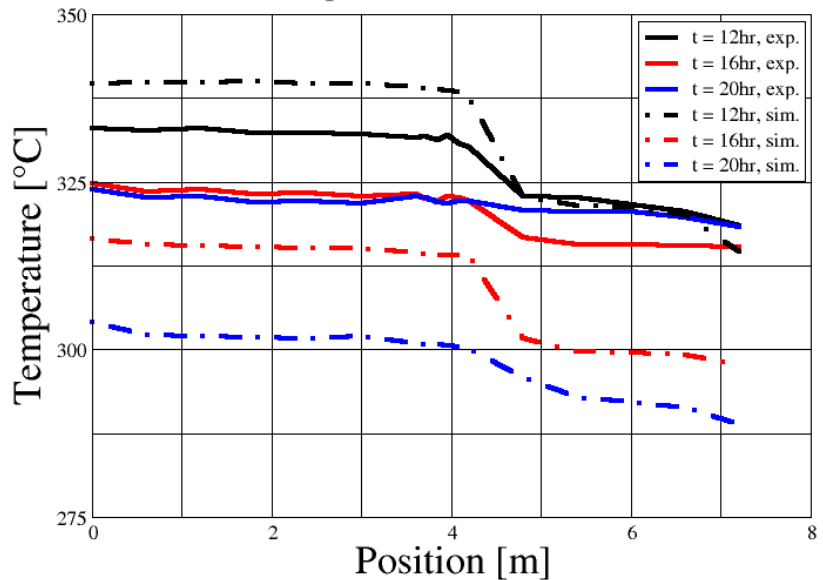



Figure 304: Comparison between the experiment and simulation of the stratification inside the main pool at three different times.

 DIVISIONE INGEGNERIA SPERIMENTALE	<u>Title</u> D3.2: CIRCE experiments: pre-test, data-set and analysis	<u>Distribution</u> PUBLIC	<u>Emission</u> 09/08/2017	<u>Pag.</u> 201 di 234
		<u>Ref.</u> CI-T-R-292	Rev. 0	

6 CONCLUSIONS AND REMARKS

The Horizon 2020 project for Thermal hydraulics Simulations and Experiments for the Safety Assessment of MEtal cooled reactors (SESAME [1]), was intended to support the development of European liquid metal-cooled fast reactors. In this frame, experiments and numerical simulations were performed to provide system designers with more information and data to enhance the safety standards and culture of these type of reactors. In particular, within Work Package 3 (WP3) of the SESAME project, four experiments were performed by ENEA Brasimone R.C. in a heavy liquid metal large pool experimental configuration (CIRCE) in order to investigate thermal hydraulics phenomena occurring during an accidental scenario considered relevant for the safety of the reactor itself (PLOHS+LOF).

Moreover, CFD simulations of the performed experiments were performed at CRS4 and NRG research center.


The first part of the document reports results of a series of four experimental tests simulating the total loss of the secondary circuit and the coolant pump trip (simulated stopping the gas enhanced circulation, with the exception of Test 4) with the consequent simulation of the reactor scram (reduction of the electric power supplied to the fuel pin simulator) and activation of DHR system to remove the decay heat power (~5% of the nominal value). Tests differ for the applied boundary conditions such as the electrical power supplied to the FPS, the duration of the test, the power removed by the HX etc., while test 4 also differs for the forced circulation maintained after the simulation of the accidental transient.

Concerning the thermal stratification inside the pool at the full power steady state, the experiment evidences the same general behaviour independently from the external conditions, characterized by the presence of a thermal gradient of about 40°C in the first 3.5 m starting from the free level (up to the outlet section of the HX). Then between the outlet sections of the HX and the DHR the slope of the vertical temperature profile increases, with a temperature drop of about 15-20 °C in less than 1 m. Moreover, the thermal stratification in the pool is purely vertical with negligible temperature variation on the horizontal planes. After transition to natural circulation, the vertical temperature profile changes. Concerning Test 1 and 2, in the upper and lower part of the vessel LBE temperature is uniform with a layer separating the two zones and where the thermal gradient concentrates. That area, after the transition from forced to natural circulation moved downwards below the DHR outlet section and the thermal gradient reduces to about 10°C. At the end of Test 1, the thermal stratification in the pool disappear. The occurrence of this phenomenon coincide with the inversion of the temperature between the inlet and outlet section observed in the DHR system probably caused by the oxide deposition in the DHR with the channel plug. Test 3 and 4 are affected by the blockage of the DHR by the oxide for the whole duration of the transient under low power condition. The cause of this had been confirmed by a visual inspection only after the extraction of the CIRCE-ICE test section.

The low power run is influenced by the DHR issue and shows a uniform temperature inside the whole pool and a reduced heat power removed by the DHR system.

The second part of the document reports the CFD analysis reproducing the experimental tests performed at CRS4 and NRG.

In particular, at CRS4, a series of numerical models of the CIRCE experimental facility were developed adopting the STAR CCM+ CFD commercial code. Attempts to model the gas driven pumping system first with an Eulerian two-phase flow and then with Lagrangian particles have shown to be either impossible in the first case or possible in the second case but

 DIVISIONE INGEGNERIA SPERIMENTALE	<u>Title</u> D3.2: CIRCE experiments: pre-test, data-set and analysis	<u>Distribution</u> PUBLIC	<u>Emission</u> 09/08/2017	<u>Pag.</u> 202 di 234
		<u>Ref.</u> CI-T-R-292	Rev. 0	

at an additional computer cost and with no additional effective modelling improvement. The numerical model is currently based on the VoF setup. After careful analysis, this setup does not look to need be maintained and alternative solutions, based of geometrically separated LBE and cover gas are to be investigated.

The pre-test simulation has highlighted the importance of the conjugate heat transfer to interpret the temperature patterns. A heat loss of almost 100 kW is seen across the Conveyor walls towards the plenum. This is about 15% of the Pin Simulator heat source and cannot be neglected.

It has not been possible to reproduce satisfactorily the experimental steady-state of reference. However, from the discrepancy between the experimental and numerical measurements, two main strong hypothesis could have been formulated:


1. About 50 kW is released in the pin bundle in the section above the active part and below the Dead Body.
2. There is a bypass between the flow separator internal and external, be it from splashing above the lateral wall caused by the highly agitated rising bubbly flow or from a leaking connexion between the Riser and the Flow Separator.

If one or both of these hypothesis result to be true, it will be a good demonstration that experimental campaigns and CFD simulation are complementary and can profit each other. The experiments were supposed to give unquestionable inputs for the CFD modelling. This is not necessarily a true assertion as the simulation can also hints on some defect or hidden feature of the experiment.


Neither CFD nor experimental results should blindly be taken as granted. Careful examination of otherwise unexplained discrepancies can help discover some flaw in one or the other investigation tool. However, when both results are in good agreement, we gain a higher level of confidence on them and a higher level of understanding provided by the more extensive access to physical data with the CFD tool.

Concerning the simulations performed at NRG, the CFD Ansys FLUENT was adopted. The developed CFD model contains various simplifications compared to the actual test facility. Geometry-wise, it only extends up to the cover gas, i.e., it's a single-phase model. Also, the electrical pins inside the Fuel Pin Simulator and the bayonet tubes inside the heat exchanger have been discarded. Instead, their influence on the flow has been taken into account by defining them as porous medium zones. Simple, constant, Volumetric Momentum and Heat Sources are used, respectively, for the FPS and the flow forcing. A more comprehensive heat sink model is used for the heat exchanger, to have more control over (potential) temperature fluctuations inside the model. Finally, since almost all interior and exterior walls are modelled as zero-thickness walls, Shell Conduction is used to allow for conjugate heat transfer from the inner loop to the main pool and from the main pool to the environment. Including VHT is crucial for getting proper 3D thermal effects inside the main pool.

Results for the steady-state and transient case of test 1 of the aforementioned work package were compared with experimental results. The steady-state conditions of this test represents a forced convection flow with a heat input of 800kW and an LBE mass flow rate of ~65 kg/s. The main heat exchanger removes about 750kW, while the remaining part is lost through conjugate heat transfer. After about 10hrs it goes into a PLOH+LOF accident scenario, with the power input being reduced to 30kW, the “pump” and primary heat exchanger switched off and the DHR system turned on.

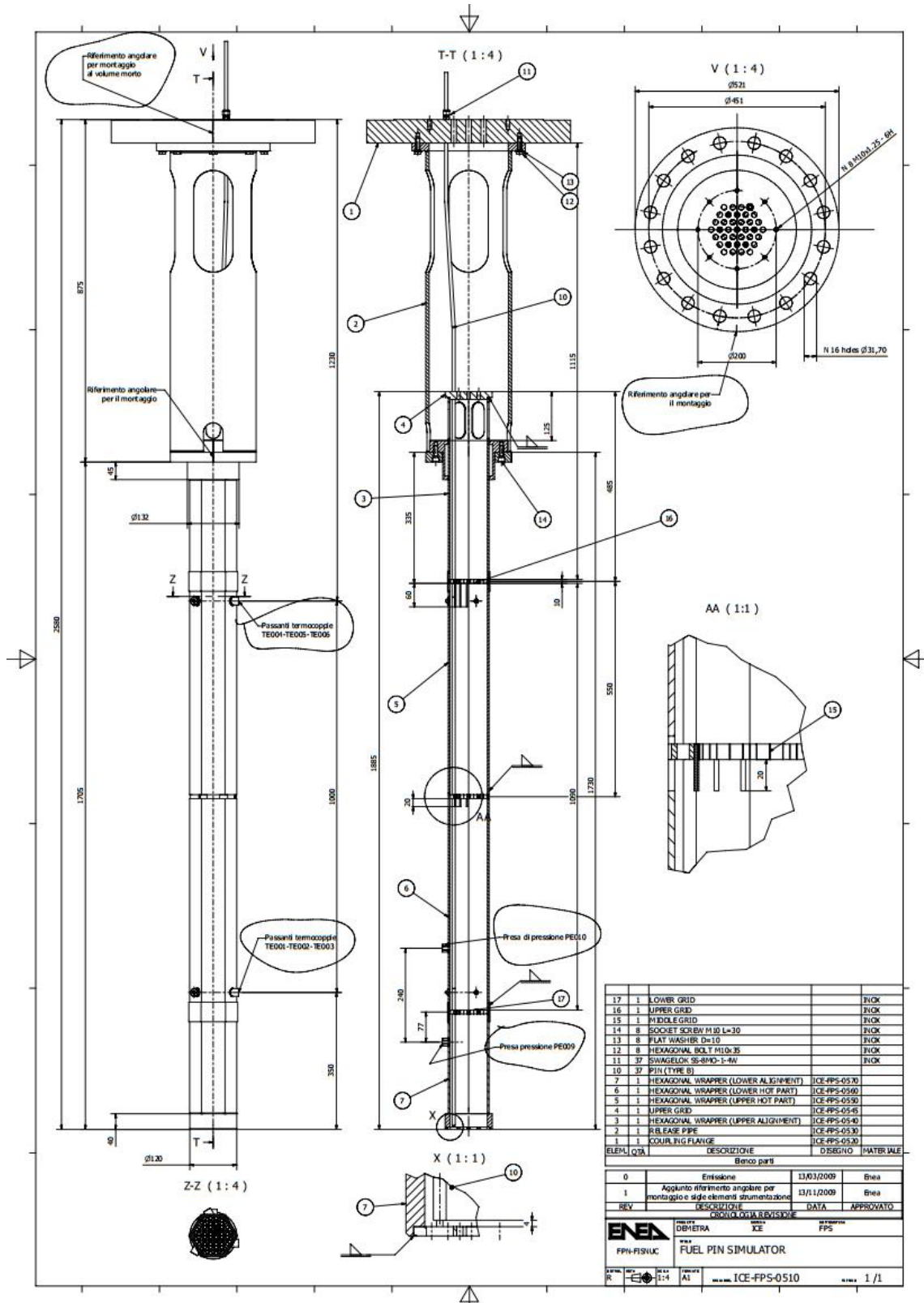
 DIVISIONE INGEGNERIA SPERIMENTALE	<u>Title</u> D3.2: CIRCE experiments: pre-test, data-set and analysis	<u>Distribution</u> PUBLIC	<u>Emission</u> 09/08/2017	<u>Pag.</u> 203 di 234
		<u>Ref.</u> CI-T-R-292	Rev. 0	

Very good agreement between the numerical and experimental results of the main pool stratification is found for the steady-state flow, especially in the middle and bottom sections of the pool. Some discrepancies exist in the top, possibly due to an incorrect representation of the conjugate heat transfer in that part. For the transient part, the numerical results agree qualitatively with the experimental ones, especially for the first two to three hours. However, temperature differences of 10-20K are observed for later times, with the differences increasing with time. Most noticeably, while the temperatures in the experiment level off in the second half of the transient flow, those in the numerical simulation keep increasing. This is possibly caused by the simple heat sink model used for the DHR. Further investigation is needed though.

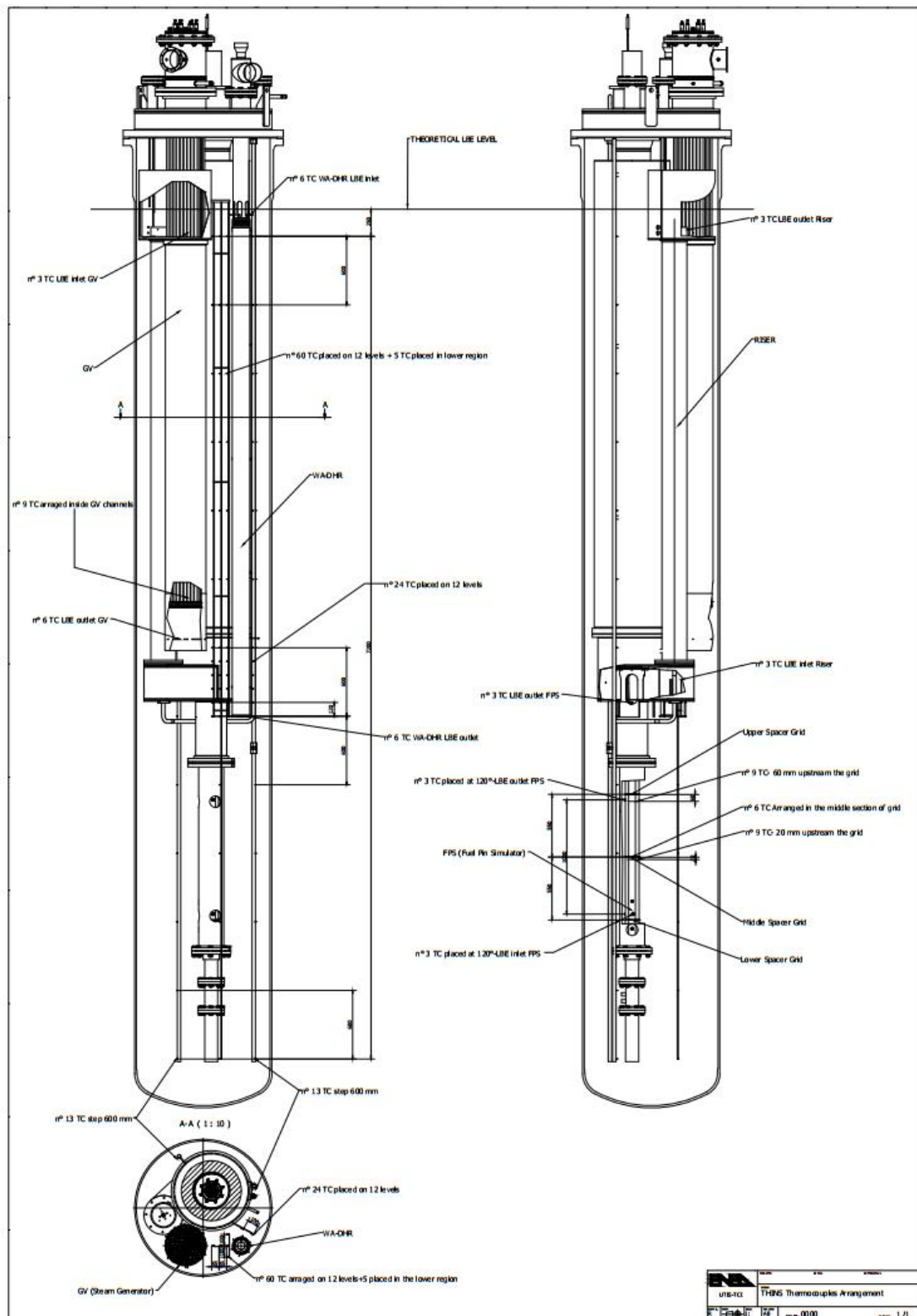
 DIVISIONE INGEGNERIA SPERIMENTALE	<u>Title</u> D3.2: CIRCE experiments: pre-test, data-set and analysis	<u>Distribution</u> PUBLIC	<u>Emission</u> 09/08/2017	<u>Pag.</u> 204 di 234
		<u>Ref.</u> CI-T-R-292	Rev. 0	

REFERENCE:

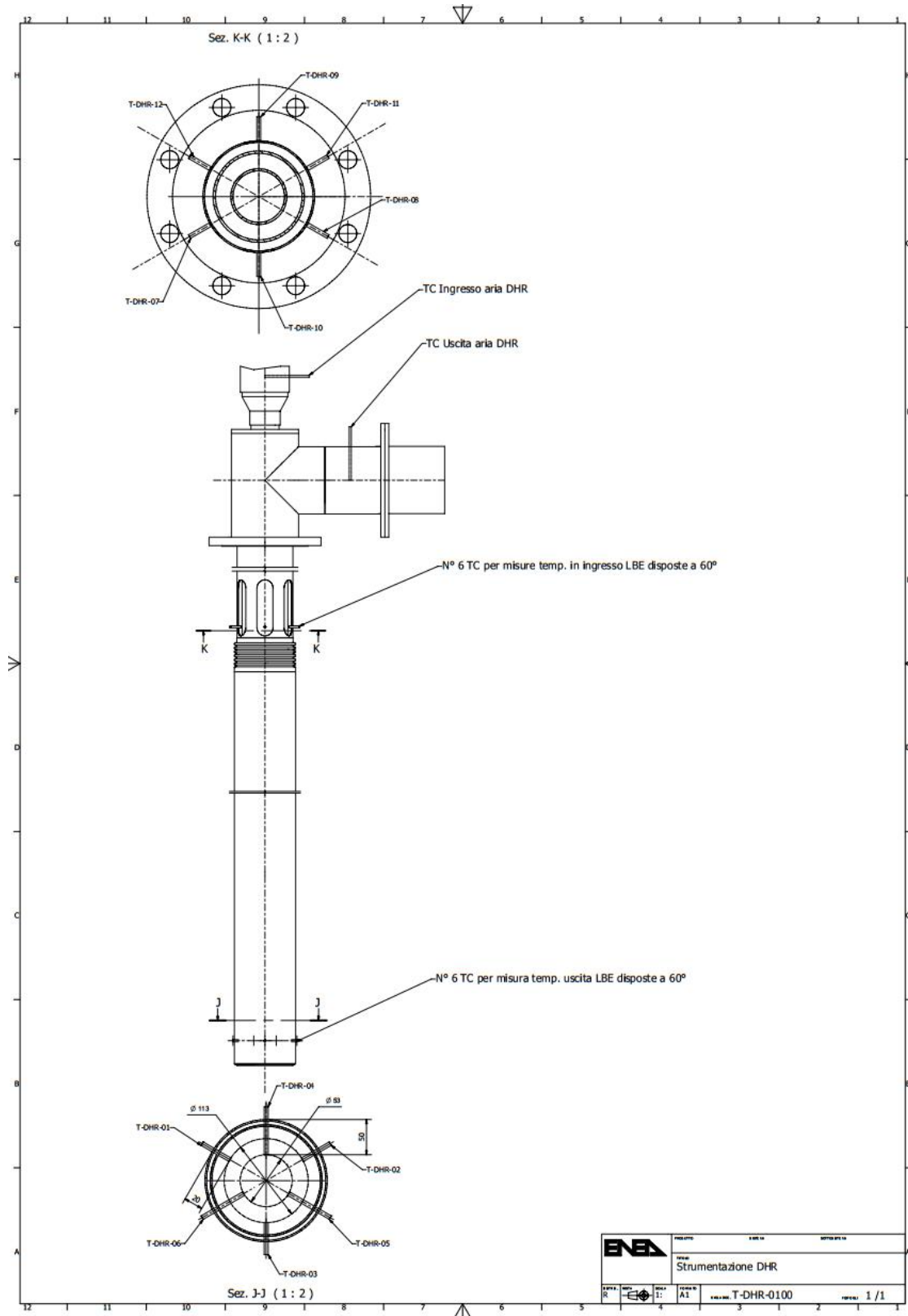
- [1] <http://sesame-h2020.eu/>
- [2] Bandini, G., Di Piazza, I., Gaggini, P., Del Nevo., A., and Tarantino, M. CIRCE experimental set-up design and test matrix definition. ENEA UTIS-TIC Technical Report, IT-F-S-001. February 2011.
- [3] D. Martelli “*CIRCE Experimental facility*” CI-R-162 ENEA Internal Report, 2015.
- [4] Tarantino, M., Scaddozzo, G. Test specifications of the Integral Circulation Experiments. Report ENEA ET-F-S-001, Deliverable D.4.15, DM4 DEMETRA, IP-EUROTRANS, 2006.
- [5] Tarantino, M. CIRCE Experimental Report. THINS deliverable D2.1.06. July 2013.
- [6] <http://www.ansys.com/Products/Fluids/ANSYS-Fluent>
- [7] Todreas, N.E., and Kazimi, M.S., (1993). *Nuclear System I, Thermal Hydraulic Fundamentals*. Taylor & Francis.
- [8] <https://www.sharcnet.ca/Software/Gambit/index.htm>
- [9] Bricteux, L., Duponcheel, M., Winckelmans, G., Tiselj, I., and Bartosiewicz, Y. (2012). Direct and large eddy simulation of turbulent heat transfer at very low Prandtl number: Application to lead-bismuth flows. *Nuclear Engineering and Design*, 246. 91-97.
- [10] Handbook on Lead-bismuth Eutectic Alloy and Lead Properties, Materials Compatibility, Thermal-hydraulics and Technologies, 2015 Edition, NEA.
- [11] Fokkens, J.H., Material Database for HFR Irradiation Experiments. Internal report.
- [12] http://www.engineeringtoolbox.com/air-properties-d_156.html



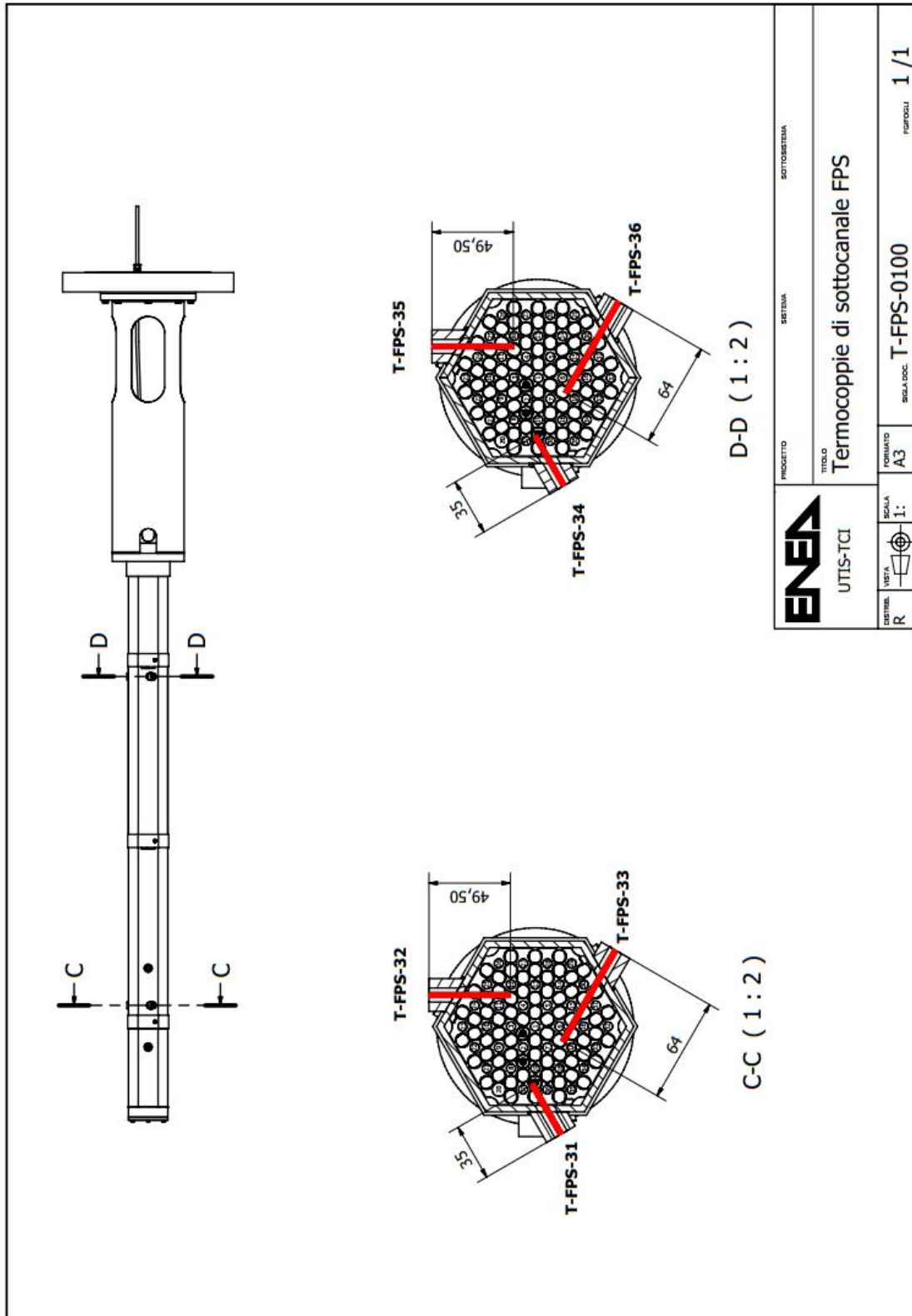
Annex A Fig. 2 0510 Rev 1-Fuel Pin Simulator.pdf



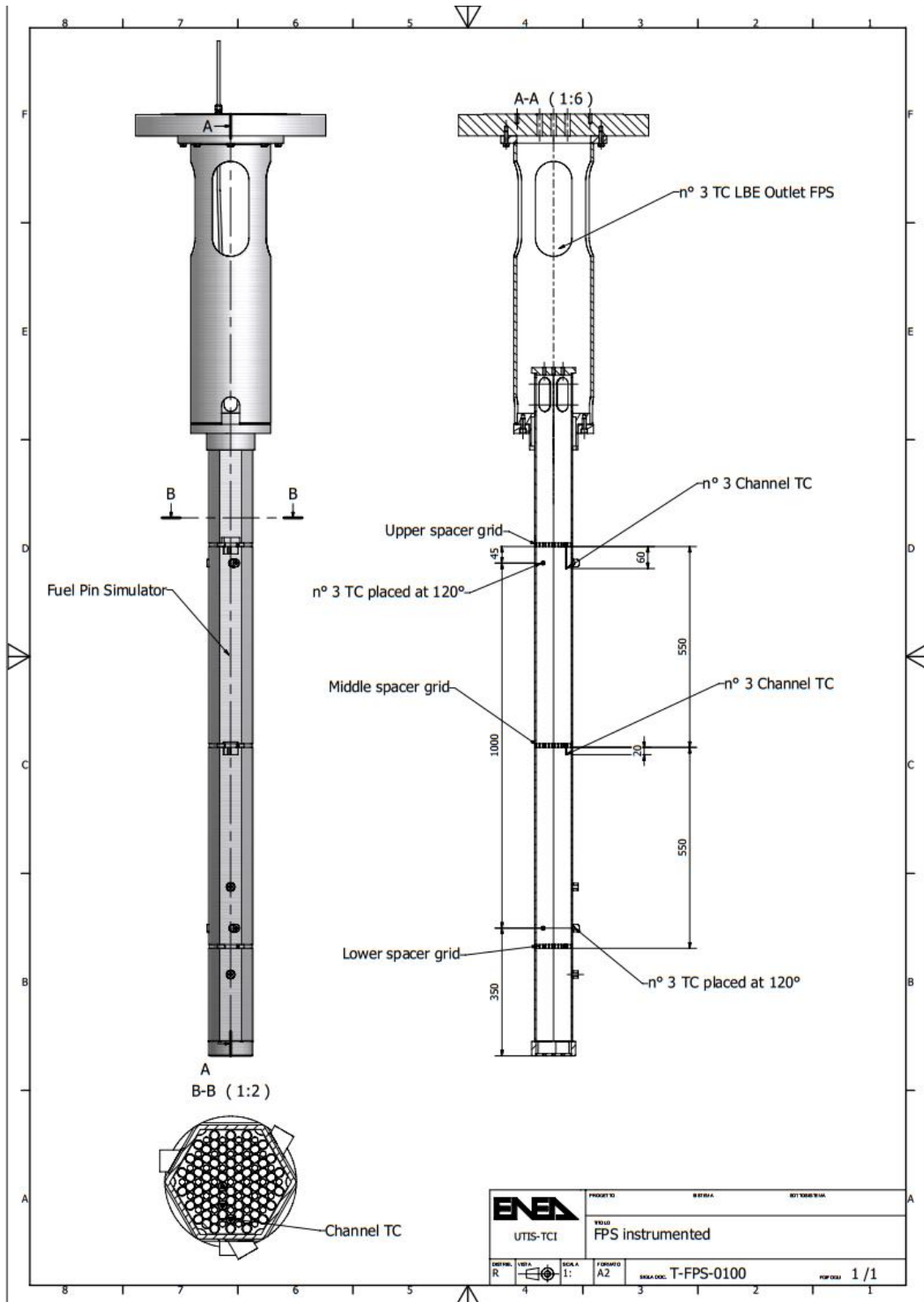
Annex A Fig. 4 THINS thermocouples arrangement.pdf




Annex A Fig. 5 T-DHR-0100-Instrumentation DHR.pdf

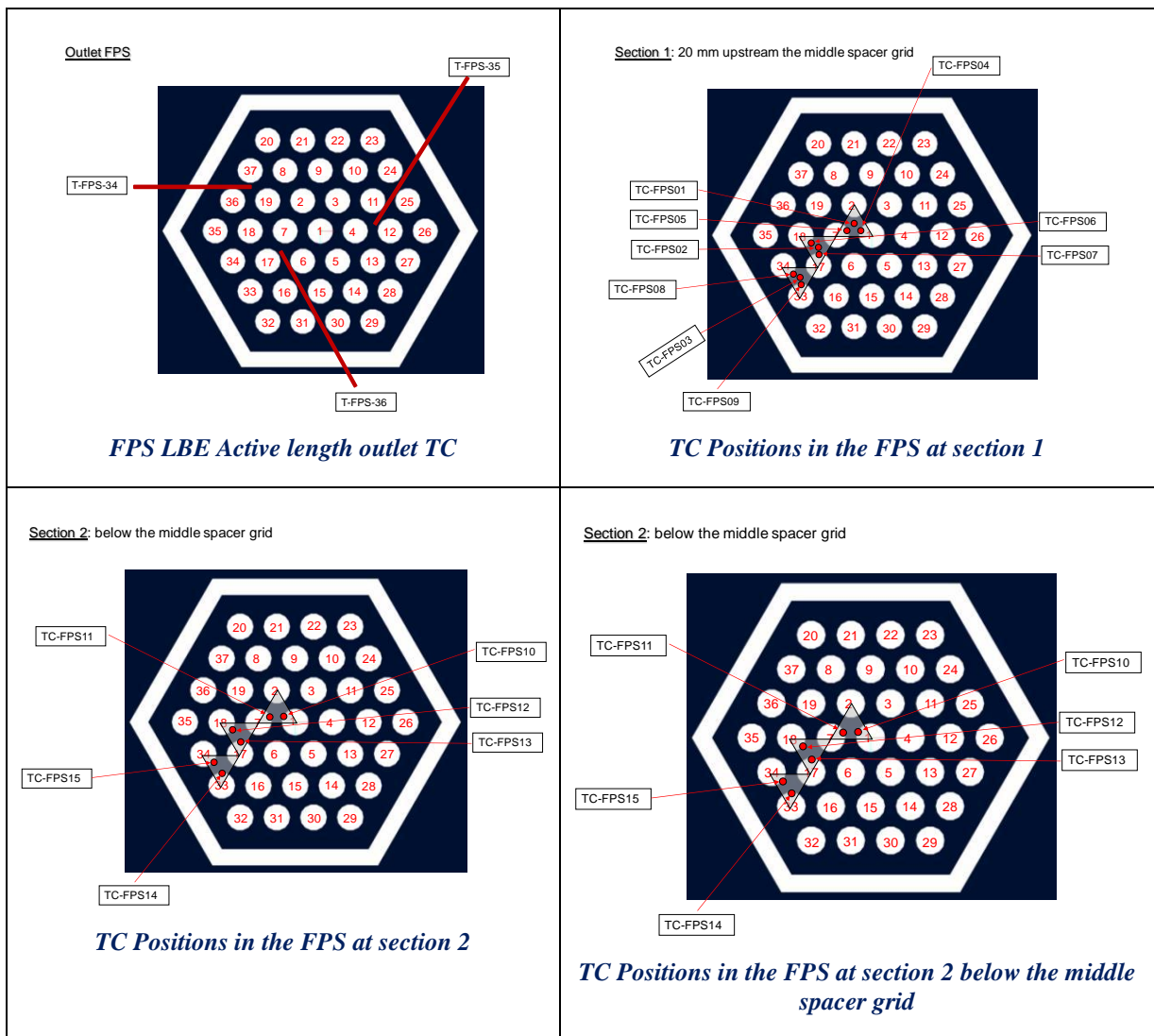


Annex A Fig. 6 T-FPS-0100 foglio2-FPS Instrumented




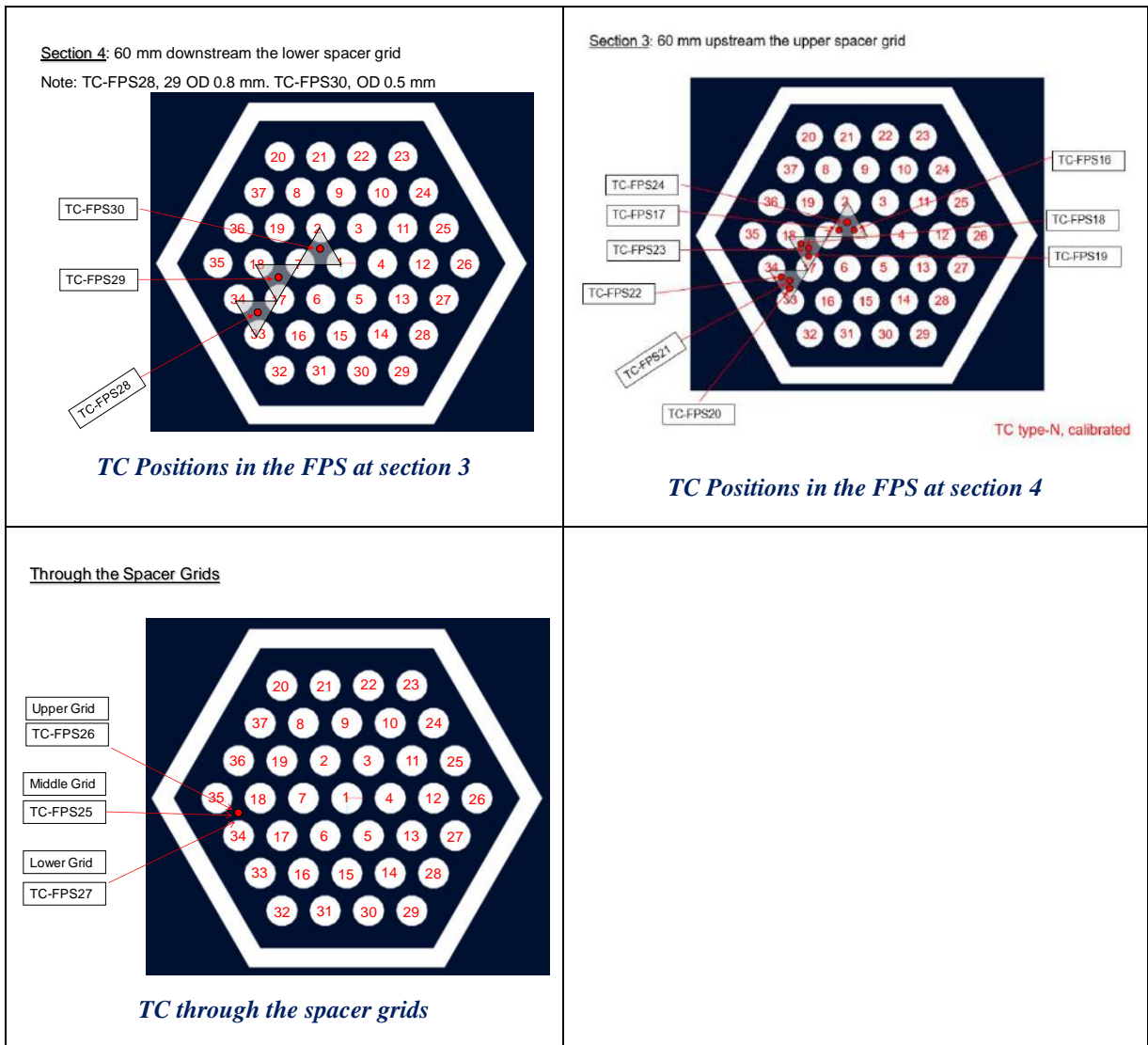
Annex A Fig. 7 T-FPS-0100 fogli1-FPS Instrumented

 DIVISIONE INGEGNERIA SPERIMENTALE	<u>Title</u> D3.2: CIRCE experiments: pre-test, data-set and analysis	<u>Distribution</u> PUBLIC	<u>Emission</u> 09/08/2017	<u>Pag.</u> 212 di 234
		<u>Ref.</u> CI-T-R-292	Rev. 0	

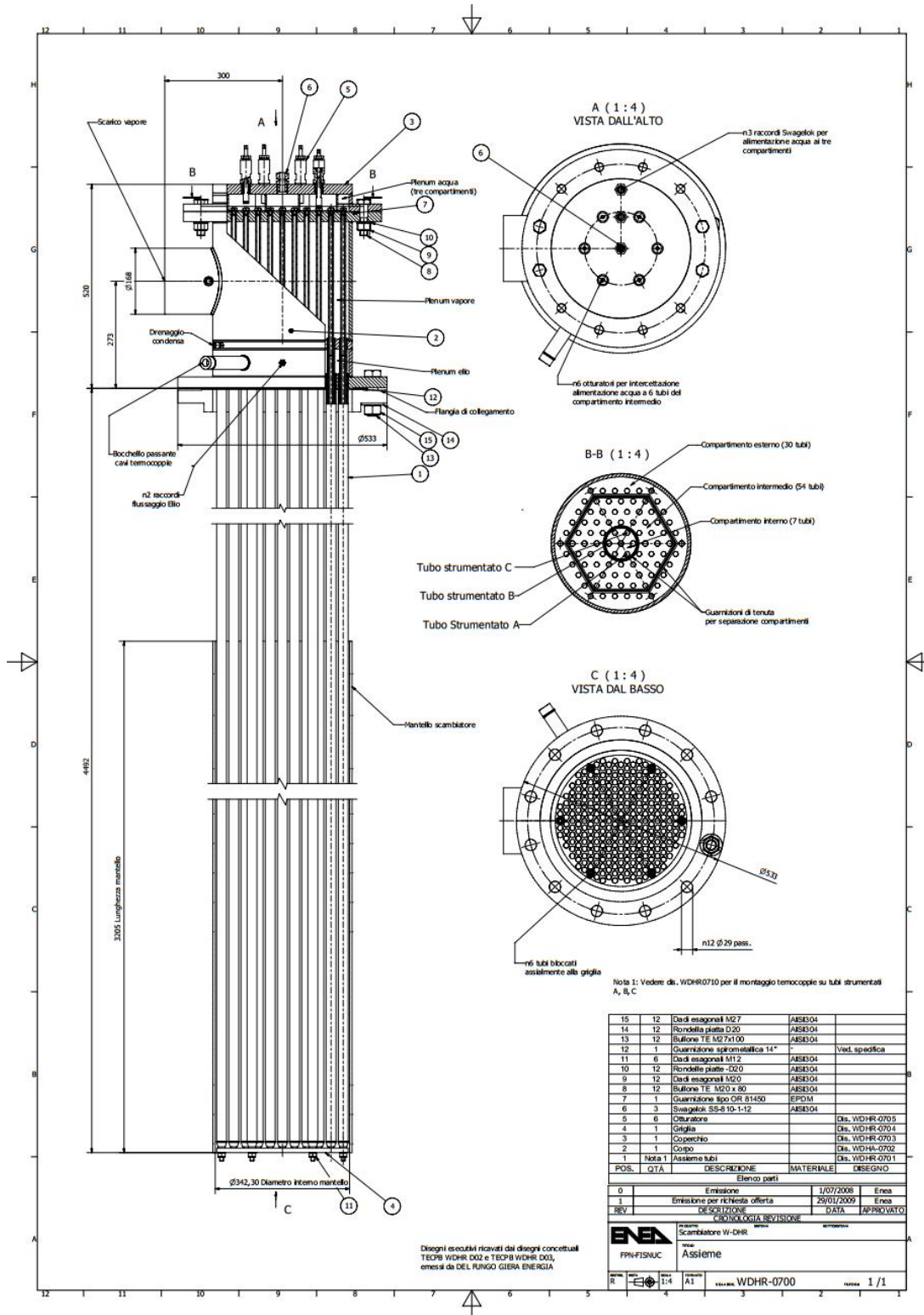


Annex A Fig. 8 T-FPS Instrumentation 1 of 2


 DIVISIONE INGEGNERIA SPERIMENTALE	<u>Title</u> D3.2: CIRCE experiments: pre-test, data-set and analysis	<u>Distribution</u> PUBLIC	<u>Emission</u> 09/08/2017	<u>Pag.</u> 213 di 234
		<u>Ref.</u> CI-T-R-292	Rev. 0	

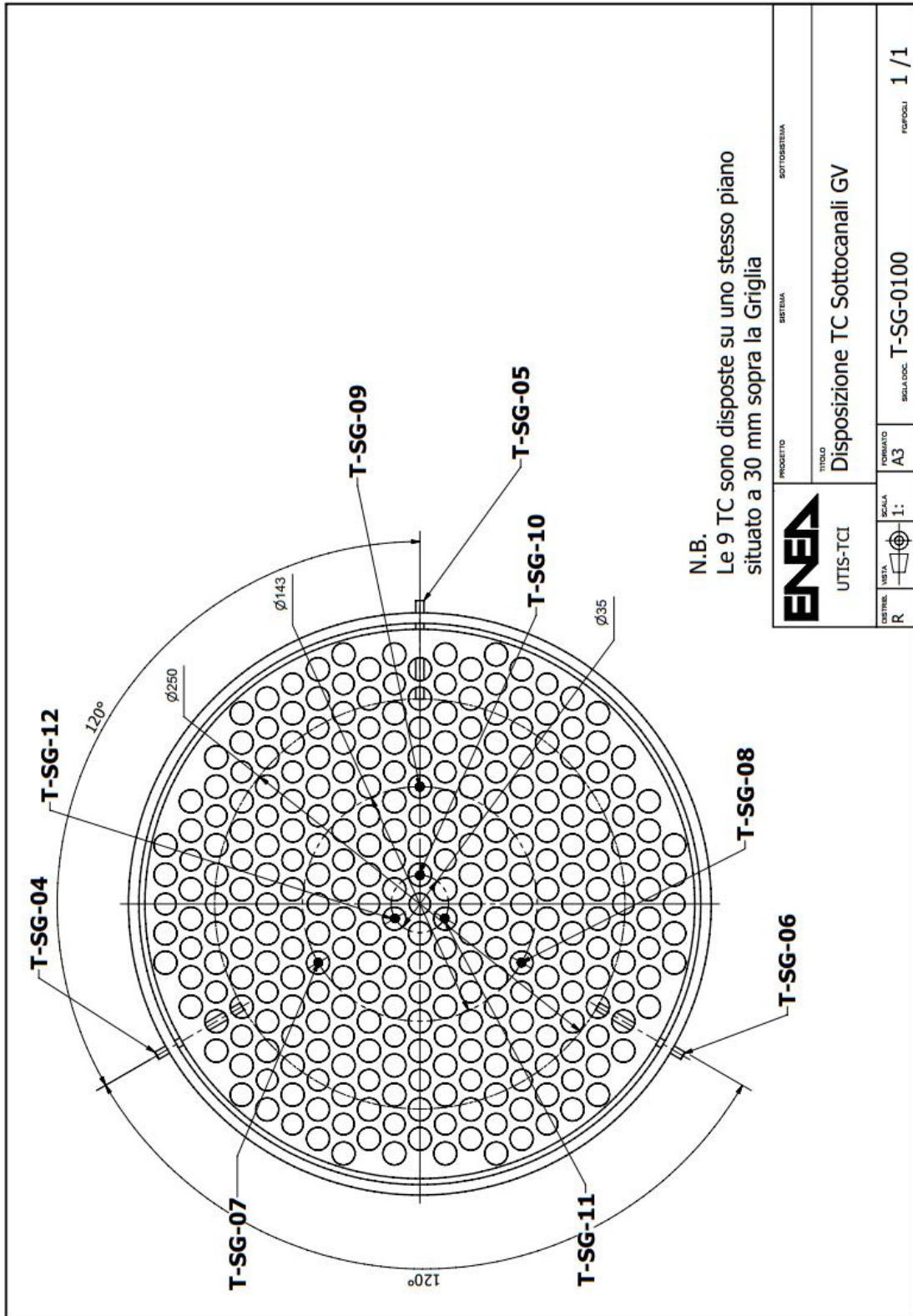


Annex A Fig. 9 T-FPS Instrumentation 2 of 2




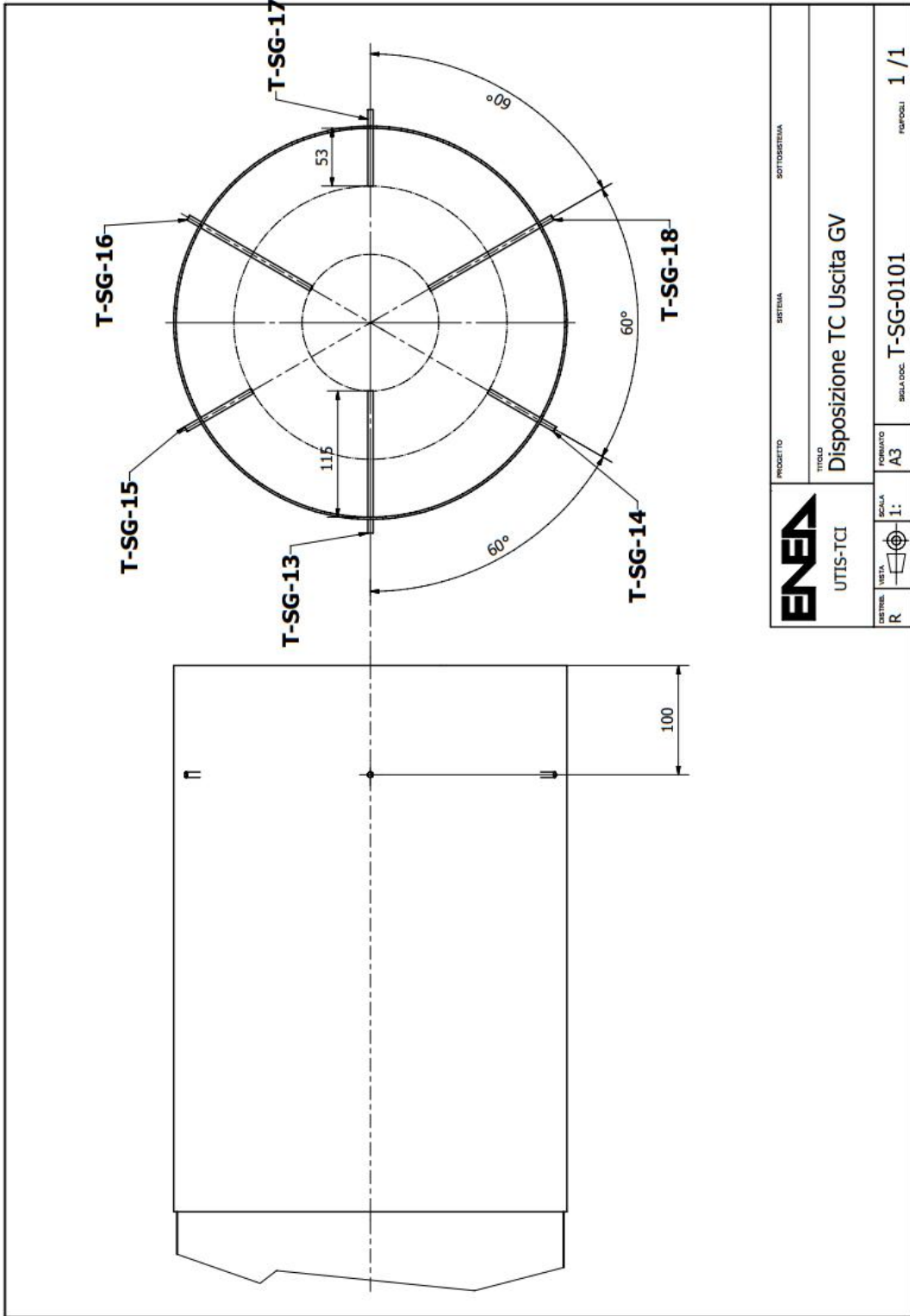
Annex A Fig. 10: 0700-Assieme-HX.pdf

 DIVISIONE INGEGNERIA SPERIMENTALE	<u>Title</u> D3.2: CIRCE experiments: pre-test, data-set and analysis	<u>Distribution</u> PUBLIC	<u>Emission</u> 09/08/2017	<u>Pag.</u> 215 di 234
		<u>Ref.</u> CI-T-R-292	Rev. 0	



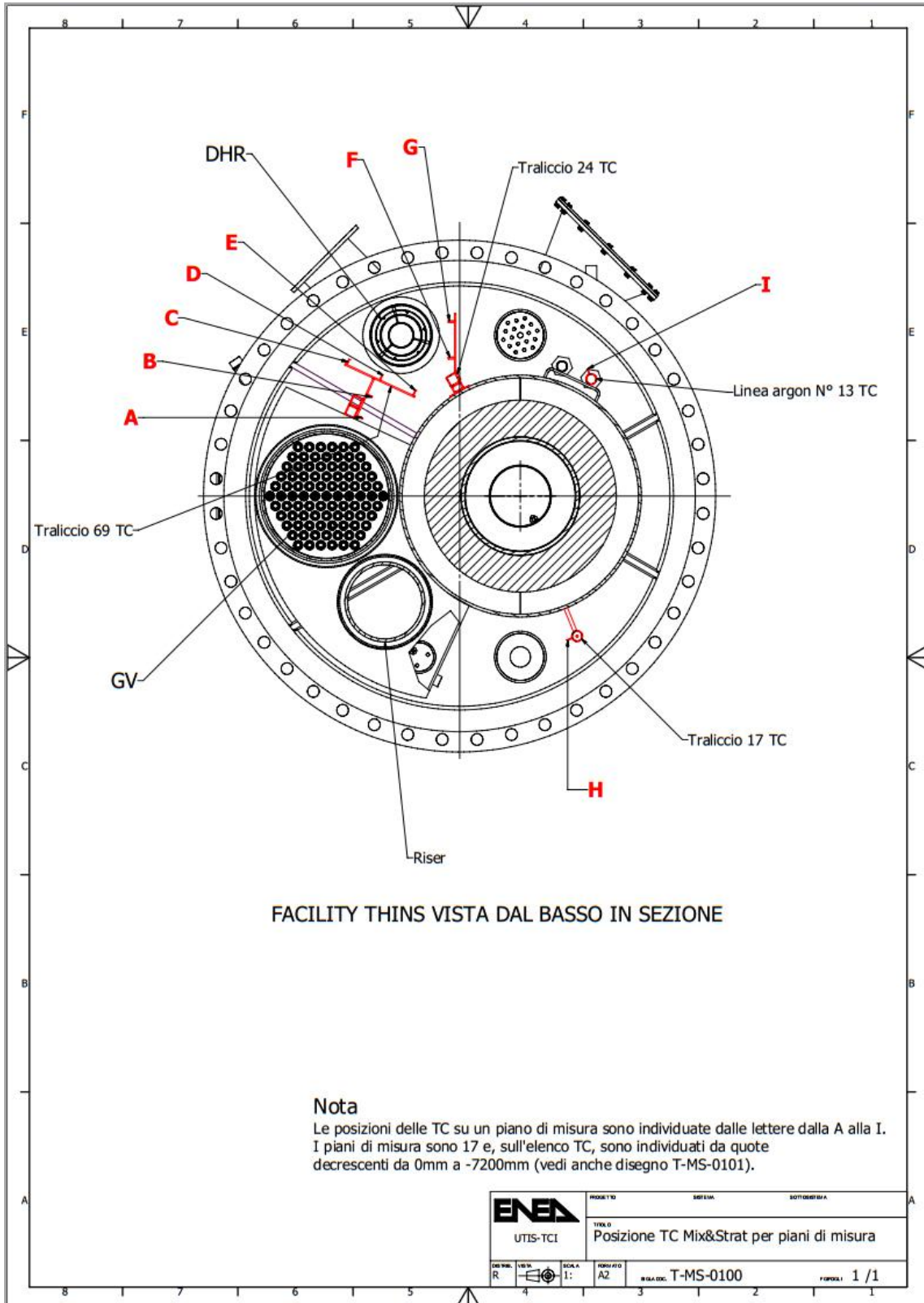
Annex A Fig. 11: T-SG-0100-Disposizione TC Sottocanali GV.pdf

 DIVISIONE INGEGNERIA SPERIMENTALE	<u>Title</u> D3.2: CIRCE experiments: pre-test, data-set and analysis	<u>Distribution</u> PUBLIC	<u>Emission</u> 09/08/2017	<u>Pag.</u> 216 di 234
		<u>Ref.</u> CI-T-R-292	Rev. 0	




		PROGETTO UTIS-TCI	SOTTOSISTEMA SISTEMI	TITOLO Disposizione TC Uscita GV
DISTRIB. R	VISTA 	SCALA 1:1	FORMATO A3	RELAZIONE T-SG-0101
			PAGINAZIONE 1 / 1	

Annex A Fig. 12: T-SG-0101-Disposizione TC Uscita GV.pdf

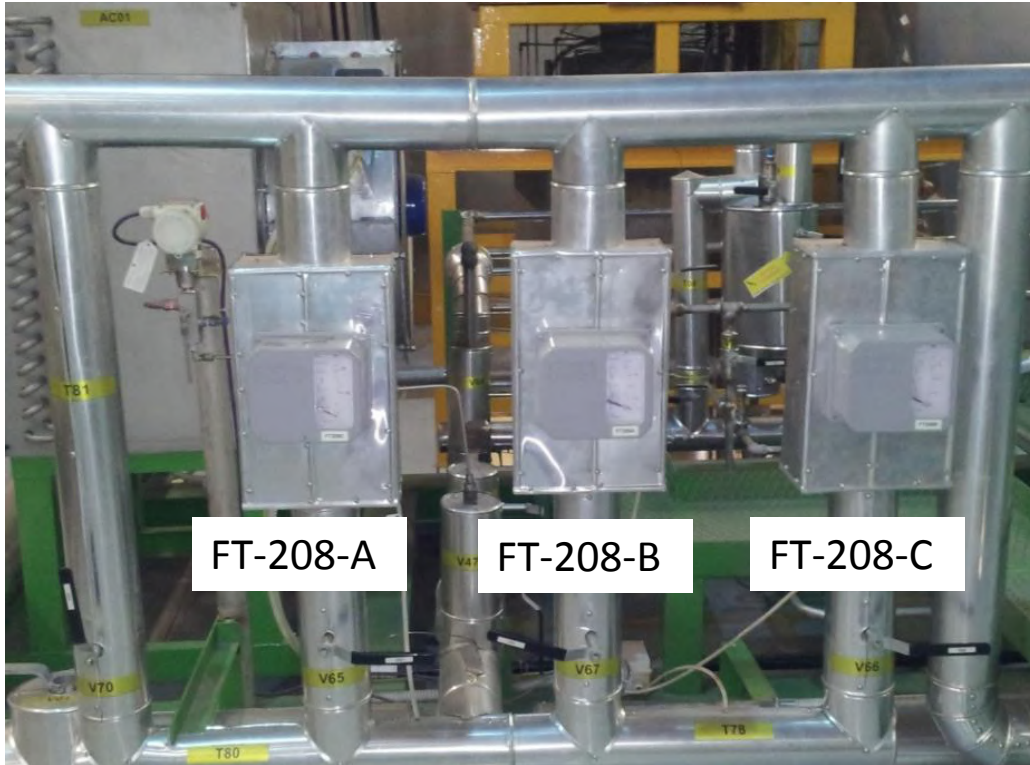


Annex A Fig. 14 T-MS-0100-Posizione TC Mix&Strat su piani di misura.pdf

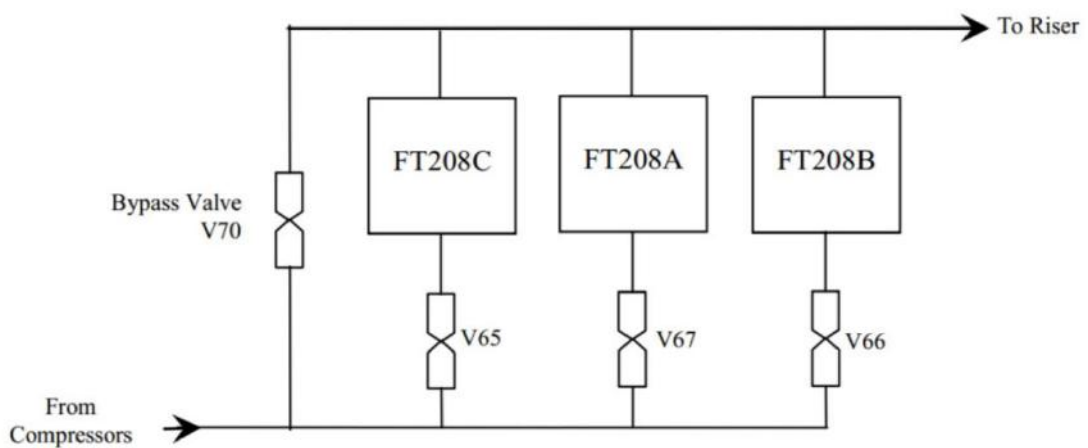
 DIVISIONE INGEGNERIA SPERIMENTALE	<u>Title</u> D3.2: CIRCE experiments: pre-test, data-set and analysis	<u>Distribution</u> PUBLIC	<u>Emission</u> 09/08/2017	<u>Pag.</u> 219 di 234
		<u>Ref.</u> CI-T-R-292	Rev. 0	

ANNEX B:


Argon Mass flow meter Test 1 and Test 2:



Annex B Fig. 1: Layout of the Argon mass flow controller




Annex B Fig. 2: Argon mass flow controller scheme

 DIVISIONE INGEGNERIA SPERIMENTALE	<u>Title</u> D3.2: CIRCE experiments: pre-test, data-set and analysis	<u>Distribution</u> PUBLIC	<u>Emission</u> 09/08/2017	<u>Pag.</u> 220 di 234
		<u>Ref.</u> CI-T-R-292	Rev. 0	


Annex B Table 1: FT208A and FT208B technical data

MISURATORI DI PORTATA			
Pos.	SIGLA	FT208A	FT208B
1	Quantità	1	1
2	Servizio	Misura di portata gas tubaz. Ingresso serbatoio S100	Misura di portata gas tubaz. Ingresso serbatoio S100
3	Fluido di processo	Argon	Argon
4	Temperatura	Norm	150°C
		Max	200°C
5	Pressione	Norm	4,5 Bar rel
		Max	10 Bar rel
6	Portata nominale	(1)	(1)
7	Tipo strumento	Ad aria variabile ed accoppiamento magnetico	Ad aria variabile ed accoppiamento magnetico
8	Campo richiesto	0,05 ÷ 0,5 NI/sec	0,35 ÷ 3.5 NI/sec
9	Precisione	± 1,5% f.s.	± 1,5% f.s.
10	Segnale di uscita	4 ÷ 20 mA a due fili	4 ÷ 20 mA a due fili
11	Tipo e lunghezza scala	Graduata 100 mm	Graduata 100 mm
12	Tubazione di processo	φ 1" sch 40	φ 1" sch 40
13	Tipo connessioni	Flangiate DN15 PN40	Flangiate DN15 PN40
14	Disposizione connessioni	Alle estremità	Alle estremità
15	Tubo di misura	AISI 316L	AISI 316L
16	Materiale connessioni	Acciaio inox	Acciaio inox
17	Materiale galleggiante	Guidato in AISI 316 L	Guidato in AISI 316 L
18	Montaggio	Verticale ingresso dal basso	Verticale ingresso dal basso
19	Accessori	Alimentatore: - Alimentaz. verso campo 24 Vcc (uscita 4-20mA) - Alimentaz. ausiliaria 220 Vac	Alimentatore: - Alimentaz. verso campo 24 Vcc (uscita 4-20mA) - Alimentaz. ausiliaria 220 Vac
20	Note	(1) La portata da misurare che sarà coperta dai tre strumenti è di 0.08÷15 NI/sec	

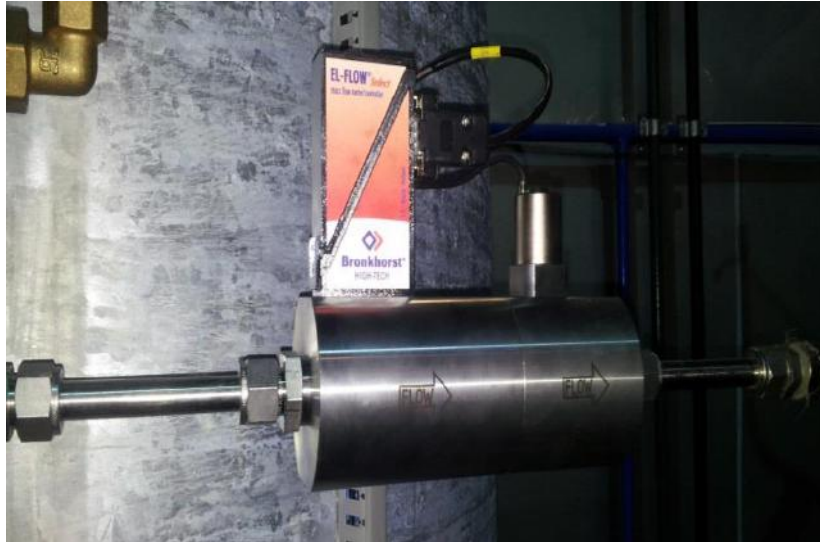
 DIVISIONE INGEGNERIA SPERIMENTALE	<u>Title</u> D3.2: CIRCE experiments: pre-test, data-set and analysis	<u>Distribution</u> PUBLIC	<u>Emission</u> 09/08/2017	<u>Pag.</u> 221 di 234
		<u>Ref.</u> CI-T-R-292	Rev. 0	

Annex B Table 2: FT208C technical data

MISURATORI DI PORTATA		
Pos.	SIGLA	FT208C
1	Quantità	1
2	Servizio	Misura di portata gas tubaz. Ingresso serbatoio S100
3	Fluido di processo	Argon
4	Temperatura	Norm 150°C
		Max 200°C
5	Pressione	Norm 4,5 Bar rel
		Max 10 Bar rel
6	Portata nominale	(1)
7	Tipo strumento	Ad aria variabile ed accoppiamento magnetico
8	Campo richiesto	2,2 ÷ 22 NI/sec
9	Precisione	± 1,5% f.s.
10	Segnale di uscita	4 ÷ 20 mA a due fili
11	Tipo e lunghezza scala	Graduata 100 mm
12	Tubazione di processo	φ 1" sch 40
13	Tipo connessioni	Flangiate DN25 PN40
14	Disposizione connessioni	Alle estremità
15	Tubo di misura	AISI 316L
16	Materiale connessioni	Acciaio inox
17	Materiale galleggiante	Guidato in AISI 316 L
18	Montaggio	Verticale ingresso dal basso
19	Accessori	Alimentatore: - Alimentaz. verso campo 24 Vcc (uscita 4-20mA) - Alimentaz. ausiliaria 220 Vac
20	Note	(1) La portata da misurare che sarà coperta dai tre strumenti è di 0.08÷15 NI/sec

 DIVISIONE INGEGNERIA SPERIMENTALE	<u>Title</u> D3.2: CIRCE experiments: pre-test, data-set and analysis	<u>Distribution</u> PUBLIC	<u>Emission</u> 09/08/2017	<u>Pag.</u> 222 di 234
		<u>Ref.</u> CI-T-R-292	Rev. 0	

Argon Mass flow meter Test 3 and Test 4:



Annex B Fig. 3: Argon mass flow controller adopted for Test 3 and 4



Annex B Fig. 4: Argon mass flow controller identification plate

Datasheet F-203AV

Mass Flow Controller for Gases

> Introduction

Bronkhorst® model F-203AV Mass Flow Controllers (MFCs) are suited for precise control of virtually all conventional process gases. The MFC consists of a thermal mass flow sensor, a precise control valve and a microprocessor based PID controller with signal and fieldbus conversion. As a function of a setpoint value, the flow controller swiftly adjusts the desired flow rate. The mass flow, expressed in normal litres per minute or normal cubic metres per hour, is provided as analog signal or digitally via RS232 or fieldbus. The flow range, wetted materials and orifice size for the control valve are determined depending of the type of gas and the process conditions of the application.

Although all specifications in this datasheet are believed to be accurate, the right is reserved to make changes without notice or obligation.



EL-FLOW Mass Flow Controller model F-203AV

> Technical specifications

Measurement / control system

Accuracy (incl. linearity)	: $\pm 0.5\%$ Rd plus $\pm 0.1\%$ FS
(Based on actual calibration)	
Turndown	: 1 : 50 (in digital mode up to 1:187.5)
Multiple fluid capability	: storage of max. 8 calibration curves
Repeatability	: $< \pm 0.2\%$ Rd
Settling time (controller)	: 2...4 seconds
Control stability	: $\pm 0.1\%$ FS
Kv-value	: 0.15...1.5
Temperature range	: -10...+70°C
Temperature sensitivity (nominal range)	: zero: $< \pm 0.05\%$ FS/°C; span: $< \pm 0.05\%$ Rd/°C
Leak integrity (outboard)	: $< 2 \times 10^{-11}$ mbar l/s He
Altitude sensitivity	: max. error at 90° off horizontal 0.2% FS at 1 bar, typical N ₂
Warm-up time	: 30 min. for optimum accuracy 2 min. for accuracy $\pm 2\%$ FS

Mechanical parts

Material (wetted parts)	: stainless steel 316L or comparable
Pressure rating	: 64 bar abs
Process connections	: compression type or face seal male
Seals	: standard: Viton; options: EPDM, Kalrez
Ingress protection (housing)	: IP40

Electrical properties

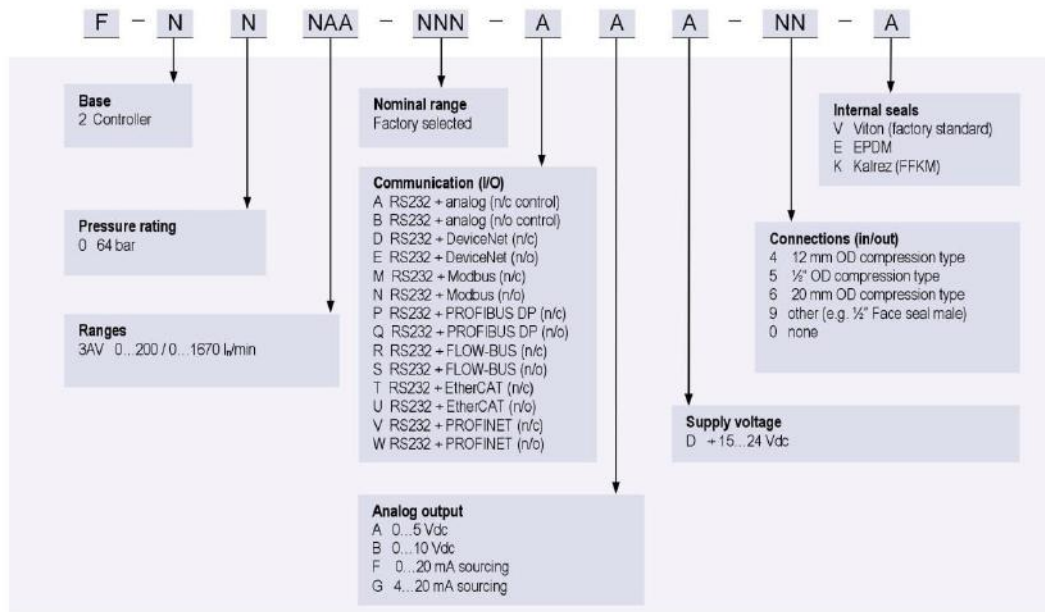
Power supply	: +15...24 Vdc $\pm 10\%$
Power consumption	: Supply at voltage I/O at current I/O
(based on N/C valve)	15 V 290 mA 320 mA 24 V 200 mA 215 mA
Extra for fieldbus:	PROFIBUS DP: add 53 mA (15 V supply) or 30 mA (24 V supply)
(if applicable)	EtherCAT®: add 66 mA (15 V supply) or 41 mA (24 V supply)
	DeviceNet™: add 48 mA (24 V supply)
	PROFINET: add 77 mA (15 V supply) or 48 mA (24 V supply)
Analog output (0...100%)	: 0...5 (10) Vdc; min. load impedance > 2 k Ω ; 0 (4)...20 mA (sourcing); max. load impedance < 375 Ω
Analog setpoint (0...100%)	: 0...5 (10) Vdc; min. load impedance > 100 k Ω ; 0 (4)...20 mA; load impedance ≈ 250 Ω
Digital communication	: standard RS232; options: PROFIBUS DP, DeviceNet™, EtherCAT®, Modbus-RTU/ASCII, FLOW-BUS, PROFINET.

> Ranges (based on Air)

Model	minimum	nominal	maximum
F-203AV-M50	4...200 L/min	4...500 L/min	15...750 L/min
F-203AV-1M0	8...400 L/min	8...1000 L/min	33...1670 L/min

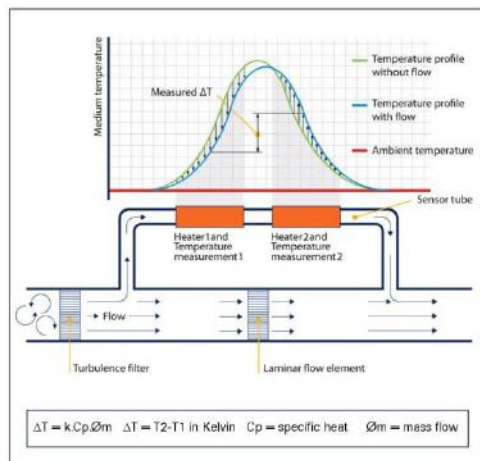
Intermediate ranges are available

> Model number identification



> Thermal mass flow measuring principle

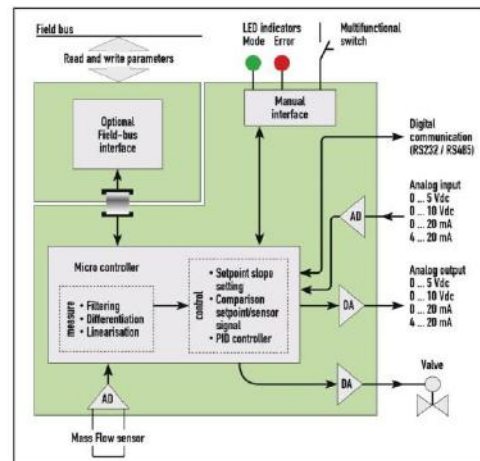
The heart of the thermal mass flow meter/controller is a sensor that consists of a stainless steel capillary tube with resistance thermometer elements. A part of the flow is diverted through this bypass style sensor, and is warmed up by heating elements. As a result, the measured temperatures T_1 and T_2 drift apart. The temperature difference is directly proportional to mass flow through the sensor. In the main channel Bronkhorst applies a patented laminar flow element consisting of a stack of stainless steel discs with precision-etched flow channels. Thanks to the perfect flow-split the sensor output is proportional to the total mass flow rate.



Functional scheme of the thermal mass flow sensor

> State of the art digital design

Today's EL-FLOW[®] series are equipped with a digital pc-board, offering high accuracy, repeatability, excellent temperature stability and fast response (settling times t_{90} down to 500 msec). The basic digital pc-board contains all of the general functions needed for measurement and control. In addition to the standard RS232 output the instruments also offer analog I/O. Furthermore, an integrated interface board provides DeviceNet[™], PROFIBUS DP, PROFINET, Modbus RTU/ASCII or FLOW-BUS protocols.



Functional scheme of the digital PC-board



DIVISIONE INGEGNERIA
SPERIMENTALE

Title
**D3.2: CIRCE experiments:
pre-test, data-set and analysis**

Distribution
PUBLIC

Emission
09/08/2017

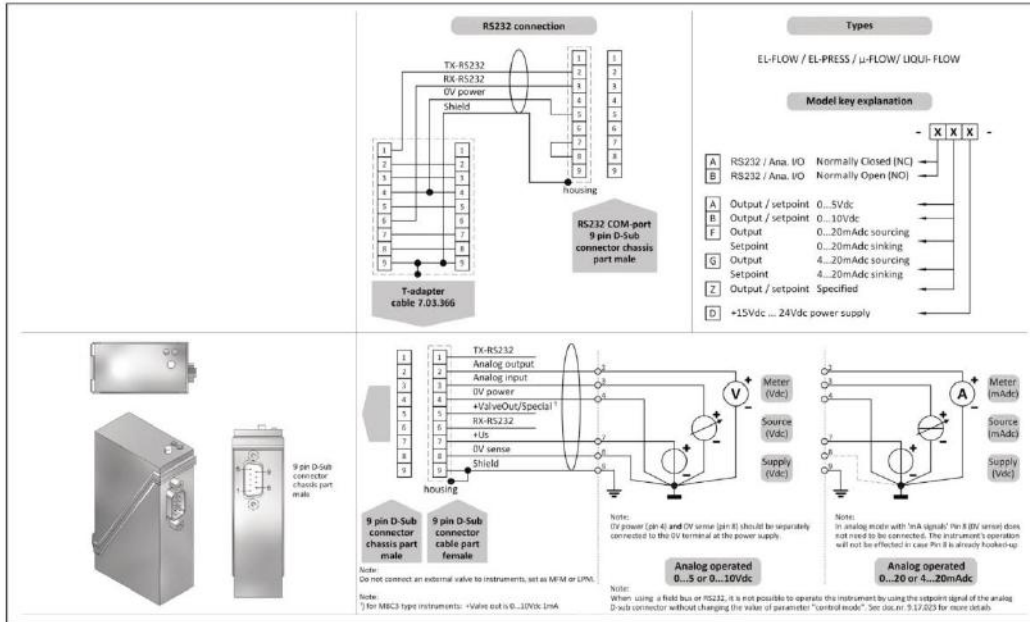
Pag.

Ref.
CI-T-R-292

Rev. 0

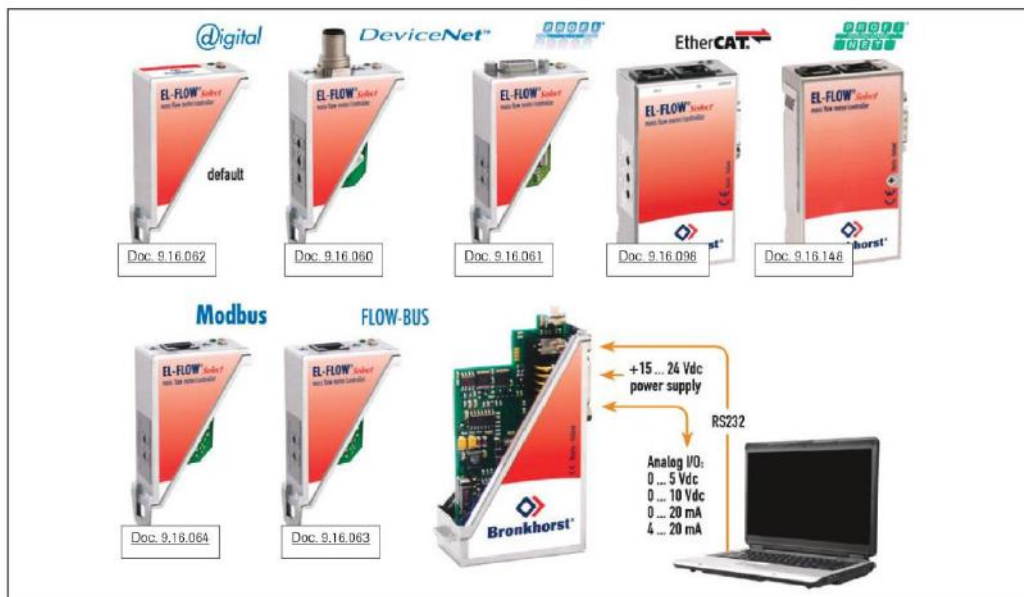
225 di 234

> Hook-up diagram for analog or RS232 communication

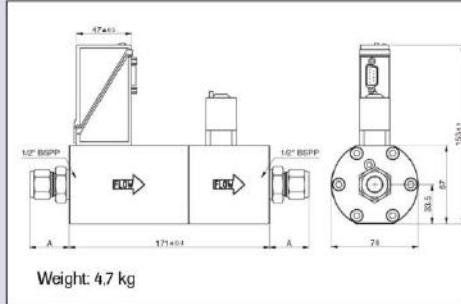


> Hook-up diagrams for fieldbus communication

For the available fieldbus options we refer to the various hook-up diagrams as indicated below. If you are viewing this datasheet in digital format, you may use the hyperlink to each of the drawings. Otherwise please visit the download section on www.bronkhorst.com or contact our local representatives.



> Dimensions (mm) and weight (kg)

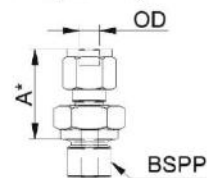


Dimension table adapters (RS-type)

Compression type	1/2" BSPP	
	Size	A
adapter 10 mm OD	31.0	
adapter 12 mm OD	33.5	
adapter 20 mm OD	36.5	
adapter 25 mm OD	42.0	
adapter 3/8" OD	30.7	
adapter 1/2" OD	33.5	
adapter 3/4" OD	34.8	

Face-seal male	1/2" BSPP	
	Size	A
adapter 1/2" inlet	27.6	
adapter 3/4" inlet	36.5	

Compression type




*) Dimension A is typical finger-tight.

> Options and accessories

- Free software support for operation, monitoring, optimizing or to interface between digital instruments and windows software.	
- IN-LINE filters for protection against particulates	
- BRIGHT compact local Readout/Control modules - E-8000 Power Supply	
- Interconnecting cables for power and analog/digital communication - PiPS Plug-in Power Supply	

> Alternatives

- IN-FLOW MFC with industrial (IP65) housing	
- IN-FLOW ^{22A} direct (no by-pass), industrial (IP65) Mass Flow Meter with close-coupled Control Valve	

 DIVISIONE INGEGNERIA SPERIMENTALE	<u>Title</u> D3.2: CIRCE experiments: pre-test, data-set and analysis	<u>Distribution</u> PUBLIC	<u>Emission</u> 09/08/2017	<u>Pag.</u> 227 di 234
		<u>Ref.</u> CI-T-R-292	Rev. 0	

ANNEX C:

In order to investigate the behavior of the DHR-system revealed during the experimental campaign, it was decided to extract the ICE test section from the CIRCE S100 pool for a visual examination to verify the integrity of the test section itself. This inspection revealed a widespread formation of oxides, such as to jeopardize the proper functioning of the DHR system. Annex C Fig. 1 show the status of the slot at the inlet section of the DHR-system before and after the experimental campaign. As evinced in the photo, the oxide formation completely clogged the DHR inlet slots.



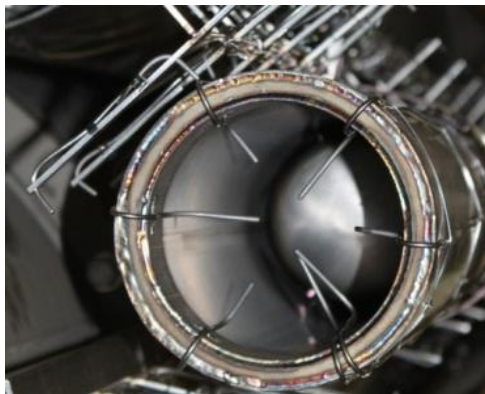
(a)



(b)

Annex C Fig. 1: DHR inlet section before (a) and after (b) the experimental campaign

Pictures showed in Annex C Fig. 2 highlight the status of the DHR outlet section before and after the experiments respectively.




(a)



(b)

Annex C Fig. 2 :DHR inlet section before (a) and after (b) the experimental campaign

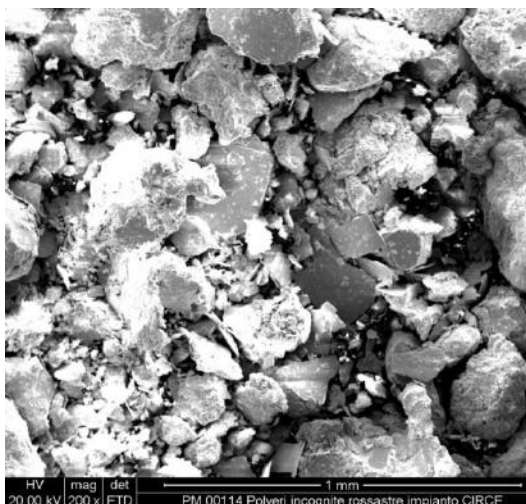
 DIVISIONE INGEGNERIA SPERIMENTALE	<u>Title</u> D3.2: CIRCE experiments: pre-test, data-set and analysis	<u>Distribution</u> PUBLIC	<u>Emission</u> 09/08/2017	<u>Pag.</u> 228 di 234
		<u>Ref.</u> CI-T-R-292	Rev. 0	

The outlet section is completely clogged by the oxides, preventing LBE circulation in the DHR-system. Moreover, as showed in Annex C Fig. 3, oxide formation was found in proximity of the external wall of the DHR and of the vertical rods for the thermocouples positioning.

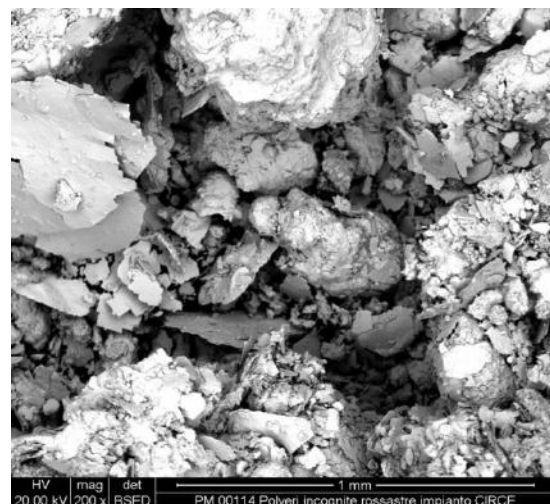


Annex C Fig. 3: Oxide formation next to the DHR-system

A sample of the oxide was collected and subjected to chemical analysis by electron microscope. This analysis did not reveal any elements making up the system (Annex C Fig. 4).




(a)



(b)

Annex C Fig. 4: Oxide Scanning Electron Microscope (SEM) analysis

 DIVISIONE INGEGNERIA SPERIMENTALE	<u>Title</u> D3.2: CIRCE experiments: pre-test, data-set and analysis	<u>Distribution</u> PUBLIC	<u>Emission</u> 09/08/2017	<u>Pag.</u> 229 di 234
		<u>Ref.</u> CI-T-R-292	Rev. 0	

The performed microanalysis confirmed the exclusive presence of lead oxides, even if it was not possible to distinguish if it was present only one type of oxide or a mixed phase of PbO and Pb₃O₄. In order to investigate the status of the FPS an endoscopic examination (Olympus IPLEX LT) was performed. This investigation highlighted the cleanness of the grids and of the electrical pins from LBE as showed in Annex C Fig. 5 and Annex C Fig. 6.



(a)

(b)


Annex C Fig. 5: Endoscopic examination (Olympus IPLEX LT) FPS entrance grid



(a)

(b)

Annex C Fig. 6: Endoscopic examination (Olympus IPLEX LT) FPS lower spacer grid (a) and electrical pins (b)

 DIVISIONE INGEGNERIA SPERIMENTALE	<u>Title</u> D3.2: CIRCE experiments: pre-test, data-set and analysis	<u>Distribution</u> PUBLIC	<u>Emission</u> 09/08/2017	<u>Pag.</u> 230 di 234
		<u>Ref.</u> CI-T-R-292	Rev. 0	

DISTRIBUTION LIST

A. Del Nevo	ENEA-FSN-ING	alessandro.delnevo@enea.it
I. Di Piazza	ENEA-FSN-ING	ivan.dipiazza@enea.it
M. Tarantino	ENEA-FSN-ING	mariano.tarantino@enea.it
N. Forgione	UNIPI-DICI	nicola.forgione@ing.unipi.it
D. Martelli	UNIPI-DICI	daniele.martelli@ing.unipi.it
V. Moreau	CRS4	mailto:moreau@crs4.it
F. Roelofs	NRG	roelofs@nrg.eu
k. Zwijzen	NRG	zwijzen@nrg.eu